Functional Self-healing Hydrogels Based on Dynamic Molecular Interactions for Biomedical Applications

by

Wenda Wang

A thesis submitted in partial fulfillment of the requirements for the degree of

Doctor of Philosophy

in

Materials Engineering

Department of Chemical and Materials Engineering
University of Alberta

Abstract

Self-healing hydrogels can autonomously heal from damage to preserve their integrity and functionalities which hold great promises in a wide range of applications. Different types of dynamic molecular interactions have been explored to develop self-healing hydrogels. Nevertheless, it remains a challenge to integrate multifunctionalities in one "smart" hydrogel platform based on different requirements in diverse biomedical applications. In addition, the molecular level understanding of different dynamic molecular interaction mechanisms is limited. In this thesis, a review of different self-healing mechanisms and some typical biomedical applications of self-healing hydrogels is first presented, followed by three original studies of developing multifunctional self-healing hydrogels for different potential biomedical applications and investigating the associated molecular interaction mechanisms.

Self-healing hydrogels with injectability, multi-stimuli-responsive and antimicrobial properties are highly desired for wound healing. In the first project, an injectable self-healing hydrogel with dual temperature-pH responsive and antimicrobial properties was developed based on dynamic Schiff base reactions between a synthetic multifunctional ABA triblock copolymer gelator, poly{(4-formylphenyl methacrylate)-co-[[2-(methacryloyloxy)ethyl] trimethylammonium chloride]}-b-poly(N-isopropylacrylamide)-b-poly{(4-formylphenyl methacrylate)-co-[[2-(methacryloyloxy)ethyl] trimethylammonium chloride]} (PFMNMF) and polyethylenimine (PEI). The self-healing

capability was characterized by rheology tests and the associated molecular interaction mechanism was studied using a surface forces apparatus (SFA). The hydrogel demonstrated excellent injectability as well as sensitive dual temperature-pH responsiveness. In addition, the hydrogel could also effectively inhibit the growth of both Gram-negative and Gram-positive bacteria (*Escherichia coli* and *Staphylococcus aureus*), while showed low cytotoxicity to both fibroblast and cancer cells (MRC-5 and HeLa). Such multifunctional self-healing hydrogel can be potentially applied as wound dressing material.

The development of biological tissue-like hydrogels with both self-healing and strain-stiffening capabilities is of great significance in various biomedical and engineering applications. In the second project, a biomimetic self-healing strain-stiffening flexible hydrogel was developed based on the dynamic boronic acid-diol interactions between diphenylboronic acid-terminated telechelic poly(ethylene glycol) (DPB-PEG) and a glycopolymer, poly(acrylamide-*co*-2-lactobionamidoethyl methacrylamide) (P(AM-*co*-LAMEA)). The hydrogel can be reversibly and repeatedly stiffened up to 8 times of its original modulus as it is strained, without showing mechanical hysteresis. In addition, the damaged hydrogel can repeatedly self-heal within seconds and fully retains the strain-stiffening capability. The associated dynamic molecular interactions were quantitatively measured using a SFA. Based on the biomimetic characteristics as well as the excellent biocompatibility, the hydrogel served as an ideal cell culture matrix to mimic the *in vivo*

mechanical environments for 3D cell culture.

In the third project, an injectable self-healing hydrogel with anti-biofouling property was developed as internal wound dressing for the treatment of gastric perforation. The hydrogel was designed based on the biological environment-adaptive supramolecular self-assembly of an ABA triblock copolymer, employing a central poly(ethylene glycol) (PEG) block and terminal thermoresponsive poly(N-isopropylacrylamide) (PNIPAM) block with pH sensitive acryloyl-6-aminocaproic acid (A6ACA) moieties randomly incorporated. Due to the thermo-sensitivity, the hydrogel could be rapidly formed at the targeted site after simple injection. The formed hydrogel dressing could smartly utilize the acidic environment to self-heal from repeated damage through the synergy of hydrophobic and pH-mediated hydrogen bonding interactions. The associated molecular interaction mechanism was studied using a SFA. Besides, the hydrogel exhibits excellent anti-biofouling performance against microorganism attachment. The *in vivo* rat model demonstrated the remarkable capabilities of the hydrogel dressing to simplify surgical procedures, reduce postoperative complications as well as enhance the healing process of gastric perforation compared with the conventional omental implantation.

This thesis work develops three novel multifunctional self-healing hydrogels based on different dynamic molecular interactions for biomedical applications, as well as investigates the self-healing mechanisms from the perspective of intermolecular interactions and surface forces. This work not only expands the applicability of self-healing

hydrogels in some new biomedical applications, but also provides fundamental insights into the development of multifunctional self-healing hydrogel in various biomedical applications.

Preface

This thesis is an original work by Wenda Wang under the supervision from Prof. Hongbo Zeng and Prof. Ravin Narain.

Part of Chapter 1 has been published as: (1) Wenda Wang, Ravin Narain, Hongbo Zeng, Rational Design of Self-healing Tough Hydrogels: A Mini Review, *Frontiers in Chemistry*, 2018, 00497. (2) Wenda Wang, Ravin Narain, Hongbo Zeng, Chapter 10-Hydrogels. In *Polymer Science and Nanotechnology*, Elsevier, 2020, 203-244. I was responsible for the manuscript composition.

Part of Chapter 2 has been published as Wenda Wang, Ravin Narain, Hongbo Zeng, Chapter 10-Hydrogels. In *Polymer Science and Nanotechnology*, Elsevier, 2020, 203-244. I was responsible for the manuscript composition.

Chapter 3 has been published as Wenda Wang, Li Xiang, Lu Gong, Wenjihao Hu, Weijuan Huang, Yangjun Chen, Anika B. Asha, Shruti Srinivas, Lingyun Chen, Ravin Narain and Hongbo Zeng, Injectable, Self-Healing Hydrogel with Tunable Optical, Mechanical, and Antimicrobial Properties, *Chemistry of Materials*, 2019, 31, 7, 2366–2376. I was responsible for material synthesis, experimental design, data collection and analysis, as well as manuscript composition. Dr. Li Xiang helped with SFA force measurements. Dr. Lu Gong helped with AFM imaging. Dr. Weijuan Huang and Anika B. Asha helped with antimicrobial assay. Shruti Srinivas helped with cytotoxicity tests. Dr. Wenjihao Hu, Dr. Yangjun Chen, Prof. Lingyun Chen helped with manuscript revision. Prof. Ravin Narain

and Prof. Hongbo Zeng were corresponding authors and were involved in the experimental design and manuscript composition.

Chapter 4 has been published as Wenda Wang, Li Xiang, Diana Diaz-Dussan, Jiawen Zhang, Wenshuai Yang, Lu Gong, Jingsi Chen, Ravin Narain and Hongbo Zeng, Dynamic Flexible Hydrogel Network with Biological Tissue-like Self-protective Functions, *Chemistry of Materials*, 2020, 32, 24, 10545–10555. I was responsible for material synthesis, experimental design, data collection and analysis, as well as manuscript composition. Dr. Li Xiang helped with SFA force measurements. Diana Diaz-Dussan helped with 3D cell culture. Dr. Jiawen Zhang, Wenshuai Yang, Dr. Lu Gong and Dr. Jingsi Chen helped with manuscript revision. Prof. Ravin Narain and Prof. Hongbo Zeng were corresponding authors and were involved in the experimental design and manuscript composition.

Chapter 5 has been submitted to *ACS Nano* and is being reviewed for publication as Wenda Wang, Zicheng Zeng, Li Xiang, Cong Liu, Diana Diaz-Dussan, Zunguo Du, Anika B. Asha, Wenshuai Yang, Yi-Yang Peng, Mingfei Pan, Ravin Narain, Jifang Liu and Hongbo Zeng, Injectable Self-healing Hydrogel via Biological-Environment Adaptive Supramolecular Assembly as Internal Wound Dressing. Some of the research conducted in this chapter belongs to an international collaboration, led by Prof. Hongbo Zeng at University of Alberta and Prof. Jifang Liu at Guangzhou Medical University. I was responsible for material synthesis, experimental design, data collection and analysis, as

well as manuscript composition. Zicheng Zeng and Cong Liu helped with *in vivo* animal study. Dr. Li Xiang helped with SFA force measurements. Diana Diaz-Dussan and Yi-Yang Peng helped with cytotoxicity tests. Zunguo Du helped with histopathological analysis. Anika B. Asha helped with anti-biofouling tests. Wenshuai Yang and Mingfei Pan helped with manuscript revision. Prof. Ravin Nrain, Prof. Jifang Liu and Prof. Hongbo Zeng were corresponding authors and were involved in the experimental design and manuscript composition.

Part of Chapter 1, 2 and Chapter 6 are originally written by Wenda Wang and have never been published before.

Acknowledgements

First and foremost, I would like to express my sincere gratitude to my supervisors Prof. Hongbo Zeng and Prof. Ravin Narain, who provide me the great opportunity to study at University of Alberta and introduced me into the world of functional polymers and intermolecular and surface forces. I really appreciate their tremendous support, immeasurable guidance and valuable suggestions during my Ph.D. study. Their passion for science, dedication for innovation and attention to details would have life-long impact on my career and life path.

Secondly, I would like to thank all the group members for their support, help and friendship. My special thanks go to Dr. Li Xiang, Dr. Lu Gong, Dr. Jiawen Zhang and Dr. Jingsi Chen for the insightful discussions on my research as well as the helpful suggestions on manuscript revision. Thank Dr. Yangjun Chen and Dr. Bin Yan for their guidance and suggestions on polymer synthesis at the beginning of my Ph.D. study. Thank Prof. Jifang Liu and Zicheng Zeng for the collaborative work on animal studies.

Thirdly, I would like to acknowledge the financial support from the Natural Sciences and Engineering Research Council of Canada (NSERC), Canada Foundation for Innovation (CFI) and the Canada Research Chairs Program.

I also wish to give many thanks to my friends, Qifeng Yu, Han Mei, Qiyuan Lin, Zhengxiang Zhao, who have kept me company since my undergraduate study. Special thanks go to my girlfriend An Zhang for the continuous encouragement and the delightful

laugh she brings to me.

Last but not least, I would like to thank my beloved parents and other family members for their generous encouragement and unconditional support during my eight-year study overseas. Special thanks go to my father, Dr. Yin Wang, who also helped me with histopathological analysis. Without their support and encouragement, I would never be able to finish my Ph.D. study.

Table of Contents

Abstract ..... *ii*

Preface ..... *vi*

Acknowledgements ..... *ix*

Table of Contents ..... *xi*

List of Figures ..... *xv*

Abbreviations and Symbols ..... *xxiii*

CHAPTER 1 General Introduction *1*

1.1 Functional Hydrogels and Self-healing Hydrogels **1**

1.2 Self-healing Mechanisms **2**

1.2.1 Extrinsic Self-healing *2*

1.2.2 Intrinsic Self-healing *4*

1.2.2.1 Dynamic Non-covalent Interactions *5*

1.2.2.2 Dynamic covalent chemistry *8*

1.3 Biomedical Applications of Self-healing Hydrogels **13**

1.3.1 Wound Healing *13*

1.3.2 3D Cell Culture Matrix *15*

1.3.3 Postoperative Anti-adhesion Barrier *17*

1.4 Objectives **19**

1.5 Structure of the Thesis **20**

References **23**

CHAPTER 2 Major Experimental Methods *37*

2.1 Polymerization Techniques **37**

2.1.1 Conventional Free Radical Polymerization *37*

2.2 Rheometer **41**

2.3 Surface forces apparatus (SFA) **44**

2.3.1 Setup of the SFA Measurement *46*

2.3.2 Force measurement using SFA *47*

References **49**

CHAPTER 3 Injectable, Self-Healing Hydrogel with Tunable Optical, Mechanical, and Antimicrobial Properties *53*

3.1 Introduction **53**

3.2 Experimental Methods **56**

3.2.1 Materials *56*

3.2.2 Polymer Synthesis *56*

3.2.3 Fabrication of the Hydrogels *58*

3.2.4 Rheological Characterization of the Hydrogels *59*

3.2.5 Self-healing Property and Measuring the Associated Polymer Interactions using SFA *59*

3.2.6 Temperature and pH Responsive Properties of the Hydrogel *61*

3.2.7 Antimicrobial Assay and Cell Cytotoxicity *62*

3.3 Results and Discussions **63**

3.3.1 Synthesis of Polymers *63*

3.3.2 Fabrication and Rheology Characterization of the Hydrogel *66*

3.3.3 Self-healing Property and Associated Polymer Interaction Mechanism *68*

3.3.4 Temperature and pH Responsive Properties of the Hydrogel *72*

3.3.5 Antimicrobial Property and Cell Cytotoxicity *76*

3.4 Conclusions **78**

Supporting Information **80**

References **85**

CHAPTER 4 Dynamic Flexible Hydrogel Network with Biological Tissue-like Self-protective Functions *93*

4.1 Introduction **93**

4.2 Experimental Methods **96**
4.2.1 Materials *96*
4.2.2 Polymer Synthesis and Characterization *96*
4.2.3 Hydrogel Preparation *97*
4.2.4 Rheology Characterization *97*
4.2.5 SFA Experiment Setup and Force Measurements *98*
4.2.6 Cell Culture *99*
4.2.7 3D cell encapsulation *99*
4.3 Results and Discussions **100**
4.3.1 Polymer Synthesis and Hydrogel Preparation *100*
4.3.2 Mechanical Analysis of Strain-stiffening Behavior *101*
4.3.3 Boronic acid/sugar Molar Ratio Dependence *101*
4.3.4 Polymer Concentration Dependence *103*
4.3.5 Temperature Dependence *104*
4.3.6 Cross-linker Chain Length Dependence *106*
4.3.7 Reversibility and Reproducibility of Strain-stiffening Behavior *107*
4.3.8 Strain-stiffening Mechanism *108*
4.3.9 Self-healing Property and Associated Interaction Mechanism *112*
4.3.10 3D Cell Encapsulation *114*
4.4 Conclusions **116**
Supporting Information **117**
References **124**
CHAPTER 5 Injectable Self-healing Hydrogel via Biological-Environment Adaptive Supramolecular Assembly as Internal Wound Dressing *130*
5.1 Introduction **130**
5.2 Experimental Methods **133**
5.2.1 Materials *133*

5.2.2 Polymer Synthesis *133*
5.2.3 Polymer Characterization *134*
5.2.4 Hydrogel Preparation *134*
5.2.5 Rheology Characterization *134*
5.2.6 SFA Force Measurements *135*
5.2.7 Bacteria Adhesion Assay *136*
5.2.8 MTT Assay *136*
5.2.9 2D/3D Cell Culture *137*
5.2.10 In vivo Gastric Perforation Repair in a Rat Model *137*
5.2.11 Histopathological Observation and Immunohistochemical Examination. *138*
5.3 Results and Discussions **138**
5.3.1 Polymer Synthesis and Characterization *138*
5.3.2 Thermo-reversibility and Injectability of ANGNA Hydrogel *139*
5.3.3 Self-healing Property and Associated Interaction Mechanism *141*
5.3.4 Anti-biofouling Property and Biocompatibility *144*
5.3.5 In vivo Gastric Perforation Repair in a Rat Model *146*
5.4 Conclusions **150**
Supporting Information **152**
References **156**
CHAPTER 6 Conclusions and Future Work *160*
6.1 Major Conclusions and Contributions **160**
6.2 Future Work **162**
Bibliography *163*

List of Figures

Figure 1.1. Schematic illustration of self-healing process of extrinsic self-healing materials.[30] 4

Figure 1.2. Hydrogen bonding interaction between (a) UPy moieties. (b) A6ACA side chains. 5

Figure 1.3. Self-healing through hydrophobic interactions between hydrophobic domains/assocaitions..... 6

Figure 1.4. Host-guest interactions between host and guest molecules. 7

Figure 1.5. Different non-covalent interactions involved in mussel-inspired chemistry. .. 8

Figure 1.6. 4-arm PEG macromonomers bearing diol or PBA derivatives for the preparation of self-healing hydrogels. 9

Figure 1.7. Dynamic Schiff base reaction between benzaldehyde and amine groups. 10

Figure 1.8. Self-healing hydrogel based on dynamic acylhydazone and disulfide bonds.[71] 11

Figure 1.9. Thiol/disulfide exchange reactions. 11

Figure 1.10. Self-healing hydrogels based on (a) BP-Ca^{2+} coordinate bonds.[76] (b) catechol-Fe^{3+} coordinate bonds.[78]..... 12

Figure 1.11. Self-healing hydrogel based on DA reaction using fulvene-modified dextran and dichloromaleic acid-terminated PEG.[83] 13

Figure 1.12. 3D cell culture using (a) physically self-healing hydrogel.[101] (b) chemically self-healing hydrogel.[60]..... 16

Figure 1.13. (a) HPMC-C12/PEG-PLA hydrogel formed via self-assembly process due to the hydrophobic interactions between HPMC-C12 and PEG-PLA nanoparticles.[106] (b) CMC-NB/GC hydrogel formed through photo-crosslinking process.[107] 19

Figure 2.1. Commonly used initiators in conventional free radical polymerization..... 37

Figure 2.2. Propagation step of conventional free radical polymerization. 38

Figure 2.3. Termination mechanisms of conventional free radical polymerization. 38

Figure 2.4. Reversible addition−fragmentation chain-transfer (RAFT) polymerization mechanism.[9] 40

Figure 2.5. General structure of thiocarbonylthio-containing chain transfer agent (CTA). 41

Figure 2.6. (a) Typical rheology measurement set-up. (b) Typical measurements of viscoelastic materials (e.g., hydrogels). 42

Figure 2.7. (a) Applied strain in an oscillatory strain amplitude test. (b) Applied strain in an oscillatory frequency test. 43

Figure 2.8. The picture of SFA 2000. 45

Figure 2.9. Cross-section of SFA 2000 through the center.[17] 46

Figure 2.10. Schematic illustration of SFA experiment setup.[22] 47

Figure 3.1. Schematic Illustration of Injectable Self-healing Hydrogel with Tunable Optical, Mechanical and Antimicrobial Properties Fabricated by PFMNMF and PEI..... 56

Figure 3.2. Synthesis Route of (a) PFMNMF ABA Triblock Copolymer and (b) PFMN Random Copolymer. 65

Figure 3.3. ^{1}H NMR spectra of (a) PFM macro-CTA and (b) PFMNMF ABA triblock copolymer. 65

Figure 3.4. (a) Gelation process of the hydrogels at 25 °C. (b) Dynamic oscillatory frequency sweeps of the hydrogels (γ = 1%, ω = 1 Hz). 67

Figure 3.5. Injectable property of Gel-9.5%. (a) Extrusion of hydrogel through a 21-G needle. (b) Writing “U of A” by using Gel-9.5% as ink. (c) Viscosity of Gel-9.5% measured as a function of shear rate. 68

Figure 3.6. (a) Demonstration of self-healing property of Gel-9.5%. (b) Dynamic strain sweep measurement of Gel-9.5% at 25 °C (ω = 1 Hz). (c) Dynamic cyclic strain sweep measurement of Gel-9.5% at 25 °C (ω = 1 Hz, γ = 1% or 200%). 70

Figure 3.7. (a) Force-distance profiles show the force magnitudes and reversibility of the

dynamic imine bonds formed between PEI and PFMNMF in PBS buffer solution (pH 7.4). (b) Force-distance profiles show the effect of contact time on the interaction forces between PEI and PFMNMF in PBS buffer solution (pH 7.4). (c) Normalized adhesion force and energy between PEI-coated and PFMNMF-coated mica surfaces in PBS buffer solution (pH 7.4) with different contact time..... 72

Figure 3.8. Transparency change of Gel-9.5% (a) 25 °C. (b) 37 °C. (c) Modulus change of Gel-9.5% at 25 °C and 37 °C (γ = 1%, ω = 1 Hz). AFM topography images of PFMNMF (d) 25 °C. (e) 37 °C. 74

Figure 3.9. (a) Reversible gel-sol-gel transitions of Gel-9.5% by changing pH. (b) Degradation profile of Gel-9.5% in PBS buffer solutions (pH 7.4 and 5.4) at 37 °C. (c) Force-distance profiles show the effect of pH on the interaction forces between PEI and PFMNMF in PBS buffer solutions (pH 7.4, 6.4 and 5.4). (d) Normalized adhesion force and energy between PEI-coated and PFMNMF-coated mica surfaces in PBS buffer solutions at different pH. 76

Figure 3.10. (a) Inhibition efficiency of S. aureus and E. coli after 24 h incubation with Gel-9.5%. (b) Cell viability of HeLa cancer cells and MRC-5 fibroblast cells after 24 h incubation with Gel-9.5% gel extracts. 78

Figure S3.1. ^{1}H NMR spectrum of 4-formylphenyl methacrylate (FPMA) in DMSO-d_6. 80

Figure S3.2. ^{1}H NMR spectrum of 2-(1-carboxy methylethylsulfanylthiocarbonylsulfanyl)-2-methylpropionic acid in DMSO-d_6. 80

Figure S3.3. ^{1}H NMR spectrum of PFMN random copolymer in D_2O..... 81

Figure S3.4. (a) Dynamic strain sweep measurement of Gel-9.5% at 37 °C (ω = 1 Hz). (b) Dynamic cyclic strain sweep measurement of Gel-9.5% at 37 °C (ω = 1 Hz, γ = 1% or 200%). 81

Figure S3.5. A typical SFA setup with asymmetric configuration for force measurement. 82

Figure S3.6. Volume phase transition temperature (VPTT) of Gel-9.5%, Gel-8.5% and Gel-7.5%. 82

Figure S3.7. Transparency change of RGel-9.5% (a) 25 °C. (b) 37 °C. 83

Figure S3.8. Modulus change of RGel-9.5% at 25 °C and 37 °C (γ = 1%, ω = 1 Hz). ... 83

Figure S3.9. AFM topography images of PFMN random copolymer (a) 25 °C. (b) 37 °C. 84

Figure S3.10. SEM images of freeze-dried Gel-9.5% after degradation in PBS buffer solutions at different pH for 24 h. (a) pH 7.4. (b) pH 5.4. 84

Figure 4.1. Preparation of biocompatible flexible hydrogel network using DPB-PEG and P(AM-co-LAEMA) and its biomimetic strain-stiffening and self-healing functions in response to mechanical deformation. 95

Figure 4.2. Mechanical properties of BL4k hydrogels (10 w/v%, T=25 °C) at different boronic acid/sugar molar ratios. (a) Differential modulus K' against stress σ. (b) Plateau modulus G_0 and critical stress σ_c against boronic acid/sugar molar ratio. (c) Normalized differential modulus (K'/ G_0) against normalized stress (σ/σ_c). (d) Stiffening index m as a function of boronic acid/sugar molar ratio. 102

Figure 4.3. Mechanical properties of BL4k hydrogels (boronic acid/sugar molar ratio=1:1, T=25 °C) at different polymer concentration. (a) Differential modulus K' against stress σ. (b) Plateau modulus G_0 and critical stress σ_c against polymer concentration. (c) Normalized differential modulus (K'/ G_0) against normalized stress (σ/σ_c). (d) Stiffening index m as a function of polymer concentration. 104

Figure 4.4. Mechanical properties of BL4k hydrogel (boronic acid/sugar molar ratio=1:1, 10 w/v%) at different temperatures. (a) Differential modulus K' against stress σ. (b) Plateau modulus G_0 and critical stress σ_c against temperature. (c) The master curve fitted to the normalized data in (a). 105

Figure 4.5. Mechanical properties of BL4k and BL8k (boronic acid/sugar molar ratio=1:1, 10 w/v%, T=25 °C). (a) Differential modulus K' against stress σ. (b) Normalized

differential modulus (K'/ G_0) against strain (γ) showing the maximum strain γ_{max} and stiffening range K'_{max}/G_0. 107

Figure 4.6. (a) Cyclic strain step tests of BL4k (boronic acid/sugar molar ratio=1:1, 10 w/v%, T=25 °C) (b) Cyclic strain step tests of BL8k (boronic acid/sugar molar ratio=1:1, 10 w/v%, T=25 °C). (c) Seven sequential strain sweeps of the hydrogel tested in (b)... 108

Figure 4.7. Illustration of the strain-stiffening mechanism. 112

Figure 4.8. The self-healing process of BL4k (boronic acid/sugar=1:1, 10 w/v%, T=25 °C). (a) original hydrogel, (b) hydrogel was cut into two pieces, (c) separated hydrogels were brought into contact, (d) self-healed hydrogel can be lifted against its own weight. (e) Sequential strain sweeps of BL4k (boronic acid/sugar molar ratio=1:1, 10 w/v%, T=25 °C). (f) Cyclic strain step tests of the hydrogel tested in (e). (g) Force-distance profiles show the interactions between P(AM-co-LAEMA) and DPB-PEG in three sequential approach−separation force measurements. 114

Figure 4.9. 3D confocal microscopy images of HeLa cells cultured in (a) 5 w/v%, (b) 10 w/v% BL4k hydrogel. (c) Cell viability quantification after 24 h incubation (live control: DMEM+10% FBS; dead control: 70% ethanol). Images were taken from randomly selected 5 fields and quantification was done using Imaris Imaging Software. Data shown represents the means ± S.D., n=5. 115

Figure S4.1. (a) Synthesis route of DPB-PEG4k/8k. (b) Synthesis route of glycopolymer P(AM-co-LAEMA).....117

Figure S4.2. ^{1}H NMR spectrum of DPB-PEG4k. δ_H (ppm)= 8.41, 8.12, 8.01, 7.57 ($B(OH_2)C_6\mathbf{H}_4$), 4.47 (-COO-C$\mathbf{H}_2$-CH_2-), 3.92 (-COO-CH_2-C$\mathbf{H}_2$-), 3.63-3.68 (-O-C$\mathbf{H}_2$-C$\mathbf{H}_2$-O-).....118

Figure S4.3. FT-IR spectra of PEG4k and DPB-PEG4k. Wavelength (cm^{-1})= 1750 (C=O stretching), 700 (C-H bending, aromatic). 119

Figure S4.4. ^{1}H NMR spectrum of P(AM-co-LAEMA). δ_H (ppm)= 4.54 (-O-C**H**-O-), 4.40 (OH-C**H**-CO-), 4.19 (-O-CH_2-O-C**H**-), 3.36 (CO-NH-C$\mathbf{H}_2$-C$\mathbf{H}_2$-NH-). 120

Figure S4.5. After mixing PBS solutions of DPB-PEG4k and P(AM-co-LAEMA), the BL4k hydrogel (boronic acid/sugar=1:1, 10 w/v%) was formed and stayed still when the vial was inverted. 120

Figure S4.6. Dynamic oscillatory strain amplitude sweeps show the well-defined non-linear strain-stiffening behavior of BL4k hydrogels (boronic acid/sugar=1:1; 10, 7.5, 5 w/v%). 121

Figure S4.7. Temperature ramp tests conducted on BL4k hydrogel (boronic acid/sugar=1:1, 10 w/v%) show the temperature-dependent mechanical properties. 121

Figure S4.8. Sequential strain amplitude tests show the self-healing capability of BL4k hydrogels (boronic acid/sugar=1:1, T=25 °C) with different polymer concentrations. (a) 15 w/v%, (b) 12.5 w/v%, (c) 7.5 w/v% and (d) 5 w/v%. 122

Figure S4.9. Illustration of symmetric configuration for SFA force measurements. 123

Figure S4.10. Force-distance profiles show the interactions between P(AM-co-LAEMA) and PEG in sequential approach−separation force measurements. 123

Figure 5.1. a) Previous acid nonresistant injectable hydrogel dressings formed through non-bioorthogonal curing process. b) The biological environmental adaptive supramolecular hydrogel as internal wound dressing. c) Chemical structure of the ABA triblock copolymer and supramolecular hydrogel network structure. 133

Figure 5.2. (a) DLS measurement showing the change of hydrodynamic radius of ANGNA with increasing temperature. (b) Thermo-sensitive storage (G') and loss (G") modulus of a 10 w/v% hydrogel. (c) Modulus change of a 10 w/v% hydrogel during multiple heating-cooling cycles. (d) Injection of a 4 °C-preserved 10 w/v% polymer solution into a PBS buffer solution (pH=3) at 37 °C and facilely writing letters "U of A" on a platform at 37°C (the hydrogel was dyed with Rhodamine B). 140

Figure 5.3. Photos of the self-healing process of a 10 w/v% ANGNA hydrogel prepared in pH=3 buffer solution at 37 °C: (a) initial hydrogel, (b) hydrogel was separated into two pieces, (c) separated hydrogels were brought into contact, and (d) the self-healed hydrogel

can be lifted against its own weight without rupture at the joint. (e) Strain amplitude measurement (left) followed by time sweep measurement (strain=1%) (right) on a 10 w/v % ANGNA hydrogel prepared in pH = 3 PBS buffer solution shows immediate recovery from damage. (f) Cyclic strain step test shows reproducible self-healing capability. (g) Strain amplitude measurement (left) followed by time sweep measurement (strain = 1%) on a 10 w/v % ANGNA hydrogel prepared in pH=7.4 PBS buffer solution. 142

Figure 5.4. (a) Force-distance profiles show the interactions between ANGNA in pH=3 or 7.4 PBS buffer solution. (b) Force-distance profiles show the reversible interactions between ANGNA in pH=3 PBS buffer solution. Schematics of interaction mechanism between ANGNA in (c) pH=3 or (d) pH =7.4 PBS buffer solution..... 144

Figure 5.5. Fluorescence microscopy images of (a) ANGNA hydrogel-coated and (b) uncoated glass surfaces after 3h incubation against E. coli attachment. Confocal microscopy images of (c) 2D and (d) 3D culture of FaDu cells using a 10 w/v % ANGNA hydrogel. 146

Figure 5.6. (a) Schematic illustration of using the supramolecular hydrogel dressing for gastric perforation repair. (b) injection of supramolecular hydrogel dressing at the perforated site. (c) implantation of an omentum majus into the stomach. Postoperative adhesion after 2 weeks of surgery. (d) hydrogel dressing group. (e) omentum patch group (control group). (f) sewing position on the stomach (left: control group, right: hydrogel dressing group). (g) histological evaluation of infiltration of inflammatory cells in hydrogel dressing and control groups in the 2^{nd}, 4^{th} and 8^{th} week. Scale bar represents 20 μm. (h) immunohistochemical evaluation of infiltration of T lymphocytes (brown) in hydrogel dressing and control groups in the 2^{nd}, 4^{th} and 8^{th} week. Scale bar represents 20 μm.... 150

Figure S5.1. Synthesis route of the ABA triblock copolymer poly[(N-isopropylacrylamide)-co-(N-acryloyl 6-aminocaproic acid)]-b-poly(ethylene glycol)-b-poly[(N-isopropylacrylamide)-co-(N-acryloyl 6-aminocaproic acid)] (ANGNA)..... 152

Figure S5.2. ^{1}H NMR spectra of ANGNA in DMSO-d_6..... 153

Figure S5.3. The reversible sol-gel-sol transitions of a 10 w/v% ANGNA liquid bandage prepared in pH=3 PBS solution. 153
Figure S5.4. Cell viabilities of HeLa and MRC-5 cells after 24 h incubation with ANGNA copolymer at different concentrations. 154
Figure S5.5. Cell viabilities of FaDu cells after 24 h 2D/3D culture using a 10 w/v% ANGNA liquid bandage..... 154
Figure S5.6. SEM image shows the porous structure of a 10 w/v% ANGNA hydrogel.155

Abbreviations and Symbols

DCPD	dicyclopentadiene
ROMP	ring-opening metathesis polymerization
PAA	polyacrylic acid
STMS	stellate mesoporous silica
EGDA	ethylene glycol dimethacrylate
BIE	benzoin isobutyl ether
GA	glutaraldehyde
PC	porous carbon
UPy	ureidopyrimidinone
PANI	polyaniline
PSS	poly(4-styrenesulfonate)
A6ACA	acryloyl-6-aminocaproic acid
AM	acrylamide
SDS	sodium dodecyl sulfate
PDMAEMA	poly(2-dimethylaminoethyl methacrylate)
SPMA	3-sulfopropyl methacrylate potassium salt
CD	cyclodextrin
CB	cucurbituril
CE	crown ether

nBu	n-butyl acrylate
Ad	adamantine
PDA	polydopamine
rGO	reduced graphene oxide
CBNP	carbon black nanoparticle
DA	dopamine
PAM	polyacrylamide
PBA	phenylboronic acid
PEG	poly(ethylene glycol)
BP	bisphosphonate
HA	hyaluronic acid
DA	Diels-Alder
QCS	quaternized chitosan
F127-CHO	benzaldehyde-terminated Pluronic®F127
PMETA	poly{[2-(methacryloyloxy)-ethyl] trimethylammonium iodide}
E. coil	*Escherichia coli*
ECM	extracellular matrix
PNIPAM	poly(N-isopropylacrylamide)
IRI	ice recrystallization inhibition
PMPC	poly(2-methacryloyloxyethyl phosphorylcholine)

HPMC-C12	dodecyl-modified hydroxypropylmethylcellulose
PEG–PLA	poly(ethylene glycol)-*b*-poly(lactic acid)
CMC-NB	o-nitrobenzyl alcohol-modified carboxymethyl cellulose
GC	glycol chitosan
PDI	polydispersity
ATRP	atom transfer radical polymerization
RAFT	reversible addition-fragmentation chain-transfer
CTA	chain transfer agent
LVR	linear viscoelastic region
SFA	surface forces apparatus
MBI	multiple beam interferometry
FECO	fringes of equal chromatic order
LCST	lower critical solution temperature
PEI	polyethylenimine
FPMA	4-formylphenyl methacrylate
META	[2-(Methacryloyloxy)ethyl] trimethylammonium chloride solution
NIPAM	N-isopropylacrylamide
ACVA	4,4′-Azobis(4-cyanovaleric acid)
DMF	dimethylformamide
GPC	gel permeation chromatography

NMR	nuclear magnetic resonance
PBS	phosphate-buffered saline
RdB	Rhodamine B
VPTT	volume phase transition temperature
AFM	atomic force microscope
HCl	hydrochloric acid
NaOH	sodium hydroxide
FESEM	field emission scanning electron microscope
S. aureus	*Staphylococcus aureus*
LB	Luria-Bertani broth
TSB	tryptic soy broth
DMEM	Dulbecco's Modified Eagle Medium
DMSO	dimethyl sulfoxide
OD	optical density
PIC	polyisocyanopeptide
BA	bolaamphiphile
DPB-PEG	diphenylboronic acid-terminated telechelic poly(ethylene glycol)
LAEMA	2-lactobionamidoethyl methacrylamide
FBS	fetal bovine serum
DMAP	4-Dimethylaminopyridine

DCC	N,N'-Dicyclohexylcarbodiimide
THF	tetrahydrofuran
AIBN	azobisisobutyronitrile
FT-IR	Fourier-transform infrared spectroscopy
H&E	Haematoxylin-Eosin
DLS	dynamic light-scattering
IHC	immunohistochemical
GI	gastrointestinal
τ	shear stress
γ	shear strain/shear deformation
δ	phase shift
G'	storage modulus
G''	loss modulus
σ_0	stress amplitude
ε_0	strain amplitude
k	spring constant
D	separation distance between two mica surfaces
$D_{applied}$	applied separation distance between two mica surfaces
$D_{measured}$	actual separation distance between two mica surfaces
R	curvature of the surface

F_{ad}	adhesion force
W_{ad}	adhesion energy
ω	angular frequency
W_t	weight of remaining hydrogel after degradation at time t
W_i	weight of initial hydrogel
M_n	number molecular weight
M_w	weight molecular weight
K'	differential modulus
G_0	plateau modulus
σ	stress
σ_c	critical stress
m	stiffening index
K'_{max}/G_0	stiffening range
γ_{max}	maximum strain
λ_{max}	maximum extension ratio
l_{max}	length of fully extended polymer
l_0	end-to-end distance of the unstretched polymer
l_p	persistence length of the polymer

CHAPTER 1 General Introduction

1.1 Functional Hydrogels and Self-healing Hydrogels

Hydrogels are three-dimensional (3D) cross-linked polymer networks, which can absorb and retain large amount of water.[1-3] Due to their tunable physical, chemical and biological properties as well as their versatile preparation methods, hydrogels with different properties (e.g., stimuli-responsive,[4-5] conductive,[6-7] anti-bacterial,[8-9] anti-fouling,[10] shape-memory,[11-12] etc.) have been developed and applied in diverse biomedical and engineering applications, ranging from tissue-engineering scaffolds,[13-14] drug-delivery systems,[15-16] soft contact lenses,[17] and antifouling coatings,[18] to sensors,[19-20] actuators,[21-22] soft robotics,[23] and wastewater treatment.[24-25] Nevertheless, conventional hydrogels can be easily damaged when they are subjected to constant mechanical forces. The accumulation of small damage (i.e., cracks, breaks, cuts, etc.) could eventually lead to the loss of structural integrity and functionalities of the hydrogels, limiting their applications.

Self-healing is a remarkable capability pervasively adopted by biological tissues but is rare in synthetic soft materials. Developing functional hydrogels with self-healing property is of great significance to improve material reliability and extend material lifespan in various biomedical and engineering applications.[26-28] Self-healing hydrogels can be designed based on two major mechanisms: extrinsic and intrinsic self-healing. The former relies on the utilization of healing agents after damage and the latter is based on different types of dynamic molecular interactions (e.g., dynamic non-covalent interactions and dynamic covalent chemistry) between polymers.

1.2 Self-healing Mechanisms

1.2.1 Extrinsic Self-healing

The extrinsic self-healing materials usually consist of three major components: 1) a non-self-healable polymer matrix and 2) the healing agent encapsulated in 3) the embedded reservoir material.[29] **Figure 1.1** shows the typical self-healing process of extrinsic self-healing materials. The cracking of polymer matrix ruptures the embedded reservoirs, which leads to the release of healing agent. Subsequently, the chemical reaction of the healing agent is triggered with the presence of catalyst, resulting in the mending of cracks. Such design strategy of extrinsic self-healing materials was pioneered by White et al. in 2001.[30] They developed a self-healing epoxy matrix which contains Grubbs' catalyst and dicyclopentadiene (DCPD)-loaded microcapsules. As the approaching crack breaks the microcapsules, Grubbs' catalyst initiates the ring-opening metathesis polymerization (ROMP) of DCPD, which bonds the crack planes. The healed epoxy matrix exhibits ~ 75% recovery in toughness.

Various healing agents (e.g., monomers, crosslinkable oligomers, etc.), reservoir materials (e.g., microcapsules, microvascular networks and hollow fibers) and healing chemistries (e.g., ROMP, polycondensation, free radical polymerization, addition reaction, etc.) have been explored to develop extrinsic self-healing materials, including self-healing hydrogels.[29, 31-32] Chen et al. reported a self-healing polyacrylic acid (PAA) hydrogel which contains stellate mesoporous silica (STMS)-based microcapsules.[33] The healing agent ethylene glycol dimethacrylate (EGDA) and the photoinitiator benzoin isobutyl ether (BIE) were loaded into the STMS microcapsules. The damaged hydrogel was healed after being exposed under 370 nm ultraviolet light for 4 h to induce the photo-polymerization of EGDA. Compared with blank PAA hydrogel, the self-healing efficiency remarkably increased from 39.2% to 86.8%. Similar concept was also demonstrated by

Liu et al. They developed a self-healing guar gum hydrogel with glutaraldehyde (GA)-loaded porous carbon (PC).[34] The self-healing was achieved by the crosslinking reactions between GA and guar gum after GA being released from PC.

Although great progress has been made in extrinsic self-healing materials, such self-healing strategy suffers from several limitations. First, the self-healing capability is strongly dependent on the amount of healing agent left in the system. Once all the healing agents are consumed, the material would be irreversibly damaged and loses the self-healing capability. Second, the healing process of extrinsic self-healing materials could be relatively slow if the healing agents suffer from low reactivity. Third, the preparation methods of healing agent-loaded microcapsules lack flexibility and adaptability, which may not be easily scaled-up for practical applications. Last but not least, the healing agents and catalysts used in the system may cause cytotoxicity, limiting the applications in bioengineering applications. Recent research interest has been shifted to the development of intrinsic self-healing materials, especially self-healing hydrogels.

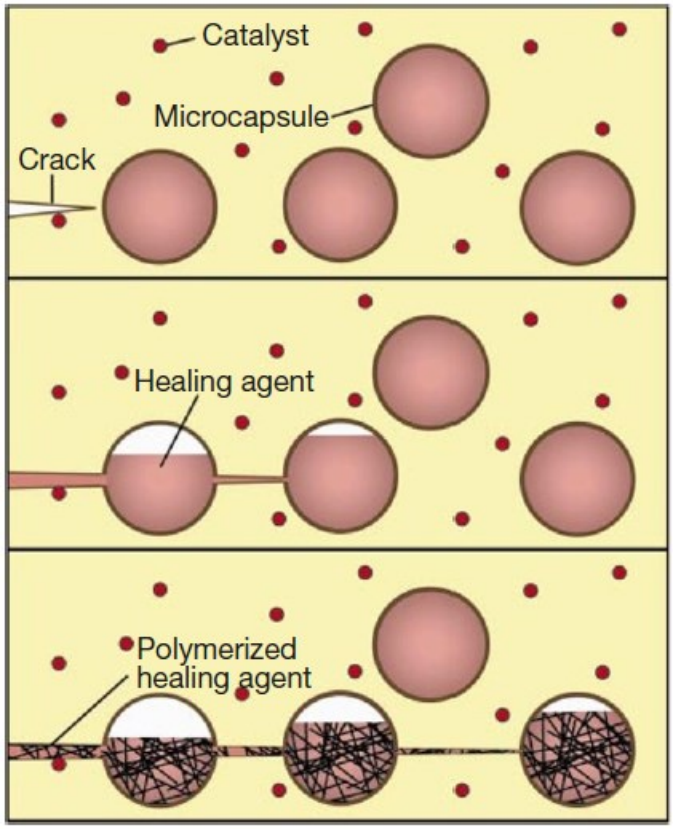

Figure 1.1. Schematic illustration of self-healing process of extrinsic self-healing materials.[30]

1.2.2 Intrinsic Self-healing

Instead of using additional healing agents and catalysts, intrinsic self-healing is enabled through the dynamic molecular interactions between polymers.[35] Modification or functionalization of polymers is required to incorporate specific molecular structures that can establish the dynamic interactions. Considering the tunable functionalities and versatile preparation methods of synthetic polymers, most of self-healing hydrogels are designed based on intrinsic self-healing mechanism. Intrinsic self-healing hydrogels can be further classified into physically and chemically self-healing hydrogels. The former recover from damage through non-covalent interactions and the latter restore the network through dynamic covalent chemistry.[27, 36]

1.2.2.1 Dynamic Non-covalent Interactions

Hydrogen bonding interaction is one of the most common non-covalent interactions used in preparing self-healing hydrogels. Hydrogels bearing ureidopyrimidinone (UPy) moieties possess self-healing property due to the reversible dimerization of two UPy units through quadruple hydrogen bonds (**Figure 1.2a)**. Chen et al. reported an UPy-containing polyaniline/poly(4-styrenesulfonate) (PANI/PSS) conductive hydrogel.[6] The damaged hydrogel could rapidly self-heal through the hydrogen bonding interactions between UPy moieties, without sacrificing the original mechanical strength and conductivity. In another example, Phadke et al. developed a self-healing hydrogel by arming the network with acryloyl-6-aminocaproic acid (A6ACA) side chains.[37] The hydrogel was rapidly healed at low pH due to the formation of hydrogen bonds between A6ACA side chains with both "face-on" and "interleaved" configurations (**Figure 1.2b)**.

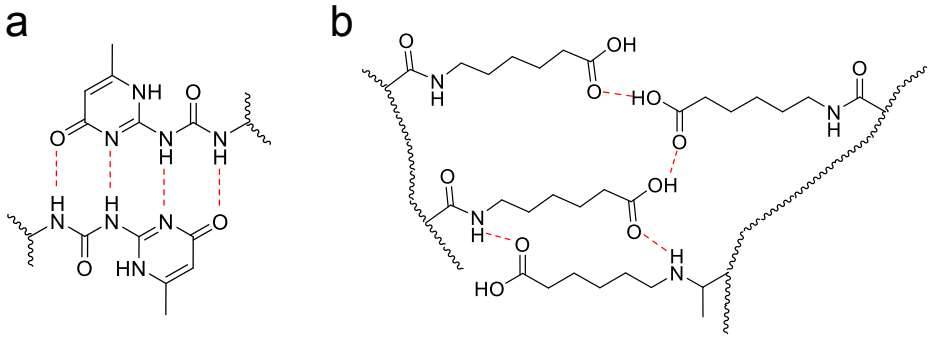

Figure 1.2. Hydrogen bonding interaction between (a) UPy moieties. (b) A6ACA side chains.

Self-healing can be achieved through hydrophobic interactions. Hydrophobic monomers can be introduced into the hydrogel system with the aid of surfactant micelles.[38-39] The hydrophobic monomers could form hydrophobic domains/associations within the micelles, which serve as the transient cross-links. Once the hydrogel is damaged, it can self-repair through hydrophobic interactions between the hydrophobic domains/associations (**Figure 1.3**). Tuncaboylu et al. developed a tough self-healing hydrogel by the copolymerization of two hydrophobic monomers,

stearyl methacrylate (C18) and dococyl acrylate (C22) with hydrophilic monomer acrylamide (AM) in a micellar solution of sodium dodecyl sulfate (SDS).[40] Both excellent mechanical and self-healing property were attributed to the strong hydrophobic interactions between the hydrophobic domains. The recovery of the elongation was about 100% after healing.

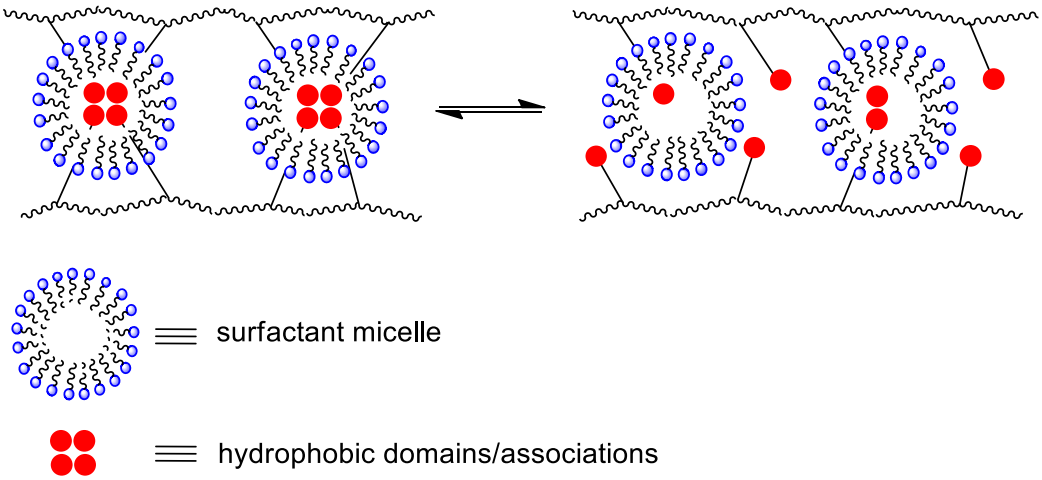

Figure 1.3. Self-healing through hydrophobic interactions between hydrophobic domains/assocaitions.

Electrostatic interactions exist between two oppositely charged components, which can be leveraged to construct self-healing hydrogels. Zheng et al. developed a self-healing hydrogel by embedding poly(2-dimethylaminoethyl methacrylate) brushes modified silica nanoparticles (SiO_2@PDMAEMA) into a PAA network.[41] The strong electrostatic interactions between the positively charged PDMAEMA and negatively charged PAA not only render the self-healing property, but also improve the mechanical properties of the hydrogel through energy dissipation mechanism. Long el al. also developed a mechanically robust self-healing hydrogel based on electrostatic interactions.[42] In their design, the hydrogel was prepared through a facile one-step polymerization of positively charged imidazolium-based ionic liquid monomers and negatively charged 3-sulfopropyl methacrylate potassium salt (SPMA). The hydrogel exhibited excellent self-

healing efficiency ~ 96% after 3 days.

Host-guest interactions refer to the complexation of host and guest molecules through specific molecular recognition, in which guest molecule can be inserted into the cavity of the cyclic host molecule through a combination of non-covalent interactions, such as hydrogen bonding, hydrophobic interactions, van der Waals forces, etc. (**Figure 1.4**).[43] The design strategy of self-healing hydrogels based on host-guest interactions is to incorporate the appropriate host-guest pairs into the hydrogel network. The commonly used host molecules include cyclodextrin (CD),[44-45] cucurbituril (CB),[46] crown ether (CE),[47] etc. Different guest molecules can bind to host molecule with different binding affinity, which would affect the self-healing efficiency of the hydrogel. Kakuta et al. developed two self-healing hydrogels based on two types of host-guest interactions, cyclodextrin-n-butyl acrylate (CD-nBu) and cyclodextrin-adamantane (CD-Ad).[48] It was found that the hydrogel based on CD-Ad interactions could self-heal damage immediately. However, the hydrogel based on CD-nBu interactions self-repaired the damage after a few hours.

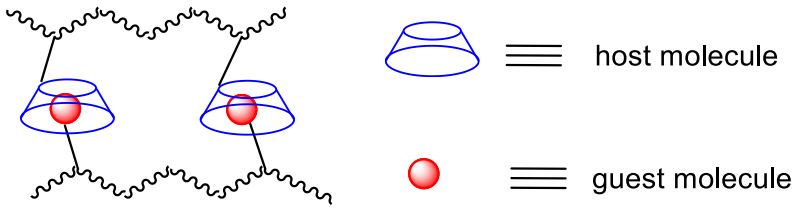

Figure 1.4. Host-guest interactions between host and guest molecules.

The self-healing properties can be resulted from a combination of multiple non-covalent interactions in the system. For example, inspired by marine mussel wet adhesion mechanism, hydrogels functionalized with catechol groups or polydopamine (PDA) possess remarkable self-healing capability through a combination of multiple non-covalent interactions including, hydrogen bonding interactions, metal-catechol coordinations, cation-π interactions, anion-π interactions, π-π interactions, etc. (**Figure 1.5**).[49-54] Li et al. reported a series of thermoresponsive

injectable self-healing hydrogels based on self-assembly of catechol-functionalized ABA tri-block thermoresponsive copolymers.[55] The hydrogel could self-heal from repeated damage due to the multiple intermolecular interactions between catechol groups. Han et al. developed a series of mussel-inspired self-healing nanocomposite hydrogels.[56-58] In their approach, nanomaterials, such as nanoclay, reduced graphene oxide (rGO) or carbon black nanoparticles (CBNPs) were coated with PDA by in situ polymerization of dopamine. The PDA-coated nanomaterials were then incorporated into polyacrylamide (PAM) network. The developed hydrogels showed great promises in various applications including, soft electronics, tissue adhesive, and wound dressing.

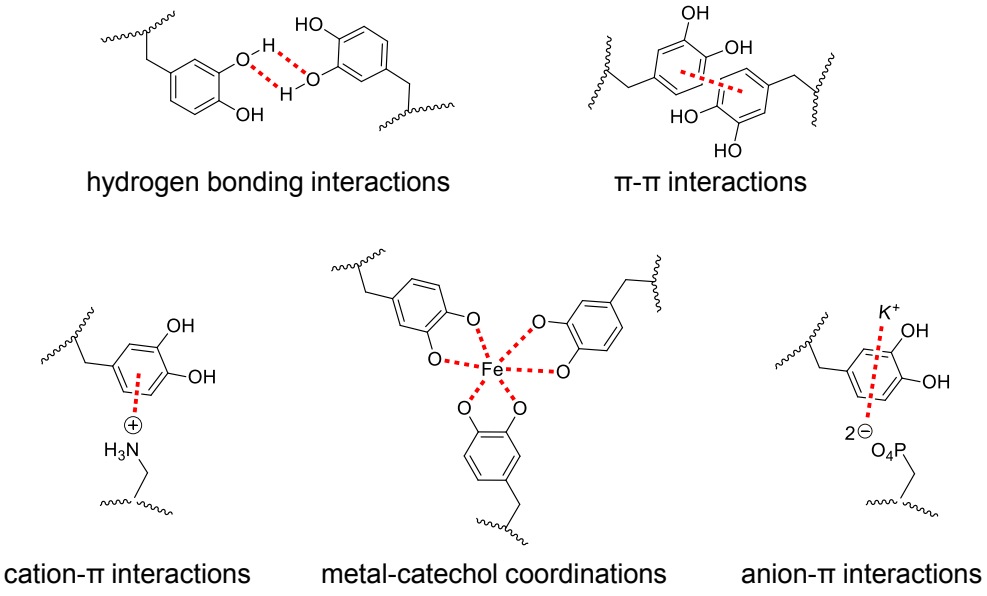

Figure 1.5. Different non-covalent interactions involved in mussel-inspired chemistry.

1.2.2.2 Dynamic covalent chemistry

Phenylboronate ester is the dynamic complex formed between phenylboronic acid (PBA) and *cis*-diol.[59] Typical molecules with *cis*-diol group includes catechol, glucose, lactose, etc.[60-61] The self-healing capability of the hydrogel depends on the relative stability of the phenylboronate ester bonds, which can be controlled by the p*K*a of PBA groups and the pH of aqueous medium.[62-63] Yesilyurt et al. studied the self-healing property of three hydrogels prepared from *cis*-diol-

terminated 4-arm polyethylene glycol (PEG) macromonomers and those bearing PBA derivatives with varied p*K*a value. (**Figure 1.6**).[64] It was found that hydrogels prepared from PEG-FPBA and PEG-PBA could rapidly self-heal, whereas the hydrogel prepared from PEG-APBA exhibited poor self-healing capability at physiological pH (~7.0). The difference in self-healing capability was resulted from the relative low p*K*a value of APBA (p*K*a~6.5-6.7) as compared with FPBA (p*K*a~7.2) and PBA (p*K*a~7.8). When pH > p*K*a, the phenylboronate ester formed between APBA and diol were thermodynamically "locked" and behaved more like a typical covalent bond, losing its dynamic nature.

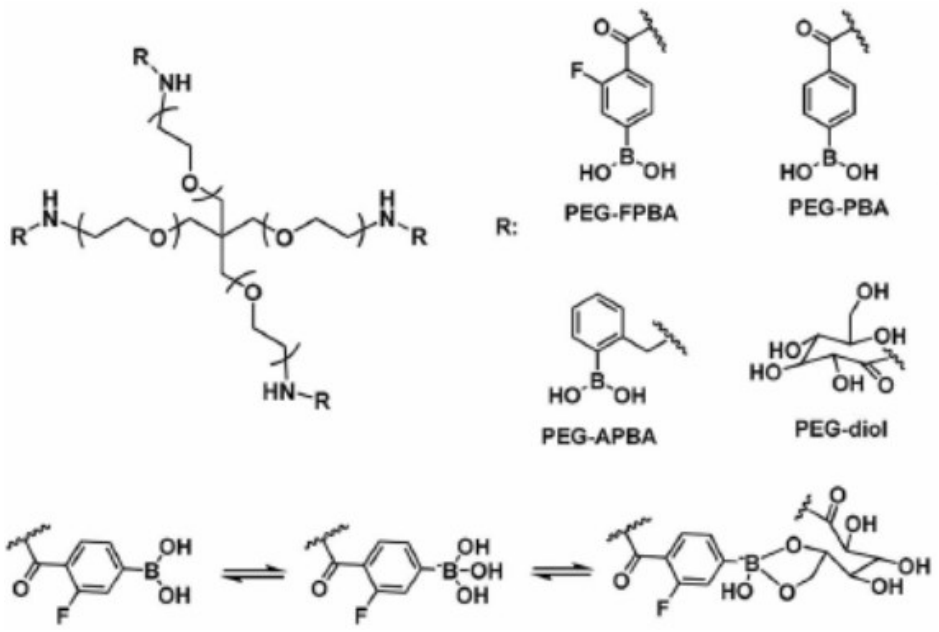

Figure 1.6. 4-arm PEG macromonomers bearing diol or PBA derivatives for the preparation of self-healing hydrogels.

Schiff base refers to the imine bonds formed by nucleophilic attack of amine to aldehyde groups (**Figure 1.7**), which have been leveraged to fabricate self-healing hydrogels.[65-67] Usually, aromatic Schiff-base linkages are preferred than aliphatic Schiff-base linkages since they can not only preserve the dynamic nature but also improve the mechanical properties of the hydrogels.[36,

[68] Zhang et al. developed a self-healing hydrogel based on dynamic Schiff base reactions using an amine-containing biopolymer, glycol chitosan, and benzaldehyde-modified PEG.[4] Due to the reversibility of Schiff-base reaction, the hydrogel possessed excellent self-healing property. In a self-healing test, two pieces of hydrogels merged into one single piece of hydrogel after being contacted for 2h. The storage modulus (*G'*) recovery was about 100% after the rupture of the network. In addition, the dynamic Schiff-base linkages are sensitive to a variety of stimuli, such as pH, vitamin B6 derivative, amino acids, and enzymes. The hydrogel network can be rapidly decomposed under these stimuli, which shows great promises in controlled drug delivery.

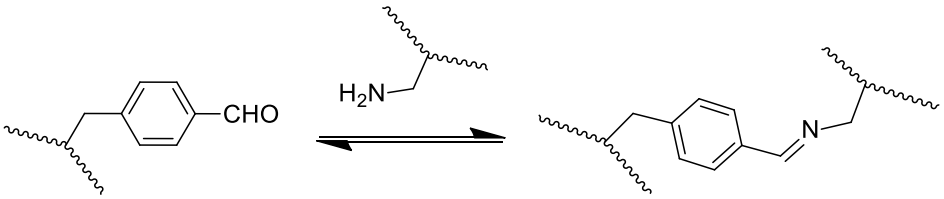

Figure 1.7. Dynamic Schiff base reaction between benzaldehyde and amine groups.

Acylhydrazone bonds are derivatives of imine bonds with higher stability, which are formed between aldehyde and hydrazine groups. Self-healing hydrogels based on acylhydrazone bonds have been reported.[69-70] However, the acylhydrazone exchange reaction only proceed under a slightly acidic environment (pH 4–6). The self-healing process of the hydrogels can only occur within a narrow pH range, which limits their applications. To solve the issue, acylhydazone bonds can be utilized along with other dynamic covalent bonds for achieving self-healing capability in a broader pH range. Deng et al. developed a self-healing hydrogel based on both acylhydazone and disulfide bonds (**Figure 1.8**).[71] The hydrogel was prepared using benzaldehyde-terminated three-arm PEG and dithiodipropionic acid dihydrazide. The hydrogel could self-heal at both acidic (pH 3–6) and basic (pH 9) conditions due to the acylhydrazone exchange or disulfide exchange reactions. In neutral condition (pH 7), the hydrogel could not self-heal because both acylhydazone

and disulfide bonds are kinetically "locked." However, the hydrogel regained the self-healing capability by accelerating the acylhydrazone exchange reactions with the addition of aniline as the catalyst.

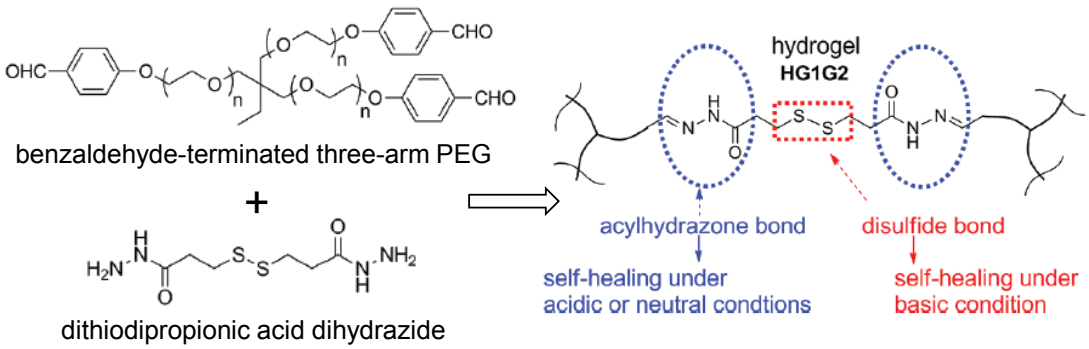

Figure 1.8. Self-healing hydrogel based on dynamic acylhydazone and disulfide bonds.[71]

Disulfide bonds are the dynamic covalent bonds based on thiol/disulfide exchange reactions, which have been employed for fabricating a wide range of self-healing materials, including rubber, polymer film, and hydrogels.[72-74] The thiol/disulfide exchange reaction needs to be triggered by external stimuli, such as heat, photo-irradiation, basic pH, and mechanical forces, in which the "old" disulfide bonds are broken into thiols and are readily to be reformed (**Figure 1.9**).[36] Fairbanks et al. reported a self-healing hydrogel prepared by the oxidation of thiol end groups of the four-arm PEG macromonomers using H_2O_2/NaI.[73] After swelling in a lithium acylphosphinate photoinitiator solution, two pieces of hydrogel could be annealed by photoinduced thiol/disulfide exchange reactions.

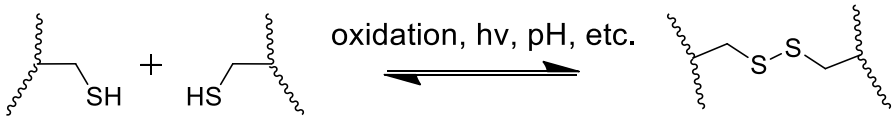

Figure 1.9. Thiol/disulfide exchange reactions.

Metal-ligand coordination is a special covalent bond formed between the binding sites on a ligand and a central metal atom. The reversible chelation between ligands and metal atoms could

endow the hydrogel with self-healing capability. The common metal-ligand coordinate bonds include bisphosphonate (BP)-Ca^{2+}/Mg^{2+},[75-76] carboxylate-Ca^{2+},[77] catechol-Fe^{3+},[52, 78-79] etc.[80] Shi et al. developed an injectable self-healing hyaluronic acid (HA) hydrogel based on BP-Ca^{2+} coordinate bonds (**Figure 1.10a**).[76] The HA was first functionalized with BP, then the hydrogel was formed after mixing of solutions of HA-BP and $CaCl_2$. The hydrogel could self-heal immediately after rheological deformation due to the reversible BP-Ca^{2+} interactions. Such dynamic hydrogel was applied as "bioink" for 3D printing applications. Holten-Andersen et al. developed a PEG-based self-healing hydrogel using catechol-Fe^{3+} coordination (**Figure 1.10b**).[78] The storage modulus (*G'*) recovery of the hydrogel was about 100% after the rheological destruction due to the reversible catechol-Fe^{3+} coordination. Moreover, the stoichiometry of catechol-Fe^{3+} complexes (mono-, bis-, or tris-) can be controlled by pH, which provides a facile approach for tuning the mechanical property of the hydrogels.

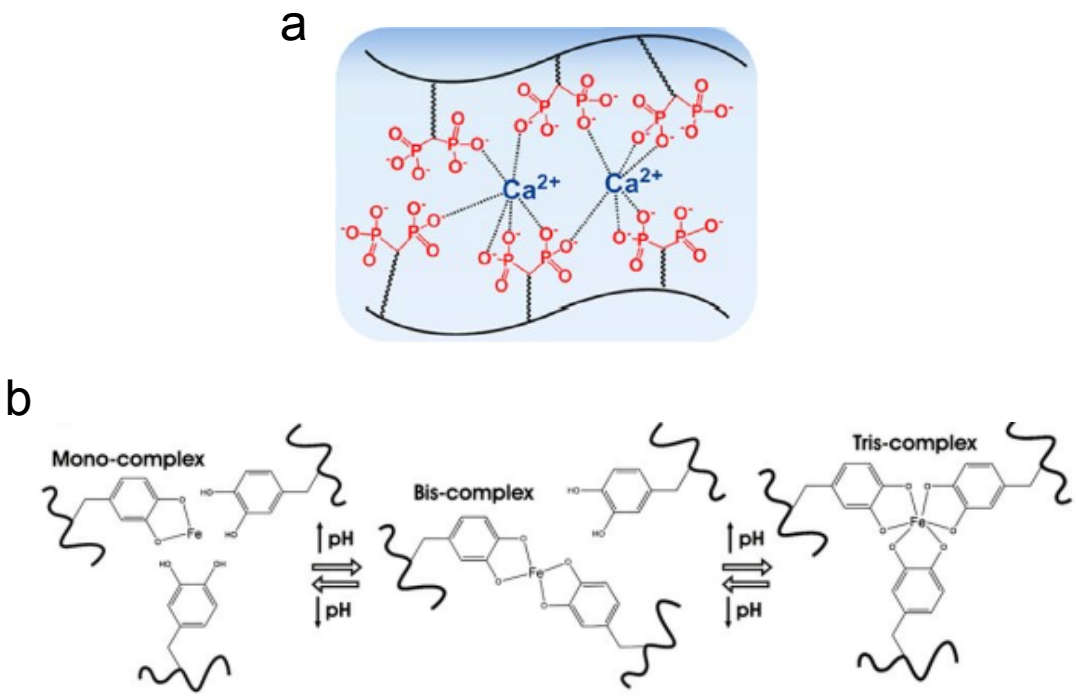

Figure 1.10. Self-healing hydrogels based on (a) BP-Ca^{2+} coordinate bonds.[76] (b) catechol-Fe^{3+}

coordinate bonds.[78]

Diels-Alder (DA) reaction is one of the "click" chemistry reactions between dienes and dienophiles for fabricating chemically crosslinked hydrogels.[81-82] The DA linkages can be cleaved on heating and reach a new equilibrium due to the thermo-reversibility of DA reaction. Thus, heating is required in order to activate the self-healing process. Wei et al. developed a self-healing hydrogel prepared by fulvene-modified dextran and dichloromaleic acid-terminated PEG (**Figure 1.11**).[83] It was found that the starch on hydrogel surface completely healed after being heated at 37°C for 7h.

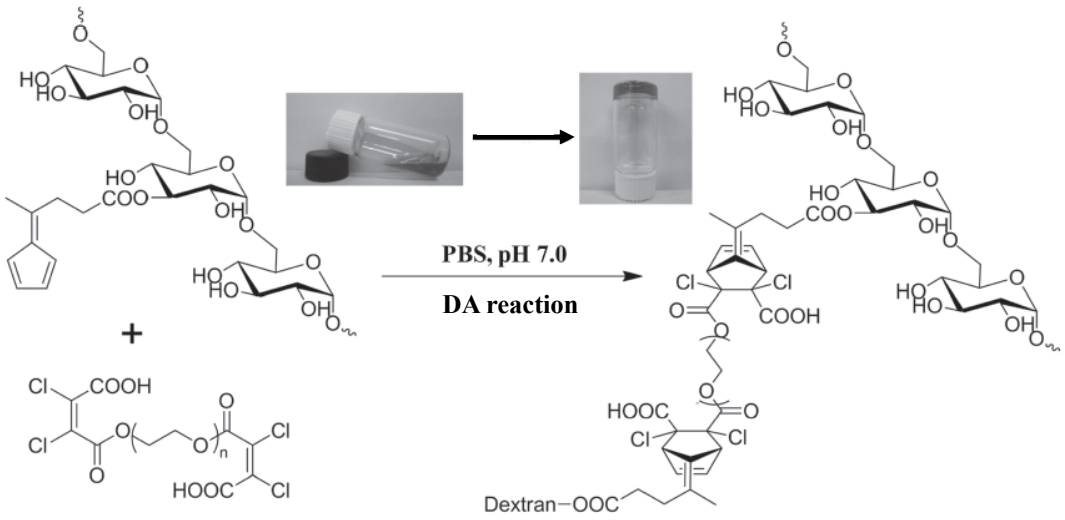

Figure 1.11. Self-healing hydrogel based on DA reaction using fulvene-modified dextran and dichloromaleic acid-terminated PEG.[83]

1.3 Biomedical Applications of Self-healing Hydrogels

1.3.1 Wound Healing

Skin is the largest human organ, which effectively protects the internal organs from mechanical impacts, microbial invasion and direct contact with chemicals and radiation.[84] Once wound is developed in the skin, dressing materials should be applied to promote the healing of the

wound. An ideal wound dressing material should include several characteristics. First, it should be able to maintain a moist wound environment for the transport of nutrients and migration of epithelial cells. Second, it can absorb tissue exudates and allow gaseous exchange. Third, it can inhibit the proliferation of bacteria or microorganisms at the wound site. Last but not least, it should be easily removed without causing secondary damage to the tissue.[85] Traditional dry dressing materials include cotton wool, gauze, bandage, etc. cannot fully fulfill these requirements. Self-healing hydrogels have attracted great research interests in wound healing due to their tunable functionalities and prolonged material lifespan.

Compared with the pre-formed hydrogel film dressings, injectable hydrogels could offer more advantages in wound healing, such as the ability to fill the irregular wound space, *in situ* drug encapsulation capability and the non-invasive accessibility to the deep wound site.[86-87] Therefore, injectable self-healing hydrogels have been developed for external wound healing.[88] Qu et al. developed an injectable self-healing hydrogel based on Schiff base reaction using quaternized chitosan (QCS) and benzaldehyde-terminated Pluronic®F127 (PF127-CHO).[89] The antioxidant drug, Curcumin, was facilely loaded into the hydrogel to promote the wound healing. The Curcumin-loaded hydrogel significantly enhanced the wound healing process as demonstrated in a full-thickness skin defect model *in vivo*.

Self-healing hydrogels with antibacterial property is highly desired in wound healing to prevent wound infections. The design strategies of antibacterial hydrogels include the incorporation of antibacterial nanoparticles (e.g., Ag nanoparticles,[90] ZnO nanoparticles,[91] etc.), encapsulation of antibiotics (e.g., Ciprofloxacin, Gentamicin, Curcumin, etc.),[92] conjugation of antibacterial peptides and inclusion of cationic polymers into the hydrogel network.[93-94] Among these approaches, introducing cationic polymers into the network is one of the simplest methods,

which can be facilely achieved by the copolymerization of cationic monomers. Li et al. developed a self-healing hydrogel with antibacterial property based on self-assembly of a catechol-functionalized ABA triblock copolymer, employing positively charged poly{[2-(methacryloyloxy)-ethyl] trimethylammonium iodide} (PMETA) as the central block.[95] The hydrogel could effectively inhibit the growth of *Escherichia coli* (*E. coil*) with over 99.8% killing efficiency.

Considering the slightly acidic environment of wounded skin, "smart" self-healing hydrogels with stimuli-responsive property (e.g., temperature-responsive, pH-responsive, redox-responsive, etc.) can be applied as drug delivery system to promote the wound healing process.[96] Dynamic covalent bonds such as Schiff base bonds, phenylboronate esters and acylhydrazone bonds are subjected to hydrolysis under acidic environment.[63, 97] Therefore, self-healing hydrogels based on these inherently pH-responsive linkages are preferred in wound healing application.

1.3.2 3D Cell Culture Matrix

Developing advanced *ex vivo* cell culture models is of great significance to decipher complex cell behaviors (e.g., migration, proliferation, differentiation, etc.) and construct artificial tissues or organs for regenerative medicines and tissue engineering.[98] Although the conventional 2D cell culture models offer great opportunities to study the basic cellular functions and screen drug cytotoxicity, the 2D culturing environment is distinct from the 3D structure of extracellular matrix (ECM) *in vivo*. Naturally derived ECM composed of collagen, elastin, actin, fibronectin, etc. has been applied for 3D cell culture. Nevertheless, their chemical, physical, mechanical properties as well as biofunctionalities are difficult to be tuned. Due to the high similarity to ECM, synthetic hydrogels with tailored properties prepared from functional "building blocks" have been widely used for 3D cell culture.[98-99]

Compared with covalently crosslinked hydrogels, dynamic self-healing hydrogels are preferred in 3D cell culture due to their *in situ* gelation and cell encapsulation capabilities. Zhang et al. reported a physically self-healing hydrogel prepared from ABA triblock copolymer containing a PEG middle block and terminal poly(N-isopropylacrylamide) (PNIPAM) block with UPy moieties randomly incorporated.[100] The formation of the hydrogel can be triggered by increasing temperature. Due to the remarkable sol-gel transition, mesenchymal stem cells could be facilely mixed with the precursor polymer solution at mild conditions and be encapsulated in the hydrogel network at physiological temperature (37 °C). Similar concept has also been demonstrated by Nagao et al, using a highly biocompatible thermosensitive zwitterionic hydrogel to encapsulate HeLa cells (**Figure 1.12a**).[101] Since the precursor polymer exhibited excellent ice recrystallization inhibition (IRI) activity, such cell culture matrix showed great promises in cryopreservation of cells.

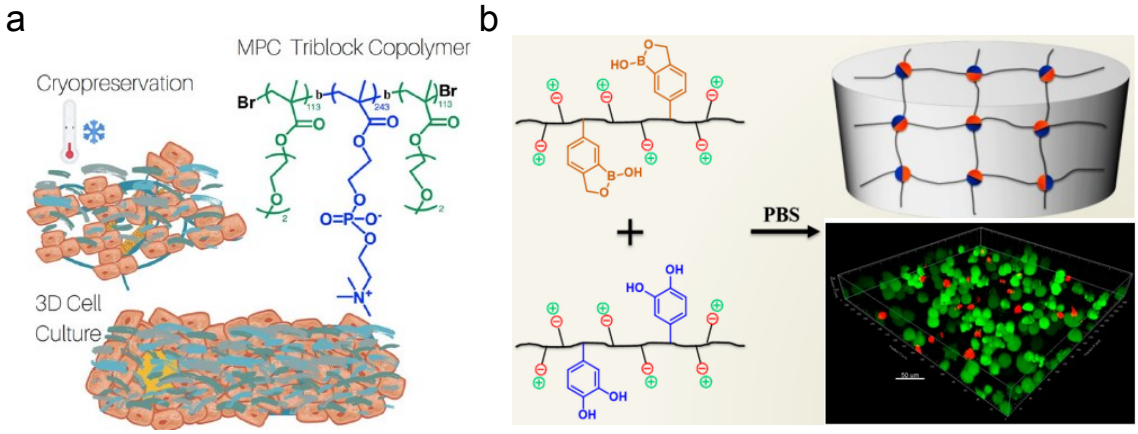

Figure 1.12. 3D cell culture using (a) physically self-healing hydrogel.[101] (b) chemically self-healing hydrogel.[60]

Chemically self-healing hydrogels can also be applied as 3D cell culture matrix. Chen et al. developed a biocompatible self-healing hydrogel prepared from boronic acid- and catechol-functionalized poly(2-methacryloyloxyethyl phosphorylcholine) (PMPC) zwitterionic polymers

(**Figure 1.11b**).[60] 3D cell encapsulation could be facilely achieved by mixing the precursor polymer solutions containing the cells. Due to the non-toxic polymer matrix and the efficient transport of nutrients through the porous structure, the cell viability could achieve ~ 86% after 24 h culture period.

Natural ECM composed of collagen, actin and intermediate filaments possesses unique strain-stiffening property (viz., the stiffness of ECM increases with applied strain or stress).[102-104] Such dynamic micro-mechanical environment plays important roles in controlling and regulating cell behaviors. Although great progress has been made in the development of advanced hydrogels for 3D cell culture, the biological strain-stiffening behavior is rarely duplicated in synthetic hydrogel materials. Therefore, the development of hydrogel-based ECM mimics with biological strain-stiffening property for 3D cell culture is of great significance while remains a challenge.

1.3.3 Postoperative Anti-adhesion Barrier

Postoperative adhesion is one common and serious complication in abdominal surgery. It can cause many diseases, including bowel obstruction, female infertility, abdominal pain, etc, raising huge health care burden.[105] One solution to the issue is to implant anti-adhesion barrier materials that can physically isolate the internal wound from adjacent tissues to lower the risk of postoperative tissue adhesion and promote the healing of injured tissues.[105] Currently, the most commonly used postoperative anti-adhesion barrier materials are polymer-based materials in the form of solution, solid film or hydrogel. Among them, hydrogels show great promises due to their high similarity to ECM and tunable functionalities. However, the application of conventional pre-formed hydrogel patch is limited when they are required to be placed to deep or narrow wounds, or to the tissues with irregular shape and those are heavily folded (e.g., small intestine, stomach, etc.).

Injectable hydrogels have attracted great research interests as postoperative anti-adhesion barrier materials due to their in-situ gelling capability, non-invasive administration method as well as the ability to fully cover the injured tissues.[87] Stapleton et al. reported an injectable supramolecular hydrogel composed of dodecyl (C12)-modified hydroxypropylmethylcellulose (HPMC-C12) and poly(ethylene glycol)-*b*-poly(lactic acid) (PEG–PLA) nanoparticles for postoperative anti-adhesion application (**Figure 1.13a**).[106] The hydrogel can be facilely prepared via a self-assembly process due to the hydrophobic interactions between HPMC-C12 and PEG-PLA NPs. In vivo rat and sheep models demonstrated the remarkable capability of the dynamic hydrogel to reduce pericardial adhesion after surgery. Yang et al. also reported a photo-crosslinked anti-adhesion hydrogel prepared from o-nitrobenzyl alcohol (NB) modified carboxymethyl cellulose (CMC-NB) and glycol chitosan (GC) (**Figure 1.13b**).[107] The hydrogel can be photo-crosslinked in situ through the formation of Schiff base. It successfully prevented the postoperative peritoneal adhesion in a cecum defect rat model. However, the non-bioorthogonal curing process of the hydrogel may associate with potential bio-safety issues.

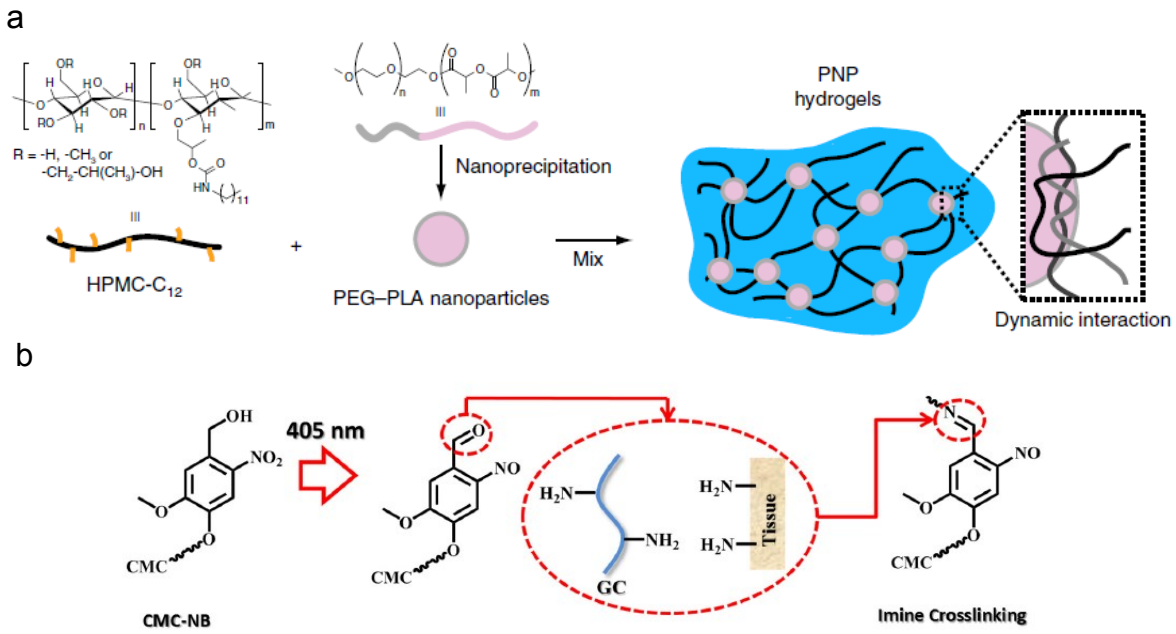

Figure 1.13. (a) HPMC-C12/PEG-PLA hydrogel formed via self-assembly process due to the hydrophobic interactions between HPMC-C12 and PEG-PLA nanoparticles.[106] (b) CMC-NB/GC hydrogel formed through photo-crosslinking process.[107]

Most of the existing injectable hydrogels used for postoperative anti-adhesion application are based on a two-component system design, in which two precursor polymers are crosslinked through a variety of crosslinking chemistries. Although some dynamic crosslinking chemistries (e.g. Schiff base,[108-109] thiol-ene click reaction,[110] etc.) render excellent self-healing property of the hydrogels, most of these chemically cross-linked hydrogels lack the adaptability to local biological environment, particularly to gastric environment (pH 1-3) since the crosslinking linkages are subjected to hydrolysis under acidic environment. Therefore, the development of anti-adhesion injectable self-healing hydrogel with local biological environment-adaptability (e.g. gastric environment) is of great significance while remains a challenge.

It is generally believed that the postoperative adhesion is triggered by the deposition/attachment of various proteins, cells (e.g. fibroblasts, inflammatory cells, etc.) and microorganisms.[111] Therefore, hydrogel barrier materials with anti-biofouling property could further improve the postoperative anti-adhesion performance.[112-113]

1.4 Objectives

Functional self-healing hydrogels hold great promises in various biomedical applications. Although the design strategies of intrinsic self-healing hydrogels based on dynamic molecular interactions have been well studied in the literature, it remains a challenge to integrate multifunctionalities (e.g., self-healing, injectability, anti-bacterial, stimuli-responsive, anti-biofouling, strain-stiffening, biocompatibility, etc.) in one hydrogel platform and explore the applicability of these materials in practical biomedical applications. Besides, the understanding of

dynamic molecular interaction mechanisms from the perspective of intermolecular and surface forces is limited, which could provide useful insights into the development of advanced self-healing materials.

The overall objective of this thesis is to develop three novel multifunctional self-healing hydrogel systems based on different types of dynamic molecular interactions for biomedical applications, and investigate the corresponding dynamic molecular interaction mechanisms at molecular level. The detailed objectives are listed as follows.

(1) Develop an injectable self-healing hydrogel with dual temperature-pH responsive and anti-bacterial properties based on Schiff base reaction, and investigate the Schiff base interaction mechanism at molecular level.

(2) Develop a biocompatible self-healing strain-stiffening flexible hydrogel based on dynamic boronic ester bonds for 3D cell culture, and investigate the boronic acid-diol interaction mechanism at molecular level.

(3) Develop an injectable self-healing hydrogel with anti-biofouling property based on biological environment-adaptive supramolecular self-assembly of multifunctional polymer as internal wound dressing for the treatment of gastric perforation, and study the associated self-healing mechanism at molecular level.

1.5 Structure of the Thesis

Chapter 1 introduces functional self-healing hydrogels, followed by a brief literature review of self-healing mechanisms and several biomedical applications of functional self-healing hydrogels. The objectives of this work are presented.

Chapter 2 describes the major experimental methods/techniques used in this work.

Chapter 3 reports an injectable self-healing hydrogel with dual temperature-pH responsive and

antibacterial properties. The hydrogel was prepared using PEI and a synthetic multifunctional gelator PFMNMF which was synthesized by reversible addition-fragmentation chain transfer (RAFT) polymerization. Due to the dynamic Schiff base reactions between two polymers, the hydrogel exhibited excellent self-healing property. The Schiff base interaction mechanism was quantitatively studied by surface force measurements using a surface forces apparatus (SFA). In addition, the injectability, dual temperature-pH responsive property, biocompatibility as well as antibacterial property of the developed hydrogel were demonstrated.

Chapter 4 introduces a biomimetic hydrogel with tissue-like strain-stiffening and self-healing properties for 3D cell culture. The hydrogel was crosslinked through dynamic boronic ester bonds formed between two linear flexible polymers, DPB-PEG and a glycopolymer, P(AM-*co*-LAMEA). The effects of boronic acid/sugar ratio, polymer concentration, temperature and crosslinker length on the strain-stiffening behavior of the hydrogel were investigated. In addition, due to the dynamic nature of boronic ester bonds, the hydrogel could self-heal from repeated damage and fully retain the strain-stiffening capability. The boronic acid-diol interaction mechanism was studied by SFA force measurements. The developed biomimetic hydrogel was successfully applied for 3D culture of HeLa cells.

Chapter 5 presents an injectable self-healing hydrogel with anti-biofouling property as internal wound dressing. The hydrogel was designed based on the biological environment-adaptive supramolecular self-assembly of an ABA triblock copolymer, employing poly[(N-isopropylacrylamide)-*co*-(N-acryloyl 6-aminocaproic acid)] (P(NIPAM-*co*-NA6ACA)) A block and PEG B block. Due to the hydrophobic interactions between the collapsed P(NIPAM-*co*-NA6ACA) block at body temperature, the hydrogel showed excellent *in situ* gelation capability. In addition, the synergy of pH-mediated hydrogen bonding and hydrophobic interactions between

the P(NIPAM-*co*-NA6ACA) block rendered the hydrogel excellent self-healing property under acidic condition. The pH-mediated hydrogen bonding interaction mechanism was investigated by SFA force measurements. The anti-biofouling property and biocompatibility of the hydrogel were demonstrated in vitro. In vivo rat model showed the remarkable capabilities of our hydrogel to simplify surgical procedures, reduce postoperative complications as well as enhance the healing process of gastric perforation compared with the conventional treatment.

Chapter 6 presents the major conclusions and contributions of this work. The suggestions for future work are also outlined.

References

(1) Wichterle, O.; Lim, D. Hydrophilic Gels for Biological Use. *Nature* **1960,** *185* (4706), 117-118.

(2) Annabi, N.; Tamayol, A.; Uquillas, J. A.; Akbari, M.; Bertassoni, L. E.; Cha, C.; Camci-Unal, G.; Dokmeci, M. R.; Peppas, N. A.; Khademhosseini, A. 25th anniversary article: Rational design and applications of hydrogels in regenerative medicine. *Adv. Mater.* **2014,** *26* (1), 85-123.

(3) Ahmed, E. M. Hydrogel: Preparation, characterization, and applications: A review. *J. Adv. Res.* **2015,** *6* (2), 105-21.

(4) Zhang, Y.; Tao, L.; Li, S.; Wei, Y. Synthesis of multiresponsive and dynamic chitosan-based hydrogels for controlled release of bioactive molecules. *Biomacromolecules* **2011,** *12* (8), 2894-901.

(5) Deng, Z.; Guo, Y.; Zhao, X.; Ma, P. X.; Guo, B. Multifunctional Stimuli-Responsive Hydrogels with Self-Healing, High Conductivity, and Rapid Recovery through Host–Guest Interactions. *Chem. Mater.* **2018,** *30* (5), 1729-1742.

(6) Chen, J.; Peng, Q.; Thundat, T.; Zeng, H. Stretchable, Injectable, and Self-Healing Conductive Hydrogel Enabled by Multiple Hydrogen Bonding toward Wearable Electronics. *Chem. Mater.* **2019,** *31* (12), 4553-4563.

(7) Wang, Z.; Chen, J.; Cong, Y.; Zhang, H.; Xu, T.; Nie, L.; Fu, J. Ultrastretchable Strain Sensors and Arrays with High Sensitivity and Linearity Based on Super Tough Conductive Hydrogels. *Chem. Mater.* **2018,** *30* (21), 8062-8069.

(8) Giano, M. C.; Ibrahim, Z.; Medina, S. H.; Sarhane, K. A.; Christensen, J. M.; Yamada, Y.; Brandacher, G.; Schneider, J. P. Injectable bioadhesive hydrogels with innate antibacterial properties. *Nat. Commun.* **2014,** *5*, 4095.

(9) Zhong, Y.; Xiao, H.; Seidi, F.; Jin, Y. Natural Polymer-Based Antimicrobial Hydrogels without

Synthetic Antibiotics as Wound Dressings. *Biomacromolecules* **2020,** *21* (8), 2983-3006.

(10) Banerjee, S. L.; Bhattacharya, K.; Samanta, S.; Singha, N. K. Self-Healable Antifouling Zwitterionic Hydrogel Based on Synergistic Phototriggered Dynamic Disulfide Metathesis Reaction and Ionic Interaction. *ACS Appl. Mater. Interfaces.* **2018,** *10* (32), 27391-27406.

(11) Zhang, Y.-c.; Le, X.-x.; Lu, W.; Jian, Y.-k.; Zhang, J.-w.; Chen, T. An "Off-the-Shelf" Shape Memory Hydrogel Based on the Dynamic Borax-Diol Ester Bonds. *Macromol. Mater. Eng.* **2018,** *303* (7), 1800144.

(12) Liu, K.; Zhang, Y.; Cao, H.; Liu, H.; Geng, Y.; Yuan, W.; Zhou, J.; Wu, Z. L.; Shan, G.; Bao, Y.; Zhao, Q.; Xie, T.; Pan, P. Programmable Reversible Shape Transformation of Hydrogels Based on Transient Structural Anisotropy. *Adv. Mater.* **2020,** *32* (28), e2001693.

(13) Khademhosseini, A.; Langer, R. Microengineered hydrogels for tissue engineering. *Biomaterials* **2007,** *28* (34), 5087-5092.

(14) Lee, K. Y.; Mooney, D. J. Hydrogels for tissue engineering. *Chem. Rev.* **2001,** *101* (7), 1869-79.

(15) Secret, E.; Kelly, S. J.; Crannell, K. E.; Andrew, J. S. Enzyme-responsive hydrogel microparticles for pulmonary drug delivery. *ACS Appl. Mater. Interfaces.* **2014,** *6* (13), 10313-21.

(16) Li, H.; Go, G.; Ko, S. Y.; Park, J.-O.; Park, S. Magnetic actuated pH-responsive hydrogel-based soft micro-robot for targeted drug delivery. *Smart Mater. Struct.* **2016,** *25* (2), 027001.

(17) Childs, A.; Li, H.; Lewittes, D. M.; Dong, B.; Liu, W.; Shu, X.; Sun, C.; Zhang, H. F. Fabricating customized hydrogel contact lens. *Sci. Rep.* **2016,** *6* (1), 34905.

(18) Tian, S.; Jiang, D.; Pu, J.; Sun, X.; Li, Z.; Wu, B.; Zheng, W.; Liu, W.; Liu, Z. A new hybrid silicone-based antifouling coating with nanocomposite hydrogel for durable antifouling properties. *Chem. Eng. J.* **2019,** *370*, 1-9.

(19) Wu, M.; Chen, J.; Ma, Y.; Yan, B.; Pan, M.; Peng, Q.; Wang, W.; Han, L.; Liu, J.; Zeng, H. Ultra elastic, stretchable, self-healing conductive hydrogels with tunable optical properties for highly sensitive soft electronic sensors. *J. Mater. Chem. A* **2020,** *8* (46), 24718-24733.

(20) Wang, J.; Tang, F.; Wang, Y.; Lu, Q.; Liu, S.; Li, L. Self-Healing and Highly Stretchable Gelatin Hydrogel for Self-Powered Strain Sensor. *ACS Appl. Mater. Interfaces.* **2020,** *12* (1), 1558-1566.

(21) Ma, Y.; Hua, M.; Wu, S.; Du, Y.; Pei, X.; Zhu, X.; Zhou, F.; He, X. Bioinspired high-power-density strong contractile hydrogel by programmable elastic recoil. *Sci. Adv.* **2020,** *6* (47), eabd2520.

(22) Ionov, L. Hydrogel-based actuators: possibilities and limitations. *Mater. Today* **2014,** *17* (10), 494-503.

(23) Zheng, W. J.; An, N.; Yang, J. H.; Zhou, J.; Chen, Y. M. Tough Al-alginate/poly(N-isopropylacrylamide) hydrogel with tunable LCST for soft robotics. *ACS Appl. Mater. Interfaces.* **2015,** *7* (3), 1758-64.

(24) Sinha, V.; Chakma, S. Advances in the preparation of hydrogel for wastewater treatment: A concise review. *J. Environ. Chem. Eng.* **2019,** *7* (5), 103295.

(25) Jiao, T.; Guo, H.; Zhang, Q.; Peng, Q.; Tang, Y.; Yan, X.; Li, B. Reduced Graphene Oxide-Based Silver Nanoparticle-Containing Composite Hydrogel as Highly Efficient Dye Catalysts for Wastewater Treatment. *Sci. Rep.* **2015,** *5* (1), 11873.

(26) Chen, Y.; Wang, W.; Wu, D.; Zeng, H.; Hall, D. G.; Narain, R. Multiresponsive and Self-Healing Hydrogel via Formation of Polymer-Nanogel Interfacial Dynamic Benzoxaborole Esters at Physiological pH. *ACS Appl. Mater. Interfaces.* **2019,** *11* (47), 44742-44750.

(27) Taylor, D. L.; In Het Panhuis, M. Self-Healing Hydrogels. *Adv. Mater.* **2016,** *28* (41), 9060-

9093.

(28) Liu, Y.; Hsu, S. H. Synthesis and Biomedical Applications of Self-healing Hydrogels. *Front. Chem.* **2018,** *6* (449), 449.

(29) Zhu, D. Y.; Rong, M. Z.; Zhang, M. Q. Self-healing polymeric materials based on microencapsulated healing agents: From design to preparation. *Prog. Polym. Sci.* **2015,** *49-50*, 175-220.

(30) White, S. R.; Sottos, N. R.; Geubelle, P. H.; Moore, J. S.; Kessler, M. R.; Sriram, S. R.; Brown, E. N.; Viswanathan, S. Autonomic healing of polymer composites. *Nature* **2001,** *409* (6822), 794-797.

(31) Diba, M.; Spaans, S.; Ning, K.; Ippel, B. D.; Yang, F.; Loomans, B.; Dankers, P. Y. W.; Leeuwenburgh, S. C. G. Self-Healing Biomaterials: From Molecular Concepts to Clinical Applications. *Adv. Mater. Interfaces* **2018,** *5* (17), 1800118.

(32) Toohey, K. S.; Sottos, N. R.; Lewis, J. A.; Moore, J. S.; White, S. R. Self-healing materials with microvascular networks. *Nat. Mater.* **2007,** *6* (8), 581-5.

(33) Chen, M.; Fan, D.; Liu, S.; Rao, Z.; Dong, Y.; Wang, W.; Chen, H.; Bai, L.; Cheng, Z. Fabrication of self-healing hydrogels with surface functionalized microcapsules from stellate mesoporous silica. *Polym. Chem.* **2019,** *10* (4), 503-511.

(34) Liu, S.; Rao, Z.; Wu, R.; Sun, Z.; Yuan, Z.; Bai, L.; Wang, W.; Yang, H.; Chen, H. Fabrication of Microcapsules by the Combination of Biomass Porous Carbon and Polydopamine for Dual Self-Healing Hydrogels. *J. Agric. Food. Chem.* **2019,** *67* (4), 1061-1071.

(35) Yang, Y.; Urban, M. W. Self-healing polymeric materials. *Chem. Soc. Rev.* **2013,** *42* (17), 7446-67.

(36) Wei, Z.; Yang, J. H.; Zhou, J.; Xu, F.; Zrinyi, M.; Dussault, P. H.; Osada, Y.; Chen, Y. M. Self-

healing gels based on constitutional dynamic chemistry and their potential applications. *Chem. Soc. Rev.* **2014,** *43* (23), 8114-31.

(37) Phadke, A.; Zhang, C.; Arman, B.; Hsu, C. C.; Mashelkar, R. A.; Lele, A. K.; Tauber, M. J.; Arya, G.; Varghese, S. Rapid self-healing hydrogels. *Proc. Natl. Acad. Sci. U. S. A.* **2012,** *109* (12), 4383-8.

(38) Han, L.; Wang, M.; Prieto-López, L. O.; Deng, X.; Cui, J. Self-Hydrophobization in a Dynamic Hydrogel for Creating Nonspecific Repeatable Underwater Adhesion. *Adv. Funct. Mater* **2019,** *30* (7), 1907064.

(39) Jeon, I.; Cui, J.; Illeperuma, W. R.; Aizenberg, J.; Vlassak, J. J. Extremely Stretchable and Fast Self-Healing Hydrogels. *Adv. Mater.* **2016,** *28* (23), 4678-83.

(40) Tuncaboylu, D. C.; Sari, M.; Oppermann, W.; Okay, O. Tough and Self-Healing Hydrogels Formed via Hydrophobic Interactions. *Macromolecules* **2011,** *44* (12), 4997-5005.

(41) Zheng, J.; Xiao, P.; Liu, W.; Zhang, J.; Huang, Y.; Chen, T. Mechanical Robust and Self-Healable Supramolecular Hydrogel. *Macromol. Rapid Commun.* **2016,** *37* (3), 265-70.

(42) Long, T.; Li, Y.; Fang, X.; Sun, J. Salt-Mediated Polyampholyte Hydrogels with High Mechanical Strength, Excellent Self-Healing Property, and Satisfactory Electrical Conductivity. *Adv. Funct. Mater* **2018,** *28* (44), 1804416.

(43) Ma, X.; Zhao, Y. Biomedical Applications of Supramolecular Systems Based on Host-Guest Interactions. *Chem. Rev.* **2015,** *115* (15), 7794-839.

(44) Hu, Q. D.; Tang, G. P.; Chu, P. K. Cyclodextrin-based host-guest supramolecular nanoparticles for delivery: from design to applications. *Acc. Chem. Res.* **2014,** *47* (7), 2017-25.

(45) Schmidt, B.; Barner-Kowollik, C. Dynamic Macromolecular Material Design-The Versatility of Cyclodextrin-Based Host-Guest Chemistry. *Angew. Chem. Int. Ed. Engl.* **2017,** *56* (29), 8350-

8369.

(46) Marquez, C.; Hudgins, R. R.; Nau, W. M. Mechanism of host-guest complexation by cucurbituril. *J. Am. Chem. Soc.* **2004,** *126* (18), 5806-16.

(47) Zhang, M.; Xu, D.; Yan, X.; Chen, J.; Dong, S.; Zheng, B.; Huang, F. Self-healing supramolecular gels formed by crown ether based host-guest interactions. *Angew. Chem. Int. Ed. Engl.* **2012,** *51* (28), 7011-5.

(48) Kakuta, T.; Takashima, Y.; Nakahata, M.; Otsubo, M.; Yamaguchi, H.; Harada, A. Preorganized hydrogel: self-healing properties of supramolecular hydrogels formed by polymerization of host-guest-monomers that contain cyclodextrins and hydrophobic guest groups. *Adv. Mater.* **2013,** *25* (20), 2849-53.

(49) Li, L.; Smitthipong, W.; Zeng, H. Mussel-inspired hydrogels for biomedical and environmental applications. *Polym. Chem.* **2015,** *6* (3), 353-358.

(50) Guo, Q.; Chen, J.; Wang, J.; Zeng, H.; Yu, J. Recent progress in synthesis and application of mussel-inspired adhesives. *Nanoscale* **2020,** *12* (3), 1307-1324.

(51) Zhang, C.; Wu, B.; Zhou, Y.; Zhou, F.; Liu, W.; Wang, Z. Mussel-inspired hydrogels: from design principles to promising applications. *Chem. Soc. Rev.* **2020,** *49* (11), 3605-3637.

(52) Zeng, H.; Hwang, D. S.; Israelachvili, J. N.; Waite, J. H. Strong reversible Fe^{3+}-mediated bridging between dopa-containing protein films in water. *Proc. Natl. Acad. Sci. U. S. A.* **2010,** *107* (29), 12850-3.

(53) Zhang, J.; Xiang, L.; Yan, B.; Zeng, H. Nanomechanics of Anion-pi Interaction in Aqueous Solution. *J. Am. Chem. Soc.* **2020,** *142* (4), 1710-1714.

(54) Gebbie, M. A.; Wei, W.; Schrader, A. M.; Cristiani, T. R.; Dobbs, H. A.; Idso, M.; Chmelka, B. F.; Waite, J. H.; Israelachvili, J. N. Tuning underwater adhesion with cation-pi interactions. *Nat.*

Chem. **2017,** *9* (5), 473-479.

(55) Li, L.; Yan, B.; Yang, J.; Chen, L.; Zeng, H. Novel mussel-inspired injectable self-healing hydrogel with anti-biofouling property. *Adv. Mater.* **2015,** *27* (7), 1294-9.

(56) Han, L.; Lu, X.; Liu, K.; Wang, K.; Fang, L.; Weng, L. T.; Zhang, H.; Tang, Y.; Ren, F.; Zhao, C.; Sun, G.; Liang, R.; Li, Z. Mussel-Inspired Adhesive and Tough Hydrogel Based on Nanoclay Confined Dopamine Polymerization. *ACS Nano* **2017,** *11* (3), 2561-2574.

(57) Han, L.; Yan, L.; Wang, K.; Fang, L.; Zhang, H.; Tang, Y.; Ding, Y.; Weng, L.-T.; Xu, J.; Weng, J.; Liu, Y.; Ren, F.; Lu, X. Tough, self-healable and tissue-adhesive hydrogel with tunable multifunctionality. *NPG Asia Mater.* **2017,** *9* (4), e372-e372.

(58) Han, L.; Lu, X.; Wang, M.; Gan, D.; Deng, W.; Wang, K.; Fang, L.; Liu, K.; Chan, C. W.; Tang, Y.; Weng, L. T.; Yuan, H. A Mussel-Inspired Conductive, Self-Adhesive, and Self-Healable Tough Hydrogel as Cell Stimulators and Implantable Bioelectronics. *Small* **2017,** *13* (2).

(59) Elshaarani, T.; Yu, H.; Wang, L.; Zain Ul, A.; Ullah, R. S.; Haroon, M.; Khan, R. U.; Fahad, S.; Khan, A.; Nazir, A.; Usman, M.; Naveed, K. U. Synthesis of hydrogel-bearing phenylboronic acid moieties and their applications in glucose sensing and insulin delivery. *J. Mater. Chem. B* **2018,** *6* (23), 3831-3854.

(60) Chen, Y.; Diaz-Dussan, D.; Wu, D.; Wang, W.; Peng, Y.-Y.; Asha, A. B.; Hall, D. G.; Ishihara, K.; Narain, R. Bioinspired Self-Healing Hydrogel Based on Benzoxaborole-Catechol Dynamic Covalent Chemistry for 3D Cell Encapsulation. *ACS Macro Lett.* **2018,** *7* (8), 904-908.

(61) Wang, W.; Xiang, L.; Diaz-Dussan, D.; Zhang, J.; Yang, W.; Gong, L.; Chen, J.; Narain, R.; Zeng, H. Dynamic Flexible Hydrogel Network with Biological Tissue-like Self-Protective Functions. *Chem. Mater.* **2020,** *32* (24), 10545-10555.

(62) Chu, C. K.; Joseph, A. J.; Limjoco, M. D.; Yang, J.; Bose, S.; Thapa, L. S.; Langer, R.;

Anderson, D. G. Chemical Tuning of Fibers Drawn from Extensible Hyaluronic Acid Networks. *J. Am. Chem. Soc.* **2020,** *142* (46), 19715-19721.

(63) Chen, Y.; Wang, W.; Wu, D.; Nagao, M.; Hall, D. G.; Thundat, T.; Narain, R. Injectable Self-Healing Zwitterionic Hydrogels Based on Dynamic Benzoxaborole–Sugar Interactions with Tunable Mechanical Properties. *Biomacromolecules* **2018,** *19* (2), 596-605.

(64) Yesilyurt, V.; Webber, M. J.; Appel, E. A.; Godwin, C.; Langer, R.; Anderson, D. G. Injectable Self-Healing Glucose-Responsive Hydrogels with pH-Regulated Mechanical Properties. *Adv. Mater.* **2016,** *28* (1), 86-91.

(65) Zhao, X.; Wu, H.; Guo, B.; Dong, R.; Qiu, Y.; Ma, P. X. Antibacterial anti-oxidant electroactive injectable hydrogel as self-healing wound dressing with hemostasis and adhesiveness for cutaneous wound healing. *Biomaterials* **2017,** *122*, 34-47.

(66) Qu, J.; Zhao, X.; Ma, P. X.; Guo, B. pH-responsive self-healing injectable hydrogel based on N-carboxyethyl chitosan for hepatocellular carcinoma therapy. *Acta. Biomater.* **2017,** *58*, 168-180.

(67) Tseng, T. C.; Tao, L.; Hsieh, F. Y.; Wei, Y.; Chiu, I. M.; Hsu, S. H. An Injectable, Self-Healing Hydrogel to Repair the Central Nervous System. *Adv. Mater.* **2015,** *27* (23), 3518-24.

(68) Wang, W.; Narain, R.; Zeng, H. Rational Design of Self-Healing Tough Hydrogels: A Mini Review. *Front. Chem.* **2018,** *6* (497), 497.

(69) Yang, X.; Liu, G.; Peng, L.; Guo, J.; Tao, L.; Yuan, J.; Chang, C.; Wei, Y.; Zhang, L. Highly Efficient Self-Healable and Dual Responsive Cellulose-Based Hydrogels for Controlled Release and 3D Cell Culture. *Adv. Funct. Mater.* **2017,** *27* (40), 1703174.

(70) Sun, C.; Jia, H.; Lei, K.; Zhu, D.; Gao, Y.; Zheng, Z.; Wang, X. Self-healing hydrogels with stimuli responsiveness based on acylhydrazone bonds. *Polymer* **2019,** *160*, 246-253.

(71) Deng, G.; Li, F.; Yu, H.; Liu, F.; Liu, C.; Sun, W.; Jiang, H.; Chen, Y. Dynamic Hydrogels

with an Environmental Adaptive Self-Healing Ability and Dual Responsive Sol–Gel Transitions. *ACS Macro Lett.* **2012,** *1* (2), 275-279.

(72) Canadell, J.; Goossens, H.; Klumperman, B. Self-Healing Materials Based on Disulfide Links. *Macromolecules* **2011,** *44* (8), 2536-2541.

(73) Fairbanks, B. D.; Singh, S. P.; Bowman, C. N.; Anseth, K. S. Photodegradable, Photoadaptable Hydrogels via Radical-Mediated Disulfide Fragmentation Reaction. *Macromolecules* **2011,** *44* (8), 2444-2450.

(74) Barcan, G. A.; Zhang, X.; Waymouth, R. M. Structurally dynamic hydrogels derived from 1,2-dithiolanes. *J. Am. Chem. Soc.* **2015,** *137* (17), 5650-3.

(75) Lopez-Perez, P. M.; da Silva, R. M. P.; Strehin, I.; Kouwer, P. H. J.; Leeuwenburgh, S. C. G.; Messersmith, P. B. Self-Healing Hydrogels Formed by Complexation between Calcium Ions and Bisphosphonate-Functionalized Star-Shaped Polymers. *Macromolecules* **2017,** *50* (21), 8698-8706.

(76) Shi, L.; Carstensen, H.; Hölzl, K.; Lunzer, M.; Li, H.; Hilborn, J.; Ovsianikov, A.; Ossipov, D. A. Dynamic Coordination Chemistry Enables Free Directional Printing of Biopolymer Hydrogel. *Chem. Mater.* **2017,** *29* (14), 5816-5823.

(77) Sun, J. Y.; Zhao, X.; Illeperuma, W. R.; Chaudhuri, O.; Oh, K. H.; Mooney, D. J.; Vlassak, J. J.; Suo, Z. Highly stretchable and tough hydrogels. *Nature* **2012,** *489* (7414), 133-6.

(78) Holten-Andersen, N.; Harrington, M. J.; Birkedal, H.; Lee, B. P.; Messersmith, P. B.; Lee, K. Y.; Waite, J. H. pH-induced metal-ligand cross-links inspired by mussel yield self-healing polymer networks with near-covalent elastic moduli. *Proc. Natl. Acad. Sci. U. S. A.* **2011,** *108* (7), 2651-5.

(79) Filippidi, E.; Cristiani, T. R.; Eisenbach, C. D.; Waite, J. H.; Israelachvili, J. N.; Ahn, B. K.; Valentine, M. T. Toughening elastomers using mussel-inspired iron-catechol complexes. *Science* **2017,** *358* (6362), 502-505.

(80) Shi, L.; Ding, P.; Wang, Y.; Zhang, Y.; Ossipov, D.; Hilborn, J. Self-Healing Polymeric Hydrogel Formed by Metal-Ligand Coordination Assembly: Design, Fabrication, and Biomedical Applications. *Macromol. Rapid. Commun.* **2019,** *40* (7), e1800837.

(81) Smith, L. J.; Taimoory, S. M.; Tam, R. Y.; Baker, A. E. G.; Binth Mohammad, N.; Trant, J. F.; Shoichet, M. S. Diels-Alder Click-Cross-Linked Hydrogels with Increased Reactivity Enable 3D Cell Encapsulation. *Biomacromolecules* **2018,** *19* (3), 926-935.

(82) Alge, D. L.; Azagarsamy, M. A.; Donohue, D. F.; Anseth, K. S. Synthetically tractable click hydrogels for three-dimensional cell culture formed using tetrazine-norbornene chemistry. *Biomacromolecules* **2013,** *14* (4), 949-53.

(83) Wei, Z.; Yang, J. H.; Du, X. J.; Xu, F.; Zrinyi, M.; Osada, Y.; Li, F.; Chen, Y. M. Dextran-based self-healing hydrogels formed by reversible diels-alder reaction under physiological conditions. *Macromol. Rapid. Commun.* **2013,** *34* (18), 1464-70.

(84) Gallo, R. L. Human Skin Is the Largest Epithelial Surface for Interaction with Microbes. *J. Invest. Dermatol.* **2017,** *137* (6), 1213-1214.

(85) Rezvani Ghomi, E.; Khalili, S.; Nouri Khorasani, S.; Esmaeely Neisiany, R.; Ramakrishna, S. Wound dressings: Current advances and future directions. *J. Appl. Polym. Sci.* **2019,** *136* (27), 47738.

(86) Bae, K. H.; Wang, L. S.; Kurisawa, M. Injectable biodegradable hydrogels: progress and challenges. *J. Mater. Chem. B* **2013,** *1* (40), 5371-5388.

(87) Yang, J.-A.; Yeom, J.; Hwang, B. W.; Hoffman, A. S.; Hahn, S. K. In situ-forming injectable hydrogels for regenerative medicine. *Prog. Polym. Sci.* **2014,** *39* (12), 1973-1986.

(88) Chen, H.; Cheng, R.; Zhao, X.; Zhang, Y.; Tam, A.; Yan, Y.; Shen, H.; Zhang, Y. S.; Qi, J.; Feng, Y.; Liu, L.; Pan, G.; Cui, W.; Deng, L. An injectable self-healing coordinative hydrogel with

antibacterial and angiogenic properties for diabetic skin wound repair. *NPG Asia Mater.* **2019,** *11* (1), 3.

(89) Qu, J.; Zhao, X.; Liang, Y.; Zhang, T.; Ma, P. X.; Guo, B. Antibacterial adhesive injectable hydrogels with rapid self-healing, extensibility and compressibility as wound dressing for joints skin wound healing. *Biomaterials* **2018,** *183*, 185-199.

(90) Fan, Z.; Liu, B.; Wang, J.; Zhang, S.; Lin, Q.; Gong, P.; Ma, L.; Yang, S. A Novel Wound Dressing Based on Ag/Graphene Polymer Hydrogel: Effectively Kill Bacteria and Accelerate Wound Healing. *AdV. Funct. Mater.* **2014,** *24* (25), 3933-3943.

(91) Schwartz, V. B.; Thétiot, F.; Ritz, S.; Pütz, S.; Choritz, L.; Lappas, A.; Förch, R.; Landfester, K.; Jonas, U. Antibacterial Surface Coatings from Zinc Oxide Nanoparticles Embedded in Poly(N-isopropylacrylamide) Hydrogel Surface Layers. *Adv. Funct. Mater.* **2012,** *22* (11), 2376-2386.

(92) Yang, K.; Han, Q.; Chen, B.; Zheng, Y.; Zhang, K.; Li, Q.; Wang, J. Antimicrobial hydrogels: promising materials for medical application. *Int. J. Nanomedicine.* **2018,** *13*, 2217-2263.

(93) Annabi, N.; Rana, D.; Shirzaei Sani, E.; Portillo-Lara, R.; Gifford, J. L.; Fares, M. M.; Mithieux, S. M.; Weiss, A. S. Engineering a sprayable and elastic hydrogel adhesive with antimicrobial properties for wound healing. *Biomaterials* **2017,** *139*, 229-243.

(94) Strassburg, A.; Petranowitsch, J.; Paetzold, F.; Krumm, C.; Peter, E.; Meuris, M.; Koller, M.; Tiller, J. C. Cross-Linking of a Hydrophilic, Antimicrobial Polycation toward a Fast-Swelling, Antimicrobial Superabsorber and Interpenetrating Hydrogel Networks with Long Lasting Antimicrobial Properties. *ACS Appl. Mater. Interfaces.* **2017,** *9* (42), 36573-36582.

(95) Li, L.; Yan, B.; Yang, J.; Huang, W.; Chen, L.; Zeng, H. Injectable Self-Healing Hydrogel with Antimicrobial and Antifouling Properties. *ACS Appl. Mater. Interfaces.* **2017,** *9* (11), 9221-9225.

(96) Mura, S.; Nicolas, J.; Couvreur, P. Stimuli-responsive nanocarriers for drug delivery. *Nat. Mater.* **2013,** *12* (11), 991-1003.

(97) Wu, M.; Chen, J.; Huang, W.; Yan, B.; Peng, Q.; Liu, J.; Chen, L.; Zeng, H. Injectable and Self-Healing Nanocomposite Hydrogels with Ultrasensitive pH-Responsiveness and Tunable Mechanical Properties: Implications for Controlled Drug Delivery. *Biomacromolecules* **2020,** *21* (6), 2409-2420.

(98) Tibbitt, M. W.; Anseth, K. S. Hydrogels as extracellular matrix mimics for 3D cell culture. *Biotechnol. Bioeng.* **2009,** *103* (4), 655-63.

(99) Lou, J.; Stowers, R.; Nam, S.; Xia, Y.; Chaudhuri, O. Stress relaxing hyaluronic acid-collagen hydrogels promote cell spreading, fiber remodeling, and focal adhesion formation in 3D cell culture. *Biomaterials* **2018,** *154*, 213-222.

(100) Zhang, G.; Chen, Y.; Deng, Y.; Ngai, T.; Wang, C. Dynamic Supramolecular Hydrogels: Regulating Hydrogel Properties through Self-Complementary Quadruple Hydrogen Bonds and Thermo-Switch. *ACS Macro Lett.* **2017,** *6* (7), 641-646.

(101) Nagao, M.; Sengupta, J.; Diaz-Dussan, D.; Adam, M.; Wu, M.; Acker, J.; Ben, R.; Ishihara, K.; Zeng, H.; Miura, Y.; Narain, R. Synthesis of Highly Biocompatible and Temperature-Responsive Physical Gels for Cryopreservation and 3D Cell Culture. *ACS Appl. Bio Mater.* **2018,** *1* (2), 356-366.

(102) Kouwer, P. H.; Koepf, M.; Le Sage, V. A.; Jaspers, M.; van Buul, A. M.; Eksteen-Akeroyd, Z. H.; Woltinge, T.; Schwartz, E.; Kitto, H. J.; Hoogenboom, R.; Picken, S. J.; Nolte, R. J.; Mendes, E.; Rowan, A. E. Responsive biomimetic networks from polyisocyanopeptide hydrogels. *Nature* **2013,** *493* (7434), 651-5.

(103) Goldenberg, C.; Goldhirsch, I. Friction enhances elasticity in granular solids. *Nature* **2005,**

435 (7039), 188-91.

(104) Burla, F.; Mulla, Y.; Vos, B. E.; Aufderhorst-Roberts, A.; Koenderink, G. H. From mechanical resilience to active material properties in biopolymer networks. *Nat. Rev. Phys.* **2019,** *1* (4), 249-263.

(105) Lih, E.; Oh, S. H.; Joung, Y. K.; Lee, J. H.; Han, D. K. Polymers for cell/tissue anti-adhesion. *Prog. Polym. Sci.* **2015,** *44*, 28-61.

(106) Stapleton, L. M.; Steele, A. N.; Wang, H.; Lopez Hernandez, H.; Yu, A. C.; Paulsen, M. J.; Smith, A. A. A.; Roth, G. A.; Thakore, A. D.; Lucian, H. J.; Totherow, K. P.; Baker, S. W.; Tada, Y.; Farry, J. M.; Eskandari, A.; Hironaka, C. E.; Jaatinen, K. J.; Williams, K. M.; Bergamasco, H.; Marschel, C.; Chadwick, B.; Grady, F.; Ma, M.; Appel, E. A.; Woo, Y. J. Use of a supramolecular polymeric hydrogel as an effective post-operative pericardial adhesion barrier. *Nat. Biomed. Eng.* **2019,** *3* (8), 611-620.

(107) Yang, Y.; Liu, X.; Li, Y.; Wang, Y.; Bao, C.; Chen, Y.; Lin, Q.; Zhu, L. A postoperative anti-adhesion barrier based on photoinduced imine-crosslinking hydrogel with tissue-adhesive ability. *Acta. Biomater.* **2017,** *62*, 199-209.

(108) Li, L.; Wang, N.; Jin, X.; Deng, R.; Nie, S.; Sun, L.; Wu, Q.; Wei, Y.; Gong, C. Biodegradable and injectable in situ cross-linking chitosan-hyaluronic acid based hydrogels for postoperative adhesion prevention. *Biomaterials* **2014,** *35* (12), 3903-3917.

(109) Song, L.; Li, L.; He, T.; Wang, N.; Yang, S.; Yang, X.; Zeng, Y.; Zhang, W.; Yang, L.; Wu, Q.; Gong, C. Peritoneal adhesion prevention with a biodegradable and injectable N,O-carboxymethyl chitosan-aldehyde hyaluronic acid hydrogel in a rat repeated-injury model. *Sci. Rep.* **2016,** *6* (1), 37600.

(110) Zhu, W.; Gao, L.; Luo, Q.; Gao, C.; Zha, G.; Shen, Z.; Li, X. Metal and light free “click”

hydrogels for prevention of post-operative peritoneal adhesions. *Polym. Chem.* **2014,** *5* (6), 2018-2026.

(111) Zhang, E.; Song, B.; Shi, Y.; Zhu, H.; Han, X.; Du, H.; Yang, C.; Cao, Z. Fouling-resistant zwitterionic polymers for complete prevention of postoperative adhesion. *Proc. Natl. Acad. Sci. U. S. A.* **2020,** *117* (50), 32046-32055.

(112) Guo, Q.; Sun, H.; Wu, X.; Yan, Z.; Tang, C.; Qin, Z.; Yao, M.; Che, P.; Yao, F.; Li, J. In Situ Clickable Purely Zwitterionic Hydrogel for Peritoneal Adhesion Prevention. *Chem. Mater.* **2020,** *32* (15), 6347-6357.

(113) Zhang, E.; Yang, J.; Wang, K.; Song, B.; Zhu, H.; Han, X.; Shi, Y.; Yang, C.; Zeng, Z.; Cao, Z. Biodegradable Zwitterionic Cream Gel for Effective Prevention of Postoperative Adhesion. *Adv. Funct. Mater* **2020,** *31* (10), 2009431.

CHAPTER 2 Major Experimental Methods

2.1 Polymerization Techniques

2.1.1 Conventional Free Radical Polymerization

Conventional free radical polymerization is one of the simplest polymerization techniques to synthesize homopolymers or statistical copolymers. Vinyl monomers and initiators are the two key components in conventional free radical polymerization. The conventional free radical polymerization can be divided into three stages: initiation, propagation and termination.

Initiation involves the generation of active free radicals by the initiators. Free radicals can be generated in several ways, including thermal or photochemical decomposition of organic peroxides and azo compounds,[1-2] high-energy radiation as well as oxidation-reduction reactions.[3-4] Figure 2.1 shows some commonly used initiators in conventional free radical polymerization.

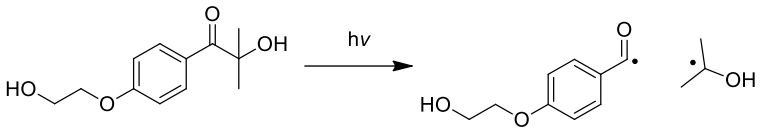

Photochemical decomposition of I2959

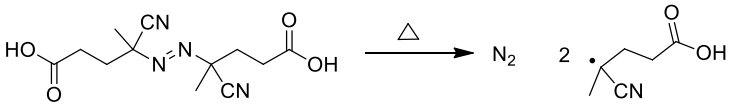

Thermal decomposition of ACVA

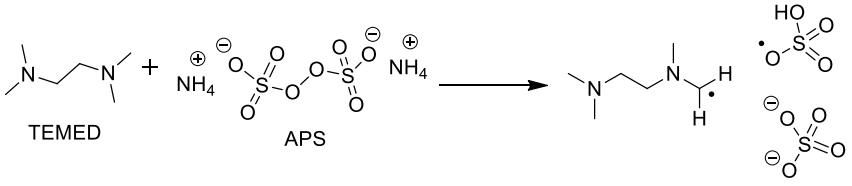

Oxidation-reduction reaction between TEMED and APS

Figure 2.1. Commonly used initiators in conventional free radical polymerization.

During propagation, active radical initiators attack the monomers and the polymer chains will continuously grow by successive addition of the monomers until termination (**Figure 2.2**). The propagation step can be affected by several factors, including radical and monomer reactivity, solvent, temperature, etc.[5]

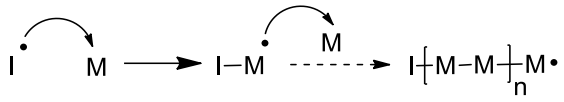

Figure 2.2. Propagation step of conventional free radical polymerization.

Termination refers to the reaction of the chain end active center with species other than monomer, leading to the removal of reactivity. Termination can occur by several mechanisms, including combination of two active chains, combination of an active chain with radical initiator, disproportionation or reaction with inhibitors, such as oxygen (**Figure 2.3**).

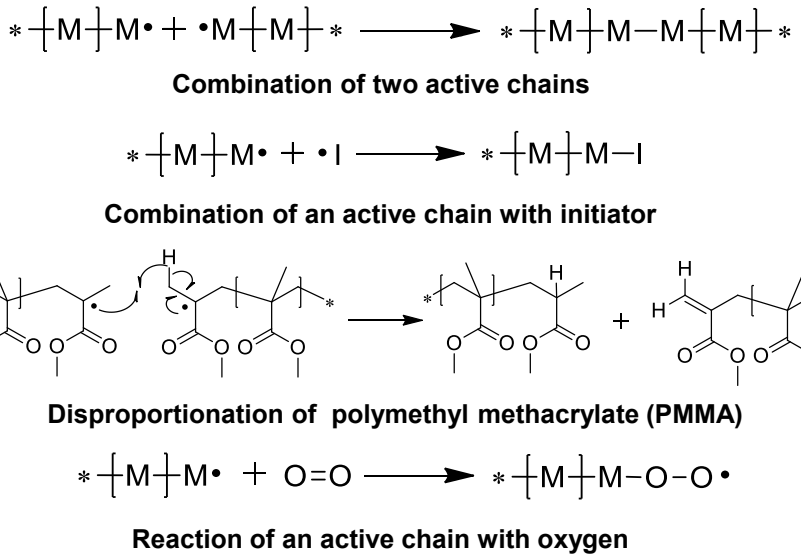

Figure 2.3. Termination mechanisms of conventional free radical polymerization.

Although conventional free radical polymerization is applicable to a wide range of commercially available monomers, it sometimes suffers from unwanted side reactions (i.e.,

chain transfer reactions). Besides, due to its uncontrolled nature, it is limited to produce well-defined polymers or block copolymers with narrow polydispersity (PDI). In some cases, living free-radical polymerization techniques (e.g., RAFT, atom transfer radical polymerization (ATRP)) are preferred for polymer synthesis.

2.1.2 Reversible addition−fragmentation chain-transfer (RAFT) Polymerization

RAFT polymerization has been an important and versatile living free-radical polymerization technique to synthesize polymers with well-controlled molecular weight, molecular weight distribution and molecular structure since the pioneering work by Thang et al. in 1998.[6] RAFT polymerization proceeds via a degenerative chain transfer process and relies on the use of highly reactive thiocarbonylthio-containing compounds as the chain transfer agents (CTAs).[7-8] **Figure 2.4** outlines the generally accepted mechanism of RAFT polymerization. After the initiation (step i), the propagating oligomeric radical (P_m•) can react with CTA (1) to form an unstable radical intermediate (2). The radical intermediate can either fragment back to the original reactants or yield a dormant oligomer chain capped with thiocarbonylthio group (3) and an active radical (R•) (step ii). The active radical (R•) can re-initiate the polymerization and produce a new propagating oligomeric radical (P_n•) (step iii). After all the CTA (1) is consumed (i.e., completion of step ii), the RAFT polymerization proceeds to its main equilibrium stage, which involves the rapid exchange between the propagating radicals (P_m• and P_n•) and the dormant compound (4) (step iv). Due to the fast initiation and rapid equilibrium, all the active radical chains (P_m• and P_n•) have equal opportunity to grow, producing polymers with narrow molecular weight distributions. Most synthesized polymer chains are “living” polymer chains, which are capped with thiocarbonylthio group. Only few dead chains can form through termination

reaction via combination or disproportionation mechanisms (step v).

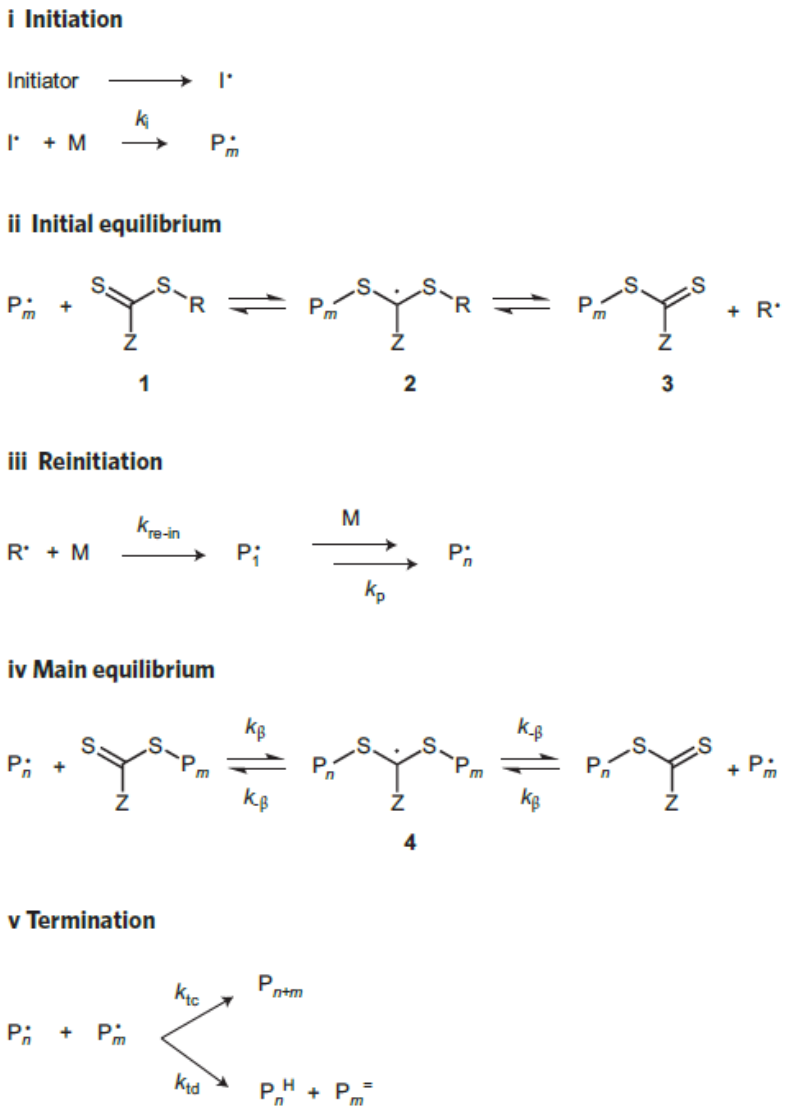

Figure 2.4. Reversible addition−fragmentation chain-transfer (RAFT) polymerization mechanism.[9]

A highly efficient thiocarbonylthio-containing CTA plays critical roles in a successful RAFT polymerization. A typical CTA contains a reactive C=S thiocarbonyl group, a free radical leaving group R which initiates the growth of polymer chains and a Z group which activates the C=S bond towards radical addition and stabilizes the intermediate radical (Figure 2.5).[7, 10] Both R and Z groups could affect the RAFT polymerization process.

Generally, the selection of CTA should be based on the type of monomers. Typical CTAs include dithiobenzoates, trithiocarbonates, xanthates and dithiocarbamates.

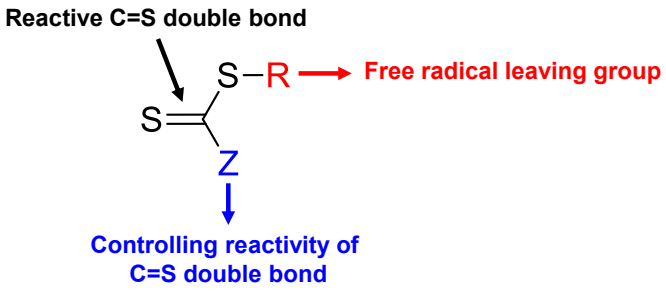

Figure 2.5. General structure of thiocarbonylthio-containing chain transfer agent (CTA).

2.2 Rheometer

Hydrogels exhibit unique viscoelastic behavior upon deformation. The viscoelastic properties of the hydrogels are usually studied through oscillatory tests using a rheometer.[1, 11-12] In a typical test, a piece of hydrogel is placed between two parallel disks (**Figure 2.6a**). The shear stress (τ) or deformation (γ) is measured as a preset sinusoidal shear strain (γ) or stress (τ) is applied to the hydrogel. For viscoelastic materials like hydrogels, there is a phase shift δ (usually between 0° and 90°) between the preset and measured parameters on the sine curves (**Figure 2.6b**). Storage modulus (*G'*) and loss modulus (*G"*), which measure the elastic and viscous response of the hydrogel respectively, are two most important parameters that can be obtained from a rheology test. Based on the measurements, the software will automatically calculate *G'* and *G"* using the following equations:

$$G' = \frac{\sigma_0}{\varepsilon_0} cos\,\delta \quad (1)$$

$$G'' = \frac{\sigma_0}{\varepsilon_0} sin\,\delta \quad (2)$$

where σ_0, ε_0 and δ are stress amplitude, strain amplitude and the phase shift between them. Generally, three types of rheology tests are commonly performed to characterize the

hydrogels.

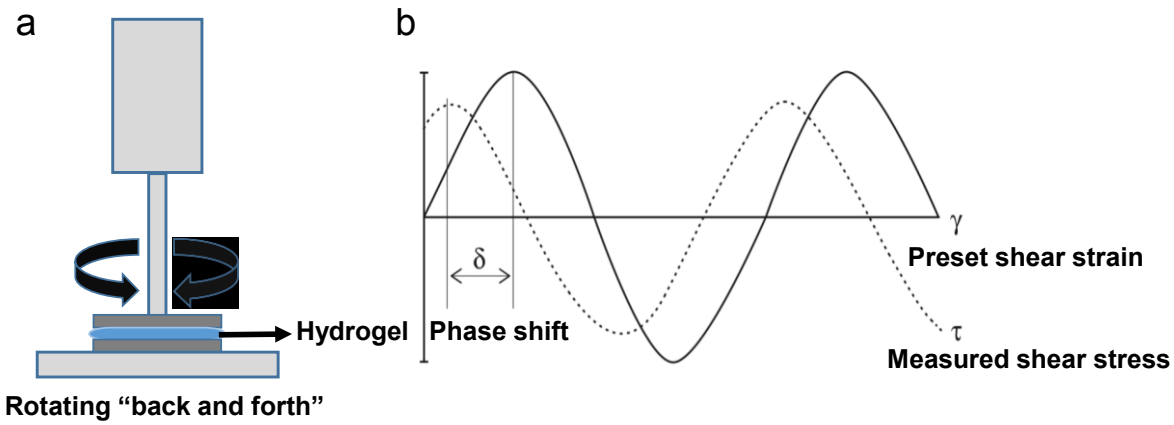

Figure 2.6. (a) Typical rheology measurement set-up. (b) Typical measurements of viscoelastic materials (e.g., hydrogels).

The first test is the oscillatory strain amplitude sweep test, in which a sinusoidal shear strain (γ) with increasing amplitude at fixed frequency is applied on the material (**Figure 2.7a**). The strain amplitude test can be used to characterize the linear viscoelastic region (LVR) and the critical strain value of the hydrogel.[13-14] In a typical strain amplitude sweep test, *G'* and *G"* of the hydrogel are measured as a function of strain amplitude. Usually, both *G'* and *G"* values are constant within small strain range. In the LVR, *G'* is always greater than *G"*, indicating the solid-like behavior of the hydrogel. *G'* value would exhibit a sharp drop and become smaller than *G"* value when certain strain is reached, indicating the destruction and liquid-like behavior of the hydrogel. The critical strain value is defined as the crossover point of *G'* and *G"*. It measures the maximum shear strain a hydrogel can withstand.

The second test is the oscillatory frequency sweep test, in which a sinusoidal shear strain (γ) with increasing frequency at fixed amplitude is applied on the material (**Figure 2.7b**). The frequency sweep test is used to characterize the equilibrium modulus of the

hydrogels in the non-destructive deformation range (i.e., applied a strain value within the LVR).[15] In a typical procedure, *G'* and *G"* are measured as a function of frequency. Typically, for the covalently crosslinked hydrogels, both *G'* and *G"* values are constant over the entire frequency range and *G'* is always greater than *G"*. However, for some hydrogels crosslinked by dynamic molecular interactions, *G'* and *G"* values may depend on the frequency. *G'* can be lower than *G"* initially. It would gradually increase and surpass *G"* until reaches the equilibrium value as the frequency increases. The variation of modulus and crossover frequency may be attributed to the change of cross-linking density, water content, and polymer concentration of the hydrogels.

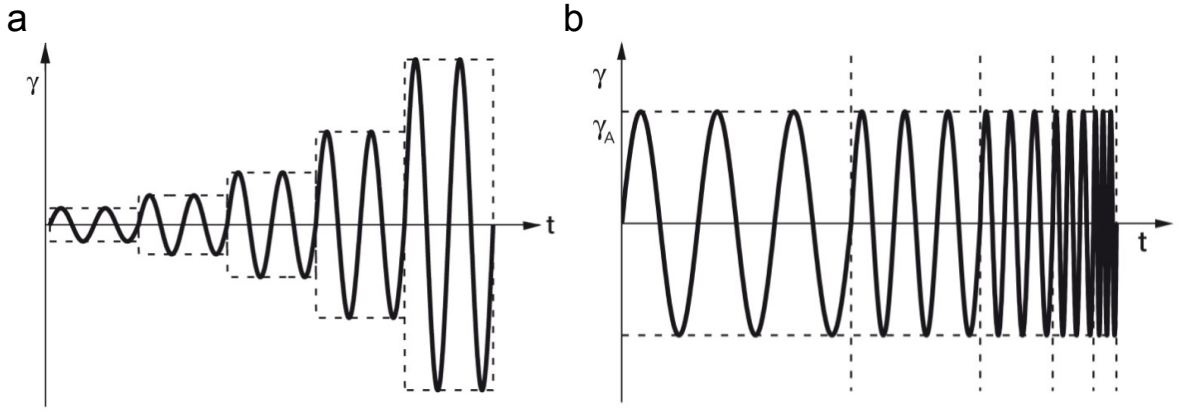

Figure 2.7. (a) Applied strain in an oscillatory strain amplitude test. (b) Applied strain in an oscillatory frequency test.

The third test is the oscillatory time sweep test, in which a sinusoidal shear strain (γ) at fixed frequency and strain amplitude is applied on the material. The time sweep test is often used to characterize the gelation time of the hydrogels.[15-16] In a typical procedure, two polymer precursor solutions are spread on upper and lower geometry respectively. After two disks are brought to the preset distance, the change of modulus is measured as a function of time. Typically, *G"* is greater than *G'* in the early stage, indicating the liquid-

like behavior of the system. As the time goes, *G'* would gradually increase and surpass *G"*, indicating the formation of hydrogel and the solid-like behavior of the system. The gelation time is defined as the crossover point of *G'* and *G"*. The *G'* value would finally reach equilibrium, indicating the formation of a stabilized hydrogel. Gelation time is an important parameter for the use of injectable hydrogels in a wide range of biomedical applications, such as tissue adhesives, hemostatic materials, etc.

For hydrogels with self-healing property, the self-healing performance can be evaluated by cyclic strain amplitude sweep test.[13-14] In a typical test, alternating strains (smaller/greater than the critical strain) are applied to the hydrogel and the change of modulus is measured as a function of time. The recovered *G'* value is compared with the initial *G'* value to determine the self-healing efficiency. Such cycle can be repeated for several times to examine the reproducibility of the self-healing capability.

2.3 Surface forces apparatus (SFA)

Surface forces apparatus (SFA) is a powerful tool for directly measuring the physical forces between surfaces (e.g., van der Waals and electrostatic forces in vapors and liquids, polymer interactions, bio-specific interactions, friction, etc.), and for studying other interfacial and thin film phenomena at the molecular level.[17] Since the pioneering work by Tabor, Winterton and Israelachvili,[18-19] SFA has been improved and developed. Based on the early versions of SFA, such as SFA Mk I, SFA Mk II and SFA Mk III, SFA 2000 (**Figure 2.8**) has been designed to have fewer parts, to be more user-friendly and to be able to accept various attachments while retains the excellent performance as the previous versions.

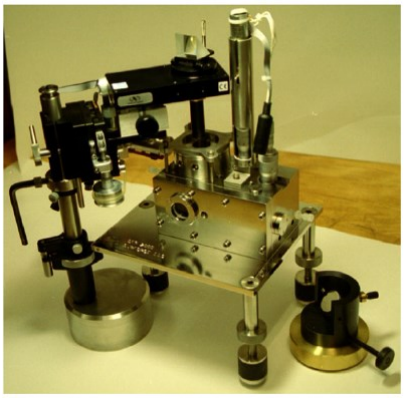

Figure 2.8. The picture of SFA 2000.

Figure 2.9 shows the cross-section of SFA 2000 through the center. The main components are the micrometers, the main stage containing the central single cantilever spring, the lower disk holder and the upper disk holder. The separation distance between the upper and lower surfaces can be precisely determined over a range of seven orders of magnitude (from millimeters to ångstroms) with 1Å (0.1 nm) resolution using four main controls.[17]

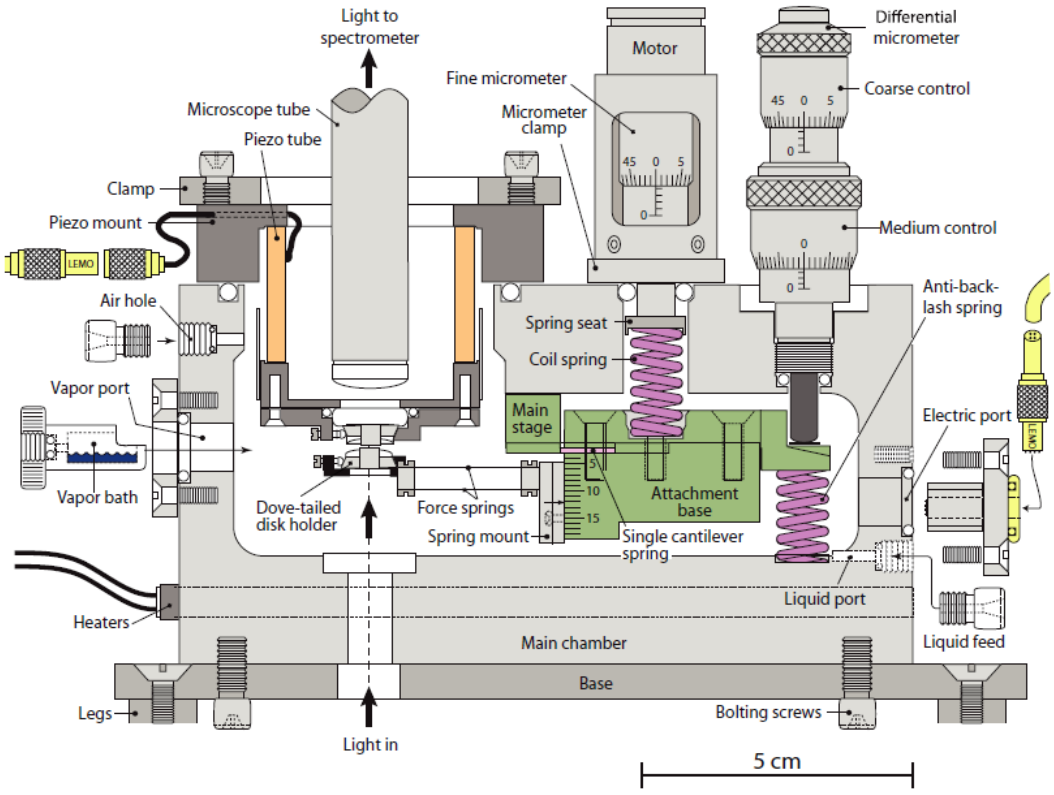

Figure 2.9. Cross-section of SFA 2000 through the center.[17]

2.3.1 Setup of the SFA Measurement

Figure 2.10 shows the typical setup of SFA experiment.[20-21] Briefly, two back-silvered mica surfaces (1−5 μm) are glued onto two cylindrical silica disks ($R \approx 2$ cm). To study the polymer interactions, the mica surfaces are coated with polymer solution for 15 min, followed by a thorough rinse with DI water to remove unbound or loosely bound polymers. Two surfaces are then mounted into the SFA chamber in a cross-cylinder configuration, and the SFA chamber is saturated with water vapor. Buffer solution or polymer solution is injected between two mica surfaces.

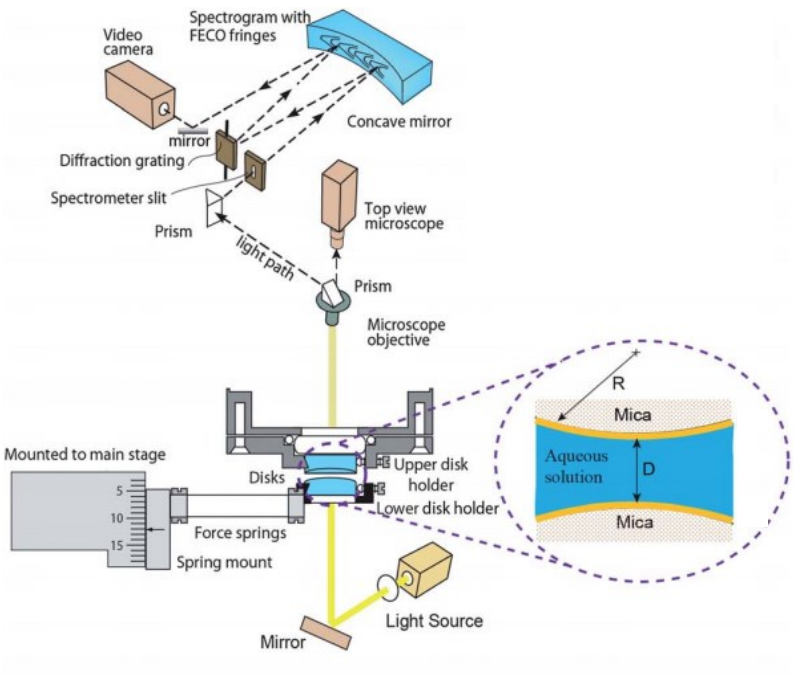

Figure 2.10. Schematic illustration of SFA experiment setup.[22]

2.3.2 Force measurement using SFA

The force measurement is conducted by bringing two surfaces to contact for some time followed by separation. Normal forces between two surfaces are determined based on the Hooke's law. The changed force between the surfaces $\Delta F(D) = k\,\Delta D$, where k is the spring constant of the force springs supporting the lower surface, and $\Delta D = D_{applied} - D_{measured}$. The applied separation distance between upper and lower surfaces $D_{applied}$ is determined by the differential micrometer and motor-driven fine micrometer. The actual separation distance between upper and lower surfaces $D_{measured}$ is measured using multiple beam interferometry (MBI) by employing fringes of equal chromatic order (FECO).[23-24] The measured interaction forces $\Delta F(D)$ is normalized by R (the curvature of the surface) and can be related to the interaction energy per unit area between two flat surfaces W_{flat} using the Derjaguin approximation:[25]

$$W_{flat}(D) = \frac{F(D)}{2\pi\sqrt{R_1 R_2}} = \frac{F(D)}{2\pi R} \quad (3)$$

when $R_1 = R_2 = R$

For soft deformable surfaces, such as polymer coating, the measured adhesion or "pull-off" force F_{ad} and adhesion energy per unit area W_{ad} are correlated by $F_{ad} = 1.5\pi R W_{ad}$.[17, 26]

References

(1) Chen, Y.; Wang, W.; Wu, D.; Nagao, M.; Hall, D. G.; Thundat, T.; Narain, R. Injectable Self-Healing Zwitterionic Hydrogels Based on Dynamic Benzoxaborole-Sugar Interactions with Tunable Mechanical Properties. *Biomacromolecules* **2018,** *19* (2), 596-605.

(2) Long, T.; Li, Y.; Fang, X.; Sun, J. Salt-Mediated Polyampholyte Hydrogels with High Mechanical Strength, Excellent Self-Healing Property, and Satisfactory Electrical Conductivity. *Adv. Funct. Mater.* **2018,** *28* (44), 1804416.

(3) Jiang, F.; Wang, X.; He, C.; Saricilar, S.; Wang, H. Mechanical properties of tough hydrogels synthesized with a facile simultaneous radiation polymerization and cross-linking method. *Radiat. Phys. Chem.* **2015,** *106*, 7-15.

(4) Han, L.; Lu, X.; Liu, K.; Wang, K.; Fang, L.; Weng, L. T.; Zhang, H.; Tang, Y.; Ren, F.; Zhao, C.; Sun, G.; Liang, R.; Li, Z. Mussel-Inspired Adhesive and Tough Hydrogel Based on Nanoclay Confined Dopamine Polymerization. *ACS Nano* **2017,** *11* (3), 2561-2574.

(5) Pojman, J. A.; Willis, J.; Fortenberry, D.; Ilyashenko, V.; Khan, A. M. Factors affecting propagating fronts of addition polymerization: Velocity, front curvature, temperatue profile, conversion, and molecular weight distribution. *J. Polym. Sci., Part A-1: Polym. Chem.* **1995,** *33* (4), 643-652.

(6) Chiefari, J.; Chong, Y. K.; Ercole, F.; Krstina, J.; Jeffery, J.; Le, T. P. T.; Mayadunne, R. T. A.; Meijs, G. F.; Moad, C. L.; Moad, G.; Rizzardo, E.; Thang, S. H. Living Free-Radical Polymerization by Reversible Addition−Fragmentation Chain Transfer: The RAFT Process. *Macromolecules* **1998,** *31* (16), 5559-5562.

(7) Perrier, S. 50th Anniversary Perspective: RAFT Polymerization—A User Guide.

Macromolecules **2017,** *50* (19), 7433-7447.

(8) Hill, M. R.; Carmean, R. N.; Sumerlin, B. S. Expanding the Scope of RAFT Polymerization: Recent Advances and New Horizons. *Macromolecules* **2015,** *48* (16), 5459-5469.

(9) Semsarilar, M.; Perrier, S. 'Green' reversible addition-fragmentation chain-transfer (RAFT) polymerization. *Nat. Chem.* **2010,** *2* (10), 811-20.

(10) Keddie, D. J.; Moad, G.; Rizzardo, E.; Thang, S. H. RAFT Agent Design and Synthesis. *Macromolecules* **2012,** *45* (13), 5321-5342.

(11) Tseng, T. C.; Tao, L.; Hsieh, F. Y.; Wei, Y.; Chiu, I. M.; Hsu, S. H. An Injectable, Self-Healing Hydrogel to Repair the Central Nervous System. *Adv. Mater.* **2015,** *27* (23), 3518-24.

(12) Li, L.; Yan, B.; Yang, J.; Huang, W.; Chen, L.; Zeng, H. Injectable Self-Healing Hydrogel with Antimicrobial and Antifouling Properties. *ACS Appl. Mater. Interfaces* **2017,** *9* (11), 9221-9225.

(13) Li, L.; Yan, B.; Yang, J.; Chen, L.; Zeng, H. Novel mussel-inspired injectable self-healing hydrogel with anti-biofouling property. *Adv. Mater.* **2015,** *27* (7), 1294-9.

(14) Wang, W.; Xiang, L.; Gong, L.; Hu, W.; Huang, W.; Chen, Y.; Asha, A. B.; Srinivas, S.; Chen, L.; Narain, R.; Zeng, H. Injectable, Self-Healing Hydrogel with Tunable Optical, Mechanical, and Antimicrobial Properties. *Chem. Mater.* **2019,** *31* (7), 2366-2376.

(15) Zhang, Y.; Fu, C.; Li, Y.; Wang, K.; Wang, X.; Wei, Y.; Tao, L. Synthesis of an injectable, self-healable and dual responsive hydrogel for drug delivery and 3D cell cultivation. *Polym. Chem.* **2017,** *8* (3), 537-544.

(16) Yang, X.; Liu, G.; Peng, L.; Guo, J.; Tao, L.; Yuan, J.; Chang, C.; Wei, Y.; Zhang, L.

Highly Efficient Self-Healable and Dual Responsive Cellulose-Based Hydrogels for Controlled Release and 3D Cell Culture. *Adv. Funct. Mater.* **2017,** *27* (40), 1703174.

(17) Israelachvili, J.; Min, Y.; Akbulut, M.; Alig, A.; Carver, G.; Greene, W.; Kristiansen, K.; Meyer, E.; Pesika, N.; Rosenberg, K.; Zeng, H. Recent advances in the surface forces apparatus (SFA) technique. *Rep. Prog. Phys.* **2010,** *73* (3), 036601.

(18) Tabor, D.; Winterton, R. H. S. The direct measurement of normal and retarded van der Waals forces. *Proceedings of the Royal Society of London. A. Mathematical and Physical Sciences* **1969,** *312* (1511), 435-450.

(19) Israelachvili, J. N.; Tabor, D. The measurement of van der Waals dispersion forces in the range 1.5 to 130 nm. *Proceedings of the Royal Society of London. A. Mathematical and Physical Sciences* **1997,** *331* (1584), 19-38.

(20) Zeng, H.; Hwang, D. S.; Israelachvili, J. N.; Waite, J. H. Strong reversible Fe^{3+}-mediated bridging between dopa-containing protein films in water. *Proc. Natl. Acad. Sci. U. S. A.* **2010,** *107* (29), 12850-12853.

(21) Lu, Q.; Oh, D. X.; Lee, Y.; Jho, Y.; Hwang, D. S.; Zeng, H. Nanomechanics of Cation–π Interactions in Aqueous Solution. *Angew. Chem. Int. Ed.* **2013,** *52* (14), 3944-3948.

(22) Faghihnejad, A.; Zeng, H. Hydrophobic interactions between polymer surfaces: using polystyrene as a model system. *Soft Matter* **2012,** *8* (9), 2746.

(23) Israelachvili, J. N. Thin film studies using multiple-beam interferometry. *J. Colloid Interface Sci.* **1973,** *44* (2), 259-272.

(24) Israelachvili, J. N. Chapter 12 - Force-Measuring Techniques. In *Intermolecular and Surface Forces (Third Edition)*; Israelachvili, J. N., Ed.; Academic Press: Boston, 2011; pp 223-252.

(25) Israelachvili, J. N. Chapter 13 - Van der Waals Forces between Particles and Surfaces. In *Intermolecular and Surface Forces (Third Edition)*; Israelachvili, J. N., Ed.; Academic Press: San Diego, 2011; pp 253-289.

(26) Lu, Q.; Huang, J.; Maan, O.; Liu, Y.; Zeng, H. Probing molecular interaction mechanisms of organic fouling on polyamide membrane using a surface forces apparatus: Implication for wastewater treatment. *Sci. Total Environ.* **2018,** *622-623*, 644-654.

CHAPTER 3 Injectable, Self-Healing Hydrogel with Tunable Optical, Mechanical, and Antimicrobial Properties

3.1 Introduction

Hydrogels are three-dimensional crosslinked polymeric networks with high water content which have great similarities to natural extracellular matrix (ECM) and have been widely applied in biomedical applications including drug delivery, tissue engineering, wound dressing, etc.[1-3] However, the conventional pre-formed hydrogels or scaffolds face the problem of invasive surgical implantation, increasing the risk of infections and improper adaption to the defect site, which could lead to the scaffold failure.[4] Injectable hydrogels have attracted great research interests over the past decade due to their ease of operation, complete filling of the defect area and minimum tissue invasion.[5-6] Nevertheless, subjected to constant mechanical forces from daily body movement, implanted hydrogels could easily be deformed or damaged. The deformation or destruction of the implanted hydrogels would not only cause the failure of tissue regeneration due to the microorganism invasion but also could lead to the sacrifice of the functionalities of the hydrogels resulting from the loss of structural integrity. To address the issue, fabricating hydrogels with self-healing property could prolong the lifetime as well as increase the reliability and durability of the implanted hydrogels.

Generally, non-covalent interactions (e.g., hydrogen bonding,[7] hydrophobic interaction[8] and host-guest interaction[9]) and dynamic covalent chemistry (e.g., phenylboronic ester complexation,[10-11] disulfide bond,[12] dynamic Schiff base[13-14] and Diels-Alder reaction[15]) are two approaches commonly adopted to construct self-healing hydrogels. Dynamic Schiff base reaction, which refers to the reversible reaction between aldehyde (-CH=O) and amine ($-NH_2$) reactants, has been studied in self-healing hydrogels for a wide range of biomedical applications including blood

capillary formation,[16] central nervous system repair,[17] and wound healing.[18-19] In most of previous studies, the self-healing hydrogels are prepared by amine-containing or aldehyde-functionalized natural polymers such as chitosan, cellulose and alginate.[20-22] However, natural polymers are difficult to be tuned in terms of structure and functionalities, which may not satisfy different requirements in diverse biomedical processes.[23-24]

Soaked in complex body fluid environment, injectable hydrogels often associate with the issue of microbial infections caused by pathogenic bacteria.[25] To tackle the obstacle, several approaches have been adopted to endow the hydrogel with antimicrobial property, such as the releasing of antibiotics, the incorporation of silver nanoparticles, the conjugation of antimicrobial peptides and the inclusion of cationic polymers into the hydrogel network through cross-linking or copolymerization.[26-30] Sensitivity to temperature and pH responsiveness is another desired feature for "smart" hydrogels since it can not only fine-tune the properties of the hydrogel, but also potentially achieve controlled release of therapeutics, detection of biomolecules and actuation of muscle.[31-33] Using functional synthetic polymers to fabricate hydrogels, both antimicrobial and multi-stimuli-responsive properties can be obtained. Nevertheless, randomly sequenced copolymers would exhibit the properties deviating from the homopolymers of each kind of monomer distinctively, especially for the thermoresponsive polymers whose lower critical solution temperature (LCST) is dependent on the ratio of hydrophobic/hydrophilic components.[34-35] Therefore, the precise design of polymer sequence is crucial for maximizing the effect from individual polymer segment. It has been reported that ABA triblock copolymers could be used to prepare thermoresponsive injectable self-healing hydrogels through non-covalent interactions.[36-38] However, the study on injectable self-healing hydrogels with tunable mechanical and optical

properties as well as antimicrobial ability, which are fabricated by functional synthetic ABA triblock copolymers through dynamic covalent chemistry is limited.

Herein, we report a new injectable self-healing hydrogel with tunable optical and mechanical properties along with the excellent antimicrobial capability, fabricated by a multifunctional ABA triblock copolymer gelator (**Figure 3.1**). The ABA triblock copolymer poly{(4-formylphenyl methacrylate)-*co*-[[2-(methacryloyloxy)ethyl] trimethylammonium chloride]}-*b*-poly(N-isopropylacrylamide)-*b*-poly{(4-formylphenyl methacrylate)-*co*-[[2-(methacryloyloxy)ethyl] trimethylammonium chloride]} (PFMNMF), was synthesized via two-step reversible addition-fragmentation chain-transfer **(**RAFT) polymerization. The ABA triblock copolymer gelator could form injectable and self-healing hydrogel with branched polyethylenimine (PEI) in a facile mixing process due to the formation of dynamic Schiff base. The hydrogel could not only respond to pH change but also show altered optical and mechanical properties in a sensitive temperature responsive manner compared to the hydrogel fabricated by the random copolymer gelator, poly{(4-formylphenyl methacrylate)-*co*-[[2-(methacryloyloxy)ethyl] trimethyl-ammonium chloride]-*co*-(*N*-isopropylacrylamide)} (PFMN). In addition, the hydrogel could effectively inhibit the growth of both Gram-negative and Gram-positive bacteria (*E. coli* and *S. aureus*), while showing low cytotoxicity to both fibroblast and cancer cells (MRC-5 and HeLa). Combining all these features, the novel multifunctional hydrogels show great potential in various bioengineering applications.

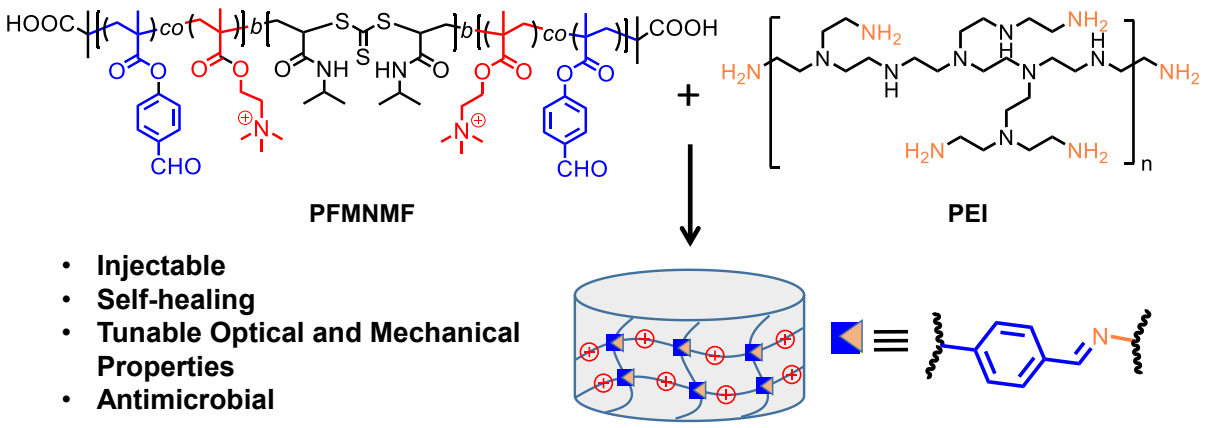

Figure 3.1. Schematic Illustration of Injectable Self-healing Hydrogel with Tunable Optical, Mechanical and Antimicrobial Properties Fabricated by PFMNMF and PEI.

3.2 Experimental Methods

3.2.1 Materials

4-formylphenyl methacrylate (FPMA) and 2-(1-carboxy methylethylsulfanylthiocarbonylsulfanyl)-2-methylpropionic acid were synthesized as previously reported.[39-40] [2-(Methacryloyloxy)ethyl] trimethylammonium chloride solution (META, 80 wt% in H_2O, stabilized with 600 ppm MEHQ), *N*-Isopropylacrylamide (NIPAM, 97%), 4,4′-Azobis(4-cyanovaleric acid) (ACVA, 98%) and branched polyethylenimine (PEI, M_w ~ 25,000) were purchased from Sigma-Aldrich. Organic solvents were purchased from Caledon Laboratories Ltd. (Canada) and used without further purification.

3.2.2 Polymer Synthesis

Poly{(4-formylphenyl methacrylate)-co-[[2-(methacryloyloxy)ethyl] trimethylammonium chloride]} Macro-CTA (PFM). The macro-CTA, PFM was synthesized by RAFT polymerization using 2-(1-carboxy methylethylsulfanylthiocarbonylsulfanyl)-2-methylpropionic acid as chain transfer agent (CTA) and ACVA as initiator. Briefly, a 50 mL polymerization tube was charged with FPMA (190 mg, 1 mmol), META chloride solution (2.2 mL, 9 mmol), CTA (28.2 mg, 0.1

mmol) and ACVA (5.6 mg, 0.02 mmol). The reagents were then dissolved in a mixed solvent of DI water and dimethylformamide (DMF). After degassing with nitrogen for 30 min, the polymerization was carried out in an oil bath at 70 °C for 24 h. The reaction was then quenched in liquid nitrogen, and the polymer was obtained by precipitation in acetone. The product was further washed with acetone to remove residual monomers and CTA and yield as white solid. Molecular weight and molecular weight distribution (PDI) were determined by gel permeation chromatography (GPC) (Viscotek model 250 dual detectors system), using 0.5 M sodium acetate/0.5 M acetic acid buffer as eluent at a flow rate of 1.0 mL/min.[41] ^{1}H NMR spectrum of the product was recorded on a Varian 500 MHz spectrometer at room temperature using D_2O as solvent. Chemical shifts are reported in parts per million (δ) relative to TMS as the internal reference.

Poly{(4-formylphenyl methacrylate)-co-[[2-(methacryloyloxy)ethyl] trimethylammonium chloride]}-b-poly(N-isopropylacrylamide)-b-poly{(4-formylphenyl methacrylate)-co-[[2-(methacryloyloxy)ethyl] trimethylammonium chloride]} ABA Triblock Copolymer (PFMNMF). PFMNMF ABA triblock copolymer was synthesized by RAFT polymerization using PFM as macro-CTA and ACVA as initiator. For a typical synthesis, a 50 mL polymerization tube was charged with NIPAM (339 mg, 3 mmol) and PFM macro-CTA (645 mg). The reagents were then dissolved in a mixed solvent of DI water and DMF, followed by adding 0.1 mL of ACVA DMF stock solution (6 mg/mL) to the mixture. After degassing with nitrogen for 30 min, the polymerization was carried out in an oil bath at 70 °C for 24 h. The reaction was then quenched in liquid nitrogen and the copolymer was precipitated in diethyl ether. The product was further purified by dialysis against DI water for 2 days and obtained as white solid after freeze-dried. ^{1}H NMR spectrum of the product was recorded on a Varian 500 MHz spectrometer at room

temperature using D_2O as solvent. Chemical shifts are reported in parts per million (δ) relative to TMS as the internal reference.

Poly{(4-formylphenyl methacrylate)-co-[[2-(methacryloyloxy)ethyl] trimethylammonium chloride]-co-(N-isopropylacrylamide)} Random Copolymer (PFMN). PFMN random copolymer was synthesized by RAFT polymerization using 2-(1-carboxy methylethylsulfanylthiocarbonylsulfanyl)-2-methylpropionic acid as chain transfer agent (CTA) and ACVA as initiator. For a typical synthesis, a 50 mL polymerization tube was charged with FPMA (47.5 mg, 0.25 mmol), META chloride solution (0.53 mL, 2.25 mmol), NIPAM (848 mg, 7.5 mmol), CTA (7.1 mg, 0.025 mmol) and ACVA (1.4 mg, 0.005 mmol). The reagents were then dissolved in a mixed solvent of DI water and DMF. After degassing with nitrogen for 30 min, the polymerization was carried out in an oil bath at 70 °C for 24 h. The reaction was then quenched in liquid nitrogen and the product was obtained as white solid after purification by dialysis against DI water for 2 days and freeze-drying. The ^1H NMR spectrum of the product was recorded on a Varian 500 MHz spectrometer at room temperature using D_2O as solvent. Chemical shifts are reported in parts per million (δ) relative to TMS as the internal reference. Molecular weight and molecular weight distribution (PDI) were determined by GPC.

3.2.3 Fabrication of the Hydrogels

The hydrogels were prepared by a simple mixing process of PFMNMF and PEI solutions. First, a PEI solution (3%, w/v) was prepared by dissolving PEI (0.30 g) in PBS buffer solution (10 mL, pH 7.4). PFMNMF solutions (12%, 14%, 16%, w/v) were prepared by dissolving the polymer (30 mg, 35 mg, 40 mg) in a PBS buffer solution (0.25 mL, pH 7.4) respectively. As a typical hydrogel preparation, the same volume (0.25 mL) of these two polymer solutions were mixed *via* pipetting. After being mixed, the resultant solution was allowed to keep still and the formation of

the hydrogel was checked by vial inversion method. The hydrogels with three different total polymer concentrations were denoted as Gel-7.5%, Gel-8.5% and Gel-9.5%, respectively. Similar procedure was followed to prepare RGel-9.5% formed by PFMN random copolymer gelator and PEI solutions.

3.2.4 Rheological Characterization of the Hydrogels

A rheometer (TA Instruments, AR-G2) fitted with a Peltier stage using a 20 mm parallel-plate configuration and with a gap of 53 μm was used to characterize both the gelation process and the mechanical properties of the hydrogels. First, the gelation process of the hydrogels with different polymer concentration was studied by dynamic time sweep rheological experiments. Briefly, PFMNMF solution was spread onto the the parallel plates of the rheometer followed by the addition of PEI solution dropwise and uniformly to the surface of PFMNMF solution. The modulus change was measured as a function of time under fixed frequency (ω = 1Hz) and strain (γ = 1%). Then, the equilibrium modulus of the hydrogels with different total polymer concentration was characterized by dynamic oscillatory frequency sweep under fixed frequency (ω = 1Hz) and strain (γ = 1%) at 25 °C. All the samples were prepared and stabilized for 1 hour before testing.

The injectability test of the hydrogel was simulated by extruding Gel-9.5% by a syringe through a 21-G needle. The change in viscosity was measured as a function of shear rate (0.1 s^{-1} to 1000 s^{-1}) by rheometer to study the shear-thinning behavior of the hydrogel.

3.2.5 Self-healing Property and Measuring the Associated Polymer Interactions using SFA

To test the self-healing property of the Gel-9.5%, two pieces of hydrogels were prepared with a trace amount of Rhodamine B (RdB) added in one piece to give a colour difference. Then, the two pieces of hydrogels were brought together and the images at different time intervals were captured to monitor the change in the appearance. Rheological analyses were carried to monitor

the self-healing process at 25 °C and 37 °C respectively.[1, 25] First, dynamic strain sweep was performed on Gel-9.5% to determine the linear viscoelastic region and the critical strain at constant frequency (ω = 1 Hz). The critical strain value was defined as the crossover point of *G'* and *G"*. Afterwards, dynamic cyclic strain tests were carried out on Gel-9.5% to monitor the modulus change of the hydrogel under alternately changing strain (γ = 1% and γ = 200%) at constant frequency (ω = 1 Hz).

A Surface Forces Apparatus (SFA) was used to quantitatively probe the interaction forces between PFMNMF and PEI which account for the self-healing property of the hydrogel. The detailed experimental setup for SFA measurements have been reported previously.[42-45] Briefly, in a typical force measurement, two back-silvered mica surfaces (1-5 μm) were glued onto two cylindrical silica disks ($R \approx 2$ cm). The mica surfaces were then coated with PFMNMF solution (10 μg/mL) or PEI solution (10 μg/mL) for 15 min, followed by a thorough rinsing with PBS buffer solution in order to remove unbound or loosely bounded polymers. Then, the two surfaces were mounted into the SFA chamber in a cross-cylinder configuration and the SFA chamber was saturated with water vapor. 100 μl of PBS buffer solution (pH 7.4) was injected between the two mica surfaces. The force measurement was conducted by bringing two surfaces to contact followed by separation. The interaction forces *F(D)* was monitored as a function of absolute surface separation distance *D* in real-time using multiple beam interferometry (MBI) by employing fringes of equal chromatic order (FECO).[46-47] For each condition, force-distance profiles was measured at least two different interaction positions on a set of surfaces and using two sets of independently prepared surfaces to confirm the reproducibility. In addition, the surfaces were approached to contact and then kept in contact for different duration time (i.e., 5 min, 10 min, 30 min and 60 min)

followed by separation to study the effect of contact time on the interaction forces. The measured adhesion or "pull-off" force F_{ad} and adhesion energy W_{ad} are correlated by eq 1:[48]

$$F_{ad} = \frac{3}{2}\pi R W_{ad} \tag{1}$$

3.2.6 Temperature and pH Responsive Properties of the Hydrogel

The volume phase transition temperature (VPTT) of the Gel-7.5%, Gel-8.5% and Gel-9.5% was determined by an optical absorption spectrometer (TECAN GENios Pro, Mainz, Germany). Briefly, the hydrogels (200 μL) were loaded into a 96-well plate and an average absorbance was measured at different temperature, ranging from 25 to 40 °C, with a 1 °C temperature increase every 5 min. VPTT was defined as the temperature at which 50% of the maximum transmission change was observed. Besides, Gel-9.5% was put in a water bath at 37 °C to monitor the change of transparency and the change of the transparency was captured by images. Additionally, dynamic oscillatory frequency sweep was performed on Gel-9.5% at different temperature (25 and 37 °C) under fixed strain (γ = 1%) to determine whether the modulus of the hydrogel changes with temperature in a responsive manner. As a control, the thermoresponsive property of RGel-9.5% was characterized following the same procedure. The topography images of PFMNMF and PFMN surfaces were obtained in air using a Bruker ICON atomic force microscope (AFM) system (Bruker, Santa Barbara, CA) operated in tapping mode. The samples for AFM imaging were prepared by depositing one drop of PFMNMF or PFMN polymer solution (100 μg/mL) onto a cleaned silica substrate, followed by drying the polymer film in air at 25 or 37 °C.[49]

For the pH responsiveness test, a trace amount of RdB was added to Gel-9.5% for better observation. Concentrated HCl solution (10 μL, 5M) was added to the hydrogel followed by shaking. After the hydrogel was completely liquefied, the pH of the solution was measured. Then, concentrated NaOH solution (10 μL, 5M) was added to regenerate the hydrogel, followed by pH

measurement. The process was repeated for 2 cycles and the reversible sol-gel transitions were captured by images.

The pH-dependent hydrolytic degradation behavior of Gel-9.5% was assessed. Briefly, the hydrogels were prepared in 1.5mL centrifuge tubes. Then the hydrogels were immersed in PBS buffer (pH 7.4 or 5.4) at 37 °C, respectively. At designed time point, the hydrogels were taken out and carefully wiped with filter paper to remove excess water, then weighted. The weight remaining ratio of hydrogels was calculated by eq 2:

$$\text{Weight remaining ratio } \% = \frac{W_t}{W_i} * 100\% \quad (2)$$

where W_t is the weight of remaining hydrogels after degradation at different time intervals and W_i is the weight of initial hydrogels.

The porous morphology of the remaining Gel-9.5% was characterized by field emission scanning electron microscopy (FESEM, Zeiss Sigma 300/VP). The hydrogels were freeze-dried and sputter-coated with gold to provide a conductive environment prior to SEM characterization. Additionally, SFA was used to quantitatively study the pH effect (7.4, 6.4 and 5.4) on the interaction forces between PEI and PFMNMF.

3.2.7 Antimicrobial Assay and Cell Cytotoxicity

Escherichia coli (ATCC®25922™) (Gram-negative bacteria) and *Staphylococcus aureus* (ATCC®25923™) (Gram-positive bacteria) were selected as the model bacteria. The culture medium (Luria-Bertani broth (LB) for *E. coli* and tryptic soy broth (TSB) for *S. aureus*) and bacterial suspension (*E. coli* and *S. aureus* suspension) were prepared as reported previously.[25] The hydrogels (Gel-9.5%) used for antimicrobial assessment were prepared by adding equal volume (35 μL) of PFMNMF and PEI solutions into each well of a 96-well plate followed by rinsing the hydrogels culture medium (LB or TSB) three times to remove any uncrosslinked

polymers. Then, a ten-fold serial dilution of the *E. coli* or *S. aureus* suspension was made and 100 μL of the dilution was added into each well with the hydrogel sample. The 96-well plate was incubated at 37 °C for 24 h. The 96-well plate was left at room temperature for 10 min and 50 μL of the suspension was transferred into a new 96-well plate. The optical density at 600 nm ($OD_{600\ nm}$) was measured by an optical absorption spectrometer. The culture medium (LB or TSB) and the bacterial suspension (*E. coli* or *S. aureus* suspension) without hydrogel served as the blank and the negative control respectively. The inhibition efficiency was calculated by eq 3:[50]

$$\text{Inhibition Efficiency (\%)} = \left(1 - \frac{OD_{600nm,sample} - OD_{600nm,blank}}{OD_{600nm,control} - OD_{600nm,blank}}\right) * 100 \quad (3)$$

Gel extracts of Gel-9.5% were used to examine the biocompatibility of the hydrogel by MTT assay. In brief, Gel-9.5% was incubated in DMEM medium for 24 h. MRC-5 fibroblast cells and HeLa cancer cells were seeded onto a 96-well plate at a density of 6000 cells per well with 100 μL of DMEM medium. After incubation of the cells for 24 h, the culture media were replaced by 100 μL of fresh DMEM media or DMEM media containing the gel extracts. The cells were allowed to be further incubated for 24 h before the addition of 15 μL of MTT solution (5mg/mL). After 3 h of incubation, the media were carefully removed and DMSO was added to dissolve the formazan crystals. The optical density at 570 nm ($OD_{570\ nm}$) was measured by an optical absorption spectrometer and the cell viability was calculated by comparing OD_{570nm} of cells treated with/without gel extracts.

3.3 Results and Discussions

3.3.1 Synthesis of Polymers

FPMA and 2-(1-carboxy methylethylsulfanylthiocarbonylsulfanyl)-2-methylpropionic acid were first synthesized as previously reported and characterized by ^{1}H NMR (**Figures S3.1 and S3.2 in Supporting Information**). PFM macro-CTA, PFMNMF ABA triblock copolymer and

PFMN random copolymer were synthesized by RAFT polymerization and characterized by ^{1}H NMR spectroscopy and GPC. PFMNMF ABA triblock copolymer was prepared by a two-step RAFT polymerization as illustrated in **Figure 3.2a**. The successful synthesis of PFM macro-CTA (PDI = 1.08) was confirmed by the characteristic peaks (δ_H (ppm) = 9.98, 8.08, 7.50) and (δ_H (ppm) = 3.33) found in the ^{1}H NMR data (**Figure 3.3a**), which correspond to the benzaldehyde groups of FPMA and the quaternary ammonium groups of META respectively. Then, PFMNMF ABA triblock copolymer was synthesized by RAFT polymerization using PFM as the macro-CTA. Due to the poor solubility in organic solvents resulting from the positively charged quaternary ammonium pendent groups and the polymer aggregation caused by the sensitive thermoresponsive property of the ABA triblock copolymer in aqueous solution, the ABA triblock copolymer could not be characterized by GPC. However, from the ^{1}H NMR data shown in **Figure 3.3b**, the characteristic peaks (δ_H (ppm) = 3.91, 1.18) corresponding to the isopropyl groups of PNIPAM were clearly observed in ABA triblock copolymer which indicates the successful synthesis. The composition of PFMFNF was determined as FPMA/META/NIPAM = 2/29/69 from the ^{1}H NMR spectrum.

PFMN random copolymer (PDI = 1.25) was synthesized to study the effect of polymer architecture on the properties of the hydrogels as illustrated in **Figure 3.2b**. The success of the synthesis was determined by the characteristic peaks observed in the ^{1}H NMR spectrum (**Figure S3.3 in Supporting Information**). The composition of PFMN was determined as FPMA/META/NIPAM = 3/24/73 from the ^{1}H NMR spectrum.

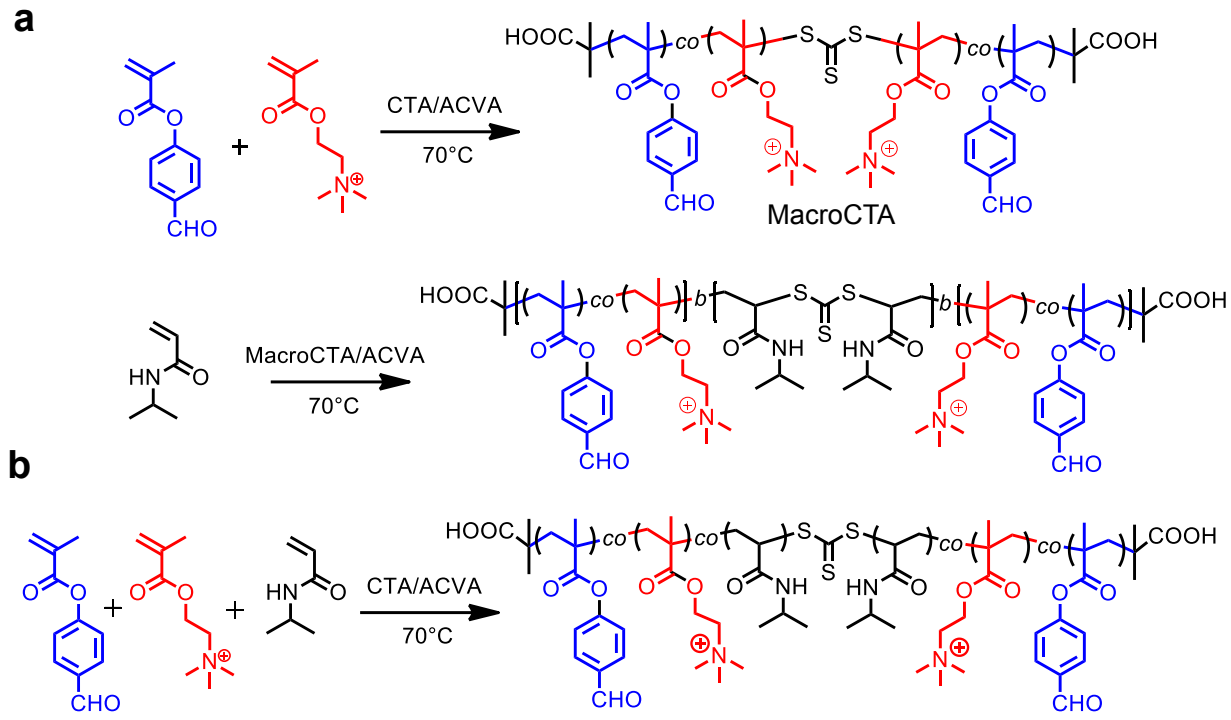

Figure 3.2. Synthesis Route of (a) PFMNMF ABA Triblock Copolymer and (b) PFMN Random Copolymer.

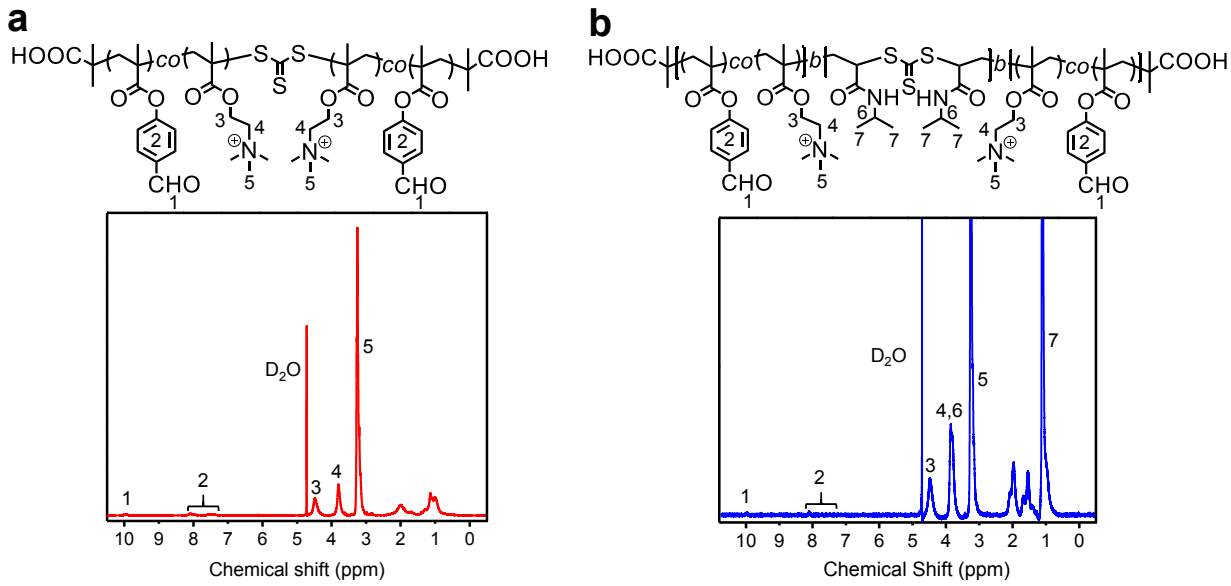

Figure 3.3. [1]H NMR spectra of (a) PFM macro-CTA and (b) PFMNMF ABA triblock copolymer.

3.3.2 Fabrication and Rheology Characterization of the Hydrogel

The hydrogels were formed after a simple mixing process of PEI solution (3%, w/v) with PFMNMF ABA triblock copolymer solutions (12%, 14%, 16%, w/v) to yield homogeneous transparent hydrogels with different polymer concentration, denoted as Gel-7.5%, Gel-8.5% and Gel-9.5% respectively. The hydrogels were formed in less than 30 sec by vial inversion tests. The rapid construction of the hydrogel network is due to the fast formation of imine bonds between benzaldehyde and amine groups. The gelation process was monitored by dynamic time sweep rheological experiments (**Figure 3.4a**). Typically, after the addition of PEI solution to the PFMNMF solution, both the storage modulus (*G'*) and loss modulus (*G"*) gradually increased and *G'* surpassed *G"* within 30 sec, indicating the formation of hydrogel network. The hydrogel with the highest total polymer concentration (Gel-9.5%) exhibited the fastest increase of *G'* during the early stage of hydrogel formation, which suggests that the gelation process was highly dependent on the total polymer concentration as a result of its significant impact on the cross-linking reaction rate.

The equilibrium modulus of the hydrogels were studied by dynamic oscillatory frequency sweep rheological experiments (**Figure 3.4b**). It was observed that *G'* was consistently greater than *G"* for all hydrogels and the value of *G'* remained unchanged regardless of the frequency change, indicating the elastic behavior of the hydrogels. In contrast, *G"* changed depending on frequency. The mechanical properties of the as-prepared hydrogels are different from the covalently cross-linked hydrogels with both constant *G'* and *G"*, which may be attributed to the dynamic nature of the hydrogel network as reported previously. In addition, as shown in Figure 2b, *G'* strongly depends on the total polymer concentration and it increased from 320 Pa to 1100 Pa with an increase of the total polymer concentration from (7.5%, w/v) to (9.5%, w/v) as a result

of the formation of much denser hydrogel networks. It is noted that the *G'* values of the hydrogels at the initial stage of hydrogel formation are lower than those for the equilibrated hydrogels of the same concentrations. The difference in the *G'* values is most likely attributed to (1) the insufficient mixing condition of the polymer solutions (in between parallel plates with diameter of 20 mm and gap of 53 μm of the rheometer)[20] and (2) the tests at the early stage of hydrogel formation in Figure 2(a).[21, 51] The mechanical properties of ECM plays an important role in a series of biological activities.[52-53] Therefore, the as-prepared hydrogels with tunable mechanical properties are desired for various biomedical applications, such as cell culture and tissue engineering.

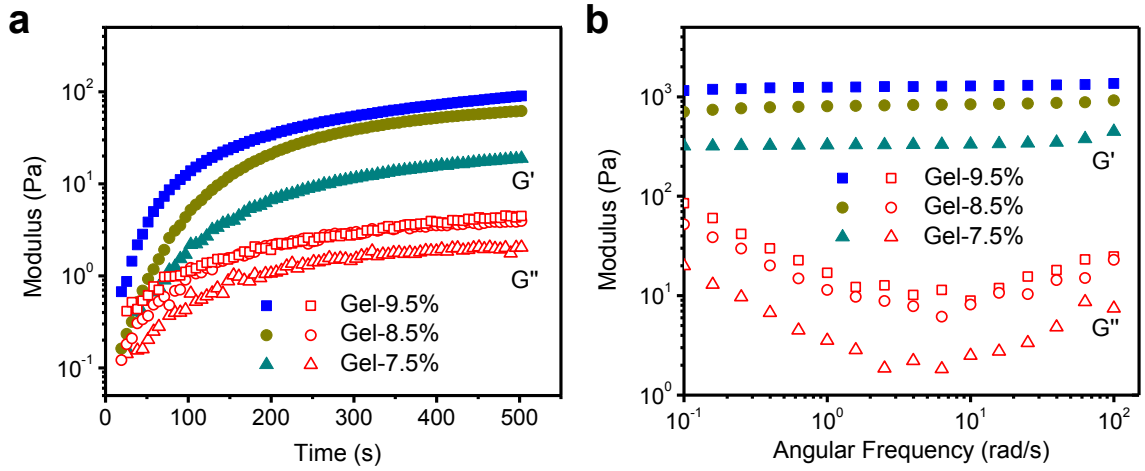

Figure 3.4. (a) Gelation process of the hydrogels at 25 °C. (b) Dynamic oscillatory frequency sweeps of the hydrogels (γ = 1%, ω = 1 Hz).

Hydrogels with injectable property can offer advantages, such as ease of operation, minimum tissue invasion, when they are used as implanted biomaterials. Gel-9.5% was used to demonstrate the injectable property of the hydrogels. As shown in **Figure 3.5a**, Gel-9.5% with a trace of RdB could be easily extruded through a 21-G needle. Moreover, the continuously extruded hydrogel could serve as ink to write typical letters of "U of A" as illustrated in **Figure 3.5b**, indicating the great potential of this novel hydrogel to be used for 3D bio-printing applications. Besides, the

viscosity of Gel-9.5% was quantitatively measured as a function of shear rate as shown in Figure **3.5c**. The viscosity decreased dramatically as the shear rate increased, which verified the shear-thinning behavior of a typical injectable hydrogel.[6]

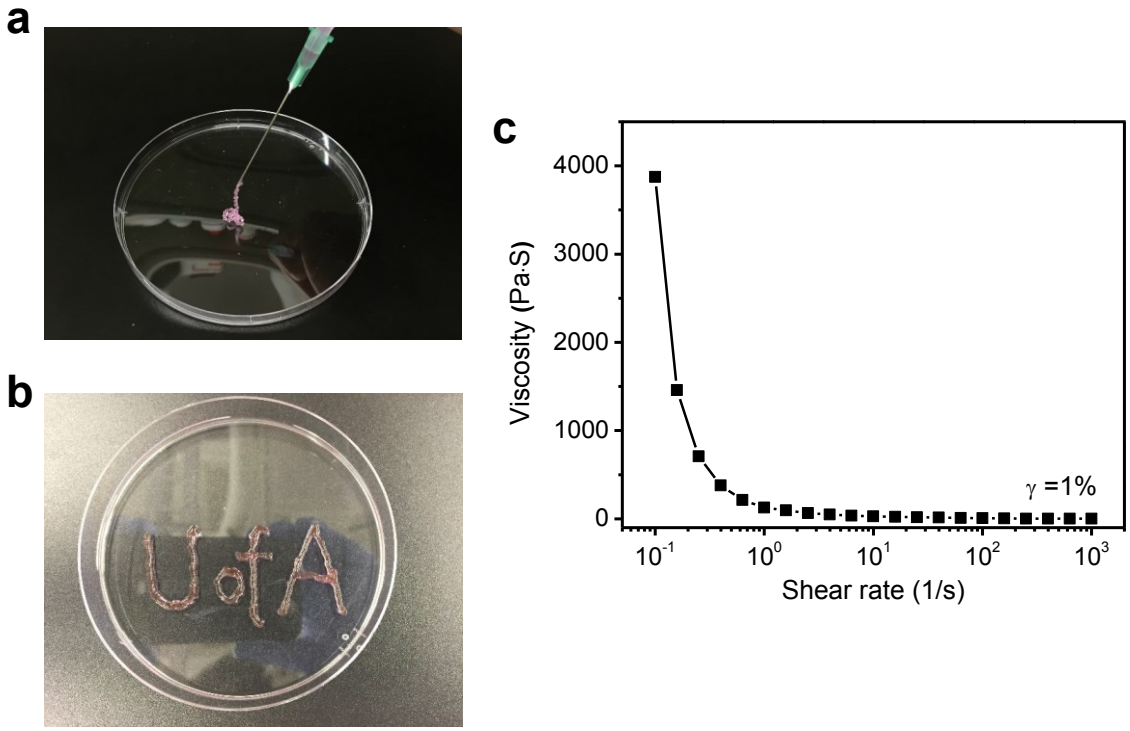

Figure 3.5. Injectable property of Gel-9.5%. (a) Extrusion of hydrogel through a 21-G needle. (b) Writing "U of A" by using Gel-9.5% as ink. (c) Viscosity of Gel-9.5% measured as a function of shear rate.

3.3.3 Self-healing Property and Associated Polymer Interaction Mechanism

It is important for the hydrogels used in bioengineering to have autonomously self-healing capability to recover form inflicted damage and maintain both structural and functional integrity. To demonstrate the self-healing property of the hydrogels, two pieces of Gel-9.5% hydrogels (one of them dyed with RdB) were prepared and brought together. As shown in **Figure 3.6a**, after two pieces of hydrogels were kept in intimate contact for 30 min at room temperature without external intervention, two pieces of hydrogels merged into one united piece and the interface between two

pieces completely disappeared. The excellent self-healing ability is attributed to the reversible formation of dynamic Schiff base across the interface of two pieces of hydrogels. The self-healing property of Gel-9.5% was studied by rheological analyses at 25 °C and 37 °C respectively. Dynamic strain sweep test (γ = 0.1% to 1000%) was first performed on Gel-9.5% to determine the linear viscoelastic region and the critical strain value for the gel-sol transition. As shown in **Figure 3.6b**, beyond the linear viscoelastic region, *G"* decreased dramatically above the critical strain value (γ = 100%), which indicates the destruction of the hydrogel network. Afterwards, dynamic cyclic strain sweep tests (γ = 1% or 200%) were conducted on Gel-9.5%. When a large strain of 200% was applied, the *G'* value decreased significantly from 1000 Pa to 100 Pa and the *G"* value exceeded the *G'* value as observed in **Figure 3.6c**, which suggests the collapse and the liquid-like behavior of the hydrogel. However, the *G'* value could almost recover to its initial value in 60s when a small strain of 1% was applied, indicating the re-construction of the hydrogel. Moreover, such recovery behavior was reproducible for multiple cycles. Similar self-healing behavior was verified at 37 °C (body temperature) (**Figure S3.4a and S3.4b in Supporting Information**). Such reproducible recovery behavior is highly desired in practical biomedical applications.

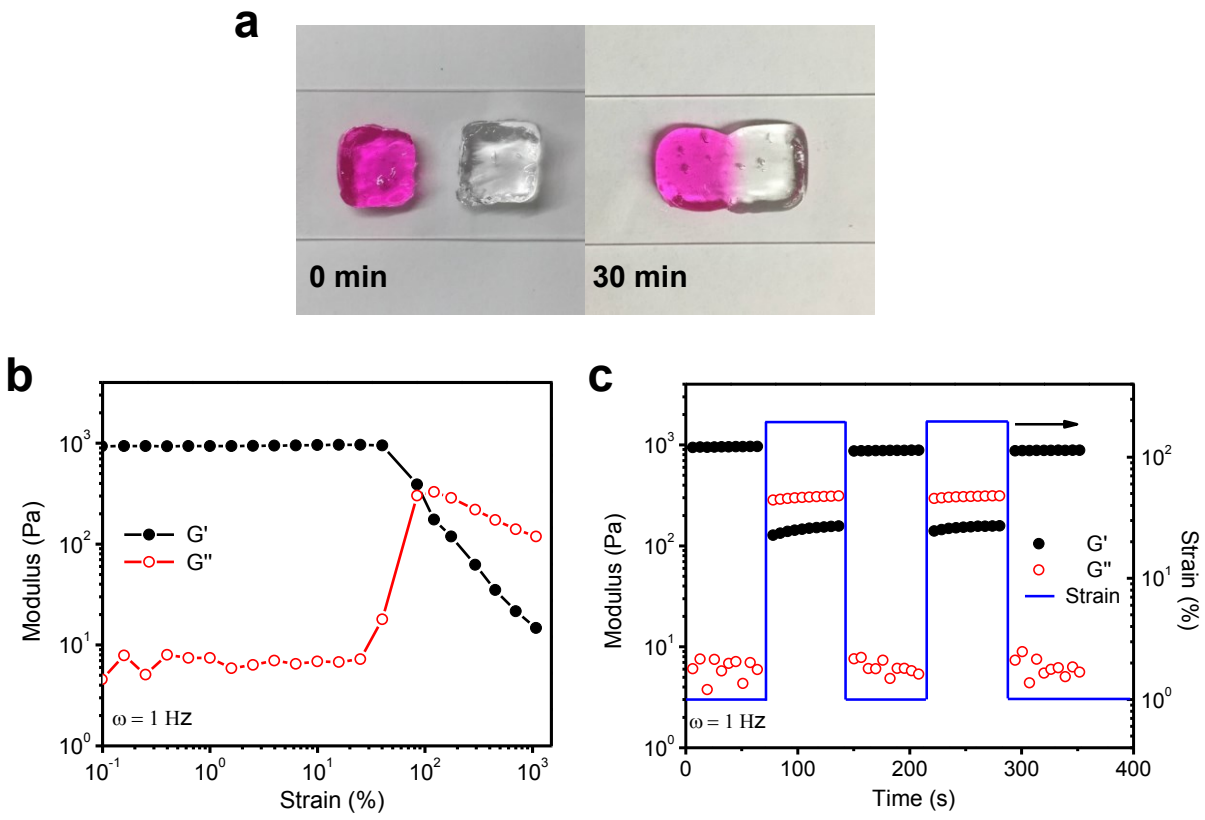

Figure 3.6. (a) Demonstration of self-healing property of Gel-9.5%. (b) Dynamic strain sweep measurement of Gel-9.5% at 25 °C (ω = 1 Hz). (c) Dynamic cyclic strain sweep measurement of Gel-9.5% at 25 °C (ω = 1 Hz, γ = 1% or 200%).

The fundamental study of the self-healing mechanism at molecular-scale and nano-scale is crucial for the comprehensive understanding of the self-healing property of the hydrogel.[54] In this work, a Surface Forces Apparatus (SFA) was employed for the *first* time to quantitatively probe the molecular interactions between PEI and PFMNMF ABA triblock copolymer, which account for the self-healing property of the hydrogels. An asymmetric configuration was adopted for SFA setup (**Figure S3.5 in Supporting Information**). The interaction forces between PEI-coated surface and PFMNMF copolymer-coated surface were first investigated in PBS buffer solution at pH 7.4. As shown in **Figure 3.7a**, an adhesion $F_{ad}/R \sim 6.0$ mN/m ($W_{ad} \sim 1.3$ mJ/m^2) was observed

between two surfaces. The adhesion is originated from the partially formed dynamic imine bonds between PEI and PFMNMF copolymer across the two surfaces. Moreover, the adhesion of the same magnitude was probed in sequential approach-separation force measurement, indicating the reversible nature of the dynamic Schiff base chemistry.[55] Since the self-healing process of the hydrogel is time dependent, the effect of contact time on the interaction forces between two polymers was studied in PBS buffer solution at pH 7.4. As shown in the force curves and the adhesion histograms in **Figure 3.7b and 3.7c**, the adhesion force (energy) exhibited an increase from $F_{ad}/R \sim 9.8$ mN/m ($W_{ad} \sim 2.1$ mJ/m^2) to $F_{ad}/R \sim 11.2$ mN/m ($W_{ad} \sim 2.38$ mJ/m^2) as the contact time increased from 5 min to 10 min and it further increased to $F_{ad}/R \sim 14.0$ mN/m ($W_{ad} \sim 3.0$ mJ/m^2) as the contact time increased to 30 min. The increase of adhesion force (energy) is attributed to the higher number of the dynamic imine bonds formed across the two surfaces as a result of longer contact time. Furthermore, the adhesion force (energy) reached a plateau at the 30 min contact time, indicating the equilibrium state of the reaction between the benzaldehyde groups and the amine groups across the two surfaces. The results of the nanomechanics experiments not only well agreed with the demonstrated self-healing capability of the as-prepared hydrogel but also provided insights at nanoscale into the self-healing mechanism.

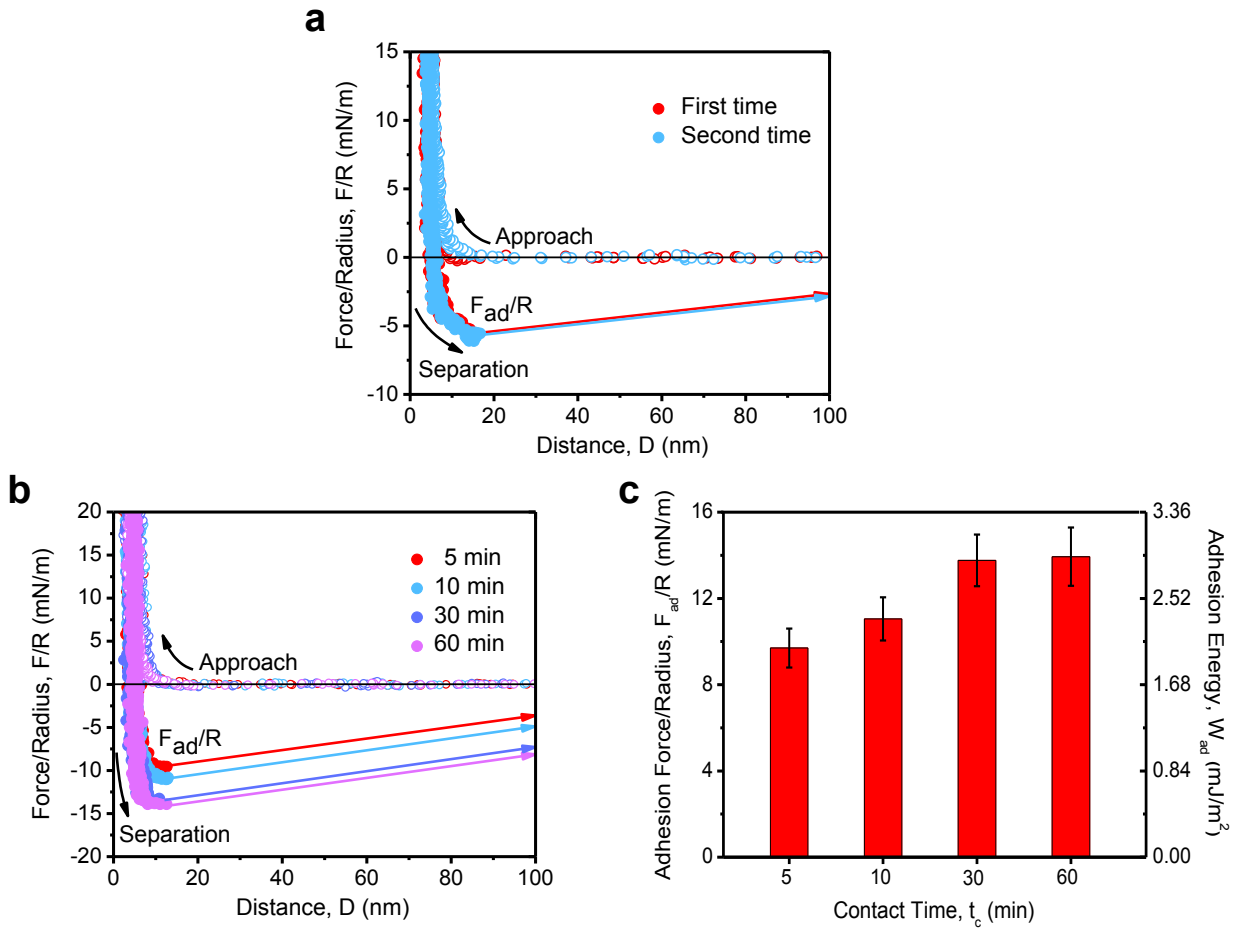

Figure 3.7. (a) Force-distance profiles show the force magnitudes and reversibility of the dynamic imine bonds formed between PEI and PFMNMF in PBS buffer solution (pH 7.4). (b) Force-distance profiles show the effect of contact time on the interaction forces between PEI and PFMNMF in PBS buffer solution (pH 7.4). (c) Normalized adhesion force and energy between PEI-coated and PFMNMF-coated mica surfaces in PBS buffer solution (pH 7.4) with different contact time.

3.3.4 Temperature and pH Responsive Properties of the Hydrogel

The volume phase transition temperature (VPTT) is a key parameter for temperature responsive hydrogels to be used under physiological conditions. All three hydrogels fabricated with ABA triblock copolymer exhibited a sharp VPTT at 32 °C (**Figure S3.6 in Supporting**

Information), which shares the same value with the LCST of the PNIPAM homopolymer in aqueous solution.[35] The results indicate that the precise sequence design of the thermoresponsive segment in hydrogel network could not only endow the hydrogel with rapid temperature responsiveness but also could avoid the deviation of the VPTT when the hydrophobic/hydrophilic ratio of the polymer within the network is changed, which is a common but undesired issue in the fabrication of temperature responsive hydrogels.[56-57] Gel-9.5% was used to further demonstrate the sensitive temperature responsive property of the hydrogels. As shown in **Figure 3.8a and 3.8b**, a sharp transparency change was observed when Gel-9.5% was heated to 37 °C, which results from the phase transition of the PNIPAM central block of the ABA triblock copolymer. In contrast, RGel-9.5% did not exhibit such rapid temperature responsiveness (**Figure S3.7a and S3.7b in Supporting Information**).

The mechanical properties of the hydrogels also varied with temperature in a responsive manner. As shown in **Figure 3.8c**, *G'* value of Gel-9.5% increased from ~ 1000 Pa to ~ 2500 Pa as the temperature increased from 25 °C to 37 °C. The enhancement of the mechanical strength is attributed to the nano-hydrophobic domains formed locally within the network upon heating, which serve as the temporary cross-linking points and lead to a denser hydrogel network.[8, 58] The formation of nano-hydrophobic domains was confirmed by AFM topography images of PFMNMF surface. As shown in **Figure 3.8d and 3.8e**, PFMNMF ABA triblock copolymer tended to form aggregation at 37 °C and the surface roughness increased from 0.43 nm at 25 °C to 27.0 nm at 37 °C. As a comparison, the mechanical strength of RGel-9.5% did not exhibit such temperature responsiveness (**Figure S3.8 in Supporting Information**) as well as the corresponding topography images of PFMN surface (**Figure S3.9a and S3.9b in Supporting Information**). The

results reveal the important role of polymer architecture in regulating the mechanical strength of temperature responsive hydrogels, which is crucial for a wide range of biomedical applications.

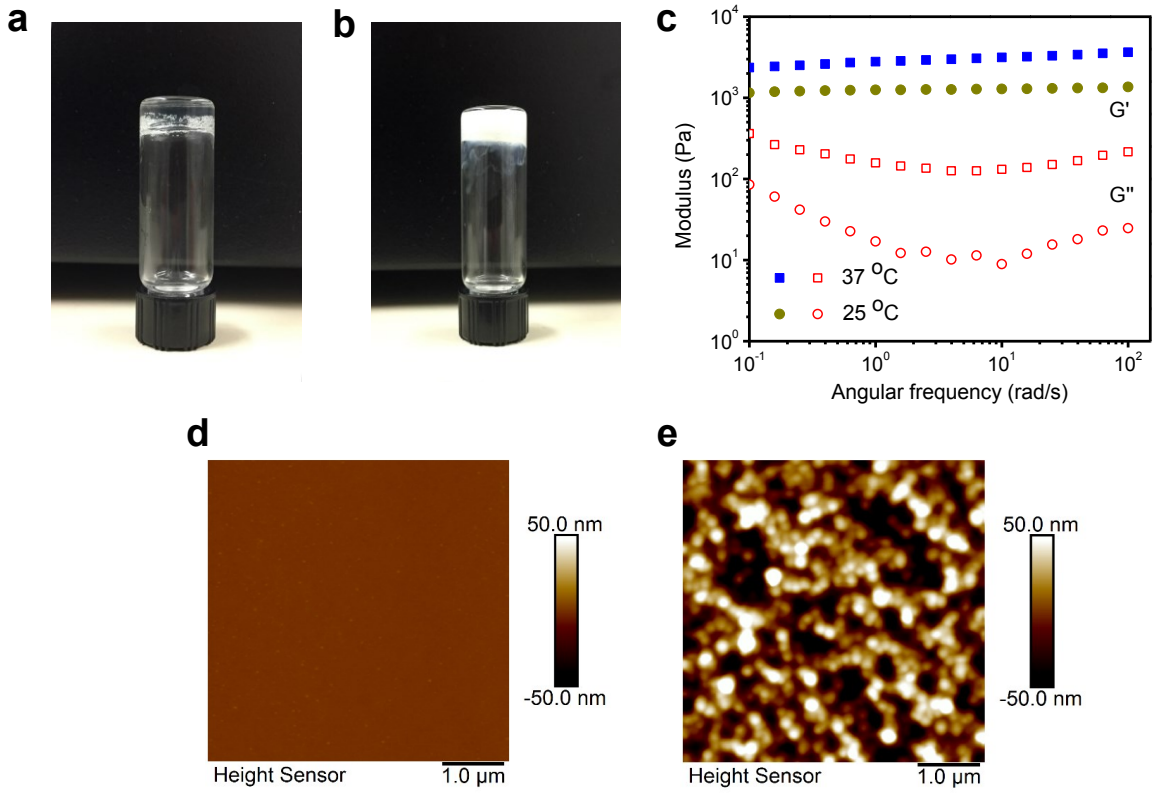

Figure 3.8. Transparency change of Gel-9.5% (a) 25 °C. (b) 37 °C. (c) Modulus change of Gel-9.5% at 25 °C and 37 °C (γ = 1%, ω = 1 Hz). AFM topography images of PFMNMF (d) 25 °C. (e) 37 °C.

The formation of dynamic Schiff base is well-known to be pH dependent as the imine bonds are sensitive to hydrolysis under acidic conditions.[20] As shown in **Figure 3.9a**, upon the addition of concentrated HCl aqueous solution (10 μL, 5M), Gel-9.5% was rapidly decomposed into liquid (pH was measured ~3), indicating the complete hydrolysis of the dynamic imine bonds formed between the benzaldehyde groups of PFMNMF and the amine groups of PEI. However, the hydrogel can be slowly regenerated after the addition of concentrated NaOH aqueous solution (10

μL, 5M) to neutralize the acid (pH was measured ~6). Such gel-sol-gel transitions can be repeated for several cycles, indicating the excellent reversibility of the dynamic hydrogel.

The degradation profile of Gel-9.5% showed that 63% of the hydrogel was left in pH 7.4 PBS buffer solution and only ~20% of the hydrogel was left in pH 5.4 PBS buffer solution after 24h (**Figure 3.9b**). The hydrogel can be degraded much more rapidly in acidic environment than in physiological environment due to the faster hydrolysis of the dynamic imine bonds in acidic condition. The morphology of the remaining hydrogels was observed by SEM (**Figure S3.10a and S3.10b in Supporting Information**). A looser structure with less polymers between the pores was observed for the hydrogel immersed in pH 5.4 PBS. The interaction forces between PEI and PFMNMF copolymer at different pH conditions (7.4, 6.4 and 5.4) was quantitatively studied using a SFA. As shown in the force curves and the adhesion histograms in **Figure 3.9c** and **3.9d**, the adhesion force (energy) between two surfaces decreased from $F_{ad}/R \sim 6.0$ mN/m ($W_{ad} \sim 1.3$ mJ/m^2) at pH 7.4 to $F_{ad}/R \sim 2.5$ mN/m ($W_{ad} \sim 0.53$ mJ/m^2) at pH 6.4 and there is no adhesion found between two surfaces at pH 5.4. The results elucidate the pH sensitivity of the dynamic imine bonds and well agree with the demonstrated gel-sol-gel transitions of Gel-9.5% induced by pH change. The novel hydrogels with sensitive dual temperature/pH responsiveness show great potential for applications, such as controlled drug delivery and biomolecules sensing.

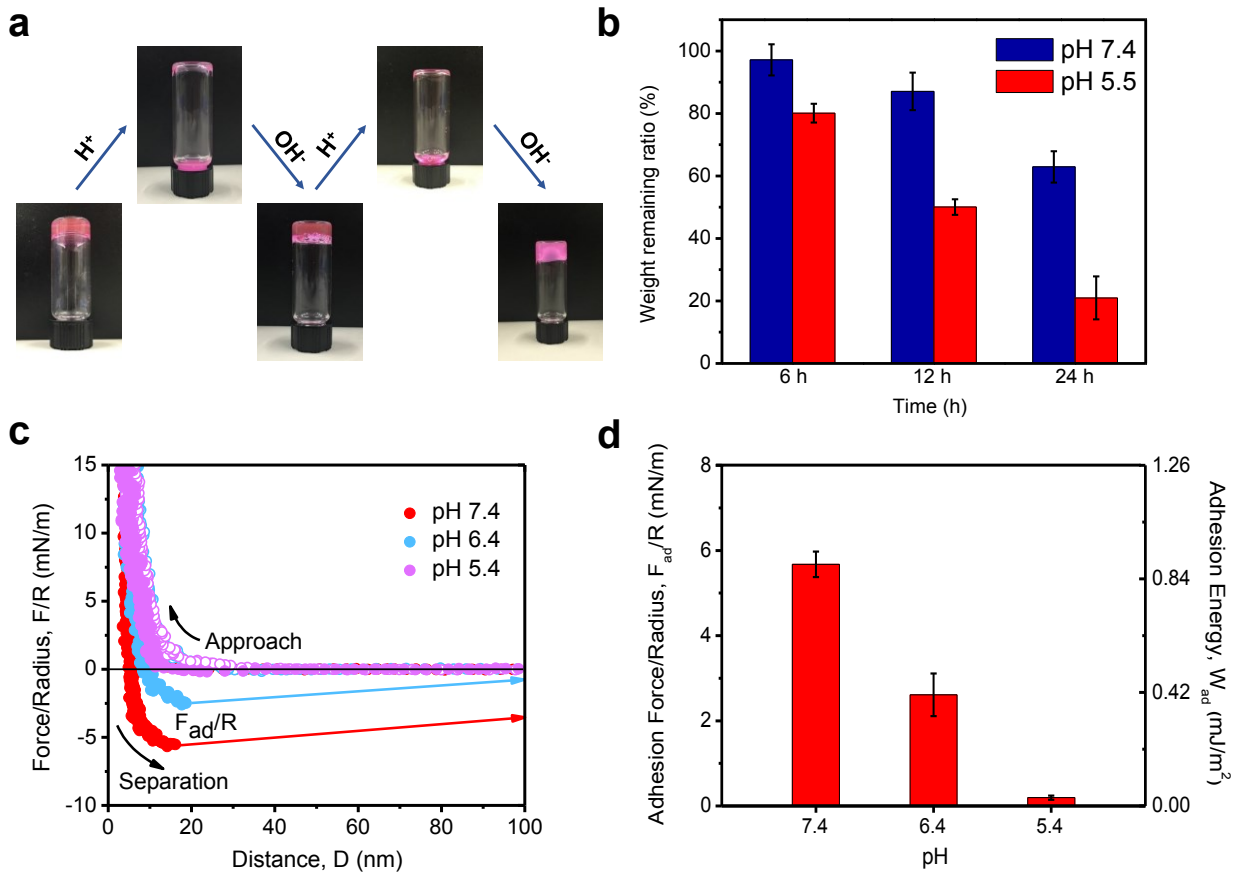

Figure 3.9. (a) Reversible gel-sol-gel transitions of Gel-9.5% by changing pH. (b) Degradation profile of Gel-9.5% in PBS buffer solutions (pH 7.4 and 5.4) at 37 °C. (c) Force-distance profiles show the effect of pH on the interaction forces between PEI and PFMNMF in PBS buffer solutions (pH 7.4, 6.4 and 5.4). (d) Normalized adhesion force and energy between PEI-coated and PFMNMF-coated mica surfaces in PBS buffer solutions at different pH.

3.3.5 Antimicrobial Property and Cell Cytotoxicity

Antimicrobial property is an essential requirement for implanted hydrogel materials since it can lower the risk of infection to the greatest extent. Therefore, Gel-9.5% was used to evaluate the antimicrobial performance against both *S. aureus* and *E. coli* with increasing concentration from 10^3 CFU/mL to 10^9 CFU/mL as shown in **Figure 3.10a**. It was found that Gel-9.5% was able to

kill more than 90% of both *S. aureus* and *E. coil* when challenged with bacterial concentration up to 10^8 CFU/mL. Even at extreme concentration (10^9 CFU/mL), Gel-9.5% was able to inhibit the growth of ~92.3% of *S. aureus* and ~ 82.6% of *E. coil* respectively. Since the hydrogel was not fully degraded within 24 h of incubation time, the antimicrobial activity is primarily through a contact-killing mechanism.[14, 50] The excellent antimicrobial property of the hydrogel is attributed to the synergistic effects of the quaternary amine groups of the ABA triblock copolymer and the partially protonated amine groups of the PEI exposed to the hydrogel surface, targeting the negatively charged microorganism lipid membrane through electrostatic interaction, which leads to lysis and cell death.[50, 59] The hydrogel demonstrated the great potential as antimicrobial biomaterial for tissue engineering and regenerative medicine.

The biocompatibility of the hydrogel (Gel-9.5%) was evaluated by MTT assay using both cancer (HeLa) and fibroblast (MRC-5) cell lines as shown in **Figure 3.10b**. After 24 h of incubation with Gel-9.5% gel extracts, cell viability of more than 80% was retained for both HeLa and MRC-5 cells. In spite of the difference in cell viability between different cell lines, the gel extracts showed low cytotoxicity to both cell lines. Although PEI has been reported to have potential cytotoxicity issue, many PEI-based hydrogels with excellent biocompatibility have been reported previously.[60-61] The good biocompatibility should be attributed to the formation of a well-interconnected hydrogel network by using low concentration of PEI solution to fabricate the hydrogel, which prevents the release of the non-crosslinked toxic PEI.[62] Therefore, the developed hydrogel serves as a potential candidate for various bioengineering applications.

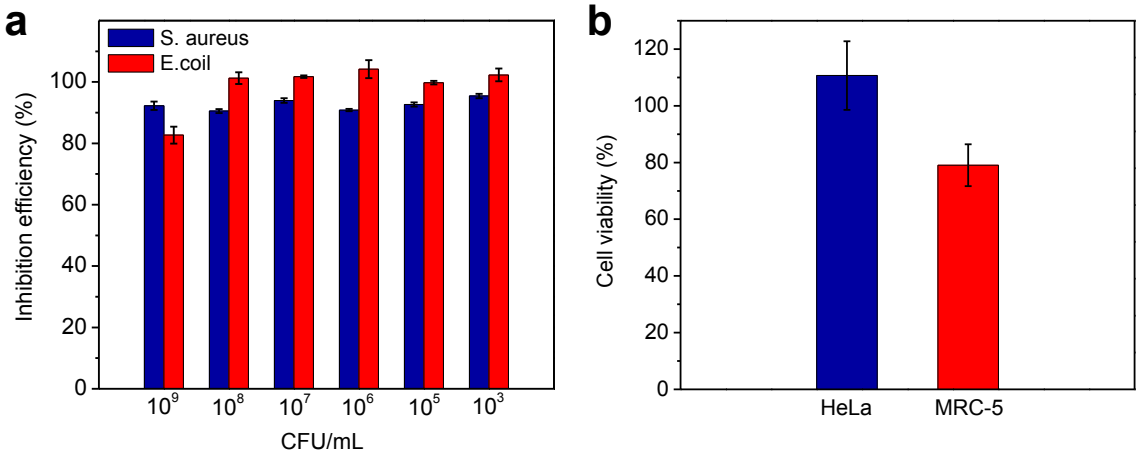

Figure 3.10. (a) Inhibition efficiency of S. aureus and E. coli after 24 h incubation with Gel-9.5%. (b) Cell viability of HeLa cancer cells and MRC-5 fibroblast cells after 24 h incubation with Gel-9.5% gel extracts.

3.4 Conclusions

Novel injectable self-healing hydrogels with tunable mechanical, optical and antimicrobial properties were designed and prepared. The hydrogels were formed after simple mixing of the multifunctional ABA triblock copolymer gelator PFMNMF solution with the PEI solution due to the formation of dynamic imine bonds as the cross-links. The hydrogel exhibited excellent injectability and self-healing capability. SFA force measurements provide insights into the self-healing mechanism of Schiff base reaction. Additionally, compared with the hydrogel fabricated by PFMN random copolymer gelator, the optical and mechanical properties of the hydrogel can be fine-tuned in a sensitive temperature responsive manner due to the nano-hydrophobic domains formed locally within the hydrogel network. The hydrogel could also undergo reversible gel-sol transitions subjected to pH change due to the pH-sensitive nature of dynamic imine bonds. Moreover, the hydrogel could effectively inhibit bacterial growth (*S. aureus* and *E. coli*) as a result of the synergistic effects of the quaternary amine groups of the PFMNMF polymer gelator

and the partially protonated amine groups of PEI exposed to the hydrogel surface, while showing low cytotoxicity to both fibroblast and cancer cells (MRC-5 and HeLa). Combining all these features, the developed novel hydrogels show great potential in various bioengineering applications.

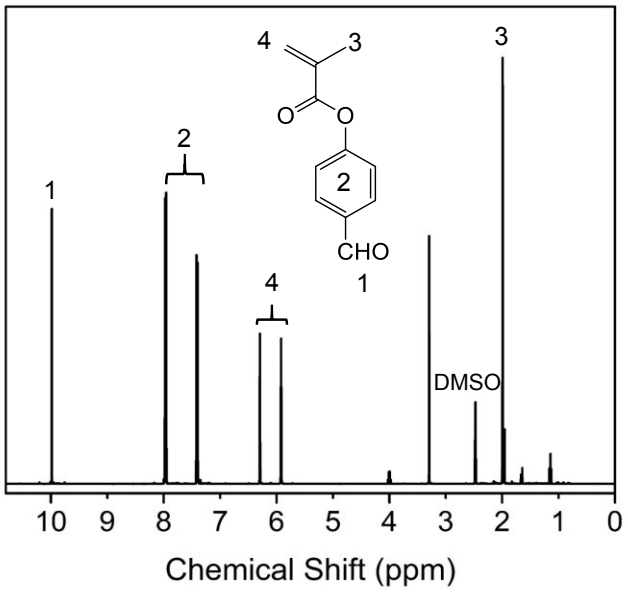

Figure S3.1. ^{1}H NMR spectrum of 4-formylphenyl methacrylate (FPMA) in DMSO-d_6.

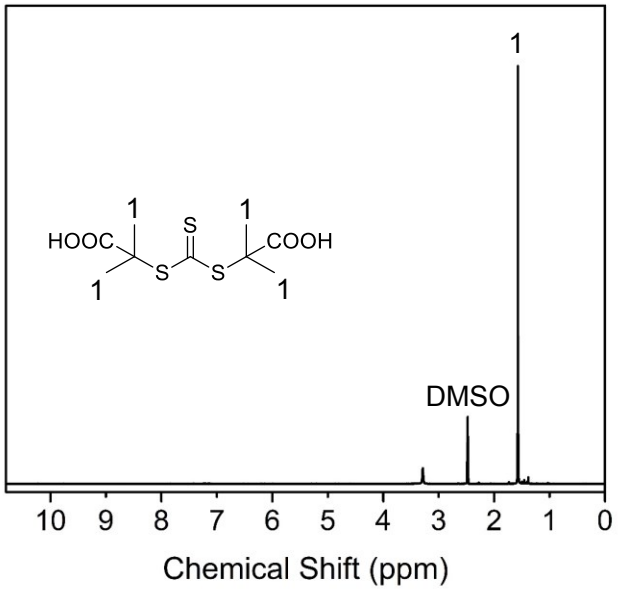

Figure S3.2. ^{1}H NMR spectrum of 2-(1-carboxy methylethylsulfanylthiocarbonylsulfanyl)-2-methylpropionic acid in DMSO-d_6.

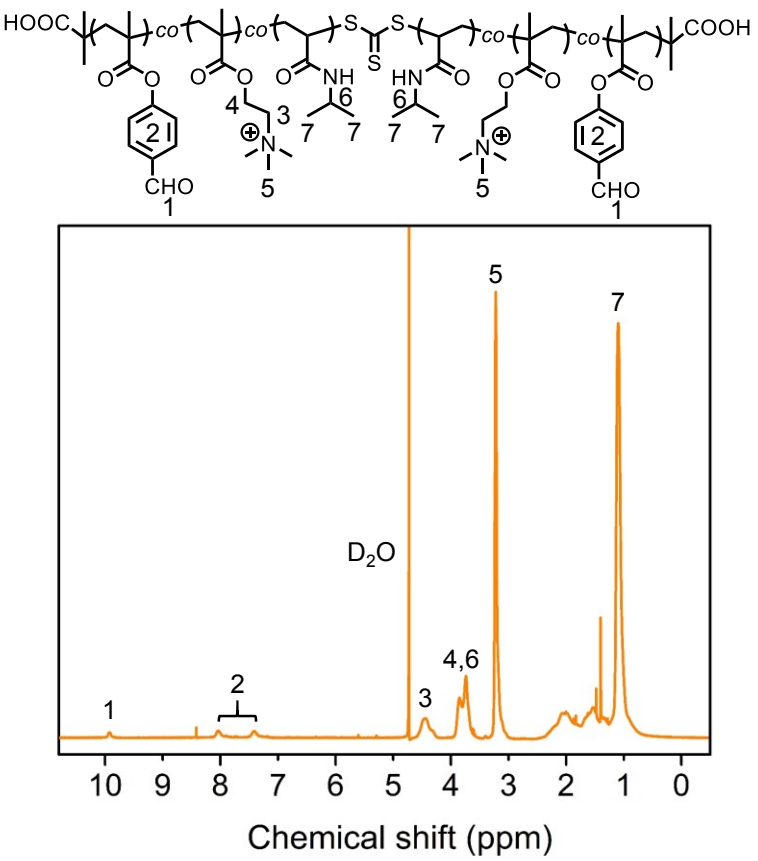

Figure S3.3. ^{1}H NMR spectrum of PFMN random copolymer in D_2O.

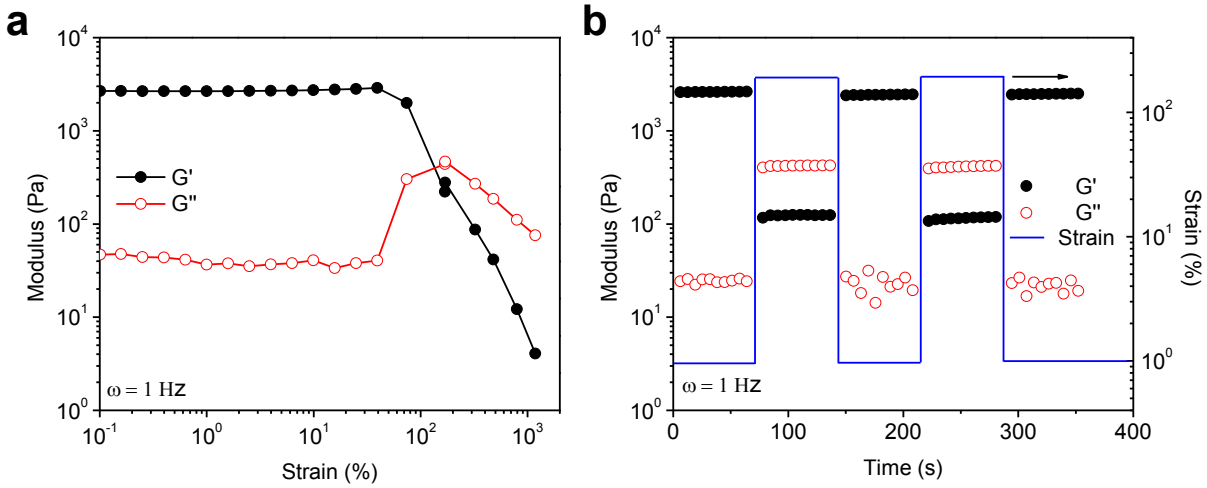

Figure S3.4. (a) Dynamic strain sweep measurement of Gel-9.5% at 37 °C (ω = 1 Hz). (b) Dynamic cyclic strain sweep measurement of Gel-9.5% at 37 °C (ω = 1 Hz, γ = 1% or 200%).

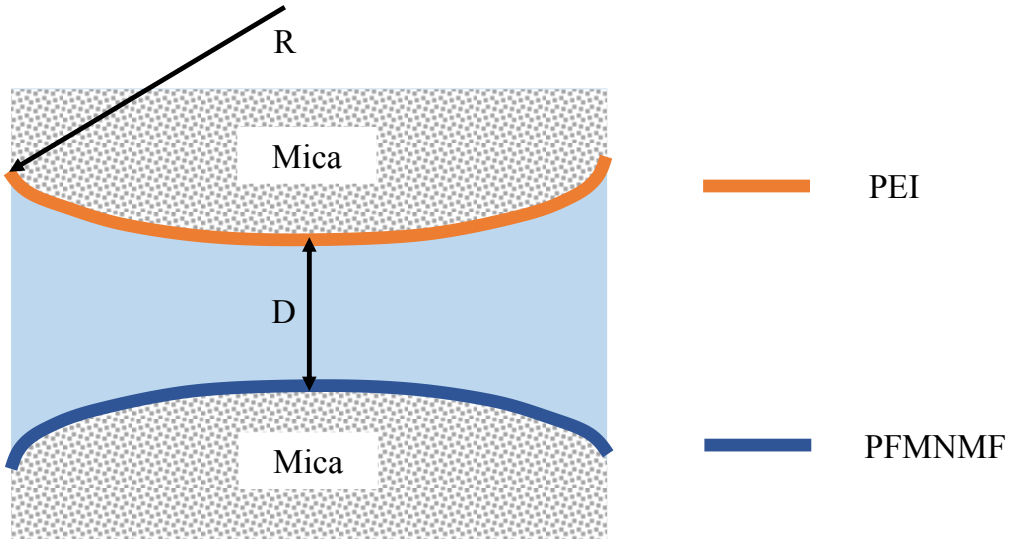

Figure S3.5. A typical SFA setup with asymmetric configuration for force measurement.

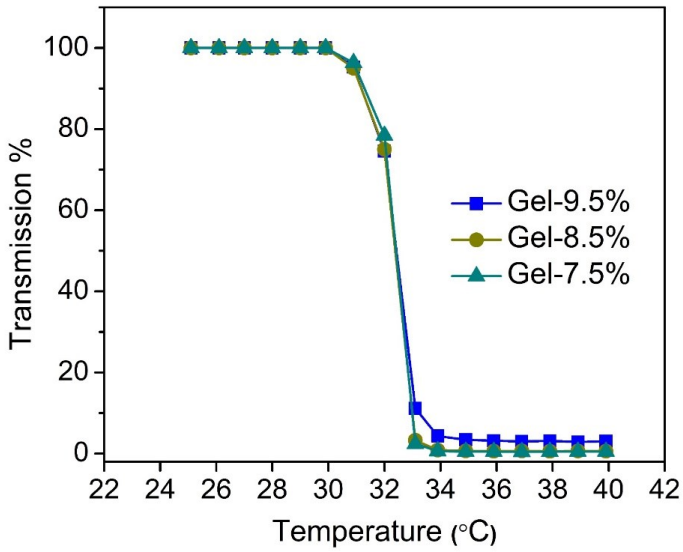

Figure S3.6. Volume phase transition temperature (VPTT) of Gel-9.5%, Gel-8.5% and Gel-7.5%.

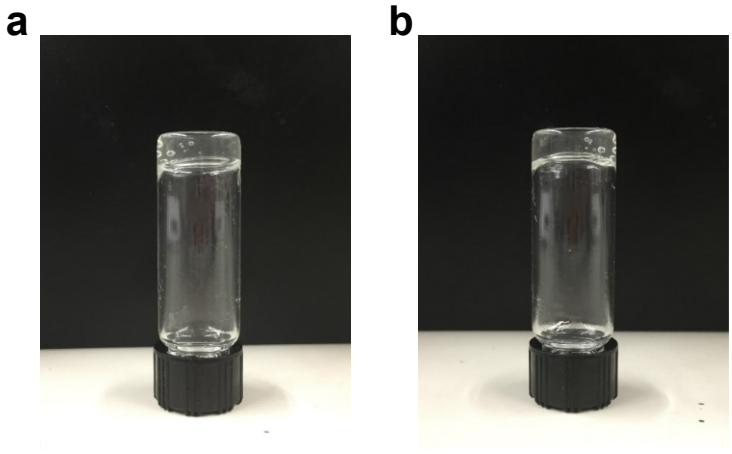

Figure S3.7. Transparency change of RGel-9.5% (a) 25 °C. (b) 37 °C.

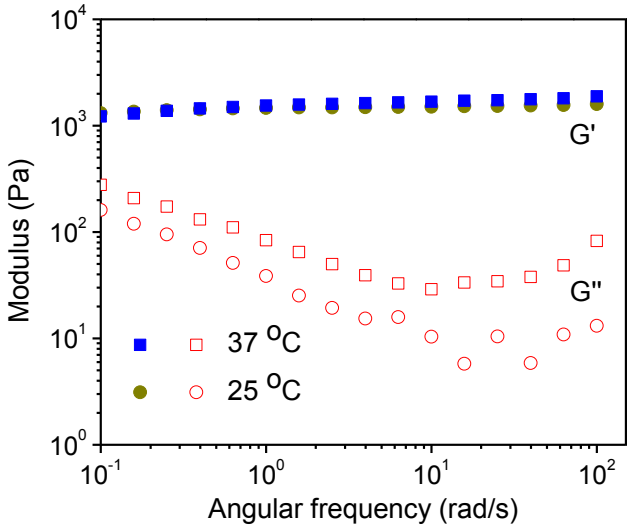

Figure S3.8. Modulus change of RGel-9.5% at 25 °C and 37 °C (γ = 1%, ω = 1 Hz).

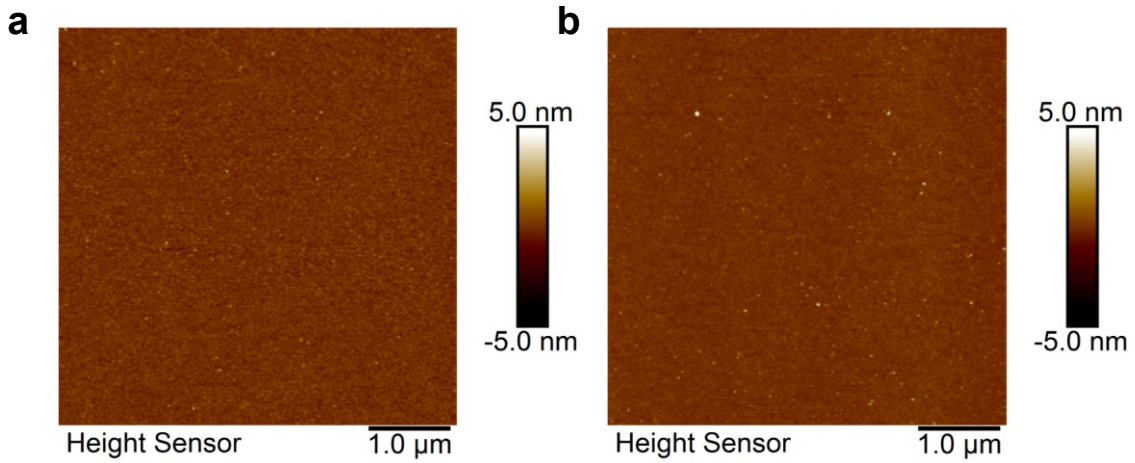

Figure S3.9. AFM topography images of PFMN random copolymer (a) 25 °C. (b) 37 °C.

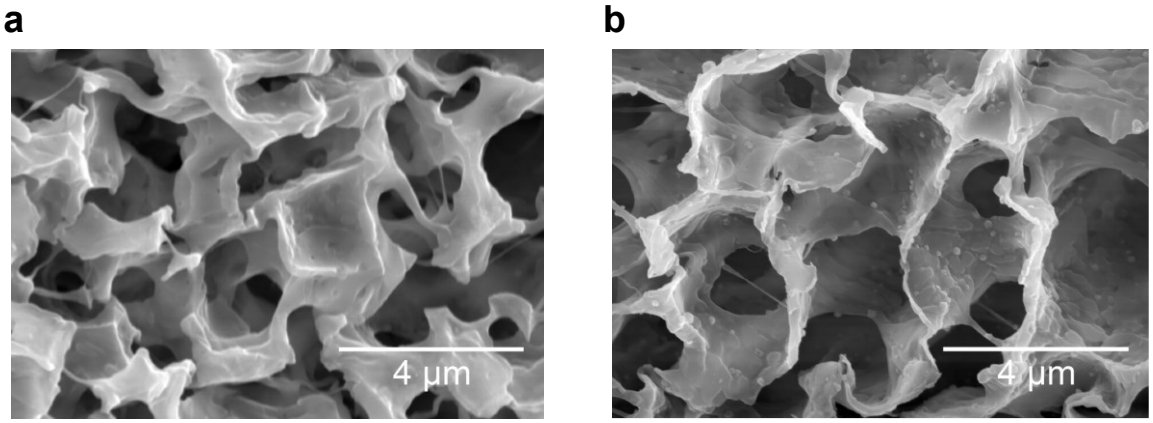

Figure S3.10. SEM images of freeze-dried Gel-9.5% after degradation in PBS buffer solutions at different pH for 24 h. (a) pH 7.4. (b) pH 5.4.

References

(1) Chen, Y.; Wang, W.; Wu, D.; Nagao, M.; Hall, D. G.; Thundat, T.; Narain, R. Injectable Self-Healing Zwitterionic Hydrogels Based on Dynamic Benzoxaborole-Sugar Interactions with Tunable Mechanical Properties. *Biomacromolecules* **2018,** *19* (2), 596-605.

(2) Zhao, X.; Li, P.; Guo, B.; Ma, P. X. Antibacterial and conductive injectable hydrogels based on quaternized chitosan-graft-polyaniline/oxidized dextran for tissue engineering. *Acta. Biomater.* **2015,** *26*, 236-48.

(3) Li, Y.; Wang, X.; Fu, Y. N.; Wei, Y.; Zhao, L.; Tao, L. Self-Adapting Hydrogel to Improve the Therapeutic Effect in Wound-Healing. *ACS Appl. Mater. Interfaces.* **2018,** *10* (31), 26046-26055.

(4) Sivashanmugam, A.; Arun Kumar, R.; Vishnu Priya, M.; Nair, S. V.; Jayakumar, R. An overview of injectable polymeric hydrogels for tissue engineering. *Eur. Polym. J.* **2015,** *72*, 543-565.

(5) Liu, M.; Zeng, X.; Ma, C.; Yi, H.; Ali, Z.; Mou, X.; Li, S.; Deng, Y.; He, N. Injectable hydrogels for cartilage and bone tissue engineering. *Bone. Res.* **2017,** *5* (1), 17014.

(6) Li, L.; Yan, B.; Yang, J.; Chen, L.; Zeng, H. Novel mussel-inspired injectable self-healing hydrogel with anti-biofouling property. *Adv. Mater.* **2015,** *27* (7), 1294-9.

(7) Zhang, G.; Chen, Y.; Deng, Y.; Ngai, T.; Wang, C. Dynamic Supramolecular Hydrogels: Regulating Hydrogel Properties through Self-Complementary Quadruple Hydrogen Bonds and Thermo-Switch. *ACS Macro Lett.* **2017,** *6* (7), 641-646.

(8) Tuncaboylu, D. C.; Sari, M.; Oppermann, W.; Okay, O. Tough and Self-Healing Hydrogels Formed via Hydrophobic Interactions. *Macromolecules* **2011,** *44* (12), 4997-5005.

(9) Xu, W.; Song, Q.; Xu, J. F.; Serpe, M. J.; Zhang, X. Supramolecular Hydrogels Fabricated from Supramonomers: A Novel Wound Dressing Material. *ACS Appl. Mater. Interfaces.* **2017,** *9* (13),

11368-11372.

(10) Chen, Y.; Diaz-Dussan, D.; Wu, D.; Wang, W.; Peng, Y.-Y.; Asha, A. B.; Hall, D. G.; Ishihara, K.; Narain, R. Bioinspired Self-Healing Hydrogel Based on Benzoxaborole-Catechol Dynamic Covalent Chemistry for 3D Cell Encapsulation. *ACS Macro Lett.* **2018,** *7* (8), 904-908.

(11) Chen, Y.; Tan, Z.; Wang, W.; Peng, Y.-Y.; Narain, R. Injectable, Self-Healing, and Multi-Responsive Hydrogels via Dynamic Covalent Bond Formation between Benzoxaborole and Hydroxyl Groups. *Biomacromolecules* **2019,** *20* (2), 1028-1035.

(12) Zhang, X.; Waymouth, R. M. 1,2-Dithiolane-Derived Dynamic, Covalent Materials: Cooperative Self-Assembly and Reversible Cross-Linking. *J. Am. Chem. Soc.* **2017,** *139* (10), 3822-3833.

(13) Qu, J.; Zhao, X.; Ma, P. X.; Guo, B. pH-responsive self-healing injectable hydrogel based on N-carboxyethyl chitosan for hepatocellular carcinoma therapy. *Acta. Biomater.* **2017,** *58*, 168-180.

(14) Dong, R.; Zhao, X.; Guo, B.; Ma, P. X. Self-Healing Conductive Injectable Hydrogels with Antibacterial Activity as Cell Delivery Carrier for Cardiac Cell Therapy. *ACS Appl. Mater. Interfaces.* **2016,** *8* (27), 17138-50.

(15) Wei, Z.; Yang, J. H.; Du, X. J.; Xu, F.; Zrinyi, M.; Osada, Y.; Li, F.; Chen, Y. M. Dextran-based self-healing hydrogels formed by reversible diels-alder reaction under physiological conditions. *Macromol. Rapid. Commun.* **2013,** *34* (18), 1464-70.

(16) Hsieh, F.-Y.; Tao, L.; Wei, Y.; Hsu, S.-h. A novel biodegradable self-healing hydrogel to induce blood capillary formation. *NPG Asia Mater.* **2017,** *9* (3), e363-e363.

(17) Tseng, T. C.; Tao, L.; Hsieh, F. Y.; Wei, Y.; Chiu, I. M.; Hsu, S. H. An Injectable, Self-Healing Hydrogel to Repair the Central Nervous System. *Adv. Mater.* **2015,** *27* (23), 3518-24.

(18) Zhao, X.; Wu, H.; Guo, B.; Dong, R.; Qiu, Y.; Ma, P. X. Antibacterial anti-oxidant

electroactive injectable hydrogel as self-healing wound dressing with hemostasis and adhesiveness for cutaneous wound healing. *Biomaterials* **2017,** *122*, 34-47.

(19) Qu, J.; Zhao, X.; Liang, Y.; Zhang, T.; Ma, P. X.; Guo, B. Antibacterial adhesive injectable hydrogels with rapid self-healing, extensibility and compressibility as wound dressing for joints skin wound healing. *Biomaterials* **2018,** *183*, 185-199.

(20) Zhang, Y.; Tao, L.; Li, S.; Wei, Y. Synthesis of Multiresponsive and Dynamic Chitosan-Based Hydrogels for Controlled Release of Bioactive Molecules. *Biomacromolecules* **2011,** *12* (8), 2894-2901.

(21) Yang, X.; Liu, G.; Peng, L.; Guo, J.; Tao, L.; Yuan, J.; Chang, C.; Wei, Y.; Zhang, L. Highly Efficient Self-Healable and Dual Responsive Cellulose-Based Hydrogels for Controlled Release and 3D Cell Culture. *Adv. Funct. Mater.* **2017,** *27* (40), 1703174.

(22) Ding, F.; Shi, X.; Wu, S.; Liu, X.; Deng, H.; Du, Y.; Li, H. Flexible Polysaccharide Hydrogel with pH-Regulated Recovery of Self-Healing and Mechanical Properties. *Macromol. Mater. Eng.* **2017,** *302* (11), 1700221.

(23) Gyles, D. A.; Castro, L. D.; Silva, J. O. C.; Ribeiro-Costa, R. M. A review of the designs and prominent biomedical advances of natural and synthetic hydrogel formulations. *Eur. Polym. J.* **2017,** *88*, 373-392.

(24) Carlini, A. S.; Adamiak, L.; Gianneschi, N. C. Biosynthetic Polymers as Functional Materials. *Macromolecules* **2016,** *49* (12), 4379-4394.

(25) Li, L.; Yan, B.; Yang, J.; Huang, W.; Chen, L.; Zeng, H. Injectable Self-Healing Hydrogel with Antimicrobial and Antifouling Properties. *ACS Appl. Mater. Interfaces.* **2017,** *9* (11), 9221-9225.

(26) Hoque, J.; Bhattacharjee, B.; Prakash, R. G.; Paramanandham, K.; Haldar, J. Dual Function

Injectable Hydrogel for Controlled Release of Antibiotic and Local Antibacterial Therapy. *Biomacromolecules* **2018,** *19* (2), 267-278.

(27) Resmi, R.; Unnikrishnan, S.; Krishnan, L. K.; Kalliyana Krishnan, V. Synthesis and characterization of silver nanoparticle incorporated gelatin-hydroxypropyl methacrylate hydrogels for wound dressing applications. *J. Appl. Polym. Sci.* **2017,** *134* (10).

(28) Gallagher, A. G.; Alorabi, J. A.; Wellings, D. A.; Lace, R.; Horsburgh, M. J.; Williams, R. L. A Novel Peptide Hydrogel for an Antimicrobial Bandage Contact Lens. *Adv. Healthc. Mater.* **2016,** *5* (16), 2013-8.

(29) Li, P.; Poon, Y. F.; Li, W.; Zhu, H. Y.; Yeap, S. H.; Cao, Y.; Qi, X.; Zhou, C.; Lamrani, M.; Beuerman, R. W.; Kang, E. T.; Mu, Y.; Li, C. M.; Chang, M. W.; Leong, S. S.; Chan-Park, M. B. A polycationic antimicrobial and biocompatible hydrogel with microbe membrane suctioning ability. *Nat. Mater.* **2011,** *10* (2), 149-56.

(30) Strassburg, A.; Petranowitsch, J.; Paetzold, F.; Krumm, C.; Peter, E.; Meuris, M.; Koller, M.; Tiller, J. C. Cross-Linking of a Hydrophilic, Antimicrobial Polycation toward a Fast-Swelling, Antimicrobial Superabsorber and Interpenetrating Hydrogel Networks with Long Lasting Antimicrobial Properties. *ACS Appl. Mater. Interfaces.* **2017,** *9* (42), 36573-36582.

(31) Dong, X.; Wei, C.; Liu, T.; Lv, F.; Qian, Z. Real-Time Fluorescence Tracking of Protoporphyrin Incorporated Thermosensitive Hydrogel and Its Drug Release in Vivo. *ACS Appl. Mater. Interfaces.* **2016,** *8* (8), 5104-13.

(32) Li, J.; Yu, J.; Huang, Y.; Zhao, H.; Tian, L. Highly Stable and Multiemissive Silver Nanoclusters Synthesized in Situ in a DNA Hydrogel and Their Application for Hydroxyl Radical Sensing. *ACS Appl. Mater. Interfaces.* **2018,** *10* (31), 26075-26083.

(33) Ma, C.; Lu, W.; Yang, X.; He, J.; Le, X.; Wang, L.; Zhang, J.; Serpe, M. J.; Huang, Y.; Chen,

T. Bioinspired Anisotropic Hydrogel Actuators with On-Off Switchable and Color-Tunable Fluorescence Behaviors. *Adv. Funct. Mater.* **2018,** *28* (7), 1704568.

(34) Ida, S.; Kitanaka, H.; Ishikawa, T.; Kanaoka, S.; Hirokawa, Y. Swelling properties of thermoresponsive/hydrophilic co-networks with functional crosslinked domain structures. *Polym. Chem.* **2018,** *9* (13), 1701-1709.

(35) Lu, H.; Wang, Y.; Li, L.; Kotsuchibashi, Y.; Narain, R.; Zeng, H. Temperature- and pH-Responsive Benzoboroxole-Based Polymers for Flocculation and Enhanced Dewatering of Fine Particle Suspensions. *ACS Appl. Mater. Interfaces.* **2015,** *7* (49), 27176-87.

(36) Nagao, M.; Sengupta, J.; Diaz-Dussan, D.; Adam, M.; Wu, M.; Acker, J.; Ben, R.; Ishihara, K.; Zeng, H.; Miura, Y.; Narain, R. Synthesis of Highly Biocompatible and Temperature-Responsive Physical Gels for Cryopreservation and 3D Cell Culture. *ACS Appl. Bio Mater.* **2018,** *1* (2), 356-366.

(37) Lee, A. L. Z.; Voo, Z. X.; Chin, W.; Ono, R. J.; Yang, C.; Gao, S.; Hedrick, J. L.; Yang, Y. Y. Injectable Coacervate Hydrogel for Delivery of Anticancer Drug-Loaded Nanoparticles in vivo. *ACS Appl. Mater. Interfaces.* **2018,** *10* (16), 13274-13282.

(38) Zhang, G.; Chen, Y.; Deng, Y.; Wang, C. A Triblock Copolymer Design Leads to Robust Hybrid Hydrogels for High-Performance Flexible Supercapacitors. *ACS Appl. Mater. Interfaces.* **2017,** *9* (41), 36301-36310.

(39) Ovdenko, V.; Kolendo, A. New bent-shaped azomethine monomers for optical applications. *Mol. Cryst. Liq. Cryst.* **2016,** *640* (1), 113-121.

(40) Haraguchi, K.; Kubota, K.; Takada, T.; Mahara, S. Highly Protein-Resistant Coatings and Suspension Cell Culture Thereon from Amphiphilic Block Copolymers Prepared by RAFT Polymerization. *Biomacromolecules* **2014,** *15* (6), 1992-2003.

(41) Kotsuchibashi, Y.; Agustin, R. V. C.; Lu, J.-Y.; Hall, D. G.; Narain, R. Temperature, pH, and Glucose Responsive Gels via Simple Mixing of Boroxole- and Glyco-Based Polymers. *ACS Macro Lett.* **2013,** *2* (3), 260-264.

(42) Israelachvili, J.; Min, Y.; Akbulut, M.; Alig, A.; Carver, G.; Greene, W.; Kristiansen, K.; Meyer, E.; Pesika, N.; Rosenberg, K.; Zeng, H. Recent advances in the surface forces apparatus (SFA) technique. *Rep. Prog. Phys.* **2010,** *73* (3), 036601.

(43) Zeng, H.; Hwang, D. S.; Israelachvili, J. N.; Waite, J. H. Strong reversible Fe^{3+}-mediated bridging between dopa-containing protein films in water. *Proc. Natl. Acad. Sci. U. S. A.* **2010,** *107* (29), 12850-3.

(44) Kim, S.; Huang, J.; Lee, Y.; Dutta, S.; Yoo, H. Y.; Jung, Y. M.; Jho, Y.; Zeng, H.; Hwang, D. S. Complexation and coacervation of like-charged polyelectrolytes inspired by mussels. *Proc. Natl. Acad. Sci. U. S. A.* **2016,** *113* (7), E847-53.

(45) Faghihnejad, A.; Zeng, H. Interaction mechanism between hydrophobic and hydrophilic surfaces: using polystyrene and mica as a model system. *Langmuir* **2013,** *29* (40), 12443-51.

(46) Israelachvili, J. N. Thin film studies using multiple-beam interferometry. *J. Colloid Interface Sci.* **1973,** *44* (2), 259-272.

(47) Zeng, H.; Tian, Y.; Anderson, T. H.; Tirrell, M.; Israelachvili, J. N. New SFA Techniques for Studying Surface Forces and Thin Film Patterns Induced by Electric Fields. *Langmuir* **2008,** *24* (4), 1173-1182.

(48) Zeng, H.; Huang, J.; Tian, Y.; Li, L.; Tirrell, M. V.; Israelachvili, J. N. Adhesion and Detachment Mechanisms between Polymer and Solid Substrate Surfaces: Using Polystyrene–Mica as a Model System. *Macromolecules* **2016,** *49* (14), 5223-5231.

(49) Chen, J.; Yan, B.; Wang, X.; Huang, Q.; Thundat, T.; Zeng, H. Core cross-linked double

hydrophilic block copolymer micelles based on multiple hydrogen-bonding interactions. *Polym. Chem.* **2017,** *8* (20), 3066-3073.

(50) Giano, M. C.; Ibrahim, Z.; Medina, S. H.; Sarhane, K. A.; Christensen, J. M.; Yamada, Y.; Brandacher, G.; Schneider, J. P. Injectable bioadhesive hydrogels with innate antibacterial properties. *Nat. Commun.* **2014,** *5* (1), 4095.

(51) Zhang, Y.; Fu, C.; Li, Y.; Wang, K.; Wang, X.; Wei, Y.; Tao, L. Synthesis of an injectable, self-healable and dual responsive hydrogel for drug delivery and 3D cell cultivation. *Polym. Chem.* **2017,** *8* (3), 537-544.

(52) Brown, T. E.; Anseth, K. S. Spatiotemporal hydrogel biomaterials for regenerative medicine. *Chem. Soc. Rev.* **2017,** *46* (21), 6532-6552.

(53) Huang, Q.; Zou, Y.; Arno, M. C.; Chen, S.; Wang, T.; Gao, J.; Dove, A. P.; Du, J. Hydrogel scaffolds for differentiation of adipose-derived stem cells. *Chem. Soc. Rev.* **2017,** *46* (20), 6255-6275.

(54) Wang, W.; Narain, R.; Zeng, H. Rational Design of Self-Healing Tough Hydrogels: A Mini Review. *Front. Chem.* **2018,** *6* (497), 497.

(55) Yan, B.; Huang, J.; Han, L.; Gong, L.; Li, L.; Israelachvili, J. N.; Zeng, H. Duplicating Dynamic Strain-Stiffening Behavior and Nanomechanics of Biological Tissues in a Synthetic Self-Healing Flexible Network Hydrogel. *ACS Nano* **2017,** *11* (11), 11074-11081.

(56) Wei, W.; Qi, X.; Li, J.; Zuo, G.; Sheng, W.; Zhang, J.; Dong, W. Smart Macroporous Salecan/Poly(N,N-diethylacrylamide) Semi-IPN Hydrogel for Anti-Inflammatory Drug Delivery. *ACS Biomater. Sci. Eng.* **2016,** *2* (8), 1386-1394.

(57) Li, X.; Zhong, H.; Li, X.; Jia, F.; Cheng, Z.; Zhang, L.; Yin, J.; An, L.; Guo, L. Synthesis of attapulgite/N-isopropylacrylamide and its use in drug release. *Mater. Sci. Eng., C* **2014,** *45*, 170-

5.

(58) Smeets, N. M. B.; Patenaude, M.; Kinio, D.; Yavitt, F. M.; Bakaic, E.; Yang, F.-C.; Rheinstädter, M.; Hoare, T. Injectable hydrogels with in situ-forming hydrophobic domains: oligo(d,l-lactide) modified poly(oligoethylene glycol methacrylate) hydrogels. *Polym. Chem.* **2014,** *5* (23), 6811-6823.

(59) Strassburg, A.; Kracke, F.; Wenners, J.; Jemeljanova, A.; Kuepper, J.; Petersen, H.; Tiller, J. C. Nontoxic, Hydrophilic Cationic Polymers-Identified as Class of Antimicrobial Polymers. *Macromol. Biosci.* **2015,** *15* (12), 1710-23.

(60) Wang, L. L.; Sloand, J. N.; Gaffey, A. C.; Venkataraman, C. M.; Wang, Z.; Trubelja, A.; Hammer, D. A.; Atluri, P.; Burdick, J. A. Injectable, Guest–Host Assembled Polyethylenimine Hydrogel for siRNA Delivery. *Biomacromolecules* **2017,** *18* (1), 77-86.

(61) Zhuang, Y.; Shen, H.; Yang, F.; Wang, X.; Wu, D. Synthesis and characterization of PLGA nanoparticle/4-arm-PEG hybrid hydrogels with controlled porous structures. *RSC Advances* **2016,** *6* (59), 53804-53812.

(62) Davoodi, P.; Ng, W. C.; Yan, W. C.; Srinivasan, M. P.; Wang, C. H. Double-Walled Microparticles-Embedded Self-Cross-Linked, Injectable, and Antibacterial Hydrogel for Controlled and Sustained Release of Chemotherapeutic Agents. *ACS Appl. Mater. Interfaces.* **2016,** *8* (35), 22785-800.

CHAPTER 4 Dynamic Flexible Hydrogel Network with Biological Tissue-like Self-protective Functions

4.1 Introduction

Biological tissues can elegantly adopt different self-protection strategies to maintain their structural integrity and biological functionalities in response to the deformation induced by external mechanical stress. For instance, biological assemblies of microtubules, actin, collagen, and intermediate filaments can stiffen before being strained to the fracture (viz., their stiffness increases as the applied strain or stress increases).[1-3] The strain-stiffening capability not only limits the biological tissues from deformation, but also plays important roles in various biological processes, such as cell differentiation and long-distance cell-cell communication.[4-5] In bioengineering applications, to endow synthetic soft materials with such strain-stiffening capability is vital in mimicking the dynamic mechanical environment to decipher cell behaviors, and fabricating artificial tissues (e.g., muscle, skin, blood vessel, etc.), implantable actuators and soft robotics. Current design strategies of strain-stiffening materials mainly rely on the use of semi-flexible polyisocyanopeptide (PIC) bundles with helical architecture or semi-flexible fibers prepared through self-assembly of gelator molecules, which possess inherent strain-stiffening property.[6-10] However, sophisticated preparation methods and limited number of candidates restrict their applications. Considering the various synthetic routes and tunable functionalities of synthetic polymers, using flexible synthetic polymers to develop novel functional hydrogels for mimicking biological tissues is highly desired. Nevertheless, the strain-stiffening behavior is rarely observed in synthetic flexible hydrogels, which, instead, generally tend to be softened when strained.

For the biological tissues, when their deformation exceed the maximum tolerable strain, they can be irreversibly damaged. In such case, the biological tissues can adopt the strategy of self-

healing to autonomously repair damage and restore the physiological functions. Inspired by biological tissues, hydrogels with self-healing capability can be designed based on two major interaction mechanisms: non-covalent interactions (e.g., hydrogen bonding,[11] hydrophobic interactions,[12] host-guest interactions,[13] etc.) and dynamic covalent chemistry (e.g., Schiff base,[14] boronic ester,[15-16] disulfide,[17] etc.). By far, only few hydrogels that possess both strain-stiffening and self-healing properties have been reported, including bolaamphiphiles (BA) fiber-based supramolecular semi-flexible hydrogels, PIC-based semi-flexible physical gels and the PVA-borax flexible hydrogel.[18-20] Recently, a flexible self-healing hydrogel with branching network architecture constructed by branched PEI and dibenzylaldehyde-functionalized PEG has been reported to have strain-stiffening property.[21] The branched PEI could cause cytotoxicity issue,[22] which potentially limits this type of hydrogel in bioengineering applications. Besides, the branching network architecture is generally difficult to achieve and control since the synthesis of well-defined precursor branched polymers should follow complicated and time-consuming processes, which could not be easily scaled-up for practical applications. Therefore, conferring both strain-stiffening and self-healing properties in a biocompatible flexible hydrogel with simple network architecture is of great significance while remains a challenge.

Herein, we report a strain-stiffening self-healing hydrogel prepared from two flexible linear polymers, both of which have excellent biocompatibility (**Figure 4.1)**. The hydrogel is cross-linked through the condensation reactions between boronic acids of diphenylboronic acid-terminated telechelic poly(ethylene glycol) (DPB-PEG) and the 1,2-/1,3-diols of a glycopolymer, poly(acrylamide-*co*-2-lactobionamidoethyl methacrylamide) (P(AM-*co*-LAMEA)) under physiological conditions. The as-prepared hydrogels exhibit remarkable biomimetic strain-stiffening behavior, which can be facilely tuned by crosslinking density, polymer concentration,

temperature and the length of the cross-linkers. The underlying strain-stiffening mechanism is elucidated as the non-linear stretching and finite extensibility of PEG, which provides novel insights into the molecular design for the functional hydrogels with tunable mechano-response. In addition, due to the dynamic boronic ester cross-linking chemistry, the damaged hydrogel can repetitively self-heal within seconds without sacrificing the strain-stiffening capability. The significant biomimetic characteristics along with the excellent biocompatibility enable the hydrogel as an ideal platform for 3D cell encapsulation. The presented biocompatible strain-stiffening self-healing hydrogel may pave the way for the development of novel multifunctional biomimetic soft materials for a wide range of biomedical and engineering applications.

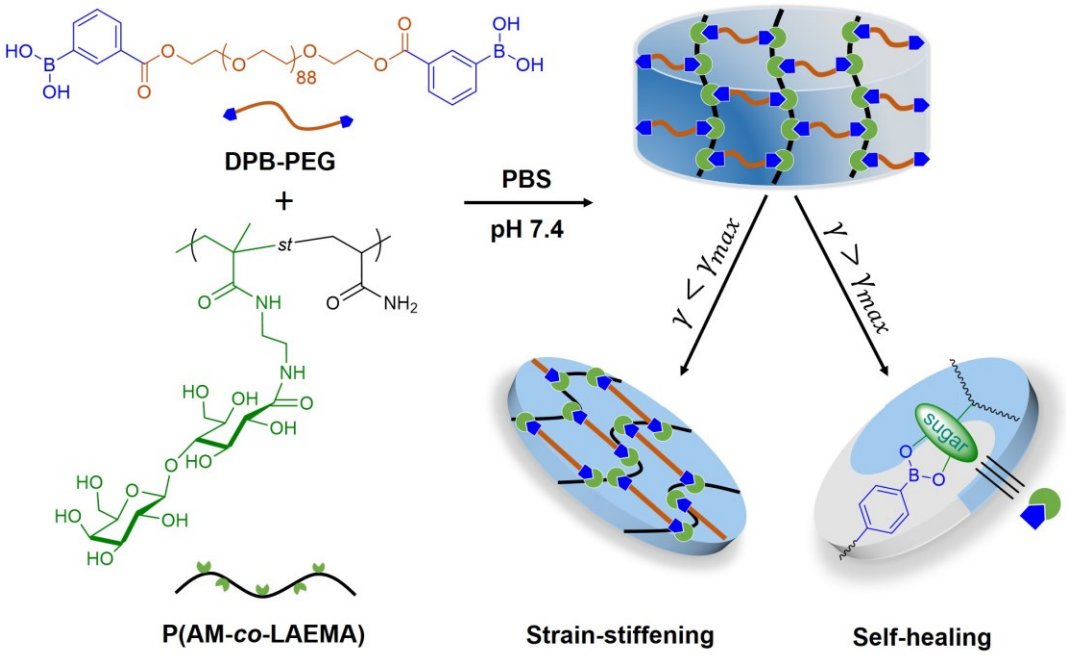

Figure 4.1. Preparation of biocompatible flexible hydrogel network using DPB-PEG and P(AM-co-LAEMA) and its biomimetic strain-stiffening and self-healing functions in response to mechanical deformation.

4.2 Experimental Methods

4.2.1 Materials

All the chemicals used for polymer synthesis were purchased from Sigma Aldrich. 2-lactobionamidoethyl methacrylamide (LAEMA) was synthesized according to the published papers.[23-24] LIVE/DEAD™ cell imaging kit was purchased from Fisher Scientific. All the cell culture products, including DMEM medium, antibiotics, fetal bovine serum (FBS), and trypsin with EDTA, were obtained from Gibco.

4.2.2 Polymer Synthesis and Characterization

DPB-PEG4k was synthesized by esterification of hydroxyl-terminated PEG with 3-carboxyphenylboronic acid. Briefly, PEG4k (0.5 mmol, 2 g), 3-carboxyphenylboronic acid (2 mmol, 332 mg) and DMAP (15 mg) were dissolved in dry THF (20 mL) in a 100-mL round-bottomed flask. DCC (2.5 mmol, 516 mg) in 10 mL of dry THF was added to the system *via* a syringe after degassing the whole system with nitrogen for 30 min. The reaction was allowed to proceed at room temperature for 24 h with vigorous stirring. The white solid was filtered and the filtrate was concentrated under vacuum. The polymer was obtained as white solid after repeated dissolution in THF and precipitation in diethyl ether for three times, followed by drying under vacuum. DPB-PEG8k was synthesized following a similar procedure, except changing the amount of the chemicals (PEG8k (0.25 mmol, 2g), 3-carboxyphenylboronic acid (1 mmol, 166mg), DMAP (8 mg), DCC (1.25 mmol, 258 mg)).

The glycopolymer P(AM-*co*-LAEMA) was synthesized by free radical polymerization. Briefly, a 50-mL round-bottomed flask was charged with acrylamide (7 mmol, 497 mg), LAEMA (3 mmol, 1.404 g) and the initiator AIBN (0.025 mmol, 4 mg). The reagents were then dissolved in a mixed solvent of DI water (9 mL) and DMF (1 mL). After degassing with nitrogen for 15 min,

the polymerization was carried out in an oil bath at 70 °C for 24 h. The polymer was obtained as white solid after dialysis against DI water for three days followed by lyophilization.

The ^{1}H NMR spectra of DPB-PEG4k and P(AM-*co*-LAEMA) were recorded on a Varian 500 MHz spectrometer at room temperature using D_2O as solvent. Chemical shifts are reported in parts per million (δ) relative to TMS used as the internal reference. The FT-IR spectra of PEG4k and DPB-PEG4k were obtained on a Thermo Scientific Nicolet iS50 Fourier transform infrared spectrophotometer equipped with diamond crystal/built-in all-reflective diamond ATR. The number (Mn) average molecular weights and polydispersity (PDI) of P(AM-*co*-LAEMA) were determined by Viscotek conventional gel permeation chromatography (GPC) system equipped with two WAT011545 Waters Ultrahydrogel linear columns using 0.5 M sodium acetate/0.5 M acetic acid buffer as eluent at a flow rate of 1.0 mL/min. The GPC was calibrated by monodisperse pullulan standards (Mw = 5900−404 000 g/mol).

4.2.3 Hydrogel Preparation

Hydrogels with designated boronic acid/sugar molar ratios and final polymer concentrations were prepared by mixing PBS solutions (pH 7.4) of DPB-PEG4k/8k and P(AM-*co*-LAEMA) at different ratios. For instance, to prepare a 10 w/v% hydrogel at boronic acid/sugar=1:1, 32 mg of DPB-PEG4k and 8 mg of P(AM-*co*-LAEMA) were firstly dissolved in 320 μL and 80 μL of PBS buffer solutions (pH 7.4) respectively. The hydrogel can be formed within ~30 s after mixing two solutions through vortex and stay still when the vial was inverted. The hydrogels using shorter crosslinkers DPB-PEG4k and longer crosslinkers DPB-PEG8k are denoted as BL4k and BL8k respectively.

4.2.4 Rheology Characterization

A rheometer (TA Instruments, AR-G2) fitted with a Peltier stage using a 20 mm parallel-plate

configuration and with a gap of 53 μm was used to characterize the mechanical behaviors of the hydrogels. All the hydrogels were stored at room temperature for 1 h to reach equilibrium before rheology measurements. For all the tests, a few drops of silicon oil is applied around the edge to prevent moisture evaporation during the tests.

A reported dynamic oscillatory strain amplitude sweep protocol (γ from 0.1 % to 1000 %) was used to investigate the strain-stiffening behavior of the hydrogels.[1, 25]

The temperature-dependent mechanical properties of hydrogel were characterized through temperature ramp tests from 15 (75) to 75 (15) °C with a heating (cooling) rate of 2 °C/min at constant strain (γ = 1%) and angular frequency (ω =10 rad/s).

The on-demand and targeted mechanical properties of the hydrogels were characterized through cyclic strain step tests by applying a low strain (γ = 5%, below γ_c) and higher strains (between γ_c and γ_{max}) at constant angular frequency (ω =10 rad/s) on the hydrogels.

To study the self-healing property of the hydrogels, sequential strain amplitude sweeps (γ from 0.1 % to 1000 %) at constant angular frequency (ω =10 rad/s) were performed on the hydrogels to monitor the recovery of the mechanical properties after a strain failure. The reproducibility of the self-healing capacity was characterized through cyclic strain step tests by applying a low strain (γ = 5%, below γ_c) and a high strain (γ = 650%, above γ_{max}) on the hydrogel at constant angular frequency (ω =10 rad/s).

4.2.5 SFA Experiment Setup and Force Measurements

A surface forces apparatus (SFA) was used to quantitatively probe the interaction forces between P(AM-*co*-LAEMA) and DPB-PEG4k or unmodified PEG4k. The detailed experiment setup for SFA measurements have been reported previously.[26-28] In this work, a symmetric configuration was adopted. Briefly, two back-silvered mica surfaces (1−5 μm) were glued onto

two cylindrical silica disks ($R \approx 2$ cm). The mica surfaces were then coated with P(AM-*co*-LAEMA) solution (100 μg/mL) for 15 min, followed by a thorough rinse with PBS buffer to remove unbound or loosely bound polymers. Two surfaces were then mounted into the SFA chamber in a cross-cylinder configuration and the SFA chamber was saturated with water vapor. PBS solution of DPB-PEG4k or unmodified PEG4k (100 μg/mL, pH 7.4) was injected between two mica surfaces. The force measurement was conducted by bringing two surfaces to contact followed by separation. The interaction forces *F(D)* were monitored as a function of absolute surface separation distance *D* in real time using multiple beam interferometry by employing fringes of equal chromatic order (FECO). For each case, force-distance profiles were measured at least two different interaction positions on a set of surfaces to confirm the reproducibility. The measured adhesion or "pull-off" force F_{ad} and adhesion energy W_{ad} are correlated by:

$$F_{ad} = \frac{3}{2}\pi R W_{ad} \quad (4)$$

4.2.6 Cell Culture

Cervical cancer cell line (HeLa ATCC® CCL-2™) were cultured in Dulbecco's Modified Eagle's medium/Nutrient Mixture F-12 media supplemented with 10% Fetal bovine serum, 2mM L-glutamine and 10% Penicillin Streptomycin. Cells were cultured in a humidified incubator at 37° C with 5 % CO_2 and divided when reached 80% confluency.

4.2.7 3D cell encapsulation

A reported procedure was followed for 3D cell culture with slight modification.[29] HeLa cells were taken as the model cell line for the demonstration of 3D cell culture in a 10 w/v% BL4k hydrogel under sterile conditions. HeLa cells at a density of 2.5×10^6 cells/mL were suspended in 320 μL of low glucose DMEM medium with 10 w/v% of DPB-PEG4k and transferred to a glass-bottomed petri-dish. Then 80 μL of 10 w/v% P(AM-co-LAEMA) PBS solution was gently mixed

with the cell suspension to form cell-loaded hydrogel. After the addition of 0.5 mL of low glucose DMEM culture medium, the cell-loaded hydrogel was incubated at 37 °C for 24 h. The cell-loaded hydrogel was visualized by CLSM 710 Meta confocal laser scanning microscope (Carl Zeiss, Jena, Germany) after stained with live/dead cell imaging kit. The live/dead staining solution is a mixture of two fluorescent dyes that are able to label live and dead cells respectively. The live cells would be stained green due to the enzymatic conversion of membrane-permeant non-fluorescent live cell dye to the intensely fluorescent molecules. The dead cells will be stained red as the membrane-impermeant dead cell dye enters the cells with damaged membrane and binds to the DNA. The cell viability was quantified using Imaris Image Analysis software.

4.3 Results and Discussions

4.3.1 Polymer Synthesis and Hydrogel Preparation

Two hydrogel precursor polymers were first synthesized. DPB-PEG with molecular weights of 4 kDa and 8 kDa (DPB-PEG4k and DPB-PEG8k) were synthesized by esterification of hydroxyl-terminated PEG with 3-carboxyphenylboronic acid. (**Figure S4.1a in Supporting Information).** The polymer was characterized by ^{1}H NMR and FT-IR spectroscopy (**Figure S4.2 and S4.3 and Supporting Information for details of polymer characterizations**). The linear glycopolymer, P(AM-*co*-LAMEA) was synthesized by free-radical polymerization of acrylamide (AM) with 2-lactobionamidoethyl methacrylamide (LAEMA) (**Figure S4.1b in Supporting Information**). The resulting polymer was characterized by ^{1}H NMR spectroscopy (**Figure S4.4 in Supporting Information**). The number average molecular weight (Mn=53800 g/mol) and polydispersity (PDI=2.9) were determined by gel permeation chromatography (GPC).

Hydrogels with designated boronic acid/sugar molar ratios and final polymer concentrations were readily prepared at physiological pH by mixing PBS solutions of DPB-

PEG4k/8k and P(AM-*co*-LAEMA) at different ratios. All the hydrogels could be rapidly formed within ~30 s (**Figure S4.5 in Supporting Information**), resulting from the efficient formation of boronic ester crosslinks between boronic acids and 1,3-diols on the sugar moieties. Hydrogels crosslinked by DPB-PEG4k and DPB-PEG8k are denoted as BL4k and BL8k respectively.

4.3.2 Mechanical Analysis of Strain-stiffening Behavior

The as-prepared hydrogels exhibited a well-defined non-linear mechano-response to deformation after a critical strain (stress) is reached (**Figure S4.6 in Supporting Information**). Such strain-stiffening behavior is commonly observed in biopolymer-based semi-flexible networks but is extremely rare in synthetic flexible hydrogel networks. Differential modulus *K'*, which is defined as the derivative of shear stress σ with respect to shear strain γ ($K' = \partial\sigma/\partial\gamma$), is employed to describe the mechano-response of the hydrogels by plotting *K'* against σ. Two distinct regimes are observed: in the low-stress linear regime, *K'* remains constant and equals to the plateau modulus G_0; while above the critical stress σ_c, *K'* starts to increase with σ as $K' \propto \sigma^m$, indicating the strain-stiffening property. The power *m* represents the stiffening index, which measures the intensity of the strain-stiffening response of the network. K'_{max}/G_0 is defined as the stiffening range, which measures the increase in stiffness relative to the initial stiffness before material failure.

4.3.3 Boronic acid/sugar Molar Ratio Dependence

The influence of different boronic acid/sugar ratios on the network mechanics of BL4k is investigated when the polymer concentration of the hydrogels is fixed at 10 w/v%. All the samples show clear linear and non-linear mechano-responsive regimes, where G_0 and σ_c can be easily tuned by varying the molar ratio between boronic acid and sugar groups (**Figure 4.2a**). As the molar ratio of boronic acid/sugar increases from 1:0.5 to 1:4, G_0 significantly increases from 32 Pa to 405 Pa (**Figure 4.2b**). The increase of G_0 could be attributed to the higher crosslinking density of

the network as more boronic esters can be formed with increasing amount of sugar groups. Consequently, σ_c also increases from 16 Pa to 209 Pa as the stiffness of the hydrogel increases (**Figure 4.2b**). Plotting normalized differential modulus (K'/G_0) against normalized stress (σ/σ_c) shows that the stiffening index m varies with different boronic acid/sugar molar ratios (**Figure 4.2c**). m decreases from 0.62 to 0.37 as the boronic acid/sugar molar ratio increases from 1:0.5 to 1:4 (**Figure 4.2d**). The stiffening index of our hydrogel is relatively lower than biopolymer-based and polyisocyanopeptide (PIC)-based semi-flexible hydrogels ($m \sim 1.5$),[7] which show purely entropic elasticity.[3] The lower m may result from the flexible nature of our polymers, which exhibit both entropic and enthalpic elasticity when being deformed.[30]

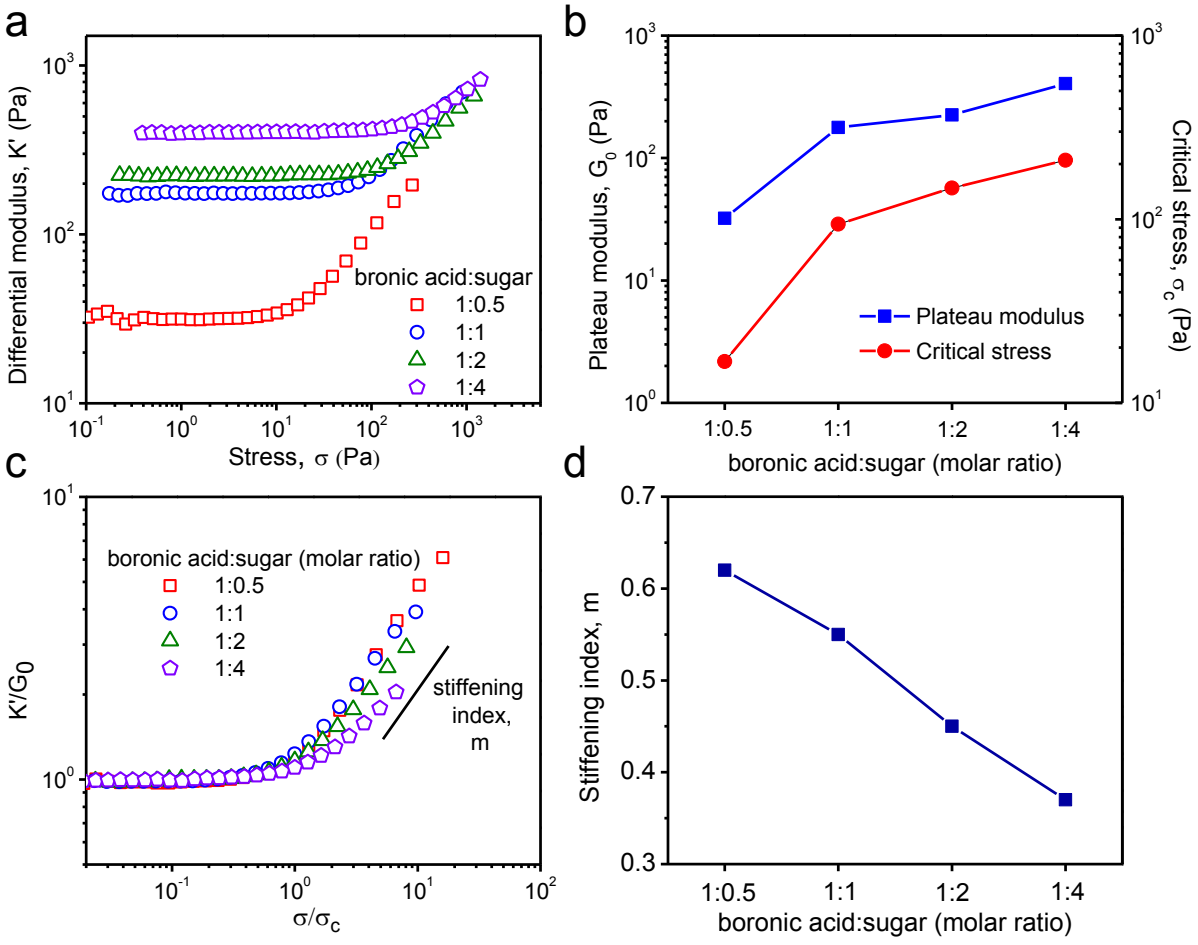

Figure 4.2. Mechanical properties of BL4k hydrogels (10 w/v%, T=25 °C) at different boronic

acid/sugar molar ratios. (a) Differential modulus K' against stress σ. (b) Plateau modulus G_0 and critical stress σ_c against boronic acid/sugar molar ratio. (c) Normalized differential modulus (K'/ G_0) against normalized stress (σ/σ_c). (d) Stiffening index m as a function of boronic acid/sugar molar ratio.

4.3.4 Polymer Concentration Dependence

A series of BL4k hydrogels with a total polymer concentration between 5.0% to 15.0% (w/v%) at boronic acid/sugar molar ratio=1:1 were prepared to tune the mechanical properties. All the samples displayed strain-stiffening behavior, with strong dependence of both G_0 and σ_c on the polymer concentration (**Figure 4.3a**). A 3-fold decrease in polymer concentration not only drops G_0 from ~500 Pa to ~10 Pa, but also drastically lowers σ_c from ~200 Pa to less than 10 Pa (**Figure 4.3b**), which falls within the biologically accessible stress range.[31] Such concentration-dependent network mechanics is similar to various biological gels based on collagen, actin and fibrin.[1-2] In addition, the strain-stiffening response of our hydrogels can be also tuned by varying the polymer concentration (**Figure 4.3c**), which is different from the universal strain-stiffening behavior adopted by semi-flexible hydrogels and PEI/PEG flexible hydrogels with branched network architecture.[7, 21] The stiffening index *m* exhibits ~30% decrease from 0.66 to 0.47 as the polymer concentration increases from 5 to 15 w/v% (**Figure 4.3d**).

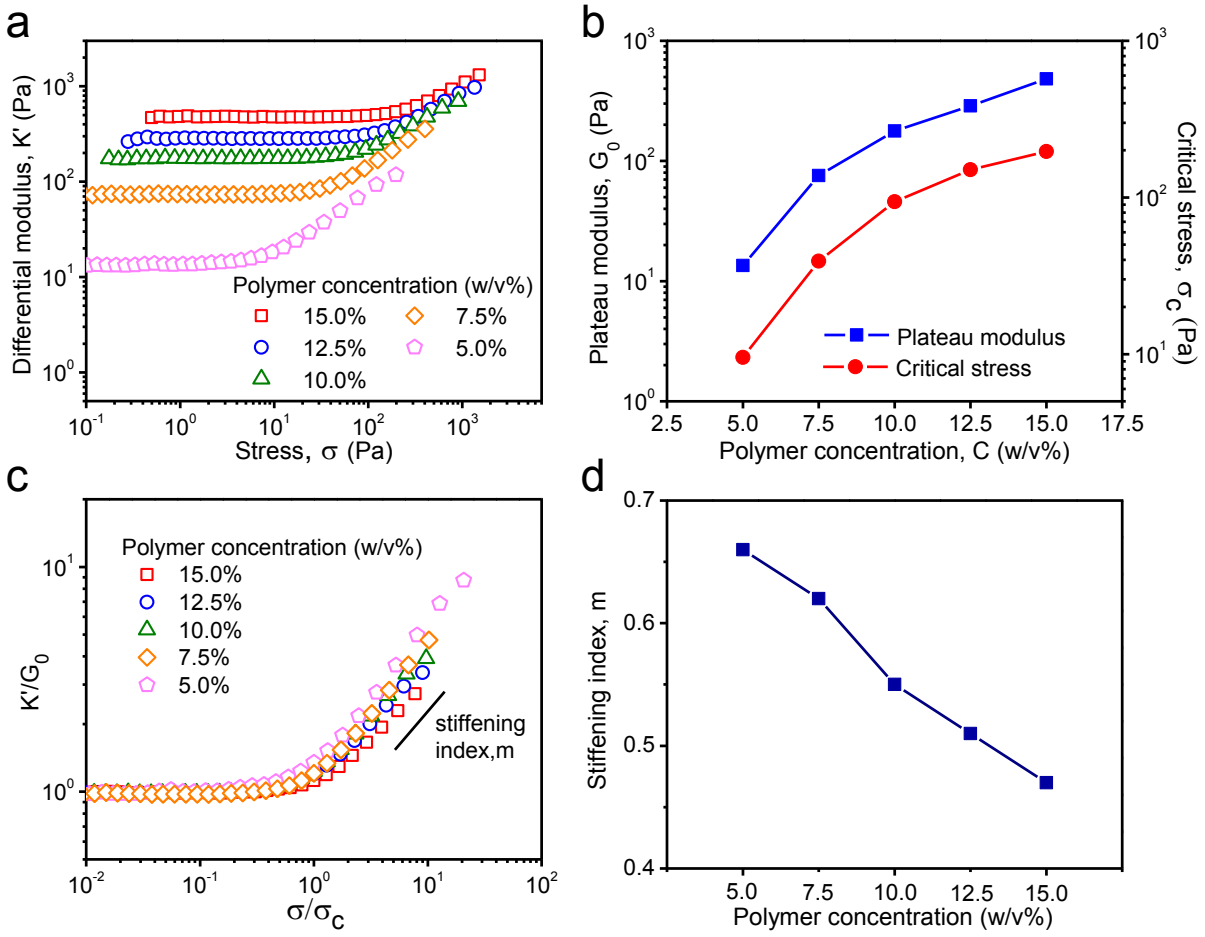

Figure 4.3. Mechanical properties of BL4k hydrogels (boronic acid/sugar molar ratio=1:1, T=25 °C) at different polymer concentration. (a) Differential modulus K' against stress σ. (b) Plateau modulus G_0 and critical stress σ_c against polymer concentration. (c) Normalized differential modulus (K'/G_0) against normalized stress (σ/σ_c). (d) Stiffening index m as a function of polymer concentration.

4.3.5 Temperature Dependence

The temperature effect on mechanical properties of BL4k (boronic acid/sugar molar ratio=1:1, 10 w/v%) was investigated through a temperature ramp test. In a heating ramp, both storage modulus *G'* and loss modulus *G"* decreased as the temperature increased from 15 to 75 °C and recovered the original values in a reversed cooling ramp (**Figure S4.7 in Supporting**

Information). The decreased hydrogel stiffness at elevated temperatures is most likely due to the "softening" behavior of PEG at high temperatures.[32-33] Nevertheless, the hydrogel retained the strain-stiffening behavior within the whole temperature range (**Figure 4.4a and 4.4b**), where both G_0 and σ_c exhibit a 4-fold decrease as the temperature increases from 20 to 70 °C. Interestingly, the normalized differential modulus (K'/G_0) against normalized stress (σ/σ_c) at different temperatures collapsed into a single master curve with m ~0.6 (**Figure 4.4c**), suggesting temperature has limited impact on the strain-stiffening response of our hydrogel.

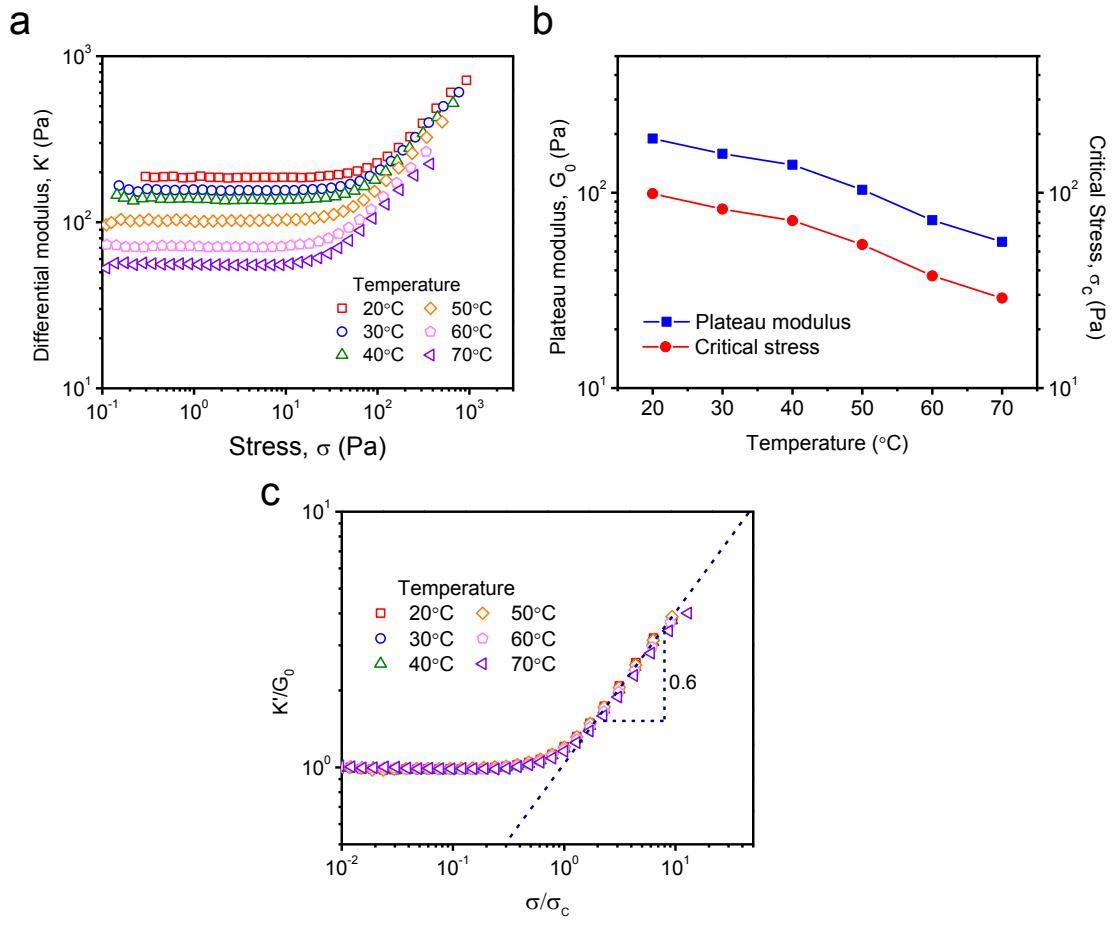

Figure 4.4. Mechanical properties of BL4k hydrogel (boronic acid/sugar molar ratio=1:1, 10 w/v%) at different temperatures. (a) Differential modulus K' against stress σ. (b) Plateau modulus G_0 and critical stress σ_c against temperature. (c) The master curve fitted to the normalized data in (a).

4.3.6 Cross-linker Chain Length Dependence

The network mechanics can be further tailored by altering the length of the cross-linking molecules. Two hydrogels (BL4k and BL8k) with different cross-linker length (DPB-PEG4k and DPB-PEG8k), but the same polymer concentration (10 w/v%) and boronic/sugar molar ratio (1:1) were prepared and measured. The stiffness of the hydrogel (BL8k) crosslinked by longer PEG is smaller than the hydrogel (BL4k) crosslinked by shorter PEG, which thereby leads to a significant decrease of σ_c from 94 to 4.8 Pa (**Figure 4.5a**). The reduction of the stiffness could be attributed to the looser and disorganized network structure. Such effect has been also found in the PIC-based and cytoskeletal polymer-based gels.[19, 34] Plotting normalized differential modulus (K'/G_0) against strain γ for both hydrogels shows that the K' continuously increases in the non-linear response regime until it reaches the maximum strain γ_{max}, where the hydrogel network is ruptured (Figure 4b). The stiffening range K'_{max}/G_0 (i.e., increase of stiffness relative to the initial stiffness before failure) is closely related to the maximum strain that the network could sustain. Due to the higher extension of the longer PEG chains, BL8k could sustain a large $\gamma_{max,}$ which consequently leads to a higher value of K'_{max}/G_0 (**Figure 4.5b**).

Biological tissues span a wide spectrum of stiffness. The stiffness of our hydrogels mainly matches those relatively soft tissues, including intestinal mucosa, neural tissue, crystalline lens, adipose tissue as well as extracellular matrix (ECM) composed of collagen, actin, fibrin and neurofilaments.[1, 35] To match the higher stiffness of other biological tissues (e.g., skin, muscle, etc.) with strain-stiffening response, one can possibly consider to introduce some stiff nanomaterials (e.g., carbon nanotubes, cellulose nanocrystals, etc.) or a 2nd semi-flexible network into the hydrogel, which could not only stiffen the material, but also preserve the biomimetic strain-stiffening mechano-repsonse.

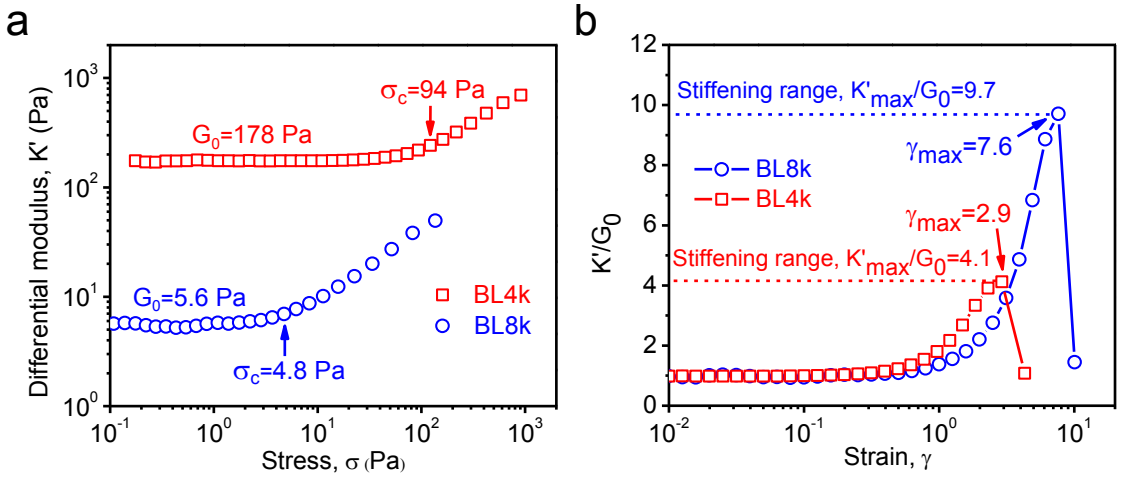

Figure 4.5. Mechanical properties of BL4k and BL8k (boronic acid/sugar molar ratio=1:1, 10 w/v%, T=25 °C). (a) Differential modulus K' against stress σ. (b) Normalized differential modulus (K'/ G_0) against strain (γ) showing the maximum strain γ_{max} and stiffening range K'_{max}/G_0.

4.3.7 Reversibility and Reproducibility of Strain-stiffening Behavior

Similar to biological tissues, our hydrogel can provide on-demand and targeted mechanical properties due to the reversible strain-stiffening capability. Both BL4k and BL8k can be repeatedly stiffened to a designated *G'* value and maintain such mechanical strength as long as a suitable strain is continuously applied (**Figure 4.6a** and **4.6b**). The original mechanical properties of the hydrogels are immediately recovered once the applied strain is reduced.

Unlike some biopolymer networks that delay the onset of strain-stiffening response at a gradually increasing strain after being repeatedly deformed,[36] the strain history does not affect the strain-stiffening response of the as-prepared hydrogel. Seven sequential strain sweeps were performed on BL8k by applying strain from 0.05 to 7.5 (below γ_{max} =7.6). The strain-stiffening profiles of the hydrogel follow the same trace and the hydrogel can be reversibly and repeatedly stiffened to 8 times of its original modulus, without showing mechanical hysteresis (**Figure 4.6c**). The reproducibility of the strain-stiffening behavior shows promises for various bioengineering

applications, such as cell culture matrices, artificial muscle, soft robotics and intelligent soft machines, which are required to tolerate repeated deformation.

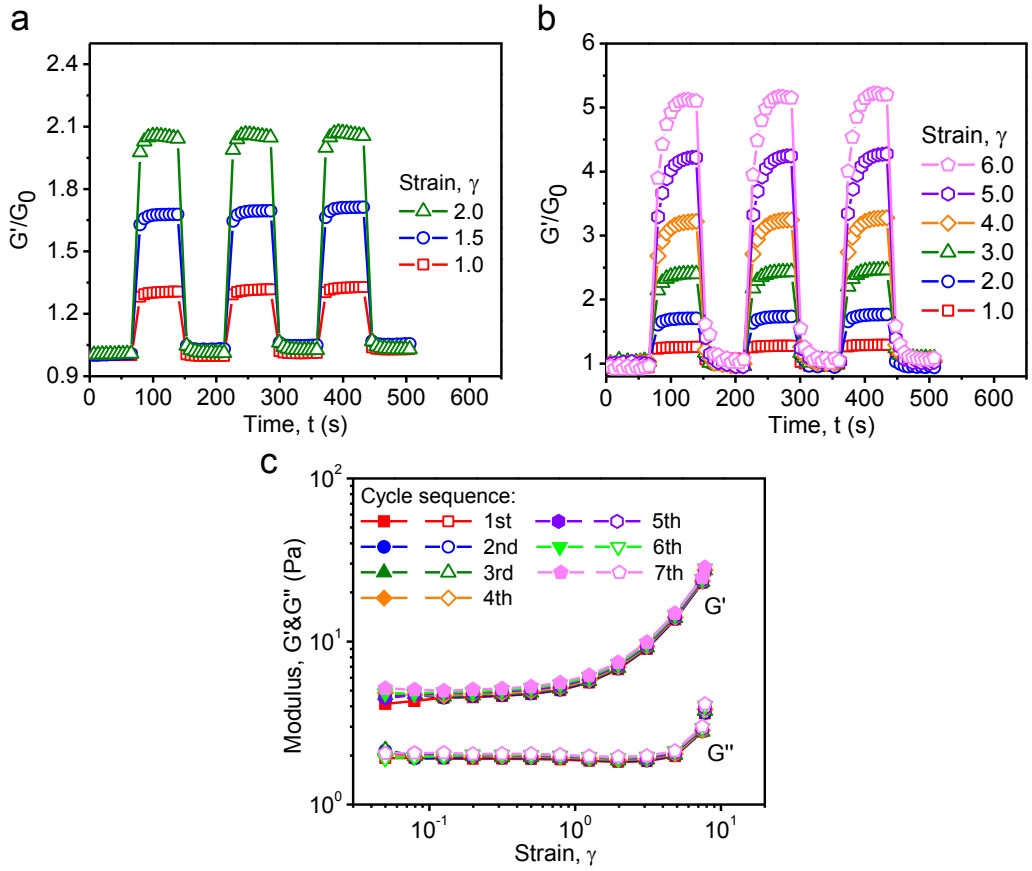

Figure 4.6. (a) Cyclic strain step tests of BL4k (boronic acid/sugar molar ratio=1:1, 10 w/v%, T=25 °C) (b) Cyclic strain step tests of BL8k (boronic acid/sugar molar ratio=1:1, 10 w/v%, T=25 °C). (c) Seven sequential strain sweeps of the hydrogel tested in (b).

4.3.8 Strain-stiffening Mechanism

In our hydrogel system, the biomimetic strain-stiffening behavior is originated from the non-linear stretching and finite extensibility of the PEG.[21, 37] The role of another linear polymer P(AM-*co*-LAEMA) is to provide sufficient amount of 1,3-diol groups, which allow both ends of DPB-PEGs to be covalently bonded through the formation of boronate esters. As shown in **Figure 4.7**, once two ends of DPB-PEGs are strongly bonded, the PEG strands could act like springs when

being strained. During deformation, the randomly oriented PEG strands tend to align parallel with the strain/stress direction. As the PEG strands are stretched to their "straightened" state, the conformational entropy is significantly reduced and the flexible PEG strands could exhibit some enthalpic elasticity due to bending or stretching of the covalent bonds within the PEG strands. The synergy of both effects could induce an opposing force against the applied strain/stress, which leads to the stiffening response of the network. The strain-stiffening effects dominate the mechanical behavior of the hydrogel, causing the drastic increase of *G'* until the PEG strands are stretched to the maximum extensibility (γ_{max}), where the rupture of the hydrogel occurs.

The theoretical value of γ_{max} can be roughly estimated from the maximum uniaxial extension ratio λ_{max} of a linear polymer chain using the following reported equations:[37-38]

$$\lambda_{max} = \frac{l_{max}}{l_0} \tag{1}$$

$$l_0 = \sqrt{2 l_p l_{max} [1 - \frac{l_p}{l_{max}} (1 - e^{-l_{max}/l_p})]} \tag{2}$$

$$\gamma_{max} = \lambda_{max} - {\lambda_{max}}^{-1} \tag{3}$$

where l_{max} is the contour length of a fully extended polymer chain, which can be calculated based on the PEO monomer repeating unit length of 0.28 nm in water;[39] l_0 is the end-to-end distance of the unstretched polymer chain, which can be calculated from the persistence length l_p of PEG in water (l_p of PEG ≈ 0.37 nm).[38] Based on **Equations (1)-(3)**, γ_{max} is calculated to be 5.7 and 8.2 for DPB-PEG4k and DPB-PEG8k respectively, which is greater than the experimental values 2.9 and 7.6.

The difference between the theoretical and experimental values may arise from: 1) the PEG are constrained and crosslinked in a network structure. The extension of the crosslinked PEG is greatly limited as compared with the case in the bulk solution. 2) the estimated l_0 may not be precise

since the PEG could adopt different conformations from those in the bulk solution, resulting from polymer entanglement and other intermolecular interactions within the network. 3) the bond strength of boronic esters is relatively low due to the dynamic nature. They can be possibly ruptured before the PEG strands being stretched to the maximum extension, leading to a lower experimental γ_{max}.

Although many hydrogels crosslinked by PEG have been reported, the strain-stiffening mechano-response is rarely observed. Several key factors play important roles in realizing and tuning the strain-stiffening response in such type of flexible hydrogels. First, the dynamic nature offers great flexibility and extensibility of the polymer network,[40] which contributes to the unique stiffening response during deformation. Second, the molecular weight of the precursor polymers could affect the network mechanics. The molecular weight of the synthetic glycopolymer P(AM-*co*-LAEMA) used in our system is relatively smaller than the natural macromolecules (e.g., chitosan, hyaluronic acid, cellulose, etc.), which are often used in the hydrogels crosslinked by PEG.[41-43] As a result, less polymer entanglement is expected in our network, which thereby permits the "free" motions of PEG upon network deformation. The selection of suitable molecular weight of our polymer could provide useful insights into the molecular design of strain-stiffening flexible hydrogels, with implications for future investigation of the molecular weight dependence of the strain-stiffening response. Third, networks with relatively low crosslinking density are more likely to obtain strain-stiffening property since the polymer strands can be stretched under less restriction. In fact, we found that the hydrogel with lower crosslinking density possesses a stronger strain-stiffening response as suggested by the increase of stiffening index. However, lower crosslinking density also leads to the reduction of material stiffness. Fourth, the total polymer concentration also plays important roles in tuning the network mechanics. Higher polymer concentration would

also enhance polymer entanglement and other intermolecular interactions (e.g., hydrogen bonding) within the network, which also limits the extension of PEG. Similar to the effect of crosslinking density, decreasing polymer concentration could achieve a stronger strain-stiffening response, while sacrificing the initial stiffness. Last but not least, the overall increase in stiffness of the material (i.e., stiffening range, K'_{max}/G_0) can be tuned by varying the length of the crosslinkers. Although using longer crosslinkers could extend the stiffening range, it also decreases the stiffness of the hydrogel due to a less compact and organized network structure. Generally, increasing the stiffness of flexible hydrogels would weaken the non-linear strain-stiffening response and make them less sensitive to the applied stress. Such trend has been also found in a strain-stiffening hybrid network based on PIC semi-flexible and polyacrylamide (PAM) flexible polymers.[44] To conclude, strain-stiffening flexible hydrogels should be constructed based on dynamic molecular interactions and one could balance the material stiffness and the strain-stiffening response by tuning the molecular weight of precursor polymers, the crosslinking density, the total polymer concentration as well as the length of the crosslinkers.

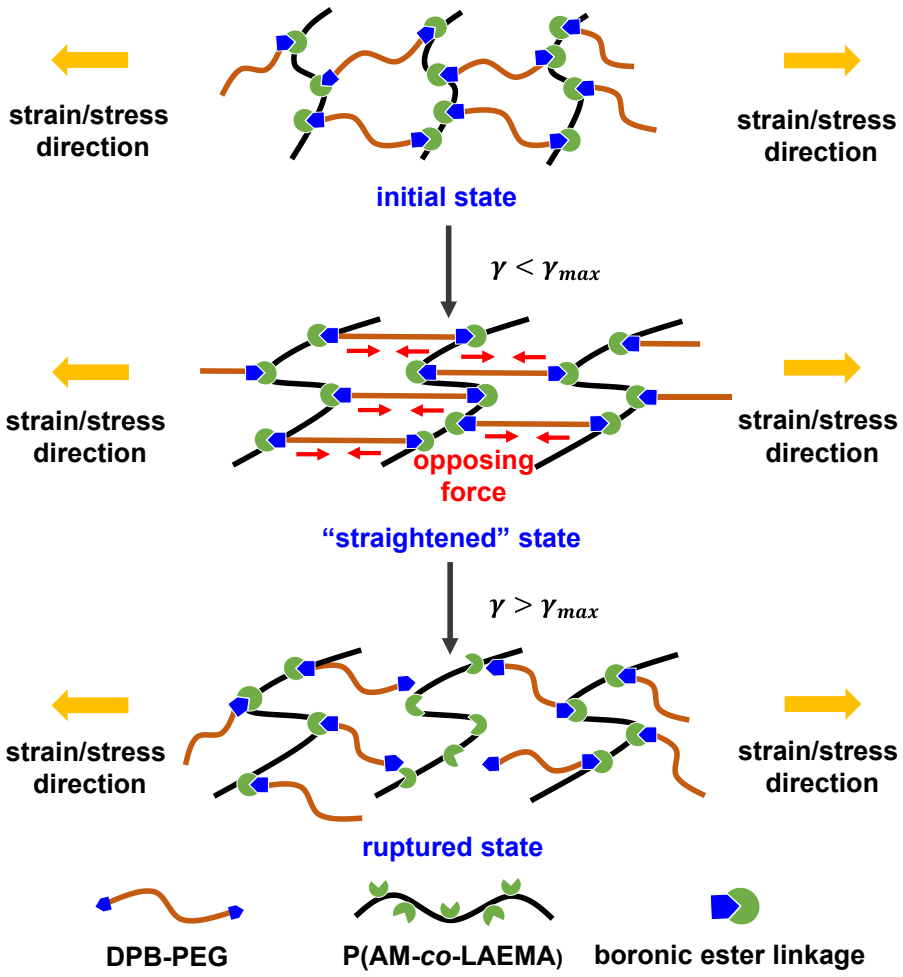

Figure 4.7. Illustration of the strain-stiffening mechanism.

4.3.9 Self-healing Property and Associated Interaction Mechanism

When strain-stiffening capability of biological tissues fails to maintain the integrity above maximum strain, they adopt the strategy of self-healing to heal the damage and recover the original properties. Our strain-stiffening hydrogel also possesses such biomimetic self-healing capability. As shown in **Figure 4.8a-d** and **Video S4.1**, after bringing two pieces of separated hydrogels into contact, the hydrogels could adhere to each other and autonomously merge into one single piece within a few seconds. The self-healed hydrogel can be easily lifted against its own weight without breakage. The self-healing property of the hydrogels was further investigated by sequential strain

sweeps. It was found that after being damaged at a high strain (γ= 6.0, above γ_{max} = 2.9), the damaged hydrogel could not only immediately self-heal to recover the original mechanical strength, but also fully retain the strain-stiffening capability (**Figure 4.8e**). Similar self-healing behavior was observed in other hydrogels with different polymer concentrations (**Figure S4.8a-S4.8d in Supporting Information**). The reproducibility of the self-healing property is further confirmed by performing cyclic strain step tests, where both *G'* and *G"* could fully recover to the original values even after the hydrogel being repeatedly ruptured (**Figure 4.8f**).

To gain insights into the self-healing mechanism, a surface forces apparatus (SFA) was employed to quantitatively probe the molecular interactions between P(AM-*co*-LAEMA) and DPB-PEG or unmodified PEG at nano-scale using symmetric configuration (**Figure S4.9 in Supporting Information**). Reversible adhesion forces of F_{ad}/R ~ 6.1 mN/m (W_{ad} ~ 1.3 mJ/m^2) were measured between P(AM-*co*-LAEMA) and DPB-PEG (**Figure 4.8g**) in three sequential approach−separation force measurements. In contrast, no adhesion was observed between P(AM-*co*-LAEMA) and the unmodified PEG (**Figure S4.10 in Supporting Information**). Considering the structural difference in end groups between two types of PEG, the adhesion is attributed to the formation of dynamic boronic ester bonds between diphenylboronic acid and 1,3-diol groups across two surfaces, which should play a dominant role in the excellent self-healing capability of our hydrogel. Moreover, the reversible nature of the adhesion force between P(AM-*co*-LAEMA) and DPB-PEG also well agrees with the reproducibility of the self-healing behavior.

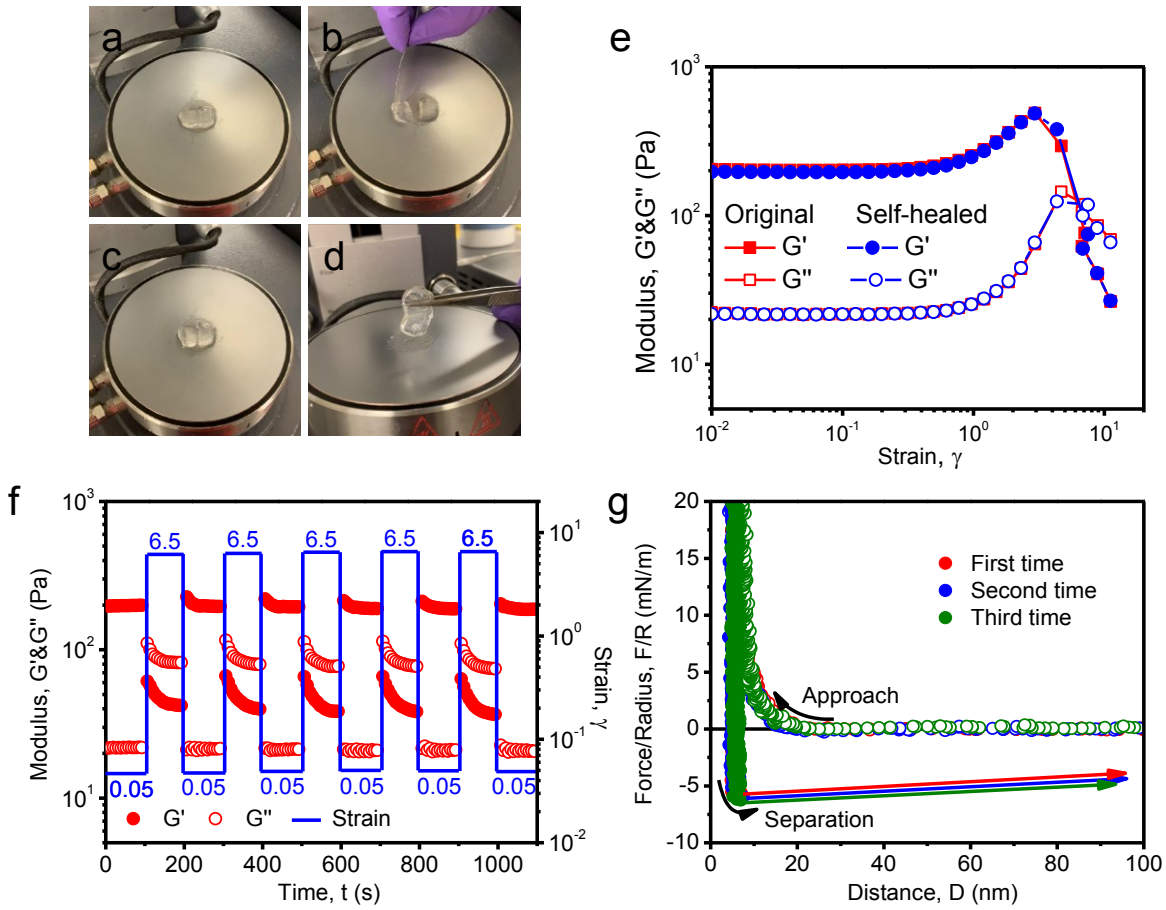

Figure 4.8. The self-healing process of BL4k (boronic acid/sugar=1:1, 10 w/v%, T=25 °C). (a) original hydrogel, (b) hydrogel was cut into two pieces, (c) separated hydrogels were brought into contact, (d) self-healed hydrogel can be lifted against its own weight. (e) Sequential strain sweeps of BL4k (boronic acid/sugar molar ratio=1:1, 10 w/v%, T=25 °C). (f) Cyclic strain step tests of the hydrogel tested in (e). (g) Force-distance profiles show the interactions between P(AM-co-LAEMA) and DPB-PEG in three sequential approach−separation force measurements.

4.3.10 3D Cell Encapsulation

The potential application of our biomimetic hydrogels is to be used as artificial ECM to encapsulate cells and further grow artificial tissues or organs for tissue engineering. Culturing cancer cells is of particular interest to create tumor tissue models for precision medicine.[45] In this

study, HeLa cells were chosen as the model cells to preliminarily investigate the cytotoxicity and 3D cell encapsulation ability of our hydrogel. As shown in **Figure 4.9a** and **4.9b**, the live cells (green colour) take the majority of the population compared with the dead cells (red colour). The cell viability is assessed to be ~80% in both 5 and 10 w/v% BL4k hydrogel after 24 h (**Figure 4.9c**), which confirms the excellent biocompatibility of our hydrogels. However, compared with the round shape morphology of HeLa cells, which are homogeneously distributed in the 10 w/v% hydrogel, the cells exhibit flat morphology and sink to the bottom in the 5 w/v% hydrogel. The results suggest that low material stiffness could not provide ideal 3D environment for the cell growth.

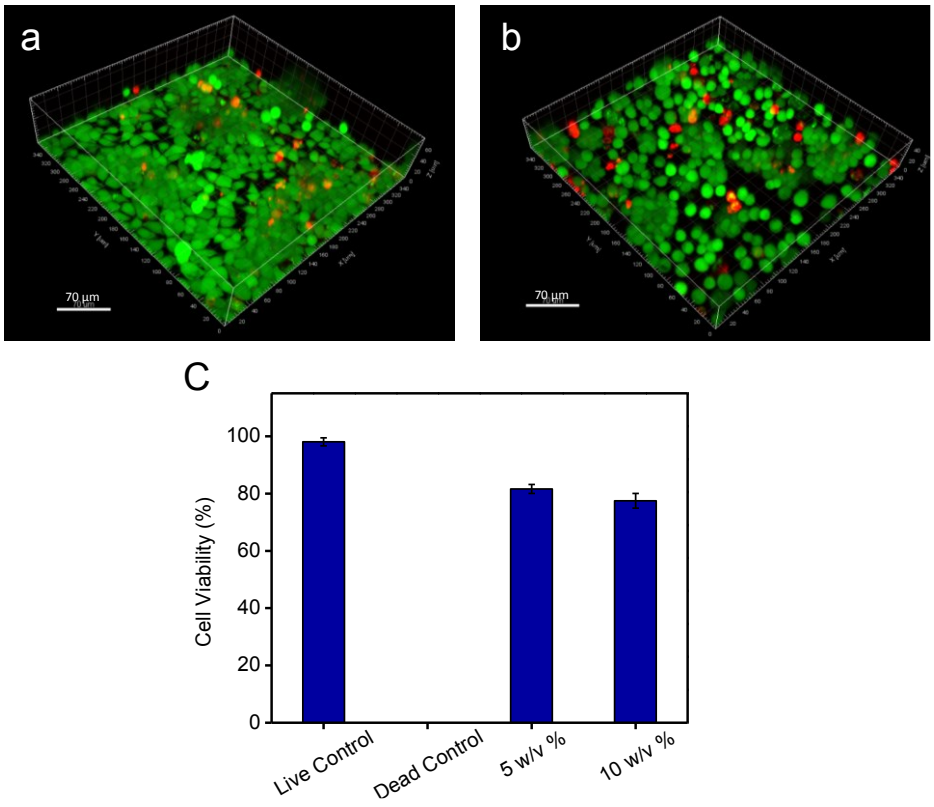

Figure 4.9. 3D confocal microscopy images of HeLa cells cultured in (a) 5 w/v%, (b) 10 w/v% BL4k hydrogel. (c) Cell viability quantification after 24 h incubation (live control: DMEM+10% FBS; dead control: 70% ethanol). Images were taken from randomly selected 5 fields and

quantification was done using Imaris Imaging Software. Data shown represents the means ± S.D., n=5.

4.4 Conclusions

In summary, we successfully realize both tissue-like strain-stiffening and self-healing functions in a flexible hydrogel network constructed by biocompatible glycopolymers and boronic acid-functionalized PEG. The biomimetic hydrogel can elegantly adopt either strain-stiffening or self-healing protective strategy to maintain the integrity and original properties in response to mechanical stress. Moreover, our novel biocompatible hydrogel shows the great promises to be used for 3D cell encapsulation. The current work provides novel insights into the molecular design of strain-stiffening materials, with useful implications for the development of biomimetic cell culture matrices, artificial tissues as well as soft machines and robotics for various biomedical and engineering applications.

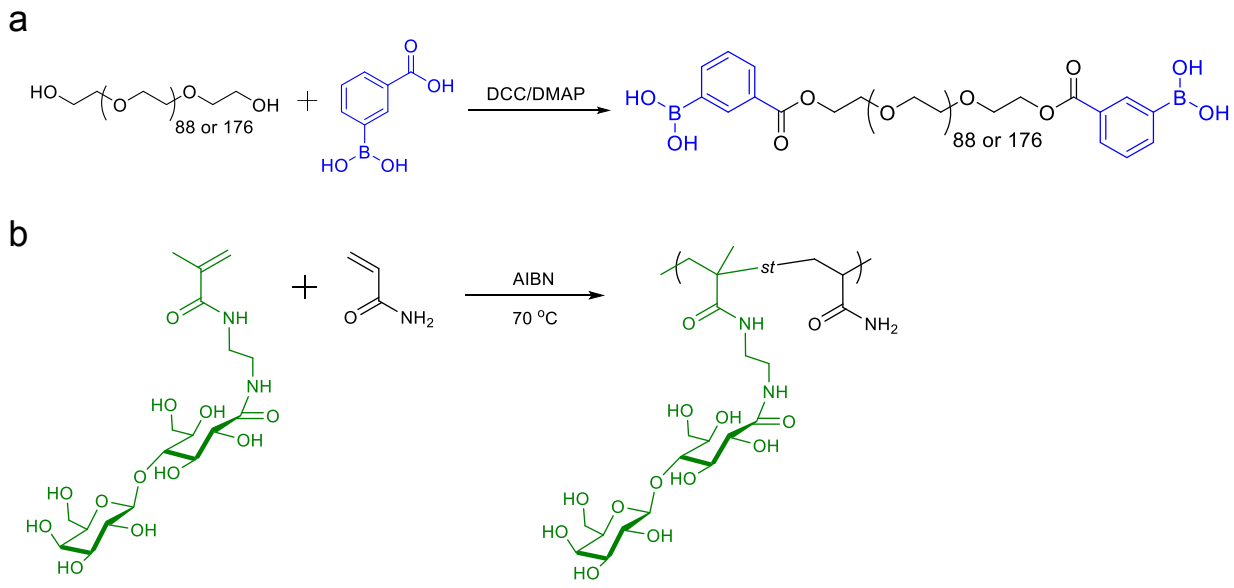

Figure S4.1. (a) Synthesis route of DPB-PEG4k/8k. (b) Synthesis route of glycopolymer P(AM-co-LAEMA)

Characterizations of Polymers

From the ^{1}H NMR spectrum of DPB-PEG4k (**Figure S4.2**), the peaks assigned to benzene ring (signal **a, b, c, d**: δ = 8.41, 8.12, 8.01, 7.57 ppm) and ester methylene (signal **e**: δ = 4.47 ppm) were clearly observed. The integration ratio among I_a, I_b, I_c, I_d and I_e was calculated to be ~1:1:1:2, indicating the hydroxyl groups at both ends of PEG were converted to phenylboronic acids. The successful synthesis of DPB-PEG4k was further confirmed by FT-IR. Compared with the spectrum of unmodified PEG4k, two new peaks appeared at 1750 and 700 cm^{-1}, which are assigned to C=O stretching of ester bond and aromatic C-H bending, respectively (**Figure S4.3**). The successful synthesis of DPB-PEG8k was verified through the similar methods.

P(AM-*co*-LAEMA) was characterized by ^{1}H NMR, in which the characteristic sugar peaks can be clearly observed (**Figure S4.4**), indicating the successful copolymerization of the LAEMA monomers. The molar percentage of AM and LAEMA was determined to be 67.8% and 32.2% by

comparing the peaks of the polymer backbone, which is consistent with the designed ratio.

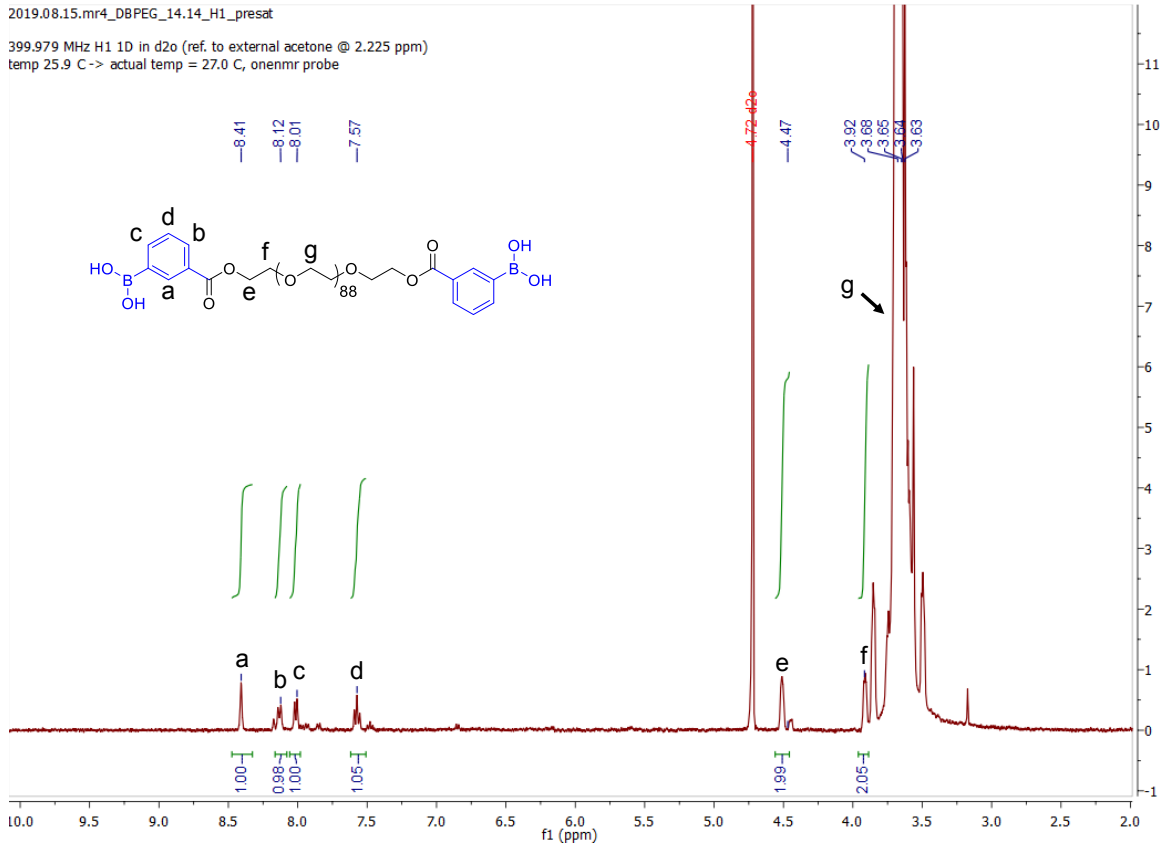

Figure S4.2. ^{1}H NMR spectrum of DPB-PEG4k. δ_H (ppm)= 8.41, 8.12, 8.01, 7.57 (B(OH$_2$)C$_6$**H**$_4$), 4.47 (-COO-C**H**$_2$-CH$_2$-), 3.92 (-COO-CH$_2$-C**H**$_2$-), 3.63-3.68 (-O-C**H**$_2$-C**H**$_2$-O-).

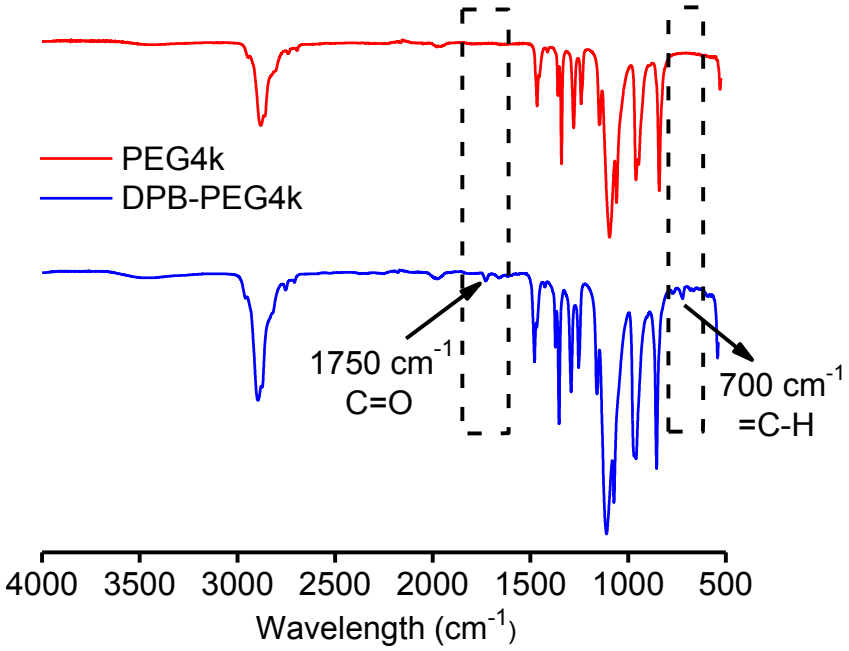

Figure S4.3. FT-IR spectra of PEG4k and DPB-PEG4k. Wavelength (cm^{-1})= 1750 (C=O stretching), 700 (C-H bending, aromatic).

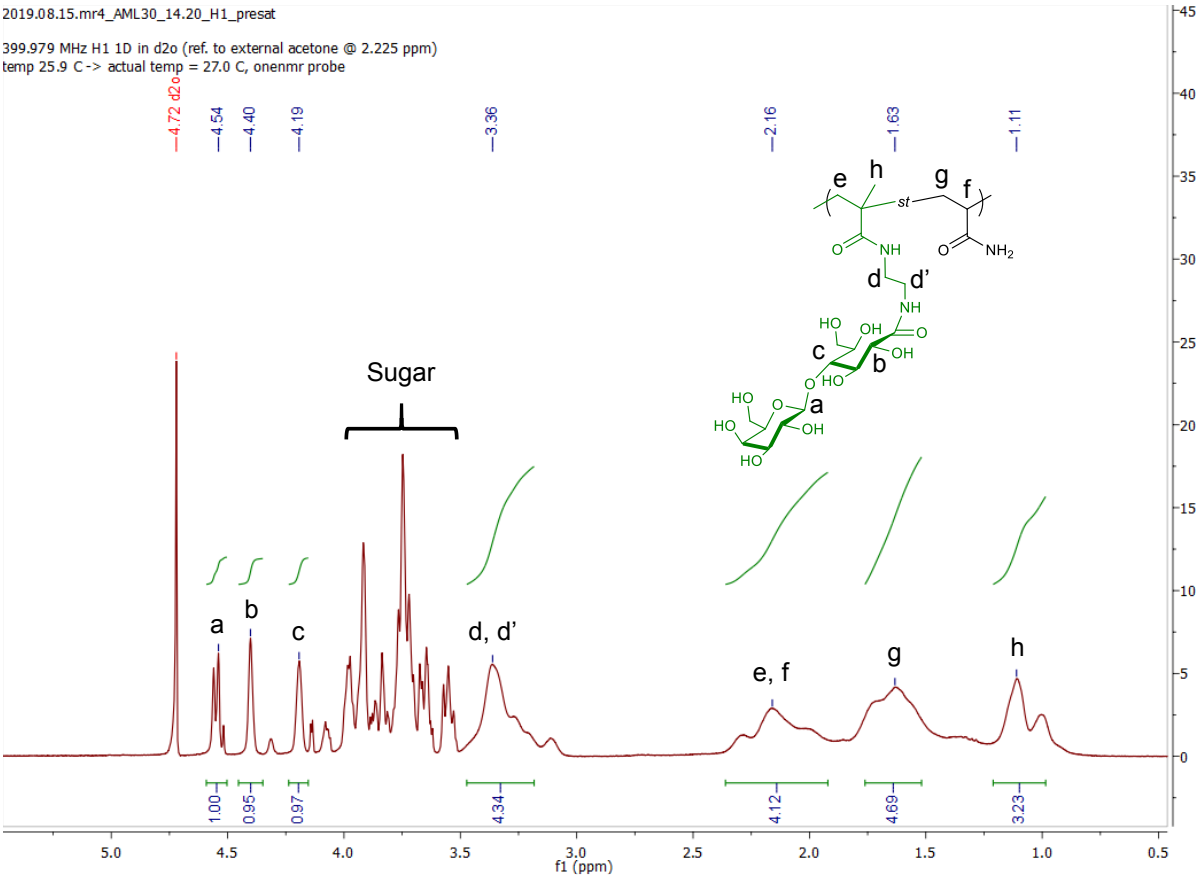

Figure S4.4. ^{1}H NMR spectrum of P(AM-co-LAEMA). δ_H (ppm)= 4.54 (-O-C**H**-O-), 4.40 (OH-C**H**-CO-), 4.19 (-O-CH_2-O-C**H**-), 3.36 (CO-NH-C$\mathbf{H}_2$-C$\mathbf{H}_2$-NH-).

Figure S4.5. After mixing PBS solutions of DPB-PEG4k and P(AM-co-LAEMA), the BL4k hydrogel (boronic acid/sugar=1:1, 10 w/v%) was formed and stayed still when the vial was inverted.

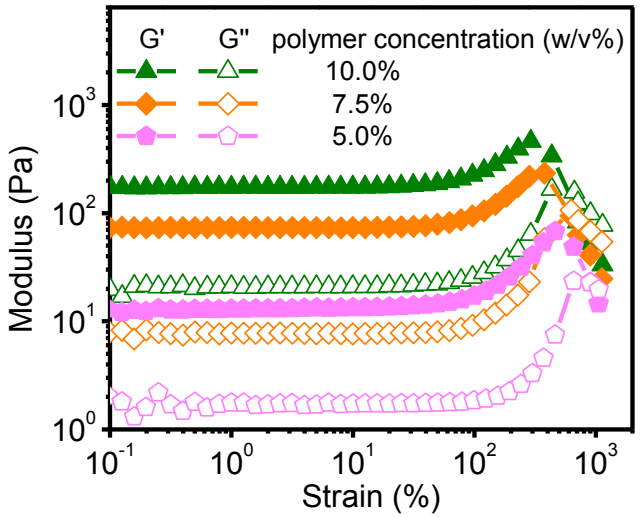

Figure S4.6. Dynamic oscillatory strain amplitude sweeps show the well-defined non-linear strain-stiffening behavior of BL4k hydrogels (boronic acid/sugar=1:1; 10, 7.5, 5 w/v%).

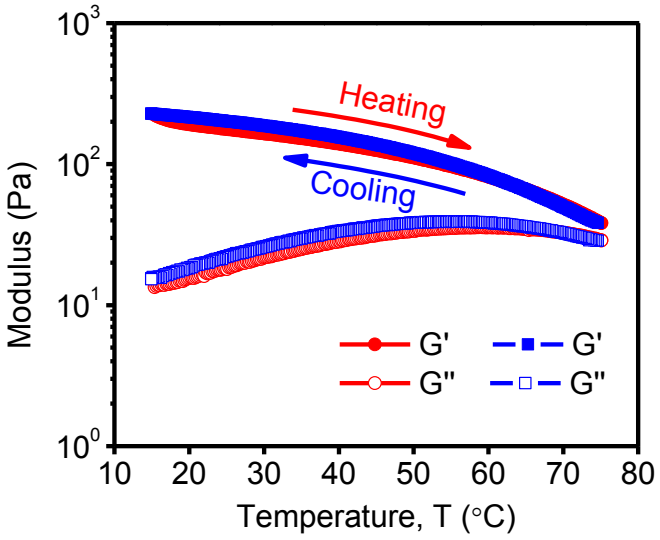

Figure S4.7. Temperature ramp tests conducted on BL4k hydrogel (boronic acid/sugar=1:1, 10 w/v%) show the temperature-dependent mechanical properties.

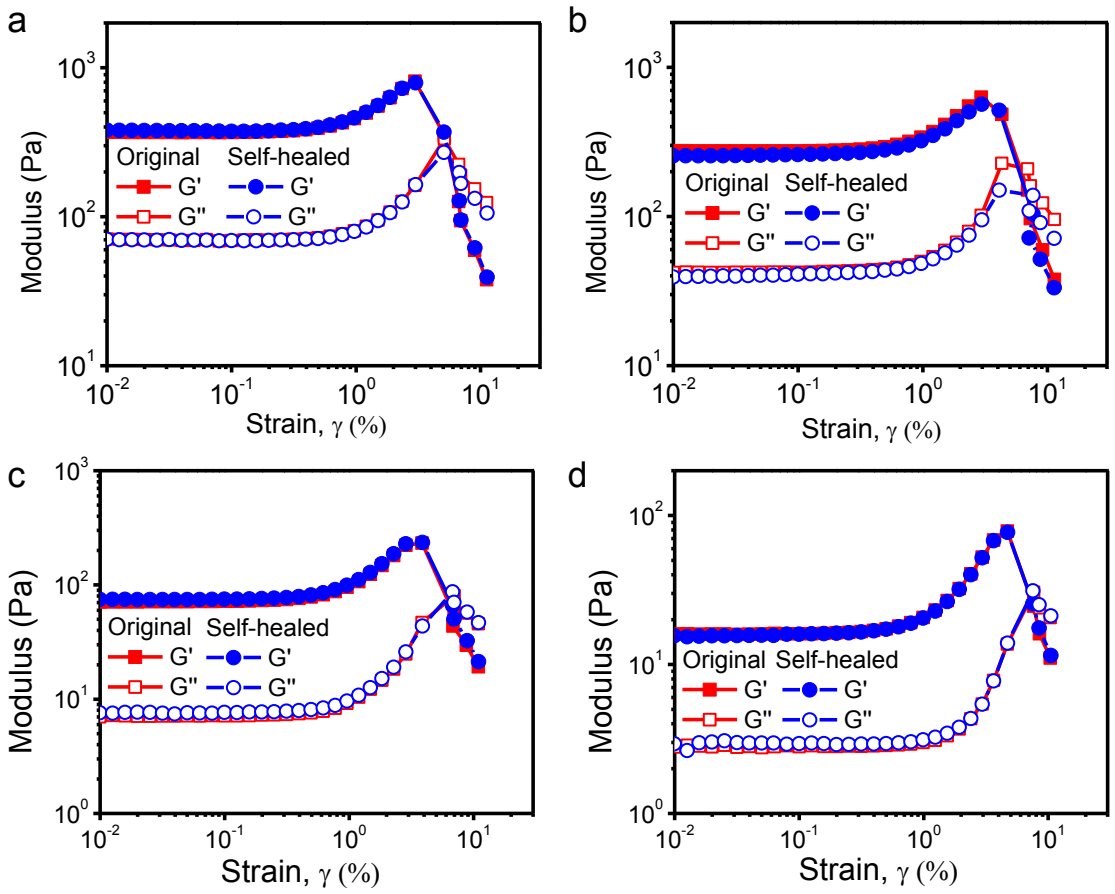

Figure S4.8. Sequential strain amplitude tests show the self-healing capability of BL4k hydrogels (boronic acid/sugar=1:1, T=25 °C) with different polymer concentrations. (a) 15 w/v%, (b) 12.5 w/v%, (c) 7.5 w/v% and (d) 5 w/v%.

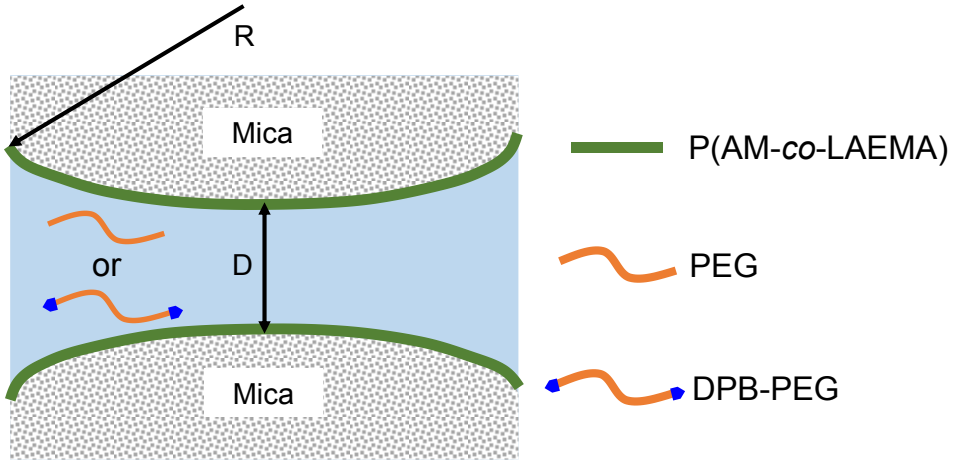

Figure S4.9. Illustration of symmetric configuration for SFA force measurements.

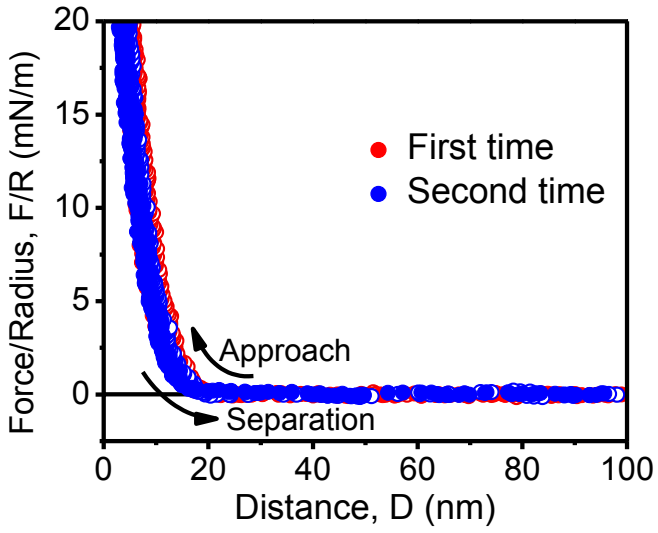

Figure S4.10. Force-distance profiles show the interactions between P(AM-co-LAEMA) and PEG in sequential approach−separation force measurements.

Video S4.1 Self-healing property of the hydrogel BL4k (boronic acid/sugar=1:1, 10 w/v%, T=25 °C).

Link for the video: https://pubs.acs.org/doi/10.1021/acs.chemmater.0c035

References

(1) Storm, C.; Pastore, J. J.; MacKintosh, F. C.; Lubensky, T. C.; Janmey, P. A. Nonlinear elasticity in biological gels. *Nature* **2005,** *435* (7039), 191-194.

(2) Licup, A. J.; Munster, S.; Sharma, A.; Sheinman, M.; Jawerth, L. M.; Fabry, B.; Weitz, D. A.; MacKintosh, F. C. Stress controls the mechanics of collagen networks. *Proc. Natl. Acad. Sci. USA* **2015,** *112* (31), 9573-9578.

(3) Pujol, T.; du Roure, O.; Fermigier, M.; Heuvingh, J. Impact of branching on the elasticity of actin networks. *Proc. Natl. Acad. Sci. USA* **2012,** *109* (26), 10364-10369.

(4) Das, R. K.; Gocheva, V.; Hammink, R.; Zouani, O. F.; Rowan, A. E. Stress-stiffening-mediated stem-cell commitment switch in soft responsive hydrogels. *Nat. Mater.* **2016,** *15* (3), 318-325.

(5) Liu, K.; Mihaila, S. M.; Rowan, A.; Oosterwijk, E.; Kouwer, P. H. J. Synthetic Extracellular Matrices with Nonlinear Elasticity Regulate Cellular Organization. *Biomacromolecules* **2019,** *20* (2), 826-834.

(6) Kouwer, P. H.; Koepf, M.; Le Sage, V. A.; Jaspers, M.; van Buul, A. M.; Eksteen-Akeroyd, Z. H.; Woltinge, T.; Schwartz, E.; Kitto, H. J.; Hoogenboom, R.; Picken, S. J.; Nolte, R. J.; Mendes, E.; Rowan, A. E. Responsive biomimetic networks from polyisocyanopeptide hydrogels. *Nature* **2013,** *493* (7434), 651-655.

(7) Jaspers, M.; Dennison, M.; Mabesoone, M. F.; MacKintosh, F. C.; Rowan, A. E.; Kouwer, P. H. Ultra-responsive soft matter from strain-stiffening hydrogels. *Nat. Commun.* **2014,** *5*, 5808.

(8) Fernandez-Castano Romera, M.; Lafleur, R. P. M.; Guibert, C.; Voets, I. K.; Storm, C.; Sijbesma, R. P. Strain Stiffening Hydrogels through Self-Assembly and Covalent Fixation of Semi-Flexible Fibers. *Angew. Chem. Int. Ed.* **2017,** *56* (30), 8771-8775.

(9) Tang, J. D.; Mura, C.; Lampe, K. J. Stimuli-Responsive, Pentapeptide, Nanofiber Hydrogel for

Tissue Engineering. *J. Am. Chem. Soc.* **2019,** *141* (12), 4886-4899.

(10) Wang, Y.; Xu, Z.; Lovrak, M.; le Sage, V. A. A.; Zhang, K.; Guo, X.; Eelkema, R.; Mendes, E.; van Esch, J. H. Biomimetic Strain-Stiffening Self-Assembled Hydrogels. *Angew. Chem. Int. Ed.* **2020,** *59* (12), 4830-4834.

(11) Li, L.; Yan, B.; Yang, J.; Chen, L.; Zeng, H. Novel mussel-inspired injectable self-healing hydrogel with anti-biofouling property. *Adv. Mater.* **2015,** *27* (7), 1294-9.

(12) Owusu-Nkwantabisah, S.; Gillmor, J.; Switalski, S.; Mis, M. R.; Bennett, G.; Moody, R.; Antalek, B.; Gutierrez, R.; Slater, G. Synergistic Thermoresponsive Optical Properties of a Composite Self-Healing Hydrogel. *Macromolecules* **2017,** *50* (9), 3671-3679.

(13) Deng, Z.; Guo, Y.; Zhao, X.; Ma, P. X.; Guo, B. Multifunctional Stimuli-Responsive Hydrogels with Self-Healing, High Conductivity, and Rapid Recovery through Host–Guest Interactions. *Chem. Mater.* **2018,** *30* (5), 1729-1742.

(14) Wang, W.; Xiang, L.; Gong, L.; Hu, W.; Huang, W.; Chen, Y.; Asha, A. B.; Srinivas, S.; Chen, L.; Narain, R.; Zeng, H. Injectable, Self-Healing Hydrogel with Tunable Optical, Mechanical, and Antimicrobial Properties. *Chem. Mater.* **2019,** *31* (7), 2366-2376.

(15) Wu, D.; Wang, W.; Diaz-Dussan, D.; Peng, Y.-Y.; Chen, Y.; Narain, R.; Hall, D. G. In Situ Forming, Dual-Crosslink Network, Self-Healing Hydrogel Enabled by a Bioorthogonal Nopoldiol–Benzoxaborolate Click Reaction with a Wide pH Range. *Chem. Mater.* **2019,** *31* (11), 4092-4102.

(16) Chen, Y.; Wang, W.; Wu, D.; Zeng, H.; Hall, D. G.; Narain, R. Multiresponsive and Self-Healing Hydrogel via Formation of Polymer-Nanogel Interfacial Dynamic Benzoxaborole Esters at Physiological pH. *ACS Appl. Mater. Interfaces* **2019,** *11* (47), 44742-44750.

(17) Kim, S. M.; Jeon, H.; Shin, S. H.; Park, S. A.; Jegal, J.; Hwang, S. Y.; Oh, D. X.; Park, J.

Superior Toughness and Fast Self-Healing at Room Temperature Engineered by Transparent Elastomers. *Adv. Mater.* **2018,** *30* (1), 1705145.

(18) Fernandez-Castano Romera, M.; Lou, X.; Schill, J.; Ter Huurne, G.; Fransen, P. K. H.; Voets, I. K.; Storm, C.; Sijbesma, R. P. Strain-Stiffening in Dynamic Supramolecular Fiber Networks. *J. Am. Chem. Soc.* **2018,** *140* (50), 17547-17555.

(19) Schoenmakers, D. C.; Rowan, A. E.; Kouwer, P. H. J. Crosslinking of fibrous hydrogels. *Nat. Commun.* **2018,** *9* (1), 2172.

(20) Schultz, R. K.; Myers, R. R. The Chemorheology of Poly(vinyl alcohol)-Borate Gels. *Macromolecules* **1969,** *2* (3), 281-285.

(21) Yan, B.; Huang, J.; Han, L.; Gong, L.; Li, L.; Israelachvili, J. N.; Zeng, H. Duplicating Dynamic Strain-Stiffening Behavior and Nanomechanics of Biological Tissues in a Synthetic Self-Healing Flexible Network Hydrogel. *ACS Nano.* **2017,** *11* (11), 11074-11081.

(22) Moghimi, S. M.; Symonds, P.; Murray, J. C.; Hunter, A. C.; Debska, G.; Szewczyk, A. A two-stage poly(ethylenimine)-mediated cytotoxicity: implications for gene transfer/therapy. *Mol. Ther.* **2005,** *11* (6), 990-995.

(23) Deng, Z.; Li, S.; Jiang, X.; Narain, R. Well-Defined Galactose-Containing Multi-Functional Copolymers and Glyconanoparticles for Biomolecular Recognition Processes. *Macromolecules* **2009,** *42* (17), 6393-6405.

(24) Narain, R.; Armes, S. P. Synthesis of low polydispersity, controlled-structure sugar methacrylate polymers under mild conditions without protecting group chemistry. *Chem. Commn.* **2002,** (23), 2776-2777.

(25) Broedersz, C. P.; Kasza, K. E.; Jawerth, L. M.; Münster, S.; Weitz, D. A.; MacKintosh, F. C. Measurement of nonlinear rheology of cross-linked biopolymer gels. *Soft Matter* **2010,** *6* (17),

4120-4127.

(26) Israelachvili, J.; Min, Y.; Akbulut, M.; Alig, A.; Carver, G.; Greene, W.; Kristiansen, K.; Meyer, E.; Pesika, N.; Rosenberg, K.; Zeng, H. Recent advances in the surface forces apparatus (SFA) technique. *Rep. Prog. Phys.* **2010,** *73* (3), 036601.

(27) Xiang, L.; Gong, L.; Zhang, J.; Zhang, L.; Hu, W.; Wang, W.; Lu, Q.; Zeng, H. Probing molecular interactions of PEGylated chitosan in aqueous solutions using a surface force apparatus. *Phys. Chem. Chem. Phys.* **2019,** *21* (37), 20571-20581.

(28) Israelachvili, J.; Min, Y.; Akbulut, M.; Alig, A.; Carver, G.; Greene, W.; Kristiansen, K.; Meyer, E.; Pesika, N.; Rosenberg, K.; Zeng, H. Recent advances in the surface forces apparatus (SFA) technique. *Rep. Prog. Phys* **2010,** *73* (3), 036601.

(29) Chen, Y.; Diaz-Dussan, D.; Wu, D.; Wang, W.; Peng, Y.-Y.; Asha, A. B.; Hall, D. G.; Ishihara, K.; Narain, R. Bioinspired Self-Healing Hydrogel Based on Benzoxaborole-Catechol Dynamic Covalent Chemistry for 3D Cell Encapsulation. *ACS Macro Lett.* **2018,** *7* (8), 904-908.

(30) Bertula, K.; Martikainen, L.; Munne, P.; Hietala, S.; Klefström, J.; Ikkala, O.; Nonappa. Strain-Stiffening of Agarose Gels. *ACS Macro Lett.* **2019,** *8* (6), 670-675.

(31) Jansen, K. A.; Bacabac, R. G.; Piechocka, I. K.; Koenderink, G. H. Cells actively stiffen fibrin networks by generating contractile stress. *Biophys. J.* **2013,** *105* (10), 2240-2251.

(32) Bao, Y.; Luo, Z.; Cui, S. Environment-dependent single-chain mechanics of synthetic polymers and biomacromolecules by atomic force microscopy-based single-molecule force spectroscopy and the implications for advanced polymer materials. *Chem. Soc. Rev.* **2020,** *49* (9), 2799-2827.

(33) Kolberg, A.; Wenzel, C.; Hackenstrass, K.; Schwarzl, R.; Ruttiger, C.; Hugel, T.; Gallei, M.; Netz, R. R.; Balzer, B. N. Opposing Temperature Dependence of the Stretching Response of Single

PEG and PNiPAM Polymers. *J. Am. Chem. Soc.* **2019,** *141* (29), 11603-11613.

(34) Wagner, B.; Tharmann, R.; Haase, I.; Fischer, M.; Bausch, A. R. Cytoskeletal polymer networks: the molecular structure of cross-linkers determines macroscopic properties. *Proc. Natl. Acad. Sci. USA* **2006,** *103* (38), 13974-13978.

(35) Guimarães, C. F.; Gasperini, L.; Marques, A. P.; Reis, R. L. The stiffness of living tissues and its implications for tissue engineering. *Nat. Rev. Mater.* **2020,** *5* (5), 351-370.

(36) Munster, S.; Jawerth, L. M.; Leslie, B. A.; Weitz, J. I.; Fabry, B.; Weitz, D. A. Strain history dependence of the nonlinear stress response of fibrin and collagen networks. *Proc. Natl. Acad. Sci. USA* **2013,** *110* (30), 12197-202.

(37) Erk, K. A.; Henderson, K. J.; Shull, K. R. Strain Stiffening in Synthetic and Biopolymer Networks. *Biomacromolecules* **2010,** *11* (5), 1358-1363.

(38) Lee, H.; Venable, R. M.; Mackerell, A. D., Jr.; Pastor, R. W. Molecular dynamics studies of polyethylene oxide and polyethylene glycol: hydrodynamic radius and shape anisotropy. *Biophys. J.* **2008,** *95* (4), 1590-1599.

(39) Oesterhelt, F.; Rief, M.; Gaub, H. E. Single molecule force spectroscopy by AFM indicates helical structure of poly(ethylene-glycol) in water. *New J Phys* **1999,** *1*, 6-6.

(40) Chu, C. K.; Joseph, A. J.; Limjoco, M. D.; Yang, J.; Bose, S.; Thapa, L. S.; Langer, R.; Anderson, D. G. Chemical Tuning of Fibers Drawn from Extensible Hyaluronic Acid Networks. *J. Am. Chem. Soc.* **2020,** *142* (46), 19715-19721.

(41) Zhang, Y.; Tao, L.; Li, S.; Wei, Y. Synthesis of multiresponsive and dynamic chitosan-based hydrogels for controlled release of bioactive molecules. *Biomacromolecules* **2011,** *12* (8), 2894-901.

(42) Yang, X.; Liu, G.; Peng, L.; Guo, J.; Tao, L.; Yuan, J.; Chang, C.; Wei, Y.; Zhang, L. Highly

Efficient Self-Healable and Dual Responsive Cellulose-Based Hydrogels for Controlled Release and 3D Cell Culture. *Adv. Funct. Mater.* **2017,** *27* (40), 1703174.

(43) Yu, F.; Cao, X.; Li, Y.; Zeng, L.; Yuan, B.; Chen, X. An injectable hyaluronic acid/PEG hydrogel for cartilage tissue engineering formed by integrating enzymatic crosslinking and Diels–Alder "click chemistry". *Polym Chem-Uk* **2014,** *5* (3), 1082-1090.

(44) Jaspers, M.; Vaessen, S. L.; van Schayik, P.; Voerman, D.; Rowan, A. E.; Kouwer, P. H. J. Nonlinear mechanics of hybrid polymer networks that mimic the complex mechanical environment of cells. *Nat. Commun.* **2017,** *8*, 15478.

(45) Bregenzer, M. E.; Horst, E. N.; Mehta, P.; Novak, C. M.; Raghavan, S.; Snyder, C. S.; Mehta, G. Integrated cancer tissue engineering models for precision medicine. *PLoS One* **2019,** *14* (5), e0216564.

CHAPTER 5 Injectable Self-healing Hydrogel via Biological-Environment Adaptive Supramolecular Assembly as Internal Wound Dressing

5.1 Introduction

Injectable hydrogels represent an ideal material candidate for internal wound dressings due to their advantages of simple administration approach, minimum tissue invasion and high similarity to extracellular matrix (ECM).[1-6] Due to their *in situ* gelation capability, the hydrogel dressing could provide complete coverage of the injured tissues with irregular shape and those are heavily folded (e.g., small intestine, stomach, etc.), which could significantly lower the risk of postoperative adhesion.[7-9] Most of existing injectable hydrogels for wound dressing is based on a two-component design, in which two precursor polymers can be cured *in situ* to from a chemically cross-linked hydrogel through various types of chemical reactions (e.g., amine-aldehyde Schiff base reactions,[10-11] boronic acid-diol reactions,[12] thiol-ene Michael addition reactions,[13] etc.). Nevertheless, such crosslinking mechanisms are generally non-bioorthogonal, which could affect the native tissues (i.e., crosslinking of native tissues) or interfere with the biological processes. Some photo-curing methods are associated with high irradiation safety risks.[14-15] Besides, most of these chemically cross-linked hydrogels lack the adaptability to local biological environment, particularly to gastric environment (pH 1-3) since the crosslinking linkages are subjected to hydrolysis under acidic environment.[16-17] The decomposition of the material would lead to the exposure of the wound to surrounding microorganisms or bacteria, resulting in various postoperative complications and delay the wound healing process (**Figure 5.1a**).[3, 18]

To conquer these limitations, we envisage that an ideal injectable hydrogel dressing for internal wound repair should exhibit two critical properties. First, the curing process should be biorthogonal to improve the bio-safety. Second, the material should be able to adapt to the local

biological environmental to promote wound healing process. Herein, we present the first injectable self-healing hydrogel based on biological-environment adaptive supramolecular assembly of an ABA triblock copolymer, and have further demonstrated its successful application in repairing gastric perforation as dressing material in a rat model (**Figure 5.1b**). The ABA triblock copolymer is composited of a central poly(ethylene glycol) (PEG) block and terminal thermoresponsive poly(N-isopropylacrylamide) (PNIPAM) block with pH sensitive acryloyl-6-aminocaproic acid (A6ACA) moieties randomly incorporated (**Figure 5.1c**). By adapting to the biological environment, the injected polymer solution can rapidly transform into a physical supramolecular hydrogel due to the hydrophobic interactions between the collapsed P(NIPAM-*co*-NA6ACA) blocks. Besides, the hydrogel could smartly utilize the acidic environment to self-heal from repeated damage through the synergy of hydrogen bonding and hydrophobic interactions between the P(NIPAM-*co*-NA6ACA) segments. In addition, the supramolecular hydrogel dressing exhibits excellent anti-biofouling performance against microorganism attachment. Compared with conventional treatment of gastric perforation in a rat model, using our supramolecular hydrogel dressing not only simplifies the surgical procedures, but also reduces various postoperative complications and promotes the healing process. The developed biological-environment adaptive supramolecular hydrogel holds great promises for internal tissue repair and other biomedical applications.

a

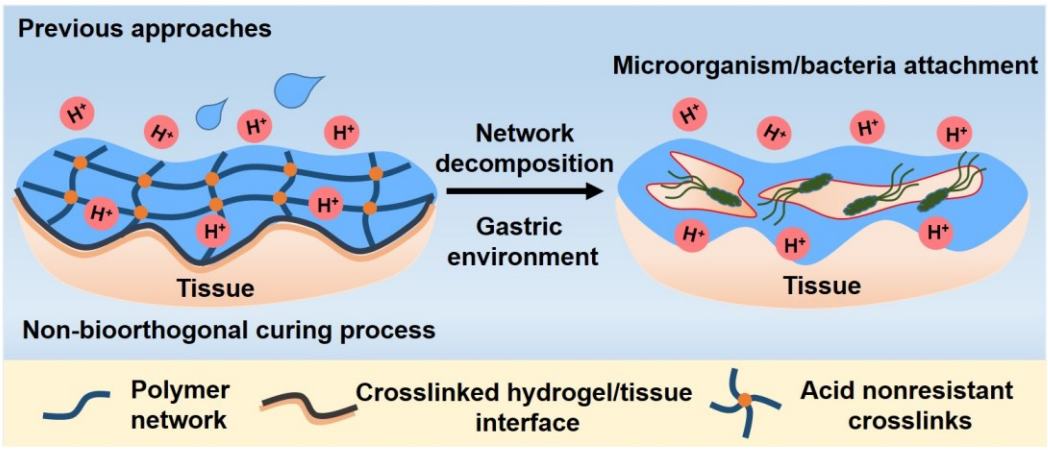
Previous approaches
Microorganism/bacteria attachment
Network decomposition
Gastric environment
Tissue
Tissue
Non-bioorthogonal curing process
Polymer network
Crosslinked hydrogel/tissue interface
Acid nonresistant crosslinks

b

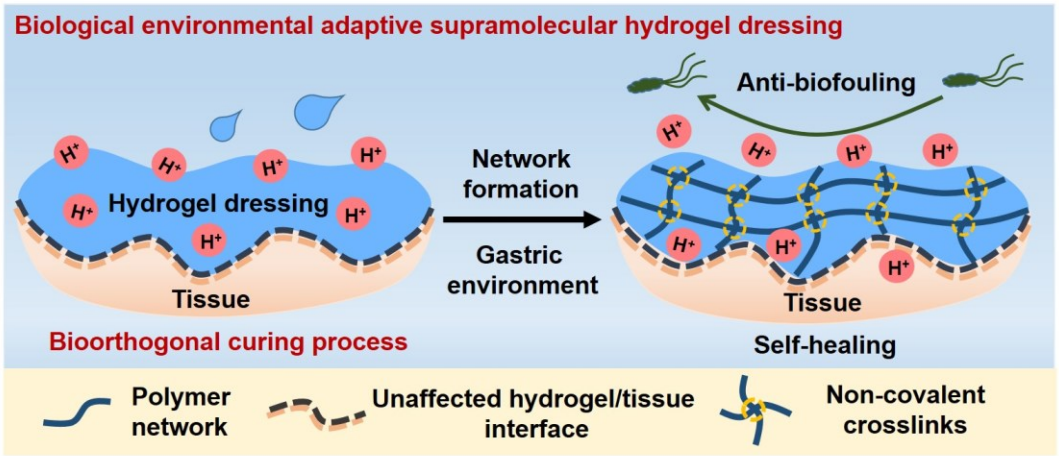
Biological environmental adaptive supramolecular hydrogel dressing
Anti-biofouling
Hydrogel dressing
Network formation
Gastric environment
Tissue
Tissue
Bioorthogonal curing process
Self-healing
Polymer network
Unaffected hydrogel/tissue interface
Non-covalent crosslinks

c

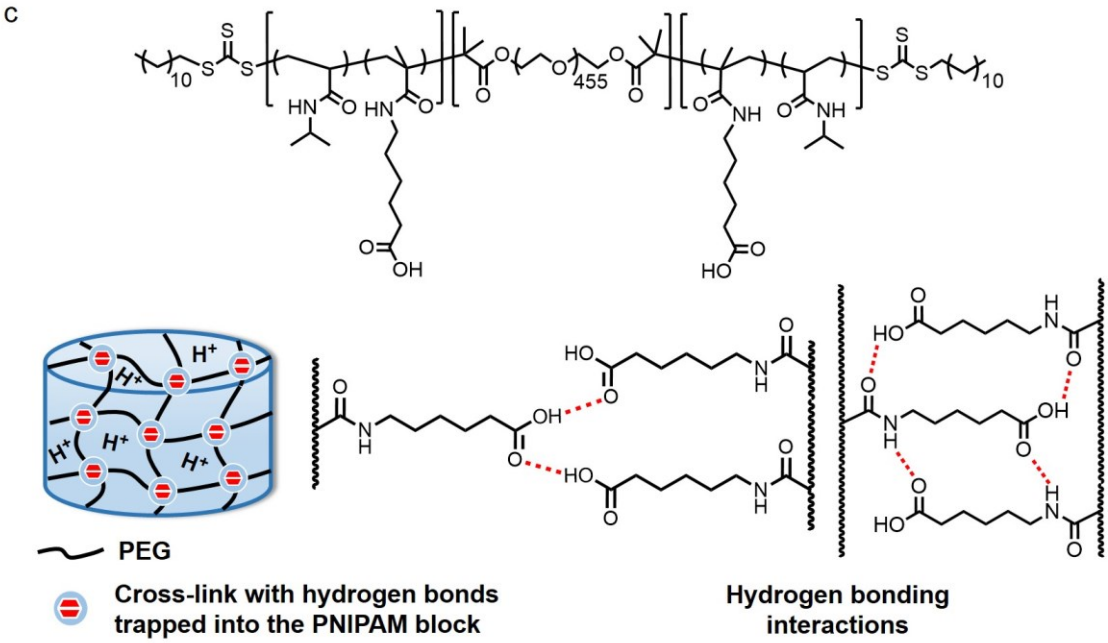
PEG
Cross-link with hydrogen bonds trapped into the PNIPAM block
Hydrogen bonding interactions

Figure 5.1. a) Previous acid nonresistant injectable hydrogel dressings formed through non-bioorthogonal curing process. b) The biological environmental adaptive supramolecular hydrogel as internal wound dressing. c) Chemical structure of the ABA triblock copolymer and supramolecular hydrogel network structure.

5.2 Experimental Methods

5.2.1 Materials

All the chemicals used for polymer synthesis were purchased from Sigma Aldrich. N-isopropylacrylamide (NIPAM) was recrystallized from hexane/toluene. N-acryloyl 6-aminocaproic acid (A6ACA) and macro-RAFT agent (CTA-PEG20K-CTA) were synthesized according to the previous reports.[19-20]

5.2.2 Polymer Synthesis

Poly[(N-isopropylacrylamide)-*co*-(N-acryloyl 6-aminocaproic acid)]-*b*-poly(ethylene glycol)-*b*-poly[(N-isopropylacrylamide)-*co*-(N-acryloyl 6-aminocaproic acid)] (ANGNA) was synthesized by one-step reversible addition-fragmentation (RAFT) polymerization. Briefly, NIPAM (904 mg, 8 mmol), A6ACA (370 mg, 2 mmol) and CTA-PEG20K-CTA (518 mg, 0.025 mmol) were dissolved in 9 mL of 1,4-dioxane in a 50-mL round bottom flask. 1 mL of N,N'-azobis-isobutyronitrile (AIBN) 1,4-dioxane stock solution (1 mg/mL) was added to the mixture. After degassing with argon for 30 min, the polymerization was allowed to proceed at 70 °C for 24 h. The polymerization was quenched by adding 5 mL of THF into the reaction mixture and the polymer was obtained after repeated dissolution in THF and precipitation in diethyl ether for three times, followed by drying under vacuum. ^{1}H NMR (DMSO-d_6, 500 MHz) : δ_H (ppm) = 3.89 (s, O=C-NH-C**H**-$(CH_3)_2$), 3.73 (m, -C**H$_2$**C**H$_2$**O-), 3.17 (s, O=C-NH-C**H$_2$**-$(CH_2)_3$-CH_2-COOH), 2.38 (s, O=C-NH-CH_2-$(CH_2)_3$-C**H$_2$**-COOH), 1.45-1.71 (br, -CH_2-C**H**(CONH)-), 1.36 (br, -C**H$_2$**-

CH(CONH)-), 1.15 (s, O=C-NH-CH-(C**H**$_3$)$_2$). (Mn = 50700 g/mol, Mw = 63600 g/mol, PDI = 1.25).

5.2.3 Polymer Characterization

The ^{1}H NMR spectra were recorded on a Varian 500 MHz spectrometer at room temperature using DMSO-d_6 as solvent. Chemical shifts are reported in parts per million (δ) relative to TMS as the internal reference. Molecular weighs (M_n and M_w) and polydispersity (PDI) of the ANGNA were determined using a Waters gel permeation chromatography (GPC) system equipped with a refractive index detector (RI 2414) and a UV/vis 2489 detector. A Waters 510 liquid chromatography pump equipped with one (HR4E) Styragel column was used at 40 °C. THF was used as the eluent at a flow rate of 1 mL min^{-1}. The GPC system was calibrated using monodisperse polystyrene standards. The hydrodynamic diameters of ANGNA in pH=3 PBS buffer solution at temperatures between 0-45 °C were characterized using a Malvern Zetasizer Nano ZSP. Samples were allowed to be stabilized for 3 min at each temperature before measurement. The lower critical solution temperature (LCST) was determined at the temperature where a sudden increase of hydrodynamic diameter occurs.

5.2.4 Hydrogel Preparation

The hydrogels were prepared by dissolving ANGNA copolymer in PBS buffer solutions (pH 3 or 7.4) with a concentration of 10 w/v%. The polymer solutions were stored at 4 °C for 24 h before use.

5.2.5 Rheology Characterization

A rheometer (TA Instruments, AR-G2) fitted with a Peltier stage using a 20 mm parallel-plate configuration and with a gap of 53 μm was used to study the rheological properties of the hydrogels. A few drops of silicon oil were applied around the edge of the sample to prevent moisture

evaporation. The temperature responsive sol-gel transition was characterized by temperature ramp test, in which both storage *G'* and loss *G"* modulus were recorded as a function of temperature from 5 to 40 °C, with a heating rate of 1°C/min, angular frequency of 10 rad/s and strain of 1 %. The gelation temperature was determined as the crossover point of *G'* and *G"*. The reversibility of the sol-gel transitions was characterized by temperature cyclic step tests between 10 and 37 °C with angular frequency of 10 rad/s and strain of 1 %.

To characterize the self-healing property of the hydrogels, a strain amplitude test was performed at 37 °C and angular frequency of 10 rad/s by applying strain from 1% to 1000% to achieve the material failure, followed by the immediate recording of *G'* and *G"* as a function of time at 1 % strain to determine the self-healing efficiency. The reproducibility of the self-healing capability was characterized by strain cyclic step tests between 1 % and 650 % at 37 °C and angular frequency of 10 rad/s.

5.2.6 SFA Force Measurements

A surface forces apparatus (SFA) was used to quantitatively probe the interaction forces between ANGNA in PBS buffer solution (100 mM) at pH 3 or 7.4. The detailed experiment setup for SFA measurements have been reported previously.[21-22] In this work, a symmetric configuration was adopted. Briefly, two back-silvered mica surfaces (1−5 μm) were glued onto two cylindrical silica disks ($R \approx 2$ cm). The mica surfaces were then coated with ANGNA solution (100 μg/mL) for 15 min, followed by a thorough rinse with PBS buffer to remove unbound or loosely bound polymers. Two surfaces were then mounted into the SFA chamber in a cross-cylinder configuration and the SFA chamber was saturated with water vapor. PBS solution (100 mM) at pH 3 or 7.4 was injected between two mica surfaces. The force measurement was conducted by bringing two surfaces to contact followed by separation. The interaction forces *F(D)* were monitored as a

function of absolute surface separation distance D in real time using multiple beam interferometry by employing fringes of equal chromatic order (FECO). For each case, force-distance profiles were measured at least two different interaction positions on a set of surfaces to confirm the reproducibility. The measured adhesion or "pull-off" force F_{ad} and adhesion energy W_{ad} are correlated by $F_{ad} = \frac{3}{2}\pi R W_{ad}$.

5.2.7 Bacteria Adhesion Assay

The anti-fouling performance of ANGNA hydrogel was evaluated through bacteria adhesion assay. Gram-negative *Escherichia coli* (*E. coli*) was used as the model bacteria. Bacterial suspension with concentration of 10^9 CFU/mL was prepared following the previous reports.[23] Bare glass substrates were used as the control. In a typical procedure, a thin layer of ANGNA hydrogel was formed to cover the glass substrates. Bacterial suspension was dropped on the top of coated and uncoated glass substrates and the samples were mildly shaken for 3 h at 37 °C to study the initial attachment of bacteria. After 3 h incubation, the substrates were rinsed with PBS solution to remove the unattached bacteria. The bacteria attached to the surface were stained with 50 μL of LIVE/DEAD stain in dark for 15 min and then washed with PBS gently, followed by observation using a fluorescence microscope.

5.2.8 MTT Assay

The cytotoxicity of ANGNA was evaluated through MTT assay. HeLa and MRC-5 cells were seeded into 96-well plates at a density of $1x10^5$ cells per well. The cells were allowed to grow for 24 h. Fresh DMEM cell culture medium containing ANGNA copolymer was added to each well to reach a final polymer concentration of 0.16, 0.32, 0.64, 1.25, 2.50 and 5.00 mg/mL respectively. The untreated cells were used as the control. After 24 h incubation, 15 μL of MTT dye solution (10 mg/mL) was added to each well. After 4 h incubation, the culture medium was carefully

removed from each well and replaced with 100 μL of lysis buffer solution (DMSO:isopropanol = 1:1). The plates were read at 570 nm using an optical absorption spectrometer and the cell viability was calculated with respect to the control group.

5.2.9 2D/3D Cell Culture

2D/3D cell culture was conducted following the reported procedures with slight modification.[24] FaDu cells were used as the model cells. For 2D cell culture, a 10 w/v% ANGNA hydrogel was prepared in PBS buffer solution at 37 °C. DMEM culture medium containing FaDu cells at a density of $1x10^6$ was then added on the top of the hydrogel. For 3D cell culture, DMEM culture medium containing Fadu cells at a density of $1x10^6$ was added to a 10 w/v % ANGNA PBS solution, followed by the formation of hydrogel/cell complex at 37 °C. Cells treated with DMEM culture medium and 70% ethanol were treated as live and dead controls respectively. After 24 h incubation, cells were stained with live/dead cell imaging kit and imaged by a confocal microscope. The cell viability was quantified using Imaris Image Analysis software.

5.2.10 In vivo Gastric Perforation Repair in a Rat Model

The *in vivo* gastric perforation repair experiment was carried out using male Sprague Dawley rats (~280 g, 8-week age). 12 rats were randomly divided into the experiment group (ANGNA hydrogel dressing) and the control group (omentum majus). First, the rats were anesthetized preoperatively with isoflurane inhalation, and prepared at the abdominal surgical site. Then, they were subjected to general anesthesia with intraperitoneal injection of sodium pentobarbital (50 mg/kg body weight). Next, the rats were placed supine on the super clean mesa, and a 2 cm incision was made to cut the skin, subdermal tissue and fascia. The gastric perforation was created by removing full thickness gastric wall with a size of 0.5cm × 0.5cm. In the experimental group, 1 mL of ANGNA solution (stored at 4 °C) was injected at the wound to form the hydrogel, and the

gastric wall at the wound was sutured with 4×0 non-absorbable suture. In the control group, an omentum majus was inserted into the serosal layer and the incision was sutured with 4×0 non-absorbable suture (To imitate the surgical method of clinical gastric perforation). The abdominal cavity was cleaned and a little ceftriaxone was injected into the abdominal cavity according to the degree of contamination of the abdominal cavity during the operation. The abdominal cavity was closed by 4×0 non-absorbable line. At 2nd, 4th and 8th week, the rats were sacrificed and the stomach samples were collected. Postoperative adhesion was compared through direct observation.

5.2.11 Histopathological Observation and Immunohistochemical Examination

For evaluation of inflammatory response after surgery, stomach tissues collected at 2nd, 4th and 8th week were fixed in 4% paraformaldehyde for 24 hours and embedded in paraffin. After being cross sectioned to ~4μm thickness, the tissues were stained with Haematoxylin-Eosin (H&E). All slides were analyzed and imaged by microscope.

T lymphocytes of the tissue sections were marked by immunohistochemical examination using CD3 biomarker. All slides were analyzed and imaged by microscope.

5.3 Results and Discussions

5.3.1 Polymer Synthesis and Characterization

The ABA triblock copolymer poly[(N-isopropylacrylamide)-*co*-(N-acryloyl 6-aminocaproic acid)]-*b*-poly(ethylene glycol)-*b*-poly[(N-isopropylacrylamide)-*co*-(N-acryloyl 6-aminocaproic acid)] (ANGNA) was synthesized by reversible addition fragmentation transfer (RAFT) polymerization (**Figure S5.1**). The synthesized polymer was characterized by ^{1}H NMR spectroscopy (**Figure S5.2**) and gel permeation chromatography (GPC) (M_n = 50700 g/mol, M_w = 63600 g/mol, PDI = 1.25).Since A blocks are thermoresponsive and B blocks are permanently hydrophilic, increasing polymer solution temperature above the lower critical solution temperature

(LCST) would trigger the formation of the hydrogel, in which the dehydrated PNIPAM blocks assemble into micellar core-like cross-links and the central PEG blocks serve as the network bridges[25] (**Figure 5.1c**). The dynamic light-scattering (DLS) measurement in pH=3 PBS buffer solution shows the ANGNA polymer chains assembled into micelles with hydrodynamic diameter ~60 nm above 15 °C (**Figure 5.2a**), which was determined as the LCST of the PNIPAM block. The hydrogel dressing was facilely prepared by dissolving the copolymer in PBS buffer solution (pH = 3).

5.3.2 Thermo-reversibility and Injectability of ANGNA Hydrogel

A 10 w/v% ANGNA sample transformed from a free-flow viscous liquid at 4 °C to a free-standing gel at 37 °C, and returned to the sol state when the temperature was decreased to 4 °C (**Figure S5.3**). The thermo-sensitivity of the material was quantitatively characterized by temperature ramp test using a rheometer, in which the changes of storage *G'* and loss modulus *G"* were measured with temperature increasing from 5 to 40 °C. *G"* was larger than *G'* at low temperature, indicating the liquid-like behavior. Upon heating, *G'* gradually increases and surpasses *G"* at the gelation temperature ~15 °C (consistent with the DLS result) until an equilibrium value is reached (**Figure 5.2b**), signifying a solid-like gel state. The thermo-reversibility was further characterized by cycling the temperature between 10 and 37 °C. The hydrogel dressing demonstrated a completely reversible sol-gel transition behavior with full recovery of the mechanical properties during multiple cooling-heating cycles (**Figure 5.2c**), indicating the dynamic cross-linking characteristic. Due to the outstanding thermo-reversibility, injecting a 4 °C-preserved 10 w/v% polymer solution into a PBS buffer solution (pH=3) at 37 °C led to the instantaneous formation of a stable hydrogel under acidic environment (**Figure 5.2d,** left). The injectability potentially allows our hydrogel dressing to be delivered through

laparoscopic surgery, which could not only simplify the surgical procedure, but also minimize tissue invasion for the treatment of gastric perforation. In addition, letters "U of A" were facilely "written" by injecting the polymer solution onto a platform at 37 °C (**Figure 5.2d,** right). Such moldable property endows the as-synthesized material with great flexibility to construct customized complex 3D structures through 3D-printing for various biomedical applications.

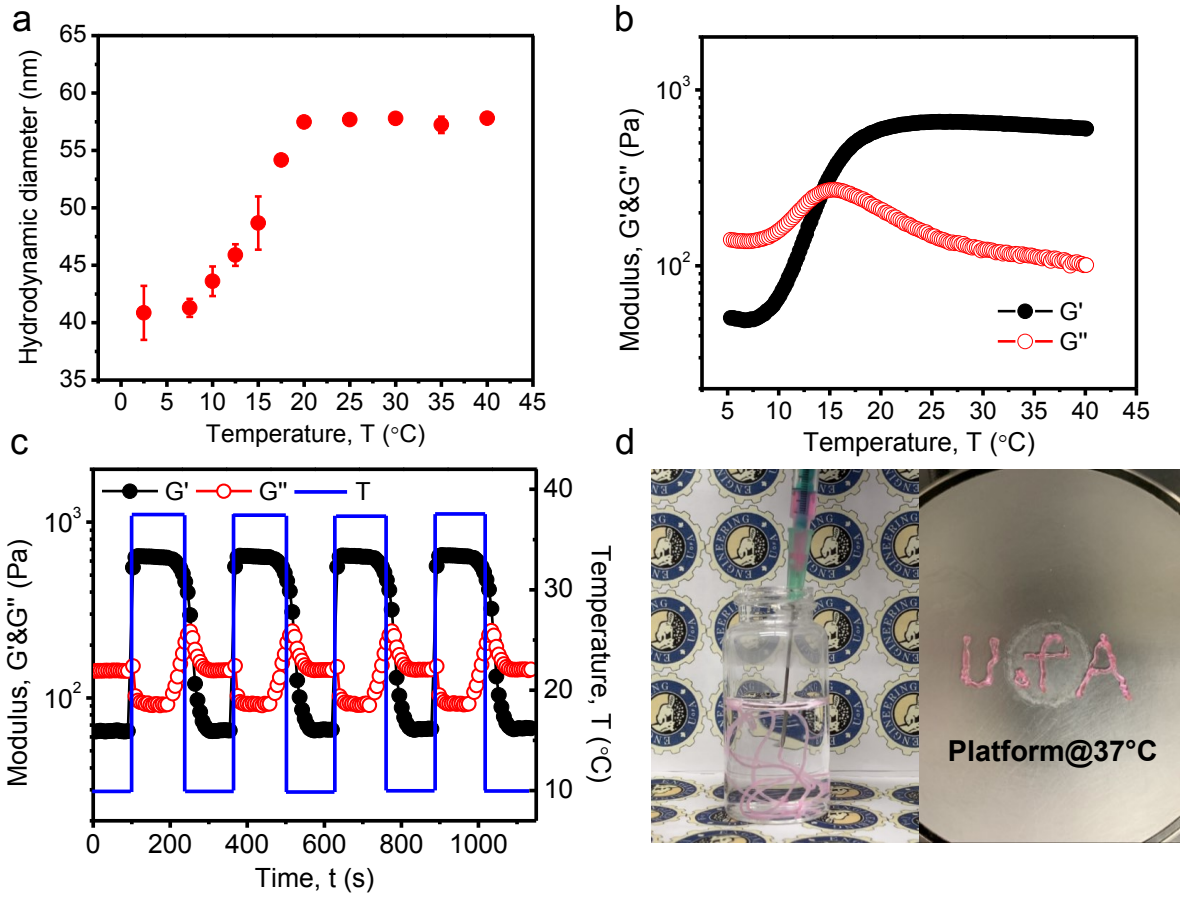

Figure 5.2. (a) DLS measurement showing the change of hydrodynamic radius of ANGNA with increasing temperature. (b) Thermo-sensitive storage (G') and loss (G") modulus of a 10 w/v% hydrogel. (c) Modulus change of a 10 w/v% hydrogel during multiple heating-cooling cycles. (d) Injection of a 4 °C-preserved 10 w/v% polymer solution into a PBS buffer solution (pH=3) at 37 °C and facilely writing letters "U of A" on a platform at 37°C (the hydrogel was dyed with Rhodamine

B).

5.3.3 Self-healing Property and Associated Interaction Mechanism

In order to maintain the integrity and functionalities after implantation under gastric environment, the dressing materials should be able to adapt to the acidic conditions and self-heal from damage for extended material lifespan. As shown in **Figure 5.3a-d**, after bringing two separated 10 w/v% hydrogels prepared in pH = 3 PBS buffer solution into contact at body temperature, the hydrogels autonomously merged into one single piece. The healed hydrogel could be lifted to support its own weight without the rupture at the joint. The self-healing capability was further investigated by rheological measurements at 37 °C. In a strain amplitude test, *G'* and *G"* initially remained constant when the strain increased from 1 to 100%. As the applied strain further increased, both *G'* and *G"* dramatically dropped with a crossover point occurring at 600%, implying the rupture of the hydrogel network. However, the hydrogel could fully regain its original mechanical strength when a small strain (1%) was immediately applied after failure (**Figure 5.3e**). Afterwards, cyclic strain step test was conducted on the hydrogel at 37 °C, in which alternating strain (1% or 650%) was applied. *G'* significantly decreased from ~700 Pa to ~20 Pa when the hydrogel was subjected to a large strain (650%). However, both *G'* and *G"* instantaneously recovered to their initial values upon the strain returning to 1% (**Figure 5.3f**). Such self-healing behavior is fully reproducible during cyclic tests, which is desirable in a wide range of bioengineering applications.

To better understand the biological environmental adaptive self-healing capability of the hydrogel, a 10 w/v% ANGNA hydrogel was prepared in pH = 7.4 PBS buffer solution to deprotonate A6ACA moieties and characterized by a rheometer. The mechanical strength of the hydrogel was significantly weakened as the equilibrium *G'* value decreased from ~750 Pa (pH =

3) to ~330 Pa (pH =7.4). Moreover, the modulus recovery could only reach ~54% after being damaged (**Figure 5.3g**). The decrease of mechanical strength and self-healing efficiency of ANGNA hydrogel at pH 7.4 is most likely due to the weakened hydrogen bonding interactions within the network as less hydrogen bonds can be formed between the deprotonated A6ACA moieties[19]. Therefore, it is evident that hydrophobic and hydrogen bonding interactions synergistically contribute to the excellent self-healing capability of as-prepared ANGNA hydrogel at low pH.

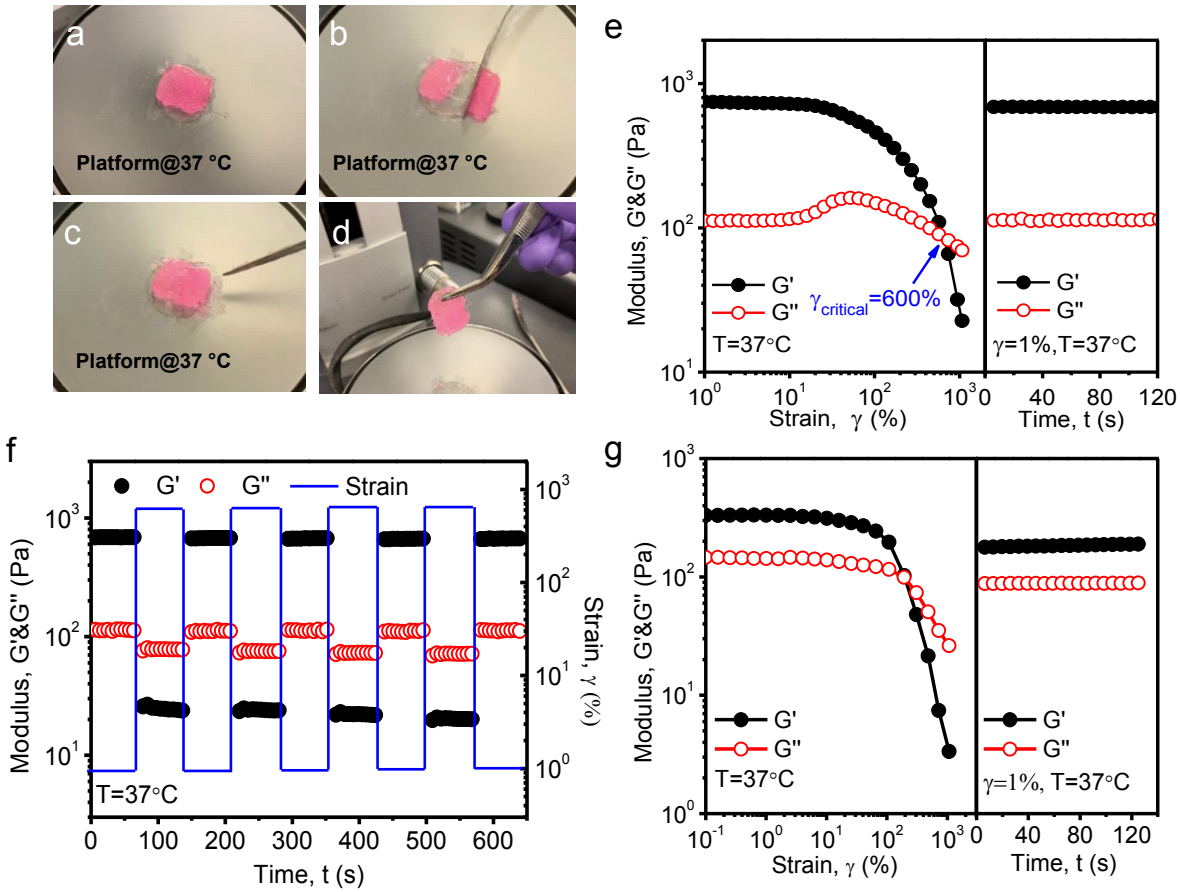

Figure 5.3. Photos of the self-healing process of a 10 w/v% ANGNA hydrogel prepared in pH=3 buffer solution at 37 °C: (a) initial hydrogel, (b) hydrogel was separated into two pieces, (c) separated hydrogels were brought into contact, and (d) the self-healed hydrogel can be lifted

against its own weight without rupture at the joint. (e) Strain amplitude measurement (left) followed by time sweep measurement (strain=1%) (right) on a 10 w/v % ANGNA hydrogel prepared in pH = 3 PBS buffer solution shows immediate recovery from damage. (f) Cyclic strain step test shows reproducible self-healing capability. (g) Strain amplitude measurement (left) followed by time sweep measurement (strain = 1%) on a 10 w/v % ANGNA hydrogel prepared in pH=7.4 PBS buffer solution.

To further elucidate the critical roles of hydrogen bonding interactions in self-healing behavior, a surface forces apparatus (SFA) was employed to quantitatively probe the molecular interactions between ANGNA in pH=7.4 and 3 buffer solutions. No adhesion was detected between ANGNA in pH=7.4 PBS buffer solution. In contrast, an adhesion ~7.9 mN/m (W_{ad} ~1.7 mJ/m^2) was measured between ANGNA in pH=3 PBS buffer solution (**Figure 5.4a**). In addition, such adhesion is fully reversible as confirmed in three sequential approach-separation force measurements (**Figure 5.4b**), which most likely results from the dynamic non-covalent interactions between ANGNA. At low pH, the carboxyl groups (pKa ~ 4.4)[19] of A6ACA moieties are protonated and electroneutral. Thus, intimate contact between terminal-carboxyl groups or amide groups on different A6ACA moieties could be realized, allowing the formation of hydrogen bonds, which thereby results in the adhesion between two surfaces (**Figure 5.4c**). However, at pH 7.4, the carboxylate groups on A6ACA moieties are deprotonated. The formation of intermolecular hydrogen bonds across the A6ACA moieties on two opposite surfaces would be significantly impeded by the electrostatic repulsion between negatively charged carboxylate groups (**Figure 5.4d**). Therefore, the hydrogen bonds formed between the protonated A6ACA moieties play important roles in achieving the self-healing performance of ANGNA hydrogel under acidic environment. Such pH-mediated hydrogen bonding interaction mechanism not only could regulate

both mechanical strength and the self-healing capability of the hydrogel, but also provides nanomechanical insights into the development of environmental adaptive self-healing materials based on tunable intermolecular interactions.

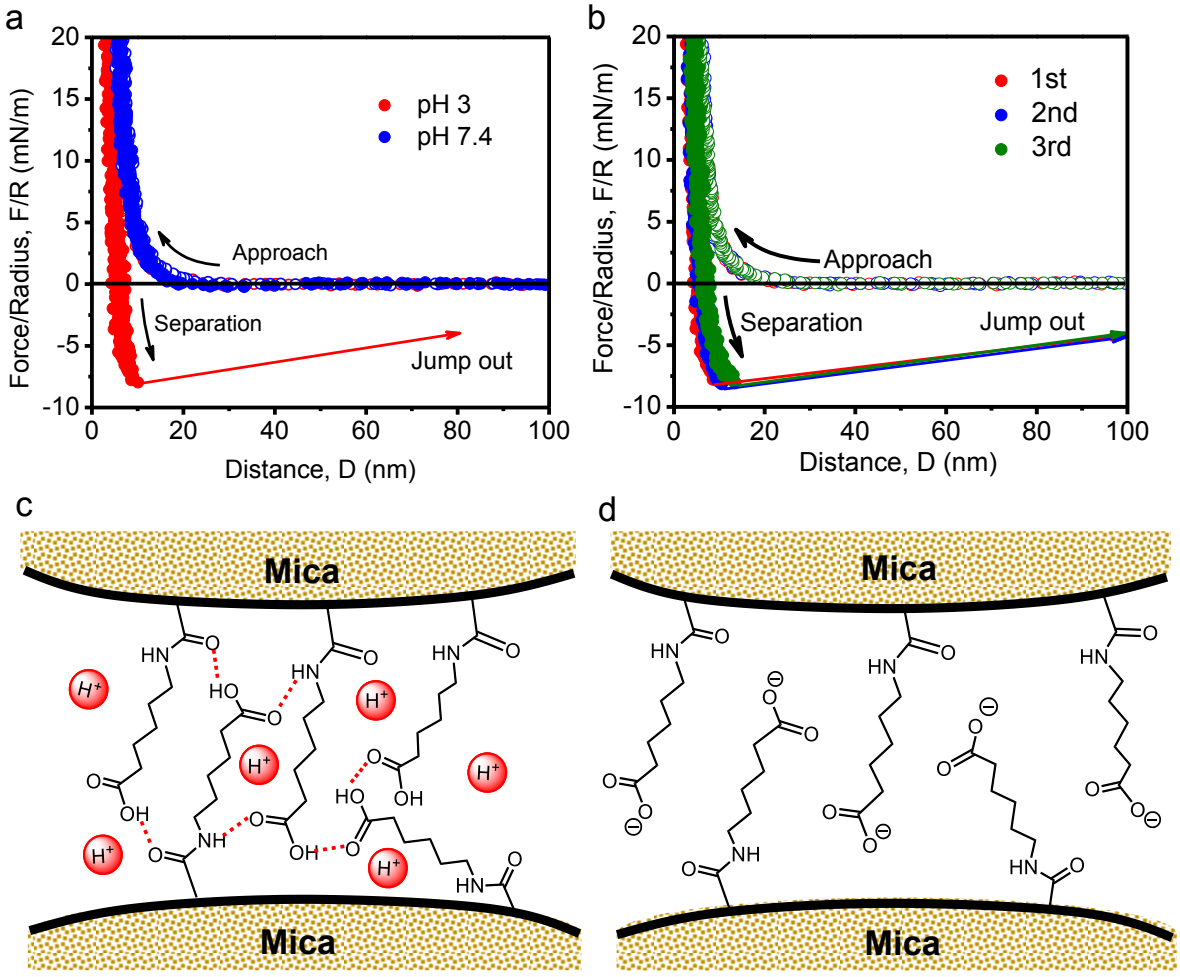

Figure 5.4. (a) Force-distance profiles show the interactions between ANGNA in pH=3 or 7.4 PBS buffer solution. (b) Force-distance profiles show the reversible interactions between ANGNA in pH=3 PBS buffer solution. Schematics of interaction mechanism between ANGNA in (c) pH=3 or (d) pH =7.4 PBS buffer solution.

5.3.4 Anti-biofouling Property and Biocompatibility

The fouling of microbes on the surface of the implanted biomaterials could trigger the

unfavorable immune response or inflammation, which delays the healing process. The number of initially attached microbes is one of the most important factors to evaluate the anti-biofouling performance of the surface. The as-prepared ANGNA hydrogel effectively prevents the initial attachment of *Escherichia coli (E. coli)*. Both hydrogel-coated and uncoated glass substrates were challenged with extremely concentrated bacterial suspension of 10^9 CFU/. After 3h incubation, no live bacteria (green spot) was observed on the hydrogel-coated glass substrate for bacteria adhesion (**Figure 5.5a**). In contrast, a large number of live bacteria (green spots) were observed on the bare glass (**Figure 5.5b**), indicating the formation of a dense layer of biofouling film. The excellent anti-biofouling performance of the ANGNA hydrogel is attributed to the presence of PEG block, which forms strong hydration layer to prevent microorganism attachment.[26-27]

It is important to evaluate the biocompatibility of our hydrogel dressing for the practical biomedical applications. The cytotoxicity of ANGNA copolymer was determined by MTT assay. The ANGNA copolymer shows extremely low cytotoxicity to both HeLa and MRC-5 cells with nearly 100% cell viability within the tested concentration range (**Figure S5.4**). Considering the outstanding biocompatibility of ANGNA, the material was further explored for 2D/3D cell culture using FaDu cells. After 24 h incubation, the live cells (green color) took the majority of the population compared with the dead cells (red color) (**Figure 5.5c and 5.5d**). The cell viabilities were assessed to be over 85% for both 2D and 3D cell culture (**Figure S5.5**). The non-toxic porous polymer matrix (**Figure S5.6**) facilitates the efficient transportation of nutrients and metabolites, maintaining the normal cellular functions. The successful demonstration of 2D/3D cell culture reveals the great potential of our supramolecular hydrogel to encapsulate and deliver biomolecules, such as proteins, DNA/RNAs and cells for tissue engineering and regenerative medicine[28].

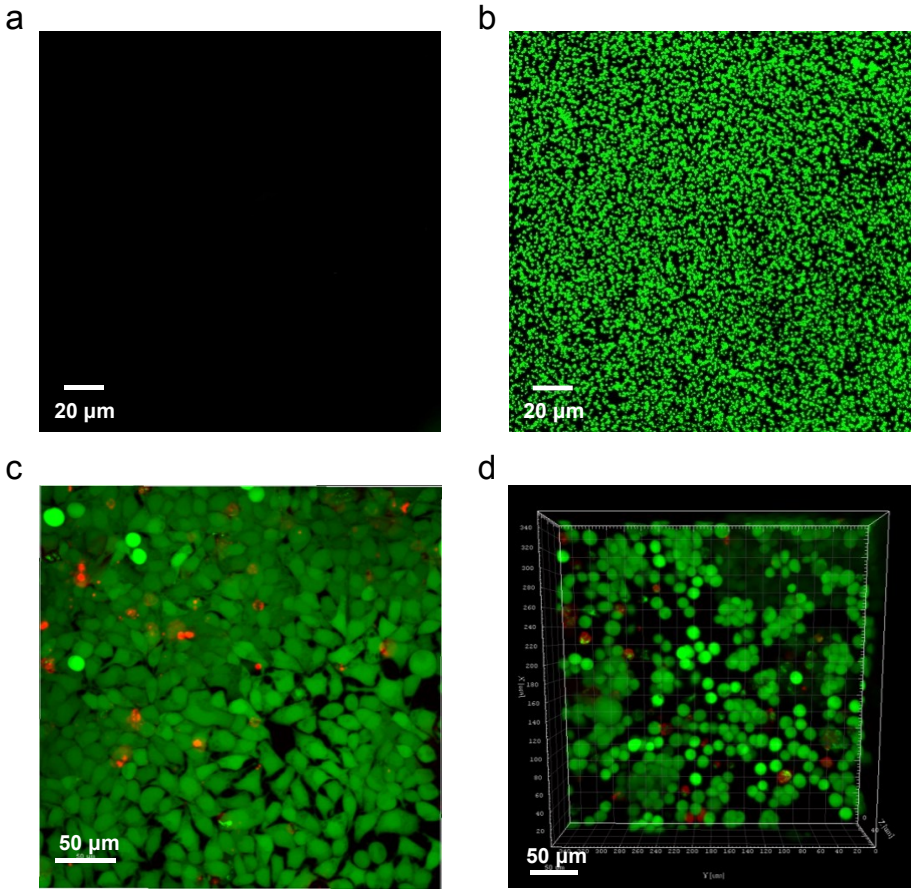

Figure 5.5. Fluorescence microscopy images of (a) ANGNA hydrogel-coated and (b) uncoated glass surfaces after 3h incubation against E. coli attachment. Confocal microscopy images of (c) 2D and (d) 3D culture of FaDu cells using a 10 w/v % ANGNA hydrogel.

5.3.5 In vivo Gastric Perforation Repair in a Rat Model

We further demonstrated the capability of the developed supramolecular hydrogel dressing to repair gastric perforation by *in vivo* study in a rat model (**Figure 5.6a**). Due to the excellent temperature responsiveness and injectibility, the hydrogel dressing could be easily delivered at the wound site through simple injection (**Figure 5.6b**). In contrast, the conventional omental implantation (control group) involved laboring sutring procedures during the surgery (**Figure 5.6c**).

There was no fatality during the observation period. Postoperative adhesion is one of the most common and serious complications after abdominal surgery.[29] After two weeks of surgery, no

obvious intraperitoneal adhesion was observed in the hydrogel group (**Figure 5.6d**). In contrast, the abdominal incision had severe adhesion with the implanted omentum and adjacent tissue in the control group (**Figure 5.6e**). In addition, white pus appeared at the sewed perforation site in the control group, while the perforated site remains smooth in the hydrogel group (**Figure 5.6f**). The use of hydrogel could reduce postoperative abdominal adhesion to a great extent, which is attributed to the prevention of direct contact between the wound and the adjacent tissue with the presence of the hydrogel as a physical barrier.

Inflammation is normally involved during the wound healing process.[10] However, extended or unfavorable inflammatory response caused by wound infection and other postoperative complications could delay the healing process.[30] The infiltration of inflammatory cells in the injured stomach tissue was investigated through histopathological observation by H&E staining (**Figure 5.6g**). In the 2nd week, both hydrogel group and control group showed similar degree of infiltration of inflammatory cells in submucosa, which indicates the establishment of inflammatory phase in both groups. In the 4th week, infiltration of inflammatory cells was significantly reduced in the hydrogel group. In contrast, the control group showed an enhaced infiltration of inflmmatory cells. The reduced inflammation in the hydrogel group implies the efficient healing of the gastric perforation. Such positive effect is most likely due to the anti-biofouling capability of our hydrogel, which prevents the accumulation of debris, bacteria and other microorganisms to cause infection. In the 8th week, no obvious inflammatory cell infiltration was observed in both groups and the gastric mucosa recovered to the normal state.

T lymphocytes are one type of inflammatory cells which appear in the late inflammatory phase of wound repair and could reflect the level of inflammation in the injured tissue.[31] The infiltration of T lymphocytes in the injured stomach tissue was specifically traced through

immunohistochemical (IHC) examination. It is clear that the number of T lymphocytes (brown) decreased over time in the hydrogel group, while the infiltration of T lymphocytes significantly enhanced in the 4^{th} week and still appeared in the tissue in the 8^{th} week for the control group (**Figure 5.6h**). These results further indicate that our hydrogel dressing could suppress the inflammatory response, which is beneficial for the healing of the gastric perforation.

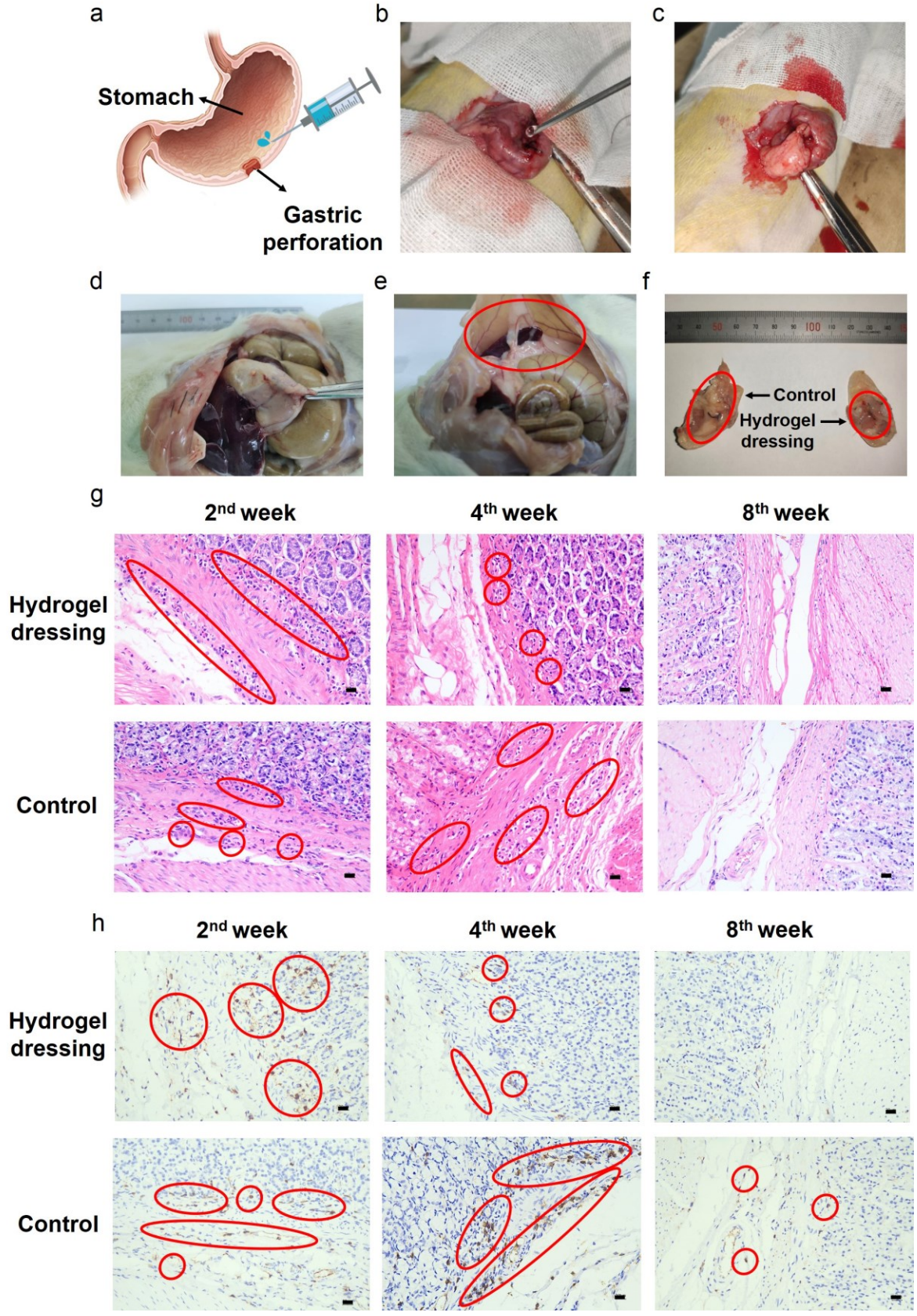
a
Stomach
Gastric perforation
b
c
d
e
f
Control
Hydrogel dressing
g
2nd week
4th week
8th week
Hydrogel dressing
Control
h
2nd week
4th week
8th week
Hydrogel dressing
Control

Figure 5.6. (a) Schematic illustration of using the supramolecular hydrogel dressing for gastric perforation repair. (b) injection of supramolecular hydrogel dressing at the perforated site. (c) implantation of an omentum majus into the stomach. Postoperative adhesion after 2 weeks of surgery. (d) hydrogel dressing group. (e) omentum patch group (control group). (f) sewing position on the stomach (left: control group, right: hydrogel dressing group). (g) histological evaluation of infiltration of inflammatory cells in hydrogel dressing and control groups in the 2^{nd}, 4^{th} and 8^{th} week. Scale bar represents 20 μm. (h) immunohistochemical evaluation of infiltration of T lymphocytes (brown) in hydrogel dressing and control groups in the 2^{nd}, 4^{th} and 8^{th} week. Scale bar represents 20 μm.

5.4 Conclusions

In this study, we have developed a novel biological-environment adaptive supramolecular hydrogel as internal wound dressing. By apatpting to the physiological termperature, the hydrogel dressing can be facilely delivered via simple injection at targeted site through supramolecular self-assembly of the ABA triblock copolymer. The formed supramolecular hydrogel could adapt to the gastric envionment and acquire remarkable self-healing capability to recover from repeated damage through the synergy of hydrophobic and hydrogen bonding interactions. The supramolecular hydrogel dressing can also effectively prevent the accumulation of microorganisms on the surface. The as-prepared state-of-art supramolecualr hydrogel dressing offers significant advantages over the conventional treatment of gastric perforation, including simplified surgical procedures, reduced postoperative adhesion as well as suppressed inflammatory response. To the best of our knowledge, this work presents the *first* design of a biological-environment adaptive supramolecuar hydrogel dressing for internal tissue repair.

Beyond the application of gastric perforation treatment, the developed material may also be

used as a 3D-printable versatile carrier of nano/micro-electronics (e.g., mini camera, nano robotics, etc.) and therapeutics (e.g., drugs, cells, siRNAs, etc.) to build gastric-retentive devices for applications such as disease diagnosis/therapy and health monitoring, which interact with gastrointestinal (GI) tract in human body. The design of our supramolecular hydrogel may pave the way for the development of biological-environment adaptive self-assembled materials, providing useful insights into the development of functional biomaterials with various biomedical applications.

Supporting Information

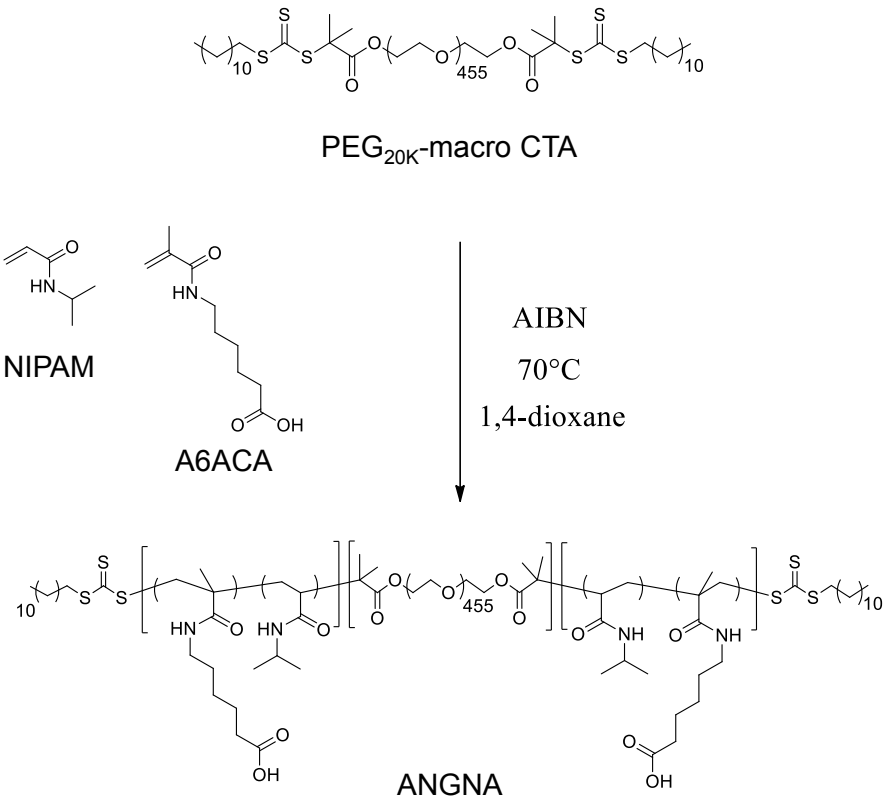

Figure S5.1. Synthesis route of the ABA triblock copolymer poly[(N-isopropylacrylamide)-co-(N-acryloyl 6-aminocaproic acid)]-b-poly(ethylene glycol)-b-poly[(N-isopropylacrylamide)-co-(N-acryloyl 6-aminocaproic acid)] (ANGNA).

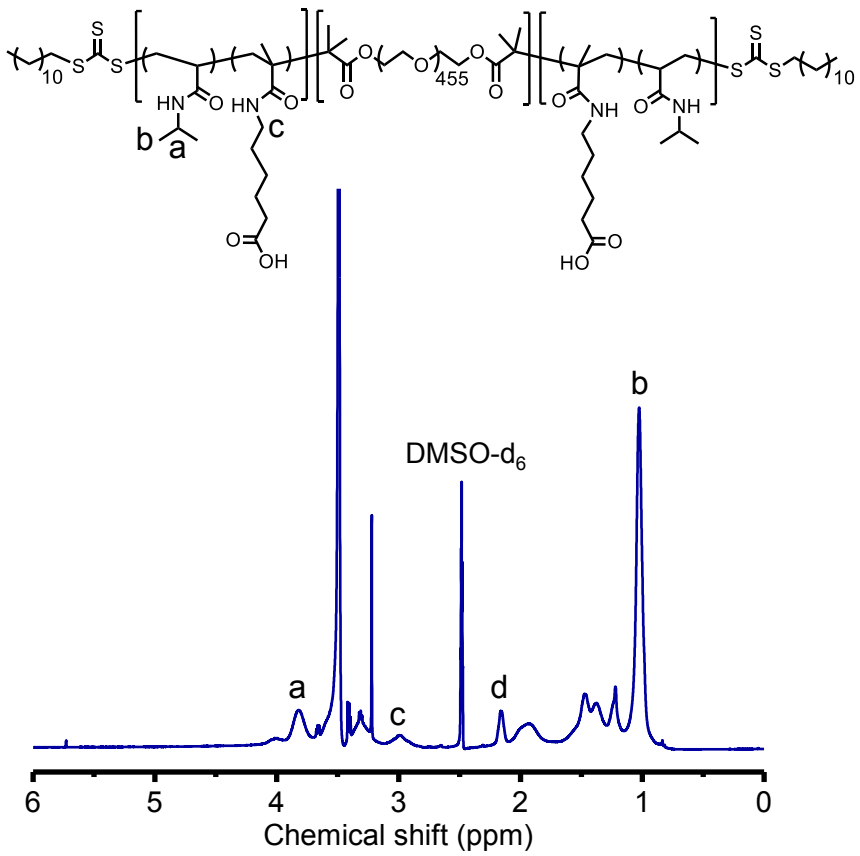

Figure S5.2. ^{1}H NMR spectra of ANGNA in DMSO-d_6.

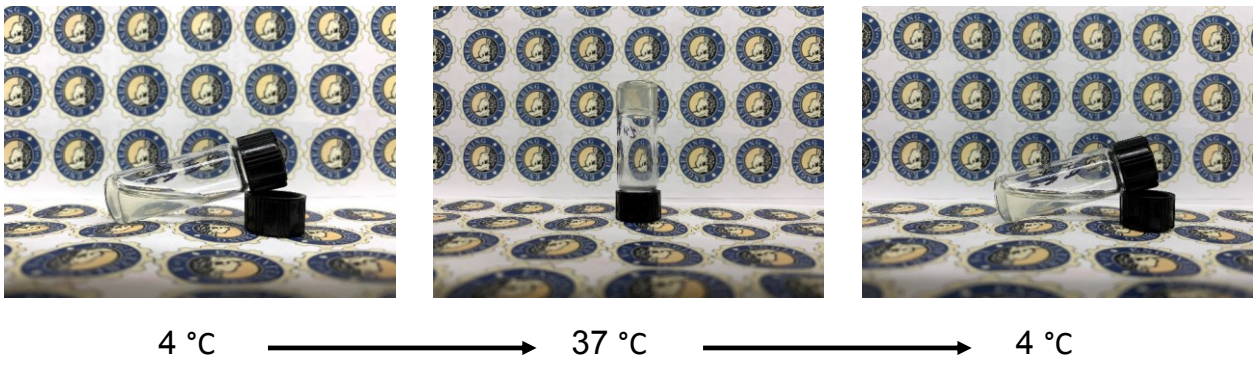

Figure S5.3. The reversible sol-gel-sol transitions of a 10 w/v% ANGNA liquid bandage prepared in pH=3 PBS solution.

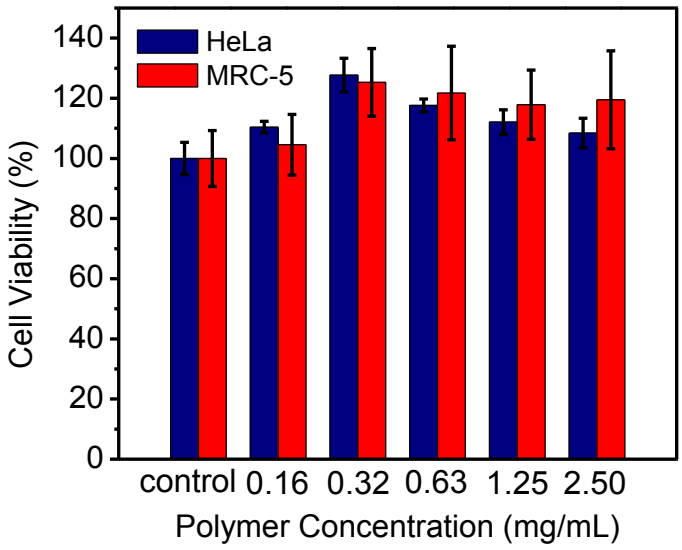

Figure S5.4. Cell viabilities of HeLa and MRC-5 cells after 24 h incubation with ANGNA copolymer at different concentrations.

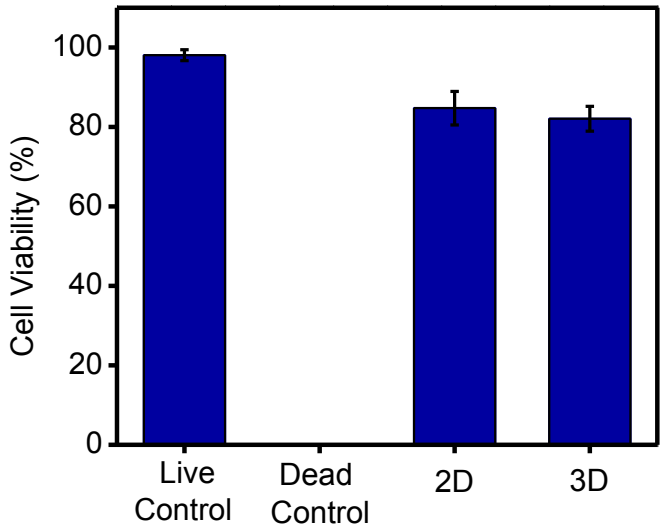

Figure S5.5. Cell viabilities of FaDu cells after 24 h 2D/3D culture using a 10 w/v% ANGNA liquid bandage.

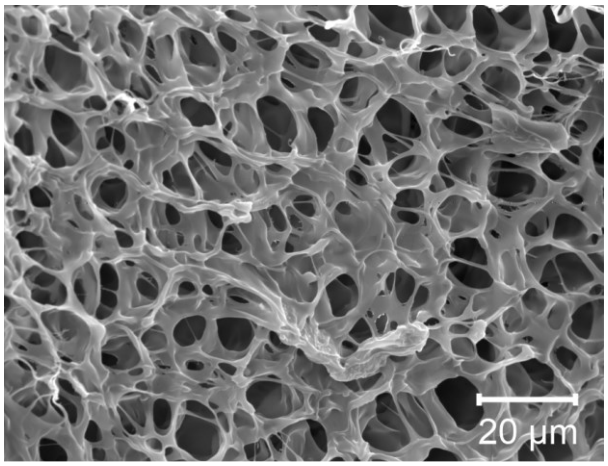

Figure S5.6. SEM image shows the porous structure of a 10 w/v% ANGNA hydrogel.

References

(1) Wang, W.; Xiang, L.; Gong, L.; Hu, W.; Huang, W.; Chen, Y.; Asha, A. B.; Srinivas, S.; Chen, L.; Narain, R.; Zeng, H. Injectable, Self-Healing Hydrogel with Tunable Optical, Mechanical, and Antimicrobial Properties. *Chem. Mater.* **2019,** *31* (7), 2366-2376.

(2) Tseng, T. C.; Tao, L.; Hsieh, F. Y.; Wei, Y.; Chiu, I. M.; Hsu, S. H. An Injectable, Self-Healing Hydrogel to Repair the Central Nervous System. *Adv. Mater.* **2015,** *27* (23), 3518-24.

(3) Li, L.; Yan, B.; Yang, J.; Chen, L.; Zeng, H. Novel mussel-inspired injectable self-healing hydrogel with anti-biofouling property. *Adv. Mater.* **2015,** *27* (7), 1294-9.

(4) Yang, J.-A.; Yeom, J.; Hwang, B. W.; Hoffman, A. S.; Hahn, S. K. In situ-forming injectable hydrogels for regenerative medicine. *Prog. Polym. Sci.* **2014,** *39* (12), 1973-1986.

(5) Griffin, D. R.; Archang, M. M.; Kuan, C. H.; Weaver, W. M.; Weinstein, J. S.; Feng, A. C.; Ruccia, A.; Sideris, E.; Ragkousis, V.; Koh, J.; Plikus, M. V.; Di Carlo, D.; Segura, T.; Scumpia, P. O. Activating an adaptive immune response from a hydrogel scaffold imparts regenerative wound healing. *Nat. Mater.* **2020**.

(6) Mandal, A.; Clegg, J. R.; Anselmo, A. C.; Mitragotri, S. Hydrogels in the clinic. *Bioeng. Transl. Med.* **2020,** *5* (2), e10158.

(7) Stapleton, L. M.; Steele, A. N.; Wang, H.; Lopez Hernandez, H.; Yu, A. C.; Paulsen, M. J.; Smith, A. A. A.; Roth, G. A.; Thakore, A. D.; Lucian, H. J.; Totherow, K. P.; Baker, S. W.; Tada, Y.; Farry, J. M.; Eskandari, A.; Hironaka, C. E.; Jaatinen, K. J.; Williams, K. M.; Bergamasco, H.; Marschel, C.; Chadwick, B.; Grady, F.; Ma, M.; Appel, E. A.; Woo, Y. J. Use of a supramolecular polymeric hydrogel as an effective post-operative pericardial adhesion barrier. *Nat. Biomed. Eng.* **2019,** *3* (8), 611-620.

(8) Guo, Q.; Sun, H.; Wu, X.; Yan, Z.; Tang, C.; Qin, Z.; Yao, M.; Che, P.; Yao, F.; Li, J. In Situ

Clickable Purely Zwitterionic Hydrogel for Peritoneal Adhesion Prevention. *Chem. Mater.* **2020,** *32* (15), 6347-6357.

(9) Zhang, E.; Yang, J.; Wang, K.; Song, B.; Zhu, H.; Han, X.; Shi, Y.; Yang, C.; Zeng, Z.; Cao, Z. Biodegradable Zwitterionic Cream Gel for Effective Prevention of Postoperative Adhesion. *Adv. Funct. Mater.* **2020**, 2009431.

(10) Zhao, X.; Wu, H.; Guo, B.; Dong, R.; Qiu, Y.; Ma, P. X. Antibacterial anti-oxidant electroactive injectable hydrogel as self-healing wound dressing with hemostasis and adhesiveness for cutaneous wound healing. *Biomaterials* **2017,** *122*, 34-47.

(11) Qu, J.; Zhao, X.; Liang, Y.; Zhang, T.; Ma, P. X.; Guo, B. Antibacterial adhesive injectable hydrogels with rapid self-healing, extensibility and compressibility as wound dressing for joints skin wound healing. *Biomaterials* **2018,** *183*, 185-199.

(12) Liu, Y.; Liu, Y.; Wang, Q.; Han, Y.; Tan, Y. Boronic ester-based self-healing hydrogels formed by using intermolecular B-N coordination. *Polymer* **2020,** *202*, 122624.

(13) Kharkar, P. M.; Rehmann, M. S.; Skeens, K. M.; Maverakis, E.; Kloxin, A. M. Thiol-ene click hydrogels for therapeutic delivery. *ACS. Biomater. Sci. Eng.* **2016,** *2* (2), 165-179.

(14) Yang, Y.; Liu, X.; Li, Y.; Wang, Y.; Bao, C.; Chen, Y.; Lin, Q.; Zhu, L. A postoperative anti-adhesion barrier based on photoinduced imine-crosslinking hydrogel with tissue-adhesive ability. *Acta. Biomater.* **2017,** *62*, 199-209.

(15) Yang, Y.; Zhang, J.; Liu, Z.; Lin, Q.; Liu, X.; Bao, C.; Wang, Y.; Zhu, L. Tissue-Integratable and Biocompatible Photogelation by the Imine Crosslinking Reaction. *Adv. Mater.* **2016,** *28* (14), 2724-30.

(16) Zhang, Y.; Tao, L.; Li, S.; Wei, Y. Synthesis of multiresponsive and dynamic chitosan-based hydrogels for controlled release of bioactive molecules. *Biomacromolecules* **2011,** *12* (8), 2894-

901.

(17) Chen, Y.; Tan, Z.; Wang, W.; Peng, Y. Y.; Narain, R. Injectable, Self-Healing, and Multi-Responsive Hydrogels via Dynamic Covalent Bond Formation between Benzoxaborole and Hydroxyl Groups. *Biomacromolecules* **2019,** *20* (2), 1028-1035.

(18) Zander, Z. K.; Becker, M. L. Antimicrobial and Antifouling Strategies for Polymeric Medical Devices. *ACS Macro Lett.* **2017,** *7* (1), 16-25.

(19) Phadke, A.; Zhang, C.; Arman, B.; Hsu, C. C.; Mashelkar, R. A.; Lele, A. K.; Tauber, M. J.; Arya, G.; Varghese, S. Rapid self-healing hydrogels. *Proc. Natl. Acad. Sci. U.S.A.* **2012,** *109* (12), 4383-8.

(20) Zhang, G.; Chen, Y.; Deng, Y.; Ngai, T.; Wang, C. Dynamic Supramolecular Hydrogels: Regulating Hydrogel Properties through Self-Complementary Quadruple Hydrogen Bonds and Thermo-Switch. *ACS Macro Lett.* **2017,** *6* (7), 641-646.

(21) Zeng, H.; Hwang, D. S.; Israelachvili, J. N.; Waite, J. H. Strong reversible Fe^{3+}-mediated bridging between dopa-containing protein films in water. *Proc. Natl. Acad. Sci. U S A.* **2010,** *107* (29), 12850-3.

(22) Zhang, J.; Xiang, L.; Yan, B.; Zeng, H. Nanomechanics of Anion-pi Interaction in Aqueous Solution. *J. Am. Chem. Soc.* **2020,** *142* (4), 1710-1714.

(23) Asha, A. B.; Chen, Y.; Zhang, H.; Ghaemi, S.; Ishihara, K.; Liu, Y.; Narain, R. Rapid Mussel-Inspired Surface Zwitteration for Enhanced Antifouling and Antibacterial Properties. *Langmuir* **2019,** *35* (5), 1621-1630.

(24) Nagao, M.; Sengupta, J.; Diaz-Dussan, D.; Adam, M.; Wu, M.; Acker, J.; Ben, R.; Ishihara, K.; Zeng, H.; Miura, Y.; Narain, R. Synthesis of Highly Biocompatible and Temperature-Responsive Physical Gels for Cryopreservation and 3D Cell Culture. *ACS Appl. Bio Mater.* **2018,**

1 (2), 356-366.

(25) Srivastava, S.; Andreev, M.; Levi, A. E.; Goldfeld, D. J.; Mao, J.; Heller, W. T.; Prabhu, V. M.; de Pablo, J. J.; Tirrell, M. V. Gel phase formation in dilute triblock copolyelectrolyte complexes. *Nat. Commun.* **2017,** *8* (1), 14131.

(26) Chen, Q.; Yu, S.; Zhang, D.; Zhang, W.; Zhang, H.; Zou, J.; Mao, Z.; Yuan, Y.; Gao, C.; Liu, R. Impact of Antifouling PEG Layer on the Performance of Functional Peptides in Regulating Cell Behaviors. *J. Am. Chem. Soc.* **2019,** *141* (42), 16772-16780.

(27) Kang, T.; Banquy, X.; Heo, J.; Lim, C.; Lynd, N. A.; Lundberg, P.; Oh, D. X.; Lee, H. K.; Hong, Y. K.; Hwang, D. S.; Waite, J. H.; Israelachvili, J. N.; Hawker, C. J. Mussel-Inspired Anchoring of Polymer Loops That Provide Superior Surface Lubrication and Antifouling Properties. *ACS Nano* **2016,** *10* (1), 930-7.

(28) He, S.; Wu, J.; Li, S. H.; Wang, L.; Sun, Y.; Xie, J.; Ramnath, D.; Weisel, R. D.; Yau, T. M.; Sung, H. W.; Li, R. K. The conductive function of biopolymer corrects myocardial scar conduction blockage and resynchronizes contraction to prevent heart failure. *Biomaterials* **2020,** *258*, 120285.

(29) Okabayashi, K.; Ashrafian, H.; Zacharakis, E.; Hasegawa, H.; Kitagawa, Y.; Athanasiou, T.; Darzi, A. Adhesions after abdominal surgery: a systematic review of the incidence, distribution and severity. *Surg. Today.* **2014,** *44* (3), 405-20.

(30) Robson, M. C. Wound infection. A failure of wound healing caused by an imbalance of bacteria. *Surg. Clin. North. Am.* **1997,** *77* (3), 637-50.

(31) Koh, T. J.; DiPietro, L. A. Inflammation and wound healing: the role of the macrophage. *Expert. Rev. Mol. Med.* **2011,** *13*, e23.

CHAPTER 6 Conclusions and Future Work

6.1 Major Conclusions and Contributions

In this thesis work, different types of dynamic molecular interactions (i.e., dynamic covalent chemistries and non-covalent physical interactions) have been leveraged to develop novel multifunctional self-healing hydrogels for various biomedical applications. The corresponding dynamic molecular interaction mechanisms have been investigated from the perspective of intermolecular and surface forces at molecular level. The major conclusions and original contributions are listed as below:

(1) An injectable self-healing hydrogel with dual temperature-pH responsive and antibacterial properties has been developed using PEI and a multifunctional gelator PFMNMF synthesized by reversible addition-fragmentation chain transfer (RAFT) polymerization. The shear-thinning rheological behavior endows the hydrogel with excellent injectability. The self-healing capability of the hydrogel is originated from the dynamic Schiff base interactions and such dynamic intermolecular interactions can be readily tuned by pH. The temperature-sensitive mechanical and optical properties of the hydrogel is resulted from the local hydrophobic domains formed by the collapsed PNIPAM block at elevated temperature. The amine-rich (quaternary or primary) groups render the hydrogel excellent antimicrobial property through a contact-killing mechanism. The as-prepared biocompatible hydrogel holds great potential for wound healing and other bioengineering applications.

(2) A biomimetic hydrogel with tissue-like strain-stiffening and self-healing properties has been developed as artificial ECM for 3D cell culture. The hydrogel is crosslinked through the dynamic boronic ester bonds formed between two linear flexible polymers, DPB-PEG and a glycopolymer, P(AM-*co*-LAMEA). Unlike the strain-softening mechanical behavior of most

flexible hydrogels, the as-prepared hydrogel possesses a well-defined nonlinear strain-stiffening mechano-response which can be facilely tuned by crosslinking density, polymer concentration, temperature and the length of crosslinker molecules. The strain-stiffening behavior is originated from the non-linear stretching and finite extensibility of the PEG strands. The self-healing property of the hydrogel is resulted from the dynamic molecular interactions between the boronic acid and *cis*-diol groups. The as-prepared biomimetic and biocompatible hydrogel can serve as an ideal platform for 3D cell culture. This work provides novel insights into molecular design of strain-stiffening self-healing materials, with useful implications for the development of biomimetic cell culture matrices, artificial tissues, as well as soft machines and robotics for various biomedical and engineering applications.

(3) An injectable self-healing hydrogel has been developed based on biological environment-adaptive supramolecular self-assembly of an ABA triblock copolymer composed of a central PEG block and terminal thermoresponsive PNIPAM block with pH sensitive A6ACA moieties randomly incorporated. The formed supramolecular hydrogel can adapt to the gastric environment and acquire remarkable self-healing capability to recover from repeated damage through the synergy of hydrophobic and pH-mediated hydrogen bonding interactions. The supramolecular hydrogel dressing can also effectively prevent the accumulation of microorganisms on the surface due to the hydration layer formed by PEG. In vivo gastric perforation rat model has demonstrated the significant advantages of our state-of-art hydrogel dressing over the conventional treatment, including simplified surgical procedures, reduced postoperative adhesion as well as suppressed inflammatory response. The design of our supramolecular hydrogel provides useful insights into the development of functional biomaterials with various biomedical applications.

6.2 Future Work

(1) Although many types of dynamic intermolecular interactions (e.g., cation-π interactions, anion-π interactions, ternary π-cation-π interactions, etc.) have been recently identified by nanomechanical force measurement techniques (e.g., SFA, AFM, etc.), it is still limited to leverage these dynamic molecular interactions to design or tune the properties and functionalities of the bulk materials (e.g., self-healing hydrogels, self-assembled materials, etc.). The development of new functional materials could be explored based on these experimentally identified intermolecular interaction mechanisms.

(2) For the self-healing hydrogels designed for wound healing and postoperative anti-adhesion applications, the materials could be further improved by integrating tissue adhesive property, particularly in wet environment, since the tissues or organs are usually covered by body fluid. Such bioadhesives with wet adhesion property could be designed based on the understanding of the interfacial molecular interaction mechanisms.

(3) The translation of these state-of-art functional hydrogels could have huge positive impact on human health. More systematic in vivo tests should be conducted in large animal models to further verify the medical outcome of the materials with the collaboration of the clinical practitioners.

Bibliography

(1) Wichterle, O.; Lim, D. Hydrophilic Gels for Biological Use. *Nature* **1960,** *185* (4706), 117-118.

(2) Annabi, N.; Tamayol, A.; Uquillas, J. A.; Akbari, M.; Bertassoni, L. E.; Cha, C.; Camci-Unal, G.; Dokmeci, M. R.; Peppas, N. A.; Khademhosseini, A. 25th anniversary article: Rational design and applications of hydrogels in regenerative medicine. *Adv. Mater.* **2014,** *26* (1), 85-123.

(3) Ahmed, E. M. Hydrogel: Preparation, characterization, and applications: A review. *J. Adv. Res.* **2015,** *6* (2), 105-21.

(4) Zhang, Y.; Tao, L.; Li, S.; Wei, Y. Synthesis of multiresponsive and dynamic chitosan-based hydrogels for controlled release of bioactive molecules. *Biomacromolecules* **2011,** *12* (8), 2894-901.

(5) Deng, Z.; Guo, Y.; Zhao, X.; Ma, P. X.; Guo, B. Multifunctional Stimuli-Responsive Hydrogels with Self-Healing, High Conductivity, and Rapid Recovery through Host–Guest Interactions. *Chem. Mater.* **2018,** *30* (5), 1729-1742.

(6) Chen, J.; Peng, Q.; Thundat, T.; Zeng, H. Stretchable, Injectable, and Self-Healing Conductive Hydrogel Enabled by Multiple Hydrogen Bonding toward Wearable Electronics. *Chem. Mater.* **2019,** *31* (12), 4553-4563.

(7) Wang, Z.; Chen, J.; Cong, Y.; Zhang, H.; Xu, T.; Nie, L.; Fu, J. Ultrastretchable Strain Sensors and Arrays with High Sensitivity and Linearity Based on Super Tough Conductive Hydrogels. *Chem. Mater.* **2018,** *30* (21), 8062-8069.

(8) Giano, M. C.; Ibrahim, Z.; Medina, S. H.; Sarhane, K. A.; Christensen, J. M.; Yamada, Y.; Brandacher, G.; Schneider, J. P. Injectable bioadhesive hydrogels with innate antibacterial properties. *Nat. Commun.* **2014,** *5*, 4095.

(9) Zhong, Y.; Xiao, H.; Seidi, F.; Jin, Y. Natural Polymer-Based Antimicrobial Hydrogels without

Synthetic Antibiotics as Wound Dressings. *Biomacromolecules* **2020,** *21* (8), 2983-3006.

(10) Banerjee, S. L.; Bhattacharya, K.; Samanta, S.; Singha, N. K. Self-Healable Antifouling Zwitterionic Hydrogel Based on Synergistic Phototriggered Dynamic Disulfide Metathesis Reaction and Ionic Interaction. *ACS Appl. Mater. Interfaces.* **2018,** *10* (32), 27391-27406.

(11) Zhang, Y.-c.; Le, X.-x.; Lu, W.; Jian, Y.-k.; Zhang, J.-w.; Chen, T. An "Off-the-Shelf" Shape Memory Hydrogel Based on the Dynamic Borax-Diol Ester Bonds. *Macromol. Mater. Eng.* **2018,** *303* (7), 1800144.

(12) Liu, K.; Zhang, Y.; Cao, H.; Liu, H.; Geng, Y.; Yuan, W.; Zhou, J.; Wu, Z. L.; Shan, G.; Bao, Y.; Zhao, Q.; Xie, T.; Pan, P. Programmable Reversible Shape Transformation of Hydrogels Based on Transient Structural Anisotropy. *Adv. Mater.* **2020,** *32* (28), e2001693.

(13) Khademhosseini, A.; Langer, R. Microengineered hydrogels for tissue engineering. *Biomaterials* **2007,** *28* (34), 5087-5092.

(14) Lee, K. Y.; Mooney, D. J. Hydrogels for tissue engineering. *Chem. Rev.* **2001,** *101* (7), 1869-79.

(15) Secret, E.; Kelly, S. J.; Crannell, K. E.; Andrew, J. S. Enzyme-responsive hydrogel microparticles for pulmonary drug delivery. *ACS Appl. Mater. Interfaces.* **2014,** *6* (13), 10313-21.

(16) Li, H.; Go, G.; Ko, S. Y.; Park, J.-O.; Park, S. Magnetic actuated pH-responsive hydrogel-based soft micro-robot for targeted drug delivery. *Smart Mater. Struct.* **2016,** *25* (2), 027001.

(17) Childs, A.; Li, H.; Lewittes, D. M.; Dong, B.; Liu, W.; Shu, X.; Sun, C.; Zhang, H. F. Fabricating customized hydrogel contact lens. *Sci. Rep.* **2016,** *6* (1), 34905.

(18) Tian, S.; Jiang, D.; Pu, J.; Sun, X.; Li, Z.; Wu, B.; Zheng, W.; Liu, W.; Liu, Z. A new hybrid silicone-based antifouling coating with nanocomposite hydrogel for durable antifouling properties. *Chem. Eng. J.* **2019,** *370*, 1-9.

(19) Wu, M.; Chen, J.; Ma, Y.; Yan, B.; Pan, M.; Peng, Q.; Wang, W.; Han, L.; Liu, J.; Zeng, H. Ultra elastic, stretchable, self-healing conductive hydrogels with tunable optical properties for highly sensitive soft electronic sensors. *J. Mater. Chem. A* **2020,** *8* (46), 24718-24733.

(20) Wang, J.; Tang, F.; Wang, Y.; Lu, Q.; Liu, S.; Li, L. Self-Healing and Highly Stretchable Gelatin Hydrogel for Self-Powered Strain Sensor. *ACS Appl. Mater. Interfaces.* **2020,** *12* (1), 1558-1566.

(21) Ma, Y.; Hua, M.; Wu, S.; Du, Y.; Pei, X.; Zhu, X.; Zhou, F.; He, X. Bioinspired high-power-density strong contractile hydrogel by programmable elastic recoil. *Sci. Adv.* **2020,** *6* (47), eabd2520.

(22) Ionov, L. Hydrogel-based actuators: possibilities and limitations. *Mater. Today* **2014,** *17* (10), 494-503.

(23) Zheng, W. J.; An, N.; Yang, J. H.; Zhou, J.; Chen, Y. M. Tough Al-alginate/poly(N-isopropylacrylamide) hydrogel with tunable LCST for soft robotics. *ACS Appl. Mater. Interfaces.* **2015,** *7* (3), 1758-64.

(24) Sinha, V.; Chakma, S. Advances in the preparation of hydrogel for wastewater treatment: A concise review. *J. Environ. Chem. Eng.* **2019,** *7* (5), 103295.

(25) Jiao, T.; Guo, H.; Zhang, Q.; Peng, Q.; Tang, Y.; Yan, X.; Li, B. Reduced Graphene Oxide-Based Silver Nanoparticle-Containing Composite Hydrogel as Highly Efficient Dye Catalysts for Wastewater Treatment. *Sci. Rep.* **2015,** *5* (1), 11873.

(26) Chen, Y.; Wang, W.; Wu, D.; Zeng, H.; Hall, D. G.; Narain, R. Multiresponsive and Self-Healing Hydrogel via Formation of Polymer-Nanogel Interfacial Dynamic Benzoxaborole Esters at Physiological pH. *ACS Appl. Mater. Interfaces.* **2019,** *11* (47), 44742-44750.

(27) Taylor, D. L.; In Het Panhuis, M. Self-Healing Hydrogels. *Adv. Mater.* **2016,** *28* (41), 9060-

9093.

(28) Liu, Y.; Hsu, S. H. Synthesis and Biomedical Applications of Self-healing Hydrogels. *Front. Chem.* **2018,** *6* (449), 449.

(29) Zhu, D. Y.; Rong, M. Z.; Zhang, M. Q. Self-healing polymeric materials based on microencapsulated healing agents: From design to preparation. *Prog. Polym. Sci.* **2015,** *49-50*, 175-220.

(30) White, S. R.; Sottos, N. R.; Geubelle, P. H.; Moore, J. S.; Kessler, M. R.; Sriram, S. R.; Brown, E. N.; Viswanathan, S. Autonomic healing of polymer composites. *Nature* **2001,** *409* (6822), 794-797.

(31) Diba, M.; Spaans, S.; Ning, K.; Ippel, B. D.; Yang, F.; Loomans, B.; Dankers, P. Y. W.; Leeuwenburgh, S. C. G. Self-Healing Biomaterials: From Molecular Concepts to Clinical Applications. *Adv. Mater. Interfaces* **2018,** *5* (17), 1800118.

(32) Toohey, K. S.; Sottos, N. R.; Lewis, J. A.; Moore, J. S.; White, S. R. Self-healing materials with microvascular networks. *Nat. Mater.* **2007,** *6* (8), 581-5.

(33) Chen, M.; Fan, D.; Liu, S.; Rao, Z.; Dong, Y.; Wang, W.; Chen, H.; Bai, L.; Cheng, Z. Fabrication of self-healing hydrogels with surface functionalized microcapsules from stellate mesoporous silica. *Polym. Chem.* **2019,** *10* (4), 503-511.

(34) Liu, S.; Rao, Z.; Wu, R.; Sun, Z.; Yuan, Z.; Bai, L.; Wang, W.; Yang, H.; Chen, H. Fabrication of Microcapsules by the Combination of Biomass Porous Carbon and Polydopamine for Dual Self-Healing Hydrogels. *J. Agric. Food. Chem.* **2019,** *67* (4), 1061-1071.

(35) Yang, Y.; Urban, M. W. Self-healing polymeric materials. *Chem. Soc. Rev.* **2013,** *42* (17), 7446-67.

(36) Wei, Z.; Yang, J. H.; Zhou, J.; Xu, F.; Zrinyi, M.; Dussault, P. H.; Osada, Y.; Chen, Y. M. Self-

healing gels based on constitutional dynamic chemistry and their potential applications. *Chem. Soc. Rev.* **2014,** *43* (23), 8114-31.

(37) Phadke, A.; Zhang, C.; Arman, B.; Hsu, C. C.; Mashelkar, R. A.; Lele, A. K.; Tauber, M. J.; Arya, G.; Varghese, S. Rapid self-healing hydrogels. *Proc. Natl. Acad. Sci. U. S. A.* **2012,** *109* (12), 4383-8.

(38) Han, L.; Wang, M.; Prieto‐López, L. O.; Deng, X.; Cui, J. Self‐Hydrophobization in a Dynamic Hydrogel for Creating Nonspecific Repeatable Underwater Adhesion. *Adv. Funct. Mater* **2019,** *30* (7), 1907064.

(39) Jeon, I.; Cui, J.; Illeperuma, W. R.; Aizenberg, J.; Vlassak, J. J. Extremely Stretchable and Fast Self-Healing Hydrogels. *Adv. Mater.* **2016,** *28* (23), 4678-83.

(40) Tuncaboylu, D. C.; Sari, M.; Oppermann, W.; Okay, O. Tough and Self-Healing Hydrogels Formed via Hydrophobic Interactions. *Macromolecules* **2011,** *44* (12), 4997-5005.

(41) Zheng, J.; Xiao, P.; Liu, W.; Zhang, J.; Huang, Y.; Chen, T. Mechanical Robust and Self-Healable Supramolecular Hydrogel. *Macromol. Rapid Commun.* **2016,** *37* (3), 265-70.

(42) Long, T.; Li, Y.; Fang, X.; Sun, J. Salt-Mediated Polyampholyte Hydrogels with High Mechanical Strength, Excellent Self-Healing Property, and Satisfactory Electrical Conductivity. *Adv. Funct. Mater* **2018,** *28* (44), 1804416.

(43) Ma, X.; Zhao, Y. Biomedical Applications of Supramolecular Systems Based on Host-Guest Interactions. *Chem. Rev.* **2015,** *115* (15), 7794-839.

(44) Hu, Q. D.; Tang, G. P.; Chu, P. K. Cyclodextrin-based host-guest supramolecular nanoparticles for delivery: from design to applications. *Acc. Chem. Res.* **2014,** *47* (7), 2017-25.

(45) Schmidt, B.; Barner-Kowollik, C. Dynamic Macromolecular Material Design-The Versatility of Cyclodextrin-Based Host-Guest Chemistry. *Angew. Chem. Int. Ed. Engl.* **2017,** *56* (29), 8350-

8369.

(46) Marquez, C.; Hudgins, R. R.; Nau, W. M. Mechanism of host-guest complexation by cucurbituril. *J. Am. Chem. Soc.* **2004,** *126* (18), 5806-16.

(47) Zhang, M.; Xu, D.; Yan, X.; Chen, J.; Dong, S.; Zheng, B.; Huang, F. Self-healing supramolecular gels formed by crown ether based host-guest interactions. *Angew. Chem. Int. Ed. Engl.* **2012,** *51* (28), 7011-5.

(48) Kakuta, T.; Takashima, Y.; Nakahata, M.; Otsubo, M.; Yamaguchi, H.; Harada, A. Preorganized hydrogel: self-healing properties of supramolecular hydrogels formed by polymerization of host-guest-monomers that contain cyclodextrins and hydrophobic guest groups. *Adv. Mater.* **2013,** *25* (20), 2849-53.

(49) Li, L.; Smitthipong, W.; Zeng, H. Mussel-inspired hydrogels for biomedical and environmental applications. *Polym. Chem.* **2015,** *6* (3), 353-358.

(50) Guo, Q.; Chen, J.; Wang, J.; Zeng, H.; Yu, J. Recent progress in synthesis and application of mussel-inspired adhesives. *Nanoscale* **2020,** *12* (3), 1307-1324.

(51) Zhang, C.; Wu, B.; Zhou, Y.; Zhou, F.; Liu, W.; Wang, Z. Mussel-inspired hydrogels: from design principles to promising applications. *Chem. Soc. Rev.* **2020,** *49* (11), 3605-3637.

(52) Zeng, H.; Hwang, D. S.; Israelachvili, J. N.; Waite, J. H. Strong reversible Fe^{3+}-mediated bridging between dopa-containing protein films in water. *Proc. Natl. Acad. Sci. U. S. A.* **2010,** *107* (29), 12850-3.

(53) Zhang, J.; Xiang, L.; Yan, B.; Zeng, H. Nanomechanics of Anion-pi Interaction in Aqueous Solution. *J. Am. Chem. Soc.* **2020,** *142* (4), 1710-1714.

(54) Gebbie, M. A.; Wei, W.; Schrader, A. M.; Cristiani, T. R.; Dobbs, H. A.; Idso, M.; Chmelka, B. F.; Waite, J. H.; Israelachvili, J. N. Tuning underwater adhesion with cation-pi interactions. *Nat.*

Chem. **2017,** *9* (5), 473-479.

(55) Li, L.; Yan, B.; Yang, J.; Chen, L.; Zeng, H. Novel mussel-inspired injectable self-healing hydrogel with anti-biofouling property. *Adv. Mater.* **2015,** *27* (7), 1294-9.

(56) Han, L.; Lu, X.; Liu, K.; Wang, K.; Fang, L.; Weng, L. T.; Zhang, H.; Tang, Y.; Ren, F.; Zhao, C.; Sun, G.; Liang, R.; Li, Z. Mussel-Inspired Adhesive and Tough Hydrogel Based on Nanoclay Confined Dopamine Polymerization. *ACS Nano* **2017,** *11* (3), 2561-2574.

(57) Han, L.; Yan, L.; Wang, K.; Fang, L.; Zhang, H.; Tang, Y.; Ding, Y.; Weng, L.-T.; Xu, J.; Weng, J.; Liu, Y.; Ren, F.; Lu, X. Tough, self-healable and tissue-adhesive hydrogel with tunable multifunctionality. *NPG Asia Mater.* **2017,** *9* (4), e372-e372.

(58) Han, L.; Lu, X.; Wang, M.; Gan, D.; Deng, W.; Wang, K.; Fang, L.; Liu, K.; Chan, C. W.; Tang, Y.; Weng, L. T.; Yuan, H. A Mussel-Inspired Conductive, Self-Adhesive, and Self-Healable Tough Hydrogel as Cell Stimulators and Implantable Bioelectronics. *Small* **2017,** *13* (2).

(59) Elshaarani, T.; Yu, H.; Wang, L.; Zain Ul, A.; Ullah, R. S.; Haroon, M.; Khan, R. U.; Fahad, S.; Khan, A.; Nazir, A.; Usman, M.; Naveed, K. U. Synthesis of hydrogel-bearing phenylboronic acid moieties and their applications in glucose sensing and insulin delivery. *J. Mater. Chem. B* **2018,** *6* (23), 3831-3854.

(60) Chen, Y.; Diaz-Dussan, D.; Wu, D.; Wang, W.; Peng, Y.-Y.; Asha, A. B.; Hall, D. G.; Ishihara, K.; Narain, R. Bioinspired Self-Healing Hydrogel Based on Benzoxaborole-Catechol Dynamic Covalent Chemistry for 3D Cell Encapsulation. *ACS Macro Lett.* **2018,** *7* (8), 904-908.

(61) Wang, W.; Xiang, L.; Diaz-Dussan, D.; Zhang, J.; Yang, W.; Gong, L.; Chen, J.; Narain, R.; Zeng, H. Dynamic Flexible Hydrogel Network with Biological Tissue-like Self-Protective Functions. *Chem. Mater.* **2020,** *32* (24), 10545-10555.

(62) Chu, C. K.; Joseph, A. J.; Limjoco, M. D.; Yang, J.; Bose, S.; Thapa, L. S.; Langer, R.;

Anderson, D. G. Chemical Tuning of Fibers Drawn from Extensible Hyaluronic Acid Networks. *J. Am. Chem. Soc.* **2020,** *142* (46), 19715-19721.

(63) Chen, Y.; Wang, W.; Wu, D.; Nagao, M.; Hall, D. G.; Thundat, T.; Narain, R. Injectable Self-Healing Zwitterionic Hydrogels Based on Dynamic Benzoxaborole–Sugar Interactions with Tunable Mechanical Properties. *Biomacromolecules* **2018,** *19* (2), 596-605.

(64) Yesilyurt, V.; Webber, M. J.; Appel, E. A.; Godwin, C.; Langer, R.; Anderson, D. G. Injectable Self-Healing Glucose-Responsive Hydrogels with pH-Regulated Mechanical Properties. *Adv. Mater.* **2016,** *28* (1), 86-91.

(65) Zhao, X.; Wu, H.; Guo, B.; Dong, R.; Qiu, Y.; Ma, P. X. Antibacterial anti-oxidant electroactive injectable hydrogel as self-healing wound dressing with hemostasis and adhesiveness for cutaneous wound healing. *Biomaterials* **2017,** *122*, 34-47.

(66) Qu, J.; Zhao, X.; Ma, P. X.; Guo, B. pH-responsive self-healing injectable hydrogel based on N-carboxyethyl chitosan for hepatocellular carcinoma therapy. *Acta. Biomater.* **2017,** *58*, 168-180.

(67) Tseng, T. C.; Tao, L.; Hsieh, F. Y.; Wei, Y.; Chiu, I. M.; Hsu, S. H. An Injectable, Self-Healing Hydrogel to Repair the Central Nervous System. *Adv. Mater.* **2015,** *27* (23), 3518-24.

(68) Wang, W.; Narain, R.; Zeng, H. Rational Design of Self-Healing Tough Hydrogels: A Mini Review. *Front. Chem.* **2018,** *6* (497), 497.

(69) Yang, X.; Liu, G.; Peng, L.; Guo, J.; Tao, L.; Yuan, J.; Chang, C.; Wei, Y.; Zhang, L. Highly Efficient Self-Healable and Dual Responsive Cellulose-Based Hydrogels for Controlled Release and 3D Cell Culture. *Adv. Funct. Mater.* **2017,** *27* (40), 1703174.

(70) Sun, C.; Jia, H.; Lei, K.; Zhu, D.; Gao, Y.; Zheng, Z.; Wang, X. Self-healing hydrogels with stimuli responsiveness based on acylhydrazone bonds. *Polymer* **2019,** *160*, 246-253.

(71) Deng, G.; Li, F.; Yu, H.; Liu, F.; Liu, C.; Sun, W.; Jiang, H.; Chen, Y. Dynamic Hydrogels

with an Environmental Adaptive Self-Healing Ability and Dual Responsive Sol–Gel Transitions. *ACS Macro Lett.* **2012,** *1* (2), 275-279.

(72) Canadell, J.; Goossens, H.; Klumperman, B. Self-Healing Materials Based on Disulfide Links. *Macromolecules* **2011,** *44* (8), 2536-2541.

(73) Fairbanks, B. D.; Singh, S. P.; Bowman, C. N.; Anseth, K. S. Photodegradable, Photoadaptable Hydrogels via Radical-Mediated Disulfide Fragmentation Reaction. *Macromolecules* **2011,** *44* (8), 2444-2450.

(74) Barcan, G. A.; Zhang, X.; Waymouth, R. M. Structurally dynamic hydrogels derived from 1,2-dithiolanes. *J. Am. Chem. Soc.* **2015,** *137* (17), 5650-3.

(75) Lopez-Perez, P. M.; da Silva, R. M. P.; Strehin, I.; Kouwer, P. H. J.; Leeuwenburgh, S. C. G.; Messersmith, P. B. Self-Healing Hydrogels Formed by Complexation between Calcium Ions and Bisphosphonate-Functionalized Star-Shaped Polymers. *Macromolecules* **2017,** *50* (21), 8698-8706.

(76) Shi, L.; Carstensen, H.; Hölzl, K.; Lunzer, M.; Li, H.; Hilborn, J.; Ovsianikov, A.; Ossipov, D. A. Dynamic Coordination Chemistry Enables Free Directional Printing of Biopolymer Hydrogel. *Chem. Mater.* **2017,** *29* (14), 5816-5823.

(77) Sun, J. Y.; Zhao, X.; Illeperuma, W. R.; Chaudhuri, O.; Oh, K. H.; Mooney, D. J.; Vlassak, J. J.; Suo, Z. Highly stretchable and tough hydrogels. *Nature* **2012,** *489* (7414), 133-6.

(78) Holten-Andersen, N.; Harrington, M. J.; Birkedal, H.; Lee, B. P.; Messersmith, P. B.; Lee, K. Y.; Waite, J. H. pH-induced metal-ligand cross-links inspired by mussel yield self-healing polymer networks with near-covalent elastic moduli. *Proc. Natl. Acad. Sci. U. S. A.* **2011,** *108* (7), 2651-5.

(79) Filippidi, E.; Cristiani, T. R.; Eisenbach, C. D.; Waite, J. H.; Israelachvili, J. N.; Ahn, B. K.; Valentine, M. T. Toughening elastomers using mussel-inspired iron-catechol complexes. *Science* **2017,** *358* (6362), 502-505.

(80) Shi, L.; Ding, P.; Wang, Y.; Zhang, Y.; Ossipov, D.; Hilborn, J. Self-Healing Polymeric Hydrogel Formed by Metal-Ligand Coordination Assembly: Design, Fabrication, and Biomedical Applications. *Macromol. Rapid. Commun.* **2019,** *40* (7), e1800837.

(81) Smith, L. J.; Taimoory, S. M.; Tam, R. Y.; Baker, A. E. G.; Binth Mohammad, N.; Trant, J. F.; Shoichet, M. S. Diels-Alder Click-Cross-Linked Hydrogels with Increased Reactivity Enable 3D Cell Encapsulation. *Biomacromolecules* **2018,** *19* (3), 926-935.

(82) Alge, D. L.; Azagarsamy, M. A.; Donohue, D. F.; Anseth, K. S. Synthetically tractable click hydrogels for three-dimensional cell culture formed using tetrazine-norbornene chemistry. *Biomacromolecules* **2013,** *14* (4), 949-53.

(83) Wei, Z.; Yang, J. H.; Du, X. J.; Xu, F.; Zrinyi, M.; Osada, Y.; Li, F.; Chen, Y. M. Dextran-based self-healing hydrogels formed by reversible diels-alder reaction under physiological conditions. *Macromol. Rapid. Commun.* **2013,** *34* (18), 1464-70.

(84) Gallo, R. L. Human Skin Is the Largest Epithelial Surface for Interaction with Microbes. *J. Invest. Dermatol.* **2017,** *137* (6), 1213-1214.

(85) Rezvani Ghomi, E.; Khalili, S.; Nouri Khorasani, S.; Esmaeely Neisiany, R.; Ramakrishna, S. Wound dressings: Current advances and future directions. *J. Appl. Polym. Sci.* **2019,** *136* (27), 47738.

(86) Bae, K. H.; Wang, L. S.; Kurisawa, M. Injectable biodegradable hydrogels: progress and challenges. *J. Mater. Chem. B* **2013,** *1* (40), 5371-5388.

(87) Yang, J.-A.; Yeom, J.; Hwang, B. W.; Hoffman, A. S.; Hahn, S. K. In situ-forming injectable hydrogels for regenerative medicine. *Prog. Polym. Sci.* **2014,** *39* (12), 1973-1986.

(88) Chen, H.; Cheng, R.; Zhao, X.; Zhang, Y.; Tam, A.; Yan, Y.; Shen, H.; Zhang, Y. S.; Qi, J.; Feng, Y.; Liu, L.; Pan, G.; Cui, W.; Deng, L. An injectable self-healing coordinative hydrogel with

antibacterial and angiogenic properties for diabetic skin wound repair. *NPG Asia Mater.* **2019,** *11* (1), 3.

(89) Qu, J.; Zhao, X.; Liang, Y.; Zhang, T.; Ma, P. X.; Guo, B. Antibacterial adhesive injectable hydrogels with rapid self-healing, extensibility and compressibility as wound dressing for joints skin wound healing. *Biomaterials* **2018,** *183*, 185-199.

(90) Fan, Z.; Liu, B.; Wang, J.; Zhang, S.; Lin, Q.; Gong, P.; Ma, L.; Yang, S. A Novel Wound Dressing Based on Ag/Graphene Polymer Hydrogel: Effectively Kill Bacteria and Accelerate Wound Healing. *AdV. Funct. Mater.* **2014,** *24* (25), 3933-3943.

(91) Schwartz, V. B.; Thétiot, F.; Ritz, S.; Pütz, S.; Choritz, L.; Lappas, A.; Förch, R.; Landfester, K.; Jonas, U. Antibacterial Surface Coatings from Zinc Oxide Nanoparticles Embedded in Poly(N-isopropylacrylamide) Hydrogel Surface Layers. *Adv. Funct. Mater.* **2012,** *22* (11), 2376-2386.

(92) Yang, K.; Han, Q.; Chen, B.; Zheng, Y.; Zhang, K.; Li, Q.; Wang, J. Antimicrobial hydrogels: promising materials for medical application. *Int. J. Nanomedicine.* **2018,** *13*, 2217-2263.

(93) Annabi, N.; Rana, D.; Shirzaei Sani, E.; Portillo-Lara, R.; Gifford, J. L.; Fares, M. M.; Mithieux, S. M.; Weiss, A. S. Engineering a sprayable and elastic hydrogel adhesive with antimicrobial properties for wound healing. *Biomaterials* **2017,** *139*, 229-243.

(94) Strassburg, A.; Petranowitsch, J.; Paetzold, F.; Krumm, C.; Peter, E.; Meuris, M.; Koller, M.; Tiller, J. C. Cross-Linking of a Hydrophilic, Antimicrobial Polycation toward a Fast-Swelling, Antimicrobial Superabsorber and Interpenetrating Hydrogel Networks with Long Lasting Antimicrobial Properties. *ACS Appl. Mater. Interfaces.* **2017,** *9* (42), 36573-36582.

(95) Li, L.; Yan, B.; Yang, J.; Huang, W.; Chen, L.; Zeng, H. Injectable Self-Healing Hydrogel with Antimicrobial and Antifouling Properties. *ACS Appl. Mater. Interfaces.* **2017,** *9* (11), 9221-9225.

(96) Mura, S.; Nicolas, J.; Couvreur, P. Stimuli-responsive nanocarriers for drug delivery. *Nat. Mater.* **2013,** *12* (11), 991-1003.

(97) Wu, M.; Chen, J.; Huang, W.; Yan, B.; Peng, Q.; Liu, J.; Chen, L.; Zeng, H. Injectable and Self-Healing Nanocomposite Hydrogels with Ultrasensitive pH-Responsiveness and Tunable Mechanical Properties: Implications for Controlled Drug Delivery. *Biomacromolecules* **2020,** *21* (6), 2409-2420.

(98) Tibbitt, M. W.; Anseth, K. S. Hydrogels as extracellular matrix mimics for 3D cell culture. *Biotechnol. Bioeng.* **2009,** *103* (4), 655-63.

(99) Lou, J.; Stowers, R.; Nam, S.; Xia, Y.; Chaudhuri, O. Stress relaxing hyaluronic acid-collagen hydrogels promote cell spreading, fiber remodeling, and focal adhesion formation in 3D cell culture. *Biomaterials* **2018,** *154*, 213-222.

(100) Zhang, G.; Chen, Y.; Deng, Y.; Ngai, T.; Wang, C. Dynamic Supramolecular Hydrogels: Regulating Hydrogel Properties through Self-Complementary Quadruple Hydrogen Bonds and Thermo-Switch. *ACS Macro Lett.* **2017,** *6* (7), 641-646.

(101) Nagao, M.; Sengupta, J.; Diaz-Dussan, D.; Adam, M.; Wu, M.; Acker, J.; Ben, R.; Ishihara, K.; Zeng, H.; Miura, Y.; Narain, R. Synthesis of Highly Biocompatible and Temperature-Responsive Physical Gels for Cryopreservation and 3D Cell Culture. *ACS Appl. Bio Mater.* **2018,** *1* (2), 356-366.

(102) Kouwer, P. H.; Koepf, M.; Le Sage, V. A.; Jaspers, M.; van Buul, A. M.; Eksteen-Akeroyd, Z. H.; Woltinge, T.; Schwartz, E.; Kitto, H. J.; Hoogenboom, R.; Picken, S. J.; Nolte, R. J.; Mendes, E.; Rowan, A. E. Responsive biomimetic networks from polyisocyanopeptide hydrogels. *Nature* **2013,** *493* (7434), 651-5.

(103) Goldenberg, C.; Goldhirsch, I. Friction enhances elasticity in granular solids. *Nature* **2005,**

435 (7039), 188-91.

(104) Burla, F.; Mulla, Y.; Vos, B. E.; Aufderhorst-Roberts, A.; Koenderink, G. H. From mechanical resilience to active material properties in biopolymer networks. *Nat. Rev. Phys.* **2019,** *1* (4), 249-263.

(105) Lih, E.; Oh, S. H.; Joung, Y. K.; Lee, J. H.; Han, D. K. Polymers for cell/tissue anti-adhesion. *Prog. Polym. Sci.* **2015,** *44*, 28-61.

(106) Stapleton, L. M.; Steele, A. N.; Wang, H.; Lopez Hernandez, H.; Yu, A. C.; Paulsen, M. J.; Smith, A. A. A.; Roth, G. A.; Thakore, A. D.; Lucian, H. J.; Totherow, K. P.; Baker, S. W.; Tada, Y.; Farry, J. M.; Eskandari, A.; Hironaka, C. E.; Jaatinen, K. J.; Williams, K. M.; Bergamasco, H.; Marschel, C.; Chadwick, B.; Grady, F.; Ma, M.; Appel, E. A.; Woo, Y. J. Use of a supramolecular polymeric hydrogel as an effective post-operative pericardial adhesion barrier. *Nat. Biomed. Eng.* **2019,** *3* (8), 611-620.

(107) Yang, Y.; Liu, X.; Li, Y.; Wang, Y.; Bao, C.; Chen, Y.; Lin, Q.; Zhu, L. A postoperative anti-adhesion barrier based on photoinduced imine-crosslinking hydrogel with tissue-adhesive ability. *Acta. Biomater.* **2017,** *62*, 199-209.

(108) Li, L.; Wang, N.; Jin, X.; Deng, R.; Nie, S.; Sun, L.; Wu, Q.; Wei, Y.; Gong, C. Biodegradable and injectable in situ cross-linking chitosan-hyaluronic acid based hydrogels for postoperative adhesion prevention. *Biomaterials* **2014,** *35* (12), 3903-3917.

(109) Song, L.; Li, L.; He, T.; Wang, N.; Yang, S.; Yang, X.; Zeng, Y.; Zhang, W.; Yang, L.; Wu, Q.; Gong, C. Peritoneal adhesion prevention with a biodegradable and injectable N,O-carboxymethyl chitosan-aldehyde hyaluronic acid hydrogel in a rat repeated-injury model. *Sci. Rep.* **2016,** *6* (1), 37600.

(110) Zhu, W.; Gao, L.; Luo, Q.; Gao, C.; Zha, G.; Shen, Z.; Li, X. Metal and light free “click”

hydrogels for prevention of post-operative peritoneal adhesions. *Polym. Chem.* **2014,** *5* (6), 2018-2026.

(111) Zhang, E.; Song, B.; Shi, Y.; Zhu, H.; Han, X.; Du, H.; Yang, C.; Cao, Z. Fouling-resistant zwitterionic polymers for complete prevention of postoperative adhesion. *Proc. Natl. Acad. Sci. U. S. A.* **2020,** *117* (50), 32046-32055.

(112) Guo, Q.; Sun, H.; Wu, X.; Yan, Z.; Tang, C.; Qin, Z.; Yao, M.; Che, P.; Yao, F.; Li, J. In Situ Clickable Purely Zwitterionic Hydrogel for Peritoneal Adhesion Prevention. *Chem. Mater.* **2020,** *32* (15), 6347-6357.

(113) Zhang, E.; Yang, J.; Wang, K.; Song, B.; Zhu, H.; Han, X.; Shi, Y.; Yang, C.; Zeng, Z.; Cao, Z. Biodegradable Zwitterionic Cream Gel for Effective Prevention of Postoperative Adhesion. *Adv. Funct. Mater* **2020,** *31* (10), 2009431.

(114) Chen, Y.; Wang, W.; Wu, D.; Nagao, M.; Hall, D. G.; Thundat, T.; Narain, R. Injectable Self-Healing Zwitterionic Hydrogels Based on Dynamic Benzoxaborole-Sugar Interactions with Tunable Mechanical Properties. *Biomacromolecules* **2018,** *19* (2), 596-605.

(115) Long, T.; Li, Y.; Fang, X.; Sun, J. Salt-Mediated Polyampholyte Hydrogels with High Mechanical Strength, Excellent Self-Healing Property, and Satisfactory Electrical Conductivity. *Adv. Funct. Mater.* **2018,** *28* (44), 1804416.

(116) Jiang, F.; Wang, X.; He, C.; Saricilar, S.; Wang, H. Mechanical properties of tough hydrogels synthesized with a facile simultaneous radiation polymerization and cross-linking method. *Radiat. Phys. Chem.* **2015,** *106*, 7-15.

(117) Pojman, J. A.; Willis, J.; Fortenberry, D.; Ilyashenko, V.; Khan, A. M. Factors affecting propagating fronts of addition polymerization: Velocity, front curvature, temperatue profile, conversion, and molecular weight distribution. *J. Polym. Sci., Part A-1: Polym. Chem.* **1995,** *33*

(4), 643-652.

(118) Chiefari, J.; Chong, Y. K.; Ercole, F.; Krstina, J.; Jeffery, J.; Le, T. P. T.; Mayadunne, R. T. A.; Meijs, G. F.; Moad, C. L.; Moad, G.; Rizzardo, E.; Thang, S. H. Living Free-Radical Polymerization by Reversible Addition−Fragmentation Chain Transfer: The RAFT Process. *Macromolecules* **1998,** *31* (16), 5559-5562.

(119) Perrier, S. 50th Anniversary Perspective: RAFT Polymerization—A User Guide. *Macromolecules* **2017,** *50* (19), 7433-7447.

(120) Hill, M. R.; Carmean, R. N.; Sumerlin, B. S. Expanding the Scope of RAFT Polymerization: Recent Advances and New Horizons. *Macromolecules* **2015,** *48* (16), 5459-5469.

(121) Semsarilar, M.; Perrier, S. 'Green' reversible addition-fragmentation chain-transfer (RAFT) polymerization. *Nat. Chem.* **2010,** *2* (10), 811-20.

(122) Keddie, D. J.; Moad, G.; Rizzardo, E.; Thang, S. H. RAFT Agent Design and Synthesis. *Macromolecules* **2012,** *45* (13), 5321-5342.

(123) Li, L.; Yan, B.; Yang, J.; Huang, W.; Chen, L.; Zeng, H. Injectable Self-Healing Hydrogel with Antimicrobial and Antifouling Properties. *ACS Appl. Mater. Interfaces* **2017,** *9* (11), 9221-9225.

(124) Wang, W.; Xiang, L.; Gong, L.; Hu, W.; Huang, W.; Chen, Y.; Asha, A. B.; Srinivas, S.; Chen, L.; Narain, R.; Zeng, H. Injectable, Self-Healing Hydrogel with Tunable Optical, Mechanical, and Antimicrobial Properties. *Chem. Mater.* **2019,** *31* (7), 2366-2376.

(125) Zhang, Y.; Fu, C.; Li, Y.; Wang, K.; Wang, X.; Wei, Y.; Tao, L. Synthesis of an injectable, self-healable and dual responsive hydrogel for drug delivery and 3D cell cultivation. *Polym. Chem.* **2017,** *8* (3), 537-544.

(126) Israelachvili, J.; Min, Y.; Akbulut, M.; Alig, A.; Carver, G.; Greene, W.; Kristiansen, K.;

Meyer, E.; Pesika, N.; Rosenberg, K.; Zeng, H. Recent advances in the surface forces apparatus (SFA) technique. *Rep. Prog. Phys.* **2010,** *73* (3), 036601.

(127) Tabor, D.; Winterton, R. H. S. The direct measurement of normal and retarded van der Waals forces. *Proceedings of the Royal Society of London. A. Mathematical and Physical Sciences* **1969,** *312* (1511), 435-450.

(128) Israelachvili, J. N.; Tabor, D. The measurement of van der Waals dispersion forces in the range 1.5 to 130 nm. *Proceedings of the Royal Society of London. A. Mathematical and Physical Sciences* **1997,** *331* (1584), 19-38.

(129) Zeng, H.; Hwang, D. S.; Israelachvili, J. N.; Waite, J. H. Strong reversible Fe^{3+}-mediated bridging between dopa-containing protein films in water. *Proc. Natl. Acad. Sci. U. S. A.* **2010,** *107* (29), 12850-12853.

(130) Lu, Q.; Oh, D. X.; Lee, Y.; Jho, Y.; Hwang, D. S.; Zeng, H. Nanomechanics of Cation–π Interactions in Aqueous Solution. *Angew. Chem. Int. Ed.* **2013,** *52* (14), 3944-3948.

(131) Faghihnejad, A.; Zeng, H. Hydrophobic interactions between polymer surfaces: using polystyrene as a model system. *Soft Matter* **2012,** *8* (9), 2746.

(132) Israelachvili, J. N. Thin film studies using multiple-beam interferometry. *J. Colloid Interface Sci.* **1973,** *44* (2), 259-272.

(133) Israelachvili, J. N. Chapter 12 - Force-Measuring Techniques. In *Intermolecular and Surface Forces (Third Edition)*; Israelachvili, J. N., Ed.; Academic Press: Boston, 2011; pp 223-252.

(134) Israelachvili, J. N. Chapter 13 - Van der Waals Forces between Particles and Surfaces. In *Intermolecular and Surface Forces (Third Edition)*; Israelachvili, J. N., Ed.; Academic Press: San Diego, 2011; pp 253-289.

(135) Lu, Q.; Huang, J.; Maan, O.; Liu, Y.; Zeng, H. Probing molecular interaction mechanisms of

organic fouling on polyamide membrane using a surface forces apparatus: Implication for wastewater treatment. *Sci. Total Environ.* **2018,** *622-623*, 644-654.

(136) Zhao, X.; Li, P.; Guo, B.; Ma, P. X. Antibacterial and conductive injectable hydrogels based on quaternized chitosan-graft-polyaniline/oxidized dextran for tissue engineering. *Acta. Biomater.* **2015,** *26*, 236-48.

(137) Li, Y.; Wang, X.; Fu, Y. N.; Wei, Y.; Zhao, L.; Tao, L. Self-Adapting Hydrogel to Improve the Therapeutic Effect in Wound-Healing. *ACS Appl. Mater. Interfaces.* **2018,** *10* (31), 26046-26055.

(138) Sivashanmugam, A.; Arun Kumar, R.; Vishnu Priya, M.; Nair, S. V.; Jayakumar, R. An overview of injectable polymeric hydrogels for tissue engineering. *Eur. Polym. J.* **2015,** *72*, 543-565.

(139) Liu, M.; Zeng, X.; Ma, C.; Yi, H.; Ali, Z.; Mou, X.; Li, S.; Deng, Y.; He, N. Injectable hydrogels for cartilage and bone tissue engineering. *Bone. Res.* **2017,** *5* (1), 17014.

(140) Xu, W.; Song, Q.; Xu, J. F.; Serpe, M. J.; Zhang, X. Supramolecular Hydrogels Fabricated from Supramonomers: A Novel Wound Dressing Material. *ACS Appl. Mater. Interfaces.* **2017,** *9* (13), 11368-11372.

(141) Chen, Y.; Tan, Z.; Wang, W.; Peng, Y.-Y.; Narain, R. Injectable, Self-Healing, and Multi-Responsive Hydrogels via Dynamic Covalent Bond Formation between Benzoxaborole and Hydroxyl Groups. *Biomacromolecules* **2019,** *20* (2), 1028-1035.

(142) Zhang, X.; Waymouth, R. M. 1,2-Dithiolane-Derived Dynamic, Covalent Materials: Cooperative Self-Assembly and Reversible Cross-Linking. *J. Am. Chem. Soc.* **2017,** *139* (10), 3822-3833.

(143) Dong, R.; Zhao, X.; Guo, B.; Ma, P. X. Self-Healing Conductive Injectable Hydrogels with

Antibacterial Activity as Cell Delivery Carrier for Cardiac Cell Therapy. *ACS Appl. Mater. Interfaces.* **2016,** *8* (27), 17138-50.

(144) Hsieh, F.-Y.; Tao, L.; Wei, Y.; Hsu, S.-h. A novel biodegradable self-healing hydrogel to induce blood capillary formation. *NPG Asia Mater.* **2017,** *9* (3), e363-e363.

(145) Zhang, Y.; Tao, L.; Li, S.; Wei, Y. Synthesis of Multiresponsive and Dynamic Chitosan-Based Hydrogels for Controlled Release of Bioactive Molecules. *Biomacromolecules* **2011,** *12* (8), 2894-2901.

(146) Ding, F.; Shi, X.; Wu, S.; Liu, X.; Deng, H.; Du, Y.; Li, H. Flexible Polysaccharide Hydrogel with pH-Regulated Recovery of Self-Healing and Mechanical Properties. *Macromol. Mater. Eng.* **2017,** *302* (11), 1700221.

(147) Gyles, D. A.; Castro, L. D.; Silva, J. O. C.; Ribeiro-Costa, R. M. A review of the designs and prominent biomedical advances of natural and synthetic hydrogel formulations. *Eur. Polym. J.* **2017,** *88*, 373-392.

(148) Carlini, A. S.; Adamiak, L.; Gianneschi, N. C. Biosynthetic Polymers as Functional Materials. *Macromolecules* **2016,** *49* (12), 4379-4394.

(149) Hoque, J.; Bhattacharjee, B.; Prakash, R. G.; Paramanandham, K.; Haldar, J. Dual Function Injectable Hydrogel for Controlled Release of Antibiotic and Local Antibacterial Therapy. *Biomacromolecules* **2018,** *19* (2), 267-278.

(150) Resmi, R.; Unnikrishnan, S.; Krishnan, L. K.; Kalliyana Krishnan, V. Synthesis and characterization of silver nanoparticle incorporated gelatin-hydroxypropyl methacrylate hydrogels for wound dressing applications. *J. Appl. Polym. Sci.* **2017,** *134* (10).

(151) Gallagher, A. G.; Alorabi, J. A.; Wellings, D. A.; Lace, R.; Horsburgh, M. J.; Williams, R. L. A Novel Peptide Hydrogel for an Antimicrobial Bandage Contact Lens. *Adv. Healthc. Mater.* **2016,**

5 (16), 2013-8.

(152) Li, P.; Poon, Y. F.; Li, W.; Zhu, H. Y.; Yeap, S. H.; Cao, Y.; Qi, X.; Zhou, C.; Lamrani, M.; Beuerman, R. W.; Kang, E. T.; Mu, Y.; Li, C. M.; Chang, M. W.; Leong, S. S.; Chan-Park, M. B. A polycationic antimicrobial and biocompatible hydrogel with microbe membrane suctioning ability. *Nat. Mater.* **2011,** *10* (2), 149-56.

(153) Dong, X.; Wei, C.; Liu, T.; Lv, F.; Qian, Z. Real-Time Fluorescence Tracking of Protoporphyrin Incorporated Thermosensitive Hydrogel and Its Drug Release in Vivo. *ACS Appl. Mater. Interfaces.* **2016,** *8* (8), 5104-13.

(154) Li, J.; Yu, J.; Huang, Y.; Zhao, H.; Tian, L. Highly Stable and Multiemissive Silver Nanoclusters Synthesized in Situ in a DNA Hydrogel and Their Application for Hydroxyl Radical Sensing. *ACS Appl. Mater. Interfaces.* **2018,** *10* (31), 26075-26083.

(155) Ma, C.; Lu, W.; Yang, X.; He, J.; Le, X.; Wang, L.; Zhang, J.; Serpe, M. J.; Huang, Y.; Chen, T. Bioinspired Anisotropic Hydrogel Actuators with On-Off Switchable and Color-Tunable Fluorescence Behaviors. *Adv. Funct. Mater.* **2018,** *28* (7), 1704568.

(156) Ida, S.; Kitanaka, H.; Ishikawa, T.; Kanaoka, S.; Hirokawa, Y. Swelling properties of thermoresponsive/hydrophilic co-networks with functional crosslinked domain structures. *Polym. Chem.* **2018,** *9* (13), 1701-1709.

(157) Lu, H.; Wang, Y.; Li, L.; Kotsuchibashi, Y.; Narain, R.; Zeng, H. Temperature- and pH-Responsive Benzoboroxole-Based Polymers for Flocculation and Enhanced Dewatering of Fine Particle Suspensions. *ACS Appl. Mater. Interfaces.* **2015,** *7* (49), 27176-87.

(158) Lee, A. L. Z.; Voo, Z. X.; Chin, W.; Ono, R. J.; Yang, C.; Gao, S.; Hedrick, J. L.; Yang, Y. Y. Injectable Coacervate Hydrogel for Delivery of Anticancer Drug-Loaded Nanoparticles in vivo. *ACS Appl. Mater. Interfaces.* **2018,** *10* (16), 13274-13282.

(159) Zhang, G.; Chen, Y.; Deng, Y.; Wang, C. A Triblock Copolymer Design Leads to Robust Hybrid Hydrogels for High-Performance Flexible Supercapacitors. *ACS Appl. Mater. Interfaces.* **2017,** *9* (41), 36301-36310.

(160) Ovdenko, V.; Kolendo, A. New bent-shaped azomethine monomers for optical applications. *Mol. Cryst. Liq. Cryst.* **2016,** *640* (1), 113-121.

(161) Haraguchi, K.; Kubota, K.; Takada, T.; Mahara, S. Highly Protein-Resistant Coatings and Suspension Cell Culture Thereon from Amphiphilic Block Copolymers Prepared by RAFT Polymerization. *Biomacromolecules* **2014,** *15* (6), 1992-2003.

(162) Kotsuchibashi, Y.; Agustin, R. V. C.; Lu, J.-Y.; Hall, D. G.; Narain, R. Temperature, pH, and Glucose Responsive Gels via Simple Mixing of Boroxole- and Glyco-Based Polymers. *ACS Macro Lett.* **2013,** *2* (3), 260-264.

(163) Kim, S.; Huang, J.; Lee, Y.; Dutta, S.; Yoo, H. Y.; Jung, Y. M.; Jho, Y.; Zeng, H.; Hwang, D. S. Complexation and coacervation of like-charged polyelectrolytes inspired by mussels. *Proc. Natl. Acad. Sci. U. S. A.* **2016,** *113* (7), E847-53.

(164) Faghihnejad, A.; Zeng, H. Interaction mechanism between hydrophobic and hydrophilic surfaces: using polystyrene and mica as a model system. *Langmuir* **2013,** *29* (40), 12443-51.

(165) Zeng, H.; Tian, Y.; Anderson, T. H.; Tirrell, M.; Israelachvili, J. N. New SFA Techniques for Studying Surface Forces and Thin Film Patterns Induced by Electric Fields. *Langmuir* **2008,** *24* (4), 1173-1182.

(166) Zeng, H.; Huang, J.; Tian, Y.; Li, L.; Tirrell, M. V.; Israelachvili, J. N. Adhesion and Detachment Mechanisms between Polymer and Solid Substrate Surfaces: Using Polystyrene–Mica as a Model System. *Macromolecules* **2016,** *49* (14), 5223-5231.

(167) Chen, J.; Yan, B.; Wang, X.; Huang, Q.; Thundat, T.; Zeng, H. Core cross-linked double

hydrophilic block copolymer micelles based on multiple hydrogen-bonding interactions. *Polym. Chem.* **2017,** *8* (20), 3066-3073.

(168) Giano, M. C.; Ibrahim, Z.; Medina, S. H.; Sarhane, K. A.; Christensen, J. M.; Yamada, Y.; Brandacher, G.; Schneider, J. P. Injectable bioadhesive hydrogels with innate antibacterial properties. *Nat. Commun.* **2014,** *5* (1), 4095.

(169) Brown, T. E.; Anseth, K. S. Spatiotemporal hydrogel biomaterials for regenerative medicine. *Chem. Soc. Rev.* **2017,** *46* (21), 6532-6552.

(170) Huang, Q.; Zou, Y.; Arno, M. C.; Chen, S.; Wang, T.; Gao, J.; Dove, A. P.; Du, J. Hydrogel scaffolds for differentiation of adipose-derived stem cells. *Chem. Soc. Rev.* **2017,** *46* (20), 6255-6275.

(171) Yan, B.; Huang, J.; Han, L.; Gong, L.; Li, L.; Israelachvili, J. N.; Zeng, H. Duplicating Dynamic Strain-Stiffening Behavior and Nanomechanics of Biological Tissues in a Synthetic Self-Healing Flexible Network Hydrogel. *ACS Nano* **2017,** *11* (11), 11074-11081.

(172) Wei, W.; Qi, X.; Li, J.; Zuo, G.; Sheng, W.; Zhang, J.; Dong, W. Smart Macroporous Salecan/Poly(N,N-diethylacrylamide) Semi-IPN Hydrogel for Anti-Inflammatory Drug Delivery. *ACS Biomater. Sci. Eng.* **2016,** *2* (8), 1386-1394.

(173) Li, X.; Zhong, H.; Li, X.; Jia, F.; Cheng, Z.; Zhang, L.; Yin, J.; An, L.; Guo, L. Synthesis of attapulgite/N-isopropylacrylamide and its use in drug release. *Mater. Sci. Eng., C* **2014,** *45*, 170-5.

(174) Smeets, N. M. B.; Patenaude, M.; Kinio, D.; Yavitt, F. M.; Bakaic, E.; Yang, F.-C.; Rheinstädter, M.; Hoare, T. Injectable hydrogels with in situ-forming hydrophobic domains: oligo(d,l-lactide) modified poly(oligoethylene glycol methacrylate) hydrogels. *Polym. Chem.* **2014,** *5* (23), 6811-6823.

(175) Strassburg, A.; Kracke, F.; Wenners, J.; Jemeljanova, A.; Kuepper, J.; Petersen, H.; Tiller, J. C. Nontoxic, Hydrophilic Cationic Polymers-Identified as Class of Antimicrobial Polymers. *Macromol. Biosci.* **2015,** *15* (12), 1710-23.

(176) Wang, L. L.; Sloand, J. N.; Gaffey, A. C.; Venkataraman, C. M.; Wang, Z.; Trubelja, A.; Hammer, D. A.; Atluri, P.; Burdick, J. A. Injectable, Guest–Host Assembled Polyethylenimine Hydrogel for siRNA Delivery. *Biomacromolecules* **2017,** *18* (1), 77-86.

(177) Zhuang, Y.; Shen, H.; Yang, F.; Wang, X.; Wu, D. Synthesis and characterization of PLGA nanoparticle/4-arm-PEG hybrid hydrogels with controlled porous structures. *RSC Advances* **2016,** *6* (59), 53804-53812.

(178) Davoodi, P.; Ng, W. C.; Yan, W. C.; Srinivasan, M. P.; Wang, C. H. Double-Walled Microparticles-Embedded Self-Cross-Linked, Injectable, and Antibacterial Hydrogel for Controlled and Sustained Release of Chemotherapeutic Agents. *ACS Appl. Mater. Interfaces.* **2016,** *8* (35), 22785-800.

(179) Storm, C.; Pastore, J. J.; MacKintosh, F. C.; Lubensky, T. C.; Janmey, P. A. Nonlinear elasticity in biological gels. *Nature* **2005,** *435* (7039), 191-194.

(180) Licup, A. J.; Munster, S.; Sharma, A.; Sheinman, M.; Jawerth, L. M.; Fabry, B.; Weitz, D. A.; MacKintosh, F. C. Stress controls the mechanics of collagen networks. *Proc. Natl. Acad. Sci. USA* **2015,** *112* (31), 9573-9578.

(181) Pujol, T.; du Roure, O.; Fermigier, M.; Heuvingh, J. Impact of branching on the elasticity of actin networks. *Proc. Natl. Acad. Sci. USA* **2012,** *109* (26), 10364-10369.

(182) Das, R. K.; Gocheva, V.; Hammink, R.; Zouani, O. F.; Rowan, A. E. Stress-stiffening-mediated stem-cell commitment switch in soft responsive hydrogels. *Nat. Mater.* **2016,** *15* (3), 318-325.

(183) Liu, K.; Mihaila, S. M.; Rowan, A.; Oosterwijk, E.; Kouwer, P. H. J. Synthetic Extracellular Matrices with Nonlinear Elasticity Regulate Cellular Organization. *Biomacromolecules* **2019,** *20* (2), 826-834.

(184) Kouwer, P. H.; Koepf, M.; Le Sage, V. A.; Jaspers, M.; van Buul, A. M.; Eksteen-Akeroyd, Z. H.; Woltinge, T.; Schwartz, E.; Kitto, H. J.; Hoogenboom, R.; Picken, S. J.; Nolte, R. J.; Mendes, E.; Rowan, A. E. Responsive biomimetic networks from polyisocyanopeptide hydrogels. *Nature* **2013,** *493* (7434), 651-655.

(185) Jaspers, M.; Dennison, M.; Mabesoone, M. F.; MacKintosh, F. C.; Rowan, A. E.; Kouwer, P. H. Ultra-responsive soft matter from strain-stiffening hydrogels. *Nat. Commun.* **2014,** *5*, 5808.

(186) Fernandez-Castano Romera, M.; Lafleur, R. P. M.; Guibert, C.; Voets, I. K.; Storm, C.; Sijbesma, R. P. Strain Stiffening Hydrogels through Self-Assembly and Covalent Fixation of Semi-Flexible Fibers. *Angew. Chem. Int. Ed.* **2017,** *56* (30), 8771-8775.

(187) Tang, J. D.; Mura, C.; Lampe, K. J. Stimuli-Responsive, Pentapeptide, Nanofiber Hydrogel for Tissue Engineering. *J. Am. Chem. Soc.* **2019,** *141* (12), 4886-4899.

(188) Wang, Y.; Xu, Z.; Lovrak, M.; le Sage, V. A. A.; Zhang, K.; Guo, X.; Eelkema, R.; Mendes, E.; van Esch, J. H. Biomimetic Strain-Stiffening Self-Assembled Hydrogels. *Angew. Chem. Int. Ed.* **2020,** *59* (12), 4830-4834.

(189) Owusu-Nkwantabisah, S.; Gillmor, J.; Switalski, S.; Mis, M. R.; Bennett, G.; Moody, R.; Antalek, B.; Gutierrez, R.; Slater, G. Synergistic Thermoresponsive Optical Properties of a Composite Self-Healing Hydrogel. *Macromolecules* **2017,** *50* (9), 3671-3679.

(190) Wu, D.; Wang, W.; Diaz-Dussan, D.; Peng, Y.-Y.; Chen, Y.; Narain, R.; Hall, D. G. In Situ Forming, Dual-Crosslink Network, Self-Healing Hydrogel Enabled by a Bioorthogonal Nopoldiol–Benzoxaborolate Click Reaction with a Wide pH Range. *Chem. Mater.* **2019,** *31* (11),

4092-4102.

(191) Chen, Y.; Wang, W.; Wu, D.; Zeng, H.; Hall, D. G.; Narain, R. Multiresponsive and Self-Healing Hydrogel via Formation of Polymer-Nanogel Interfacial Dynamic Benzoxaborole Esters at Physiological pH. *ACS Appl. Mater. Interfaces* **2019,** *11* (47), 44742-44750.

(192) Kim, S. M.; Jeon, H.; Shin, S. H.; Park, S. A.; Jegal, J.; Hwang, S. Y.; Oh, D. X.; Park, J. Superior Toughness and Fast Self-Healing at Room Temperature Engineered by Transparent Elastomers. *Adv. Mater.* **2018,** *30* (1), 1705145.

(193) Fernandez-Castano Romera, M.; Lou, X.; Schill, J.; Ter Huurne, G.; Fransen, P. K. H.; Voets, I. K.; Storm, C.; Sijbesma, R. P. Strain-Stiffening in Dynamic Supramolecular Fiber Networks. *J. Am. Chem. Soc.* **2018,** *140* (50), 17547-17555.

(194) Schoenmakers, D. C.; Rowan, A. E.; Kouwer, P. H. J. Crosslinking of fibrous hydrogels. *Nat. Commun.* **2018,** *9* (1), 2172.

(195) Schultz, R. K.; Myers, R. R. The Chemorheology of Poly(vinyl alcohol)-Borate Gels. *Macromolecules* **1969,** *2* (3), 281-285.

(196) Yan, B.; Huang, J.; Han, L.; Gong, L.; Li, L.; Israelachvili, J. N.; Zeng, H. Duplicating Dynamic Strain-Stiffening Behavior and Nanomechanics of Biological Tissues in a Synthetic Self-Healing Flexible Network Hydrogel. *ACS Nano.* **2017,** *11* (11), 11074-11081.

(197) Moghimi, S. M.; Symonds, P.; Murray, J. C.; Hunter, A. C.; Debska, G.; Szewczyk, A. A two-stage poly(ethylenimine)-mediated cytotoxicity: implications for gene transfer/therapy. *Mol. Ther.* **2005,** *11* (6), 990-995.

(198) Deng, Z.; Li, S.; Jiang, X.; Narain, R. Well-Defined Galactose-Containing Multi-Functional Copolymers and Glyconanoparticles for Biomolecular Recognition Processes. *Macromolecules* **2009,** *42* (17), 6393-6405.

(199) Narain, R.; Armes, S. P. Synthesis of low polydispersity, controlled-structure sugar methacrylate polymers under mild conditions without protecting group chemistry. *Chem. Commun.* **2002,** (23), 2776-2777.

(200) Broedersz, C. P.; Kasza, K. E.; Jawerth, L. M.; Münster, S.; Weitz, D. A.; MacKintosh, F. C. Measurement of nonlinear rheology of cross-linked biopolymer gels. *Soft Matter* **2010,** *6* (17), 4120-4127.

(201) Xiang, L.; Gong, L.; Zhang, J.; Zhang, L.; Hu, W.; Wang, W.; Lu, Q.; Zeng, H. Probing molecular interactions of PEGylated chitosan in aqueous solutions using a surface force apparatus. *Phys. Chem. Chem. Phys.* **2019,** *21* (37), 20571-20581.

(202) Israelachvili, J.; Min, Y.; Akbulut, M.; Alig, A.; Carver, G.; Greene, W.; Kristiansen, K.; Meyer, E.; Pesika, N.; Rosenberg, K.; Zeng, H. Recent advances in the surface forces apparatus (SFA) technique. *Rep. Prog. Phys* **2010,** *73* (3), 036601.

(203) Bertula, K.; Martikainen, L.; Munne, P.; Hietala, S.; Klefström, J.; Ikkala, O.; Nonappa. Strain-Stiffening of Agarose Gels. *ACS Macro Lett.* **2019,** *8* (6), 670-675.

(204) Jansen, K. A.; Bacabac, R. G.; Piechocka, I. K.; Koenderink, G. H. Cells actively stiffen fibrin networks by generating contractile stress. *Biophys. J.* **2013,** *105* (10), 2240-2251.

(205) Bao, Y.; Luo, Z.; Cui, S. Environment-dependent single-chain mechanics of synthetic polymers and biomacromolecules by atomic force microscopy-based single-molecule force spectroscopy and the implications for advanced polymer materials. *Chem. Soc. Rev.* **2020,** *49* (9), 2799-2827.

(206) Kolberg, A.; Wenzel, C.; Hackenstrass, K.; Schwarzl, R.; Ruttiger, C.; Hugel, T.; Gallei, M.; Netz, R. R.; Balzer, B. N. Opposing Temperature Dependence of the Stretching Response of Single PEG and PNiPAM Polymers. *J. Am. Chem. Soc.* **2019,** *141* (29), 11603-11613.

(207) Wagner, B.; Tharmann, R.; Haase, I.; Fischer, M.; Bausch, A. R. Cytoskeletal polymer networks: the molecular structure of cross-linkers determines macroscopic properties. *Proc. Natl. Acad. Sci. USA* **2006,** *103* (38), 13974-13978.

(208) Guimarães, C. F.; Gasperini, L.; Marques, A. P.; Reis, R. L. The stiffness of living tissues and its implications for tissue engineering. *Nat. Rev. Mater.* **2020,** *5* (5), 351-370.

(209) Munster, S.; Jawerth, L. M.; Leslie, B. A.; Weitz, J. I.; Fabry, B.; Weitz, D. A. Strain history dependence of the nonlinear stress response of fibrin and collagen networks. *Proc. Natl. Acad. Sci. USA* **2013,** *110* (30), 12197-202.

(210) Erk, K. A.; Henderson, K. J.; Shull, K. R. Strain Stiffening in Synthetic and Biopolymer Networks. *Biomacromolecules* **2010,** *11* (5), 1358-1363.

(211) Lee, H.; Venable, R. M.; Mackerell, A. D., Jr.; Pastor, R. W. Molecular dynamics studies of polyethylene oxide and polyethylene glycol: hydrodynamic radius and shape anisotropy. *Biophys. J.* **2008,** *95* (4), 1590-1599.

(212) Oesterhelt, F.; Rief, M.; Gaub, H. E. Single molecule force spectroscopy by AFM indicates helical structure of poly(ethylene-glycol) in water. *New J Phys* **1999,** *1*, 6-6.

(213) Yu, F.; Cao, X.; Li, Y.; Zeng, L.; Yuan, B.; Chen, X. An injectable hyaluronic acid/PEG hydrogel for cartilage tissue engineering formed by integrating enzymatic crosslinking and Diels–Alder “click chemistry”. *Polym Chem-Uk* **2014,** *5* (3), 1082-1090.

(214) Jaspers, M.; Vaessen, S. L.; van Schayik, P.; Voerman, D.; Rowan, A. E.; Kouwer, P. H. J. Nonlinear mechanics of hybrid polymer networks that mimic the complex mechanical environment of cells. *Nat. Commun.* **2017,** *8*, 15478.

(215) Bregenzer, M. E.; Horst, E. N.; Mehta, P.; Novak, C. M.; Raghavan, S.; Snyder, C. S.; Mehta, G. Integrated cancer tissue engineering models for precision medicine. *PLoS One* **2019,** *14* (5),

e0216564.

(216) Griffin, D. R.; Archang, M. M.; Kuan, C. H.; Weaver, W. M.; Weinstein, J. S.; Feng, A. C.; Ruccia, A.; Sideris, E.; Ragkousis, V.; Koh, J.; Plikus, M. V.; Di Carlo, D.; Segura, T.; Scumpia, P. O. Activating an adaptive immune response from a hydrogel scaffold imparts regenerative wound healing. *Nat. Mater.* **2020**.

(217) Mandal, A.; Clegg, J. R.; Anselmo, A. C.; Mitragotri, S. Hydrogels in the clinic. *Bioeng. Transl. Med.* **2020,** *5* (2), e10158.

(218) Zhang, E.; Yang, J.; Wang, K.; Song, B.; Zhu, H.; Han, X.; Shi, Y.; Yang, C.; Zeng, Z.; Cao, Z. Biodegradable Zwitterionic Cream Gel for Effective Prevention of Postoperative Adhesion. *Adv. Funct. Mater.* **2020**, 2009431.

(219) Liu, Y.; Liu, Y.; Wang, Q.; Han, Y.; Tan, Y. Boronic ester-based self-healing hydrogels formed by using intermolecular B-N coordination. *Polymer* **2020,** *202*, 122624.

(220) Kharkar, P. M.; Rehmann, M. S.; Skeens, K. M.; Maverakis, E.; Kloxin, A. M. Thiol-ene click hydrogels for therapeutic delivery. *ACS. Biomater. Sci. Eng.* **2016,** *2* (2), 165-179.

(221) Yang, Y.; Zhang, J.; Liu, Z.; Lin, Q.; Liu, X.; Bao, C.; Wang, Y.; Zhu, L. Tissue-Integratable and Biocompatible Photogelation by the Imine Crosslinking Reaction. *Adv. Mater.* **2016,** *28* (14), 2724-30.

(222) Chen, Y.; Tan, Z.; Wang, W.; Peng, Y. Y.; Narain, R. Injectable, Self-Healing, and Multi-Responsive Hydrogels via Dynamic Covalent Bond Formation between Benzoxaborole and Hydroxyl Groups. *Biomacromolecules* **2019,** *20* (2), 1028-1035.

(223) Zander, Z. K.; Becker, M. L. Antimicrobial and Antifouling Strategies for Polymeric Medical Devices. *ACS Macro Lett.* **2017,** *7* (1), 16-25.

(224) Phadke, A.; Zhang, C.; Arman, B.; Hsu, C. C.; Mashelkar, R. A.; Lele, A. K.; Tauber, M. J.;

Arya, G.; Varghese, S. Rapid self-healing hydrogels. *Proc. Natl. Acad. Sci. U.S.A.* **2012,** *109* (12), 4383-8.

(225) Zeng, H.; Hwang, D. S.; Israelachvili, J. N.; Waite, J. H. Strong reversible Fe^{3+}-mediated bridging between dopa-containing protein films in water. *Proc. Natl. Acad. Sci. U S A.* **2010,** *107* (29), 12850-3.

(226) Asha, A. B.; Chen, Y.; Zhang, H.; Ghaemi, S.; Ishihara, K.; Liu, Y.; Narain, R. Rapid Mussel-Inspired Surface Zwitteration for Enhanced Antifouling and Antibacterial Properties. *Langmuir* **2019,** *35* (5), 1621-1630.

(227) Srivastava, S.; Andreev, M.; Levi, A. E.; Goldfeld, D. J.; Mao, J.; Heller, W. T.; Prabhu, V. M.; de Pablo, J. J.; Tirrell, M. V. Gel phase formation in dilute triblock copolyelectrolyte complexes. *Nat. Commun.* **2017,** *8* (1), 14131.

(228) Chen, Q.; Yu, S.; Zhang, D.; Zhang, W.; Zhang, H.; Zou, J.; Mao, Z.; Yuan, Y.; Gao, C.; Liu, R. Impact of Antifouling PEG Layer on the Performance of Functional Peptides in Regulating Cell Behaviors. *J. Am. Chem. Soc.* **2019,** *141* (42), 16772-16780.

(229) Kang, T.; Banquy, X.; Heo, J.; Lim, C.; Lynd, N. A.; Lundberg, P.; Oh, D. X.; Lee, H. K.; Hong, Y. K.; Hwang, D. S.; Waite, J. H.; Israelachvili, J. N.; Hawker, C. J. Mussel-Inspired Anchoring of Polymer Loops That Provide Superior Surface Lubrication and Antifouling Properties. *ACS Nano* **2016,** *10* (1), 930-7.

(230) He, S.; Wu, J.; Li, S. H.; Wang, L.; Sun, Y.; Xie, J.; Ramnath, D.; Weisel, R. D.; Yau, T. M.; Sung, H. W.; Li, R. K. The conductive function of biopolymer corrects myocardial scar conduction blockage and resynchronizes contraction to prevent heart failure. *Biomaterials* **2020,** *258*, 120285.

(231) Okabayashi, K.; Ashrafian, H.; Zacharakis, E.; Hasegawa, H.; Kitagawa, Y.; Athanasiou, T.; Darzi, A. Adhesions after abdominal surgery: a systematic review of the incidence, distribution

and severity. *Surg. Today.* **2014,** *44* (3), 405-20.

(232) Robson, M. C. Wound infection. A failure of wound healing caused by an imbalance of bacteria. *Surg. Clin. North. Am.* **1997,** *77* (3), 637-50.

(233) Koh, T. J.; DiPietro, L. A. Inflammation and wound healing: the role of the macrophage. *Expert. Rev. Mol. Med.* **2011,** *13*, e23.